# Durham E-Theses

*Non-intrusive support of ground vehicle wind tunnel models through superconducting magnetic levitation*

Muscroft, Robert J. M.

**How to cite:**

**Use policy**

# Non-Intrusive Support of Ground Vehicle Wind Tunnel

# Models through Superconducting Magnetic Levitation

## Robert J. M. Muscroft

**Thesis submitted for degree of Doctor of Philosophy**

**University of Durham**

**School Of Engineering**

**2006**

# Abstract

Wind tunnel testing of racing cars is performed with a moving ground plane to take into account the downforce generated by the low ground clearance of these vehicles. Struts and wheel stings, mounted from the roof and walls of the tunnel, are used to hold the vehicle in position within the test section. These supports disrupt the airflow around the model, thereby deviating from on-track conditions. Where the vehicle's aerodynamics are already highly refined, the effects of subtle shape changes such as those made in Formula 1, may be much smaller than the errors introduced by the supporting struts. Support interference can also lead to incorrect optimisation of aerodynamic elements.

A magnet will stably levitate over a High Temperature Superconductor (HTS) cooled below its critical temperature. The magnetic flux of the magnet becomes pinned within the bulk HTS microstructure in the form of individual flux quanta, each of which is surrounded by a current vortex at sites of imperfection in the superconducting matrix. This mechanism formed the basis of the superconducting pod which achieved stable passive levitation. Finite element analysis simulation was used to optimise the effectiveness of the electromagnets providing a restoring force to the levitating magnets. To augment the superconducting levitation, without introducing excessive instability to the levitation, the magnetic rail was invented. Traverses of both the superconducting pod and the magnetic rail were performed to map the forces each produced.

The feasibility of a non-intrusive method of supporting ground vehicle wind tunnel models has been investigated. The Superconducting Magnetic Levitation System combines the inherent stability and damping of superconducting levitation with the high ground clearance of magnet only levitation. Stable passive levitation has been achieved, with six degree of freedom control. The system uses a combination of type II high temperature superconductors, rare earth permanent magnets, and electromagnets to support a model under test.

The final prototype of the superconducting magnetic levitation system was designed to support a 40% scale Formula 1 model. The system was capable of supporting 250N of downforce on top of the weight of the model and 90N of drag at ground clearances comparable to 40% scale Formula 1 clearances. The Superconducting Magnetic Levitation System is the largest wind tunnel magnetic levitation system in the world and has been successfully tested at speeds of up to 20ms$^{-1}$ in the Durham 2m wind tunnel.

# Contents

**Declaration**

I confirm that no part of the material offered has previously been submitted by me for a degree in this or any other University and is all my own work except where indicated otherwise and referenced.

Signed: ..............................................

Robert J. M. Muscroft

Date:...21/5/2007...........................

**Copyright**

The copyright of this thesis rests solely with the author. No quotation from it should be published without the author's prior written consent, and information derived from it should be acknowledged.

# Acknowledgements

## Nomenclature

| | | |
|---|---|---|
| Å | x | Angstrom |
| Al | | Aluminium |
| B | | Boron |
| Ba | | Barium |
| BF | | Bluntness Factor |
| $(BH)_{max}$ | | Energy Product |
| $_BH_c$ | | Normal Coercivity |
| Bi | | Bismuth |
| $B_r$ | | Magnetic Flux |
| Ca | | Calcium |
| Co | | Cobalt |
| Cu | | Copper |
| E | | Electric Field |
| Fe | | Iron |
| H | | Magnetic Field |
| $H_c$ | | Critical Magnetic Field Strength |
| Hg | | Mercury |
| $H_{n_1}$ | | Magnetic Field in Loop 1 |
| $H_{n_2}$ | | Magnetic Field in Loop 2 |
| HTS | | High Temperature Superconductor |
| I | | Current |
| $I_{s_A}$ | | Current in Superconducting Loop A |
| $I_{s_B}$ | | Current in Superconducting Loop B |
| $_iH_c$ | | Intrinsic Coercivity |
| J | | Current Density |
| $J_c$ | | Critical Current |
| $J_s$ | | Saturation Polarization Field |
| K | | Kelvin |
| kg | | Kilograms |
| La | | Lanthanum |
| $L_A$ | | Length of Loop A |
| $L_B$ | | Length of Loop B |

| | |
|---|---|
| Mg | Magnesium |
| Nb | Niobium |
| Nd | Neodymium |
| Ni | Nickel |
| O | Oxygen |
| P | Power |
| Pb | Lead |
| R | Resistance |
| $R_0$ | Leading Edge Radius |
| $r_{S_A}$ | Resistance in Superconducting Loop A |
| $r_{S_B}$ | Resistance in Superconducting Loop B |
| Sm | Samarium |
| Sr | Strontium |
| $S_T$ | Distance from leading edge of the aerofoil surface to the point of maximum thickness |
| t | Time |
| t | Maximum Thickness of Aerofoil |
| T | Tesla |
| T | Temperature |
| $T_c$ | Transition Temperature |
| Ti | Titanium |
| Tl | Thallium |
| $U_\infty$ | Free Stream Velocity |
| $X_T$ | Chordwise position of the maximum thickness |
| Y | Yttrium |
| $\delta$ | Boundary layer thickness |
| $\delta_1$ | Displacement thickness |
| $\varepsilon$ | Resistivity |
| $\lambda$ | Penetration Depth |
| $\sigma$ | Conductivity |
| $\varphi$ | Charge Potential |

# 1. Introduction

## 1.1 Summary

This thesis investigates the feasibility of a non-intrusive method of supporting ground vehicles under test in a wind tunnel with a moving ground plane. Without such a system struts and stings, mounted to the roof and walls of the test section, are required to support the weight of the vehicle, and transmit forces to a force balance for measurement. In cases where the vehicle's aerodynamics are already highly refined, the effects of subtle shape changes, such as those made in Formula 1, may be considerably smaller than the errors introduced by the supporting struts. Hetherington & Sims-Williams (2006) discusses the effects that struts and stings have on lift and drag measurements and showed that the results are considerably affected and that the effects were dependant of the model and strut configuration; precluding the use of correction factors. Considerable resources are spent each year by automotive manufacturers on wind tunnel testing for new models, and some Formula 1 teams have multiple wind tunnels running 24 hours a day, yet the resulting data is affected by the supporting struts and stings.

The Superconducting Magnetic Levitation System detailed in this thesis is based on the facility of type II high temperature superconductors (HTS) to trap magnetic flux within their volume. This mechanism allows levitation to occur without the need for any active control. The magnetic flux of a permanent magnet becomes trapped or pinned within the bulk HTS microstructure in the form of individual flux quanta, each of which is surrounded by a current vortex at sites of imperfections (such as second phase inclusions) in the superconducting matrix, (Feng et al 2001). A magnet will stably levitate over a type II superconductor in the vortex state and will oppose any force acting on it. This superconducting levitation is passive and intrinsically damped thereby insulating the system from the effects of high frequency oscillation in the air flow.

Computational analysis of a simplified geometry of the superconducting levitation was undertaken using an electromagnetic finite element analysis program called MEGA (MEGA 2000). Simulations of multiple arrangements of the permanent magnet,

1

superconductor, and electromagnet system were tested to find the most efficacious configuration.

Through the use of superconducting levitation, stable passive levitation can be achieved. However the height at which such levitation can occur is limited. In order to expand the operating range of the system a permanent magnet only levitation system, which is capable of acting over considerably larger air gaps, was constructed to reinforce the superconducting levitation. Rare earth permanent magnets composed of a Neodymium-Iron-Boron alloy were used throughout this project. These magnets possess far superior field strength-to-weight ratio than that of ferrite or ceramic magnets (Coey 2002), an essential attribute for any levitation application. Table 1.1.1 shows that $Nd_2Fe_{14}B$ has the highest value of magnetic flux, $B_r$, and, more importantly, by far the largest maximum energy product $(BH)_{max}$ which is a measure of the useful work that a magnet can produce at a distance from its volume.

| Characteristic <br> Material | $B_r$ (T) | $(BH)_{max}$ $(kJm^{-3})$ |
|---|---|---|
| $Nd_2Fe_{14}B$ | 1.28 | 300 |
| $Sm_2Co_{17}$ | 1.08 | 220 |
| $SmCo_5$ | 0.88 | 150 |
| AlNiCo | 1.25 | 43 |
| $SrFe_{12}O_{19}$ | 0.41 | 34 |

Table 1.1.1, Properties of Magnetic Material (Coey 2002)

## 1.2 Existing test techniques

Wind tunnel tests involving the use of a moving ground plane requires the use of struts and stings to hold the vehicle under test in position. For vehicles with high ground clearance, such as road cars, testing is generally performed with a static ground plane and the wheels of the model are pinned through the floor of the wind tunnel. This technique provides a reasonably realistic airflow over the top half of the model and, given the high ride height of these vehicles, a moderately representative airflow underneath the model. However when

performing testing on vehicles with low ground clearance or refining under body elements for high ground clearance vehicles, it is important to simulate the relative motion of the moving ground plane and the model, due to the interaction of the ground plane with the under floor of the model. When a moving ground plane is used in the testing of racing cars the model is usually held in position by the use of five stings. One sting locates the main body of the model and four locate the wheels, as shown in figure 1.2.1.



Rolling Road

Figure 1.2.1, The Sauber Wind tunnel (Motorsport.com 2003).

1.2.1 Support Strut Interference

Wind tunnel testing of aeroplane models also require the use of stings, as shown in figure 1.2.2 which shows the A380 being tested at ONERA (2005). The model is supported by a strut attached to the base of the fuselage, which is connected to a force balance to measure the forces acting on the model and the supporting strut. However it is well established that the measurements of the forces acting on supporting struts in cases such as these change when the model is introduced, and equally the forces acting on the model change when the supporting struts are introduced (Barlow et al 1999). The sum of the separate forces acting

on the model and strut in most cases is less than the combined forces acting on both together.



Figure 1.2.2, Airbus A380 under test at ONERA (2005).

The join between the strut and the model body produces a horseshoe vortex, so called because it wraps around the strut and has two trailing legs that progress down either side of the strut, as shown in figure 1.2.3.
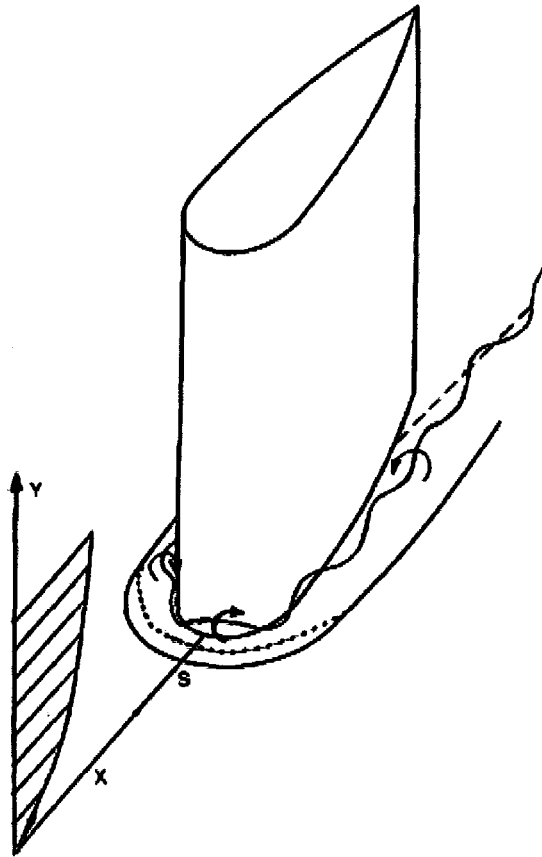
Figure 1.2.3 Horseshoe Vortex System, from Simpson (2001)

The horseshoe vortex is subject to large-scale, low-frequency unsteadiness (Simpson 2001), and acts to bring high momentum, free stream fluid into the corner of the strut-body joint which energises the flow, increasing the shear stress adding to the drag. This effect can also act to change the point at which separation may occur on aerodynamic elements downstream (Devenport et al 1990), and so may change the perceived effect on part of the model even if the overall forces are accounted for.

The same principles apply to the testing of ground vehicle wind tunnel models but with the added complexity that a moving ground plane introduces. Given the importance that is placed upon the under floor flow of racing cars in providing downforce quantifying the effects of the supporting struts and stings would be essential to validate the accuracy of the results. However there is little published work on the subject.

It is possible to attempt to quantify the effects of the struts on the models through the use of dummy struts. The model is supported by another strut and the strut being evaluated is replaced by a mock strut, the effect of the strut on the force measurement can then be evaluated. This process must be repeated for any change made to the model or the supporting strut and is time consuming. This approach is more effective for aircraft as supporting struts can be used both above and below the model where the struts cause little interference with the flow around each other. For ground vehicles this approach is more limited as there is less scope for mounting supports in positions where they will not affect the flow around each other. However whilst this method allows the effect of an isolated strut to be quantified it does not entirely solve the problem as the supporting struts still disturb the airflow from the path it would otherwise be taking and the flow in the wake of such a strut will possess a momentum deficiency that will affect any aerodynamic element downstream of the strut.

### 1.2.2 Support Strut Interference Factors

Simpson (2001) discusses how the shape of a strut supporting a model directly affects the aerodynamic interference that it causes. The amount of drag produced mainly depends on the strength of the horseshoe vortex formed at the leading edge of the strut. The strength of the horseshoe vortex produced increases with the bluntness factor of the strut. Where bluntness factor is defined as;

$$\mathrm{BF} = \frac{1}{2}\frac{R_0}{X_T}\left[\frac{T}{S_T} + \frac{S_T}{X_T}\right]$$
(1.1)

Where $R_0$ is the leading edge radius, $X_T$ is the chordwise position of the maximum thickness $T$, and $S_T$ is the distance from the leading edge along the aerofoil surface to the maximum thickness. It was found that struts with bluntness factors of 0.0133 and 0.0287 did not produce horseshoe vortices, but that struts with bluntness factors of 0.0452 and higher caused the creation of vortices. The distances between a model and the wall of the wind tunnel that support struts have to span means that the required stiffness of the struts necessitates the struts possessing a bluntness factor greater than 0.0452. When testing is

done with a yawed model and consequently a yawed strut, the angle of attack becomes non-zero and the flow encounters a strut that becomes more blunt with increasing angle of attack. As a result the strength of the horseshoe vortices also increases with the increasing angle of attack (Simpson 2001).

## 1.2.3, Support Strut Interference Reduction

Given that the production of horseshoe vortices is virtually unavoidable for large scale model testing with a moving ground plane, methods of reducing the vortices produced by the struts have been investigated. Devenport et al (1990) have shown that a constant radius fillet at the strut/body junction can reduce the interference drag on a strut. However the fillet also has the effect of making the nose of the strut more blunt, strengthening the horseshoe vortices produced. A more successful approach was to apply the fillet to the leading edge only, Devenport et al (1992) showed that this configuration eliminated separation at the leading edge of the strut by reducing the adverse pressure gradient experienced by the boundary layer on the body upstream of the strut/body junction. The leading edge fillet also prevented the formation of the horseshoe vortices. It has also been show that by applying a fillet, with a radius of around 6% of the wing chord extending one strut chord from the trailing edge, the interference drag can be reduced by 10% (Hoerner 1965). Leading and trailing edge fillets also act to decrease the effective bluntness of the struts by increasing the strut chord at the strut/body junction. However given the need for vehicle support struts which penetrate the body shell without contact, and regular changes of the model under test, applying fillets effectively in a wind tunnel can be complicated. Another method of drag reduction was investigated by Lafleur and Langston (1993) which involved producing an indentation in front of the leading edge of the strut which allowed for an 18% reduction in interference drag. The indentation allows for lower velocities and lower peak vorticity magnitudes around the strut due to the increased flow area that results (Simpson 2001). However for this to be feasible for testing it would require reshaping the model and as such is impractical. The impact of the strut interference on aerodynamic elements downstream was found to be reduced by ejecting high pressure air from the trailing edge of the strut (Akehurst 2003); however strut wake interference constitutes only a small part of the total interference, and so this method is limited in its effectiveness.

Among the factors that contribute to the overall drag increase caused by supporting struts are the nose bluntness of the support, the Reynolds number and displacement thickness of the approach boundary layer, the free-stream turbulence, the roughness of the surfaces, the boundary layers, separations, and vortices around the obstacles (Simpson 2001). While it is possible to account for some of these effects that are caused by these factors, the complex interactions between them means there is no way to apply correction factors to completely negate their effects.

1.2.4 Boundary Layer Control

Unlike wind tunnel testing of aircraft, boundary layer removal is important for ground vehicle testing due to the proximity of the vehicle underfloor and the floor of the wind tunnel. It is especially so for racing cars due to their very low ground clearance. Figure 1.2.4 shows common methods of boundary layer control.
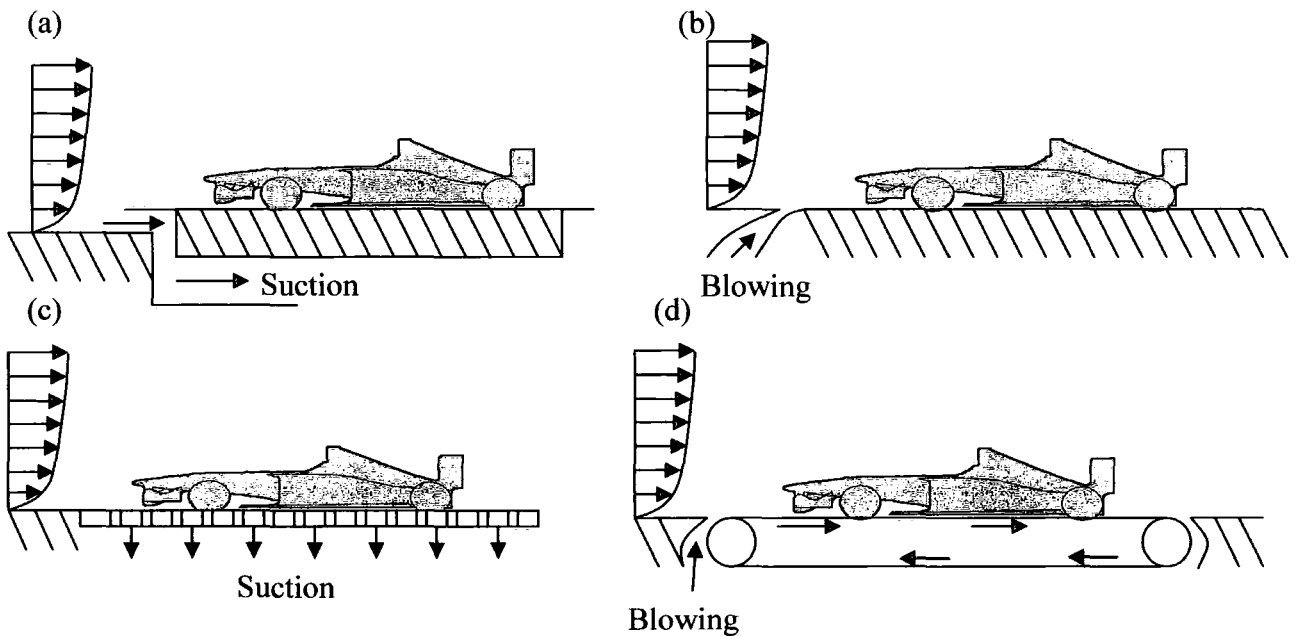


Figure 1.2.4, Boundary Layer Control Methods

In figure 1.2.4 (a) the boundary layer is removed by suction before the start of the test section. In figure 1.2.4 (b) the flow is re-energised by injecting air into the boundary layer before the start of the test section. Figure 1.2.4 (c) shows the slotted floor boundary layer

control method. Low pressure below the floor of the wind tunnel constantly removes the low speed air of the boundary layer. In figure 1.2.4 (d) the flow is re-energised before the test section at which point the moving ground plane, which moves at the same speed as the air, eliminates the boundary layer.

The boundary layer on an empty test section has a deficit of both mass and momentum fluxes. The mass deficit is characterised by the displacement thickness $\delta_1$, which is the amount by which the boundary displaces flow field above it away from the floor, as shown in figure 1.2.5 (Hucho 1998). The thickness of the boundary layer increases as it progresses downstream. The presence of the boundary layer caused by the stationary floor is a considerable deviation from on road conditions where the vehicle is moving over the road and through the air at the same speed as the air, especially in vehicles with low ground clearances.
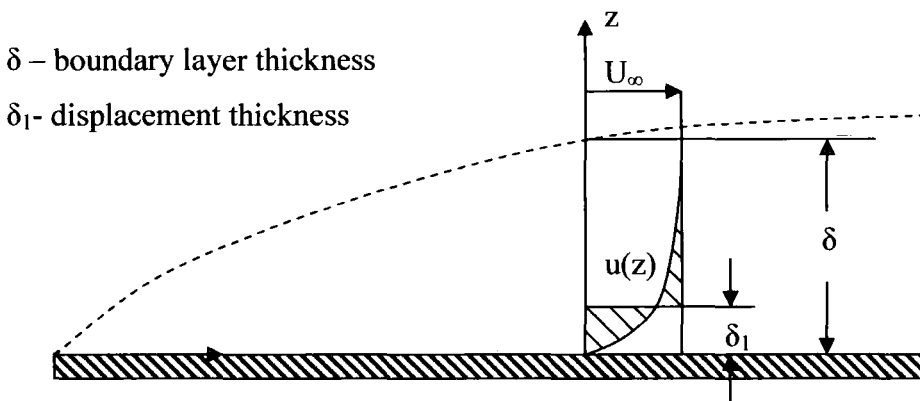


Figure 1.2.5, Boundary Layer Development

Separation of the boundary layer may occur when it is subjected to an adverse pressure gradient such as occurs in front of the wheels of a model or where the underfloor of a model is shaped like a diffuser. Flow separation below a diffuser can render the diffuser ineffective during wind tunnel testing, severely affecting the resulting data. For these reasons, wind tunnel testing employing a moving ground plane is important for racing car models with low ground clearance in order to facilitate accurate representation of on-track conditions.

1.2.5 Support Strut Interference Quantification

Tests were performed by Knowles et al (2002) on an isolated racing car wheel in contact with a moving ground plane to measure the effect of a supporting strut. This was done by first measuring the forces acting on the wheel and suspension alone, then introducing a supporting strut and measuring the resulting forces. The strut was found to decrease the lift of the wheel by 16%, increase the drag by 2%, and increase the mass flow through the hub by 83%. The strut was also found to cause the point of flow separation to advance by 4 degrees compared to the wheel on its own. Significantly the changed flow over the wheel will also affect the flow over other aerodynamic elements downstream, further affecting the results. Page et al (2002) conducted a CFD study at the Swift wind tunnel using a NASCAR model to investigate the effect on the flow field of supporting struts. An overhead strut was found to reduce the pressure coefficient by 0.1 one chord length in front of the leading edge and after the trailing edge, and continued to disrupt the flow downstream of the strut.

More in-depth work has been done into the effects of support strut interference at Durham University School of Engineering using the 2m Durham Wind Tunnel, which is a ¾ open jet tunnel as described by Sims-Williams and Dominy (2002). Hetherington and Sims-Williams (2006) used four different models to investigate the effect of supporting struts on the airflow;

- 25% scale notchback saloon. The model has stationary wheels, a semi-detailed under floor, simplified engine cooling flow and limited exterior trim. The area blockage of the model in the tunnel jet was 6%, as shown in figure 1.2.6 (a).
- 40% scale hatchback. The model has stationary wheels and limited exterior trim. The area blockage of the model in the tunnel jet was 15%, as shown in figure 1.2.6 (b).
- 35% scale Le Mans prototype closed-wheel race car. The model has stationary wheels, a detailed under floor with front splitter and rear diffuser, engine and brake cooling ducts, and full exterior trim. The area blockage of the model in the tunnel test was 5%, as shown in figure 1.2.6 (c).

- 25% scale generic open-wheel race car. The model has stationary wheels, a detailed under floor, simplified engine cooling and suspension and full exterior trim. The area blockage of the model in the tunnel jet was 5%, as shown in figure 1.2.6 (d).



Figure 1.2.6. Support strut interference test models.

All the models were tested with a fixed ground plane in the 2m Durham wind tunnel and connected to a six component under floor force balance at each of the model's wheels. The models were tested at a wind speed of $29ms^{-1}$ both with and without mock struts and stings. Four mock wheel stings and one mock supporting overhead strut were used to measure the interference on the airflow. Wake traverses were performed on the models and flow visualisation was utilised to show local flow effects.

The mock overhead strut used was a NACA $66_4$-021, which was selected for its low drag profile in order to minimise the effect of strut wake on the rear wing of the models under test, and possessed a bluntness factor (Fleming et al 1991) of 0.045. The strut had a chord of 100mm which if steel would provide it with sufficient stiffness to support a 40% model. The strut was mounted to a faired support that housed actuators for controlling model pitch and ride height. The mock wheel stings that were used were existing wheel stings that had had their wheel mounting points removed. The wheel stings had a circular mounting boss and an aerofoil shape over the rest of their length. The wheel stings were mounted onto the floor of the wind tunnel outside the tunnel jet.

1.2.6, Support Strut Interference Quantification Results.

Figure 1.2.7 shows the separate and combined effects of an overhead strut and wheel stings on the drag coefficient. The results show that the struts caused different effects on the drag depending on the model being tested and that the effects were not cumulative.
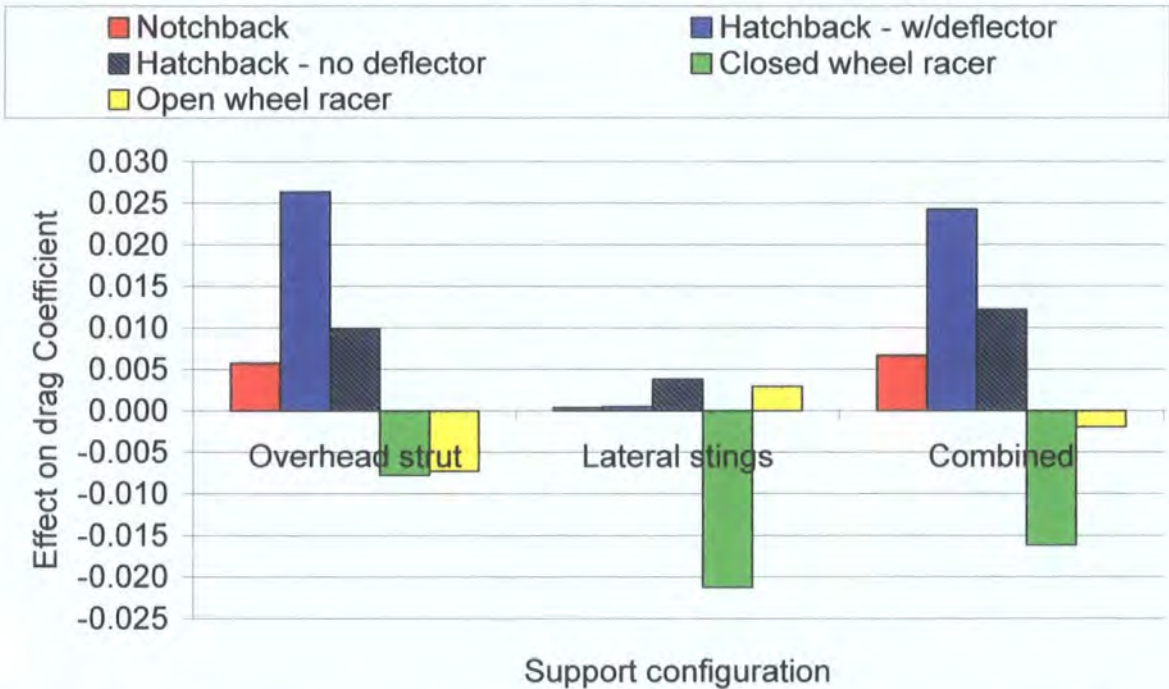


Figure 1.2.7, Effects of Support Interference on Drag Coefficient (Hetherington and Sims-Williams 2006)

Figure 1.2.8 show the effects of supporting overhead strut and sting on the lift coefficient of the models. As with the changes shown for the drag coefficient the struts had different effects depending on which model they were used on and again the effects were not summative. It was also found for the closed wheel race car that the introduction of an overhead strut affected the flow underneath the car. It was thought that this was due the wake of the supporting strut impinging on the rear wing and reducing its effectiveness and so decreasing the pumping effect of the wing that sucks air from the underneath of the vehicle.

These results show that the effects of supporting struts and stings considerably disrupt the airflow around vehicles under test and that the effects differ considerably depending on the model and that the effects of the struts and stings are not cumulative.
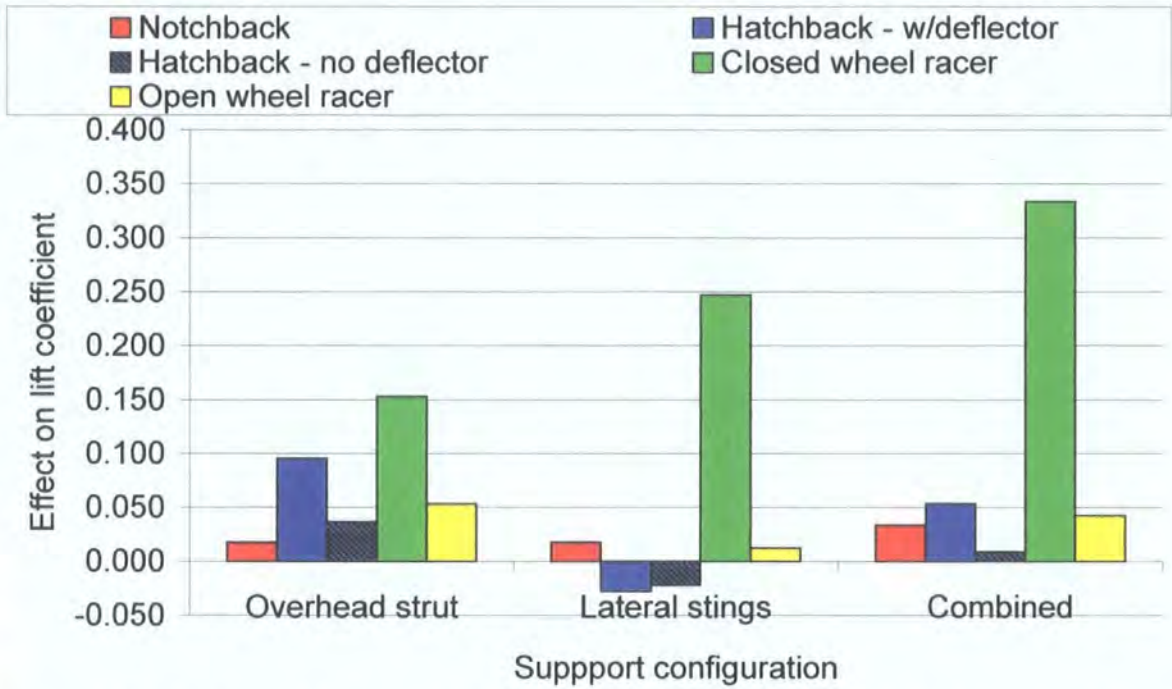


Figure 1.2.8, Effects of Support Interference on Lift Coefficient (Hetherington and Sims-Williams 2006)

1.3 Magnetic Suspension and Balance System

A technique for supporting wind tunnel models by non-intrusive means would provide a more realistic testing environment and would eliminate the problems caused by support strut interference. This can be achieved through the use of magnetic levitation. Holmes (1937) developed a non-intrusive method of supporting a spinning rotor using magnetic fields, this idea was further developed by Beams (1954) who created a frictionless bearing and with it achieved rotational speeds of 50,000,000 rpm. Tournier and Laurenceau (1957) were the first to build a magnetic suspension and balance system (MSBS) wind tunnel to support a stationary model at ONERA, the French National Office of Aerospace Study and Research.

1.3.1, MIT/NASA/ODU MSBS

NASA used an active non-intrusive electromagnetic support system, called the Magnetic Suspension and Balance System (MSBS) (NASA 1991), to test the space shuttle at mach 0.6 in a 158mm diameter wind tunnel, as shown in figure 1.3.1. The system was originally developed at the Massachusetts Institute of Technology (Stephens 1969). The system was moved to NASA Langley Research Centre in 1984, before being moved to Old Dominion University in 1994.



Figure 1.3.1, NASA's MSBS 158mm Wind Tunnel (NASA 1991) showing reflection of test vehicle in mirrored walls.

The NASA 158mm Magnetic Suspension and Balance System supported the model under test using a combination of Helmholtz coils, saddle coils, and iron core magnet assemblies (Yang 1997). The Helmholtz coils provided an axial magnetisation field, compensating for the drag force acting on the model; multiple Helmholtz coils were positioned along the test section to provide a uniform magnetic field over the test section. The saddle coils provided the transverse magnetic field components; multiple coils were used at right angles to each

other and spaced along the test section to allow for pitch and yaw control of the model. Lift and side force was provided by iron cored magnets; again the magnets were spaced along the test section to produce an even magnetic field to act on the model. All of the coils were required to be water cooled in order to dissipate the considerable heat produced by the large currents. In order to avoid electrolysis and silting the water had to be demineralised and de-aerated to facilitate prolonged operation. The large coils of the electromagnets are visible through the perspex walls of the wind tunnel shown in figure 1.3.1.

The need for the Magnetic Suspension and Balance System to have multiple large electromagnets around the test section meant that the space available was restricted preventing the use of an optical positioning system. An electromagnetic position sensor was used instead which utilised the principle of a differential transformer with the model acting as the core to resolve the components of the models position and orientation. A pair of Helmholtz coils acted as the excitation winding while seven pairs of coils were used as the pickup coils. The axial pickup coils were Helmholtz coils while the models horizontal and vertical position and pitch and yaw readings were measured using six pairs of saddle coils. The excitation coils produced a uniform magnetic field throughout the centre of the test section; when a ferromagnetic model was aligned with the axis of the excitation coils it became magnetized at the same frequency as the excitation field. The position of the model could then be ascertained by measuring the outputs of the pickup coils.

NASA also used a larger MSBS tunnel; The NASA Langley Research Centre (LaRC) 13 inch Magnetic Suspension and Balance System was developed from a system originally constructed at the Arnold Engineering Development Centre in the 1960's. (Boyden et al, 1985). Various other MSBS tunnels have been developed including systems at the University of Southampton and Oxford University (Tuttle et al 1991)

However there were many drawbacks with the Magnetic Suspension and Balance System, the most significant being the massive power supplies required to power the electromagnets. The 158mm MSBS was recently recommissioned with considerably improved and more efficient electromagnets yet the system still drew 400kW (Britcher 1997). Such high power consumption is very expensive for prolonged operation and scaling

the system up would exponentially increase the power requirements because of the inverse cube law of forces between magnetic dipoles. Despite the lack of any physical supports the results from the MIT/NASA/ODU tunnel were affected by the proximity of the tunnel walls to the test subject; the diameter of the tunnel was only marginally larger than that of the model which had a wingspan of 127mm.

1.3.2, National Aerospace Laboratory of Japan MSBS

More recently the National Aerospace Laboratory of Japan has built several MSBS wind tunnels, ranging in size from the smallest with a test section of 100mm x 100mm to the largest with a 600mm x 600mm test section which is shown in figure 1.3.2 (Sawada 2001). The arrangement of electromagnets required to support the model is shown in Figure 1.3.3. Coils 0 and 9 produced an axial magnetisation field, compensating for the drag force acting on the model in the x axis. Coils 1, 3, 5, and 7 provided lift and also controlled the pitch of the model in the z axis. Coils 2, 4, 6, and 8, provided side force in the y axis and also controlled the roll and yaw of the model. An optical positioning system monitored the position of the model in the test section providing feedback for the active control system to keep the model centred in the wind tunnel. This system is currently the largest active Magnetic Suspension and Balance System in operation, and is considerably larger than the system used by NASA. However it is still limited in the maximum weight that it can support; only models weighing less than 7kg and producing less than 16N of drag force can be used. Despite the low weight and drag of the models the MSBS tunnel still requires 40kW to operate.

The National Aerospace Laboratory of Japan is currently working to develop a system to allow heavier models to be supported. By replacing the magnets in the model with low temperature superconducting electromagnets, capable of producing stronger magnetic fields, the load bearing capacity of the system is increased. However this approach is problematical as superconducting electromagnets are very expensive and difficult to manufacture and also limit the time the tunnel can be operated to just a few minutes before the superconducting coil either saturates or warms up. Low temperature superconductors also require expensive liquid helium to operate.
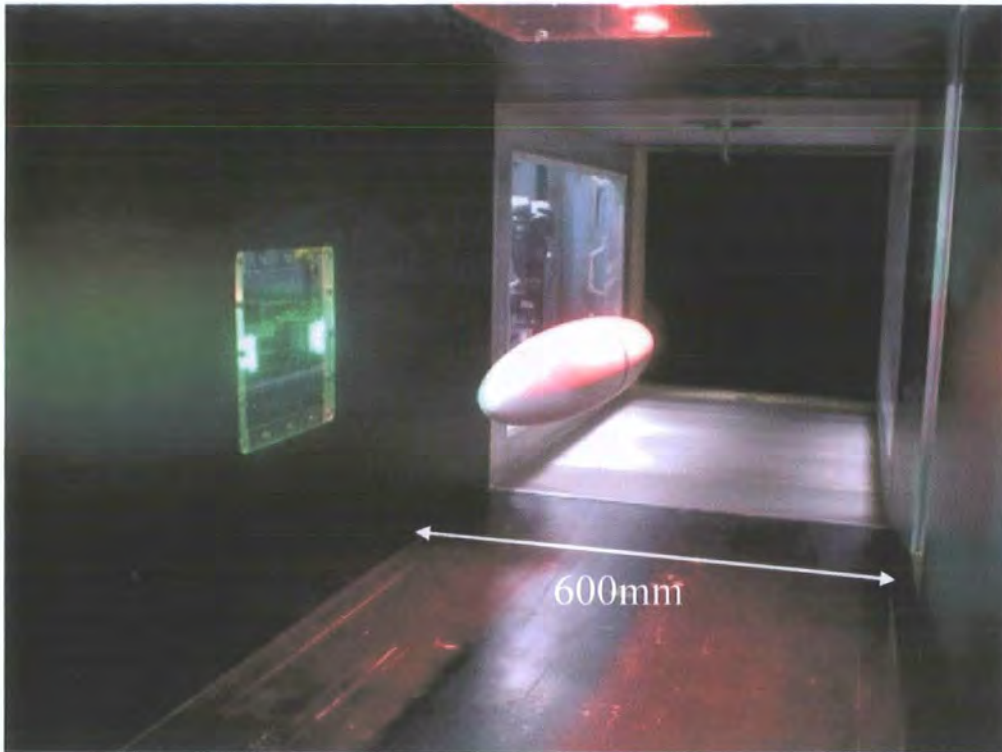
Figure 1.3.2, MSBS at the National Aerospace Laboratory of Japan (Sawada 2001)
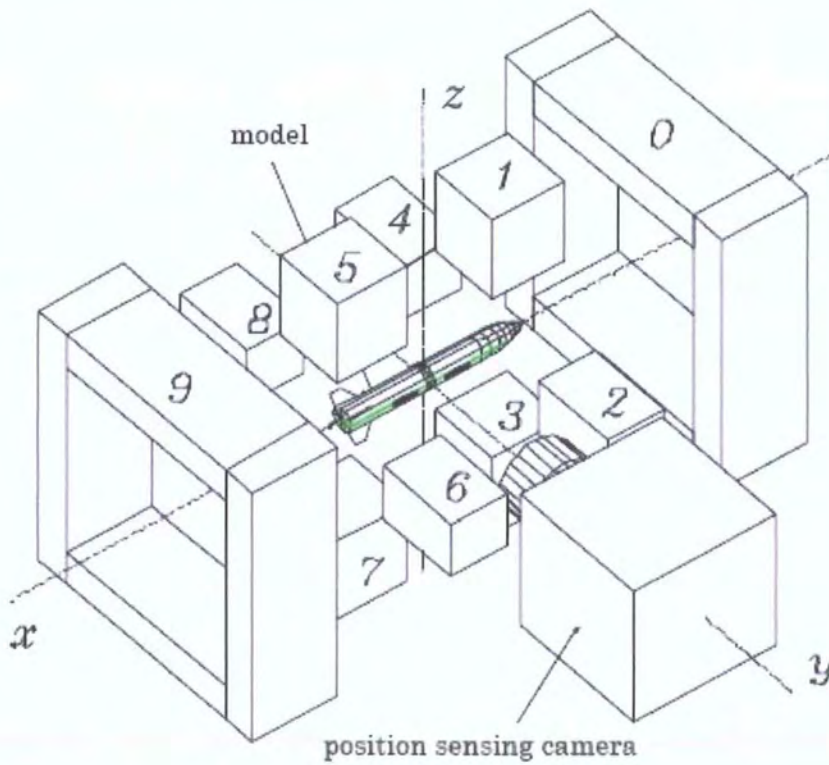


Figure 1.3.3, Electromagnet arrangement for the 600mm NAL MSBS Wind Tunnel (Sawada 2001)

1.3.3, Limitations of the Magnetic Suspension and Balance System.

While all the incarnations of the Magnetic Suspension and Balance Systems provide a non-intrusive method of supporting wind tunnel models, even the largest is limited to operation in a wind tunnel with dimensions of 600mm x 600mm and can only support light weight and low drag models. None of the systems would be suitable for ground vehicle wind tunnel testing, unless the testing was performed at an extremely small scale. When testing ground vehicle models in a wind tunnel, a suitably low blockage ratio must be achieved in order to approximate real conditions. On the road, a car is subject to open air on three sides, in order to replicate these conditions in the wind tunnel, the walls and ceiling of the tunnel must be a significant distance away from the model. Adapting an MSBS system to test a ground vehicle model would require the introduction of a floor in the middle of the tunnel, effectively halving the size of the tunnel at a stroke. The magnetic interaction between two dipoles decreases with the inverse cube of the distance between them, so increasing the size of the tunnel causes the power requirements of the tunnel to increase exponentially. An electromagnet capable of producing a field strong enough to act on the model from a distance of at least a metre would either be prohibitively large or would have to be an expensive and complex low temperature superconducting coil. The output of such a coil would be likely to interfere with the other electrical equipment in the tunnel, even if the cost and power requirements for such a system were not a consideration.

The development of a magnetic levitation system that would be capable of supporting a model from one side only would allow the solution of the problem of magnetic fields acting over large distances. A system that could support a ground vehicle wind tunnel model solely from below the floor would allow the walls and ceiling of the tunnel to be as far away as desired facilitating testing in an open jet wind tunnel to provide a low blockage ratio.

1.4 Preliminary work

A non-intrusive method of supporting ground vehicle wind tunnel models was developed by the author for an M.Eng thesis at the School of Engineering at Durham University

(Muscroft 2002). During this project the superconducting pod was designed and built that used a combination of high temperature superconductors (HTS), permanent magnets, and electromagnets. The pod that was built proved to be stationary and stable when tested in a wind tunnel at $20ms^{-1}$, achieving stable levitation without the need for active control. The research detailed in this thesis is a continuation of that work, investigating the feasibility of a non-intrusive method of support for use in the aerodynamic testing of 40% scale Formula 1 cars.

1.5 Overview of research

This thesis details the design and development of a non-intrusive support system for ground vehicle wind tunnel models. The aim of this research was to investigate the feasibility of such a system built to support a 40% Formula 1 car under test in a wind tunnel with a moving ground plane.

Chapter 2 discusses the key mechanism underpinning this research; flux trapping in type II high temperature superconductors. This mechanism allows the stable levitation of a permanent magnet over a superconductor and, crucially, is also intrinsically damped. This allows magnetic reinforcement of the superconducting levitation without rendering the system unstable.

Chapter 3 covers the design and development of the superconducting "pod" system that is the vital constituent of the larger system. Electromagnetic finite element analysis was undertaken to model a simplified geometry of the superconductor, permanent magnet, and electromagnet system. This work was done to optimise the layout of the system to achieve the maximum restoring force acting on a levitating magnet from an electromagnet. The larger three pod superconducting levitation system is also discussed.

Chapter 4 details the conception, development, and testing of the magnetic "rail" configuration designed to reduce the instability of permanent magnet only levitation. Multiple rare-earth permanent magnets of varying shapes and sizes were tested to ascertain

which was the most suitable for the magnetic reinforcement of the superconducting levitation.

Chapter 5 covers the development and testing of both the medium and large scale hybrid superconducting magnetic levitation systems.

Chapter 6 draws together the results of the work and discusses the experimental techniques.

Chapter 7 covers the conclusions that were drawn from this work as to the feasibility of the system for use in testing 40% models in wind tunnels with a moving ground plane. Recommendations for future work are also covered.

## 2. Theory

### 2.1 Superconductivity

Superconductivity was first discovered when Heike Kamerlingh Onnes developed refrigeration to a sufficient degree to solidify mercury. Using the Leyden Cascade, a series of refrigeration loops that each used a refrigerant with a lower boiling point than the previous loop, he achieved temperatures below the boiling point of Helium, 4.2K. When a current was passed through the solid form of mercury at 4.15K it was found to have an extremely low value of resistance. The value of the resistance was measured to be less than $10^{-6}$ $\Omega$, which was the limit to the sensitivity of the equipment that was available at the time (Kamerlingh Onnes 1913). Advances in the sensitivity of measurement equipment have decreased this upper limit. Kedves et al (1987) and Yeh et al (1987) studied the decay rates of persistent currents in an YBaCuO superconducting ring and found values of resistance of less than $2 \times 10^{-16}$ $\Omega$, and $1 \times 10^{-16}$ $\Omega$ respectively.
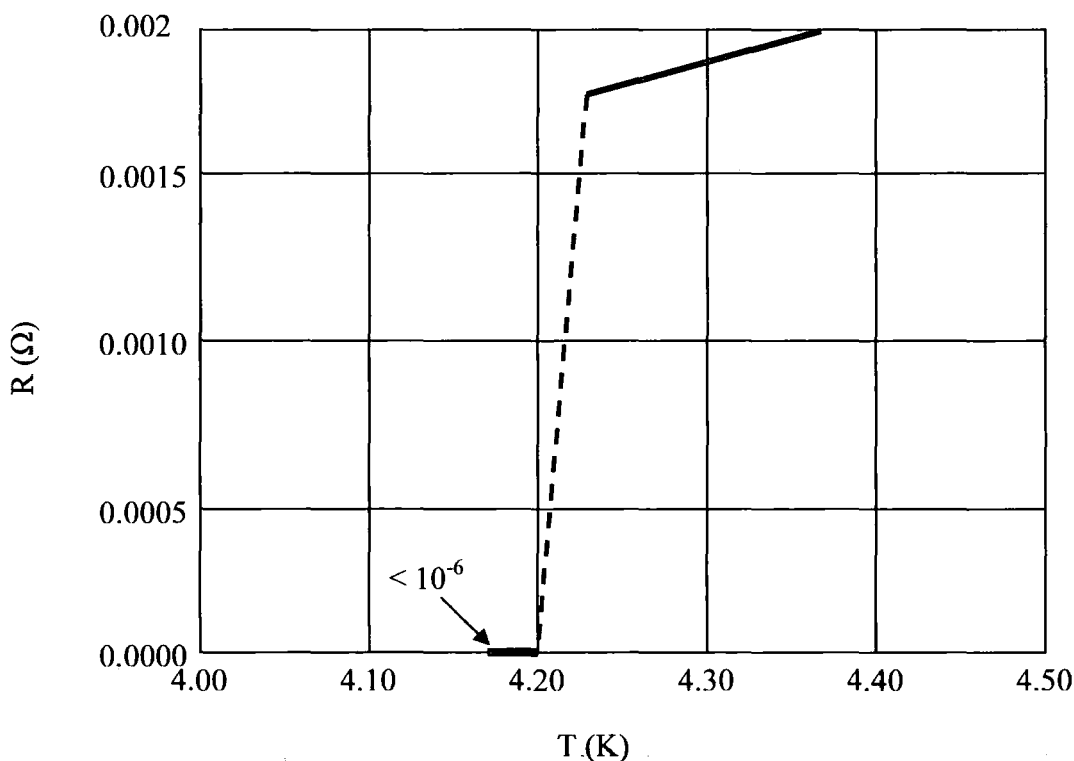


Figure 2.1.1, Graph showing the resistance of mercury at liquid helium temperatures (Kamerlingh Onnes 1913).

## 2.1.1, Zero Resistance in a Superconducting Wire

Sarangi et al (2005) showed that the value of resistance in a Niobium Titanium (NbTi) superconducting wire is zero. To show this they used a 300cm coil of NbTi wire, designated coil B, in parallel with an 8cm loop of NbTi wire, designated coil A. A 6 Amp current was passed through the wires, and the magnetic field in the coil measured using a Hall probe with and without the 8cm loop connected. The magnetic field from the large coil, $H_{n_1}$, without the short loop connected was found to be 174 Gauss. With the short loop connected the magnetic field from the coil, $H_{n_2}$, was found to be 4.5 Gauss. These results corresponded to the equation;

$$H_{n_2} = H_{n_1} / (\frac{L_B}{L_A} + 1) \qquad (2.1)$$

Where $L_B/L_A$ is the ratio of lengths of the two NbTi coils. These measured values fitted with the expected result as the resistance in the large coil is $L_B/L_A$ times more than the resistance in the short coil.

The NbTi coils were then cooled to liquid helium temperatures, below the critical temperature of NbTi (9.3K), and the magnetic fields in the coils were measured again using the Hall probe. If the superconducting wire possessed even a small resistivity, $\varepsilon$, of the order $10^{-20}$ $\Omega cm^{-1}$, then the resistance of the short loop, $r_{s_A}$, would be equal to $\varepsilon$ $L_A$ multiplied by the area of the cross section of the wire. The resistance of the large coil, $r_{s_B}$, would be equal to $\varepsilon$ $L_B$ multiplied by the area of the cross section of the wire, so that $r_{s_B} = k\, r_{s_A}$. As a result $I_{s_B} = I_{s_A}/k$, and the magnetic field from the large coil B, $H_{s_2}$, would be equal to $H_{n_2}$.

However if the resistance of the superconducting wire is zero, then both coils have equal resistances and would therefore carry equal currents, I/2. As a result the magnetic field generated by the large loop, coil B, would be $H_{n_1}/2$. The magnetic field in coil B was measured to be 87 Gauss; half of the original field of 174 Gauss, showing that the resistance of the wire in the superconducting state is effectively zero (Sarangi et al, 2005).

## 2.1.2 Elements Displaying Superconductivity

As well as mercury many elements were also found to have superconducting properties at liquid helium temperatures, as shown in table 2.1.1. It was found that some elements that do not display superconductivity at low temperatures alone can be induced into displaying superconductivity through the application of high pressure (Buzea and Robbie 2005). However, all the elemental superconductors that were discovered were type I superconductors. Type I superconductors possess a low critical field strength, as a result of which superconductivity breaks down when only a small current is passed through them, generating a magnetic field, rendering them to be of little use for current carrying applications. For this reason and because of the difficulty and high cost involved in producing liquid helium the applications of superconductivity were not further explored until much later in the twentieth century.

**PERIODIC TABLE OF SUPERCONDUCTING ELEMENTS**

Legend:
- Atomic number, Symbol, Critical temperature of bulk at normal pressure
- Example: 4 Be, 0.026 K, 9.95 K film
- Critical temperature under certain conditions; Condition type (e.g. pressure value, film form)
- superconducting element only under certain conditions (pressure or film form)
- superconducting element at normal pressure in bulk form
- alkali metals, alkaline earth metals, transition metals, metals, semi-metals, non-metals

| Z | Symbol | $T_c$ (normal, bulk) | $T_c$ (condition) | Condition |
|---|--------|---------------------|-------------------|-----------|
| 3 | Li | | 20 K | 50 GPa |
| 4 | Be | 0.026 K | 9.95 K | film |
| 5 | B | | 11.2 K | 250 GPa |
| 6 | C | | 15 K | nanotube |
| 8 | O | | 0.6 K | 120 GPa |
| 13 | Al | 1.18 K | 3.6 K | film |
| 14 | Si | | 8.5 K | 12 GPa |
| 15 | P | | 18 K | 30 GPa |
| 16 | S | | 17 K | 160 GPa |
| 20 | Ca | | 15 K | 150 GPa |
| 21 | Sc | 0.5 K | 0.34 K | 21 GPa |
| 23 | V | 5.4 K | 17.2 K | 120 GPa |
| 24 | Cr | | 3 K | film |
| 26 | Fe | | 2 K | 21 GPa |
| 30 | Zn | 0.85 K | 1.6 K | film |
| 31 | Ga | 1.08 K | 8.6 K | film |
| 32 | Ge | | 5.4 K | 11.5 GPa |
| 33 | As | | 2.7 K | 24 GPa |
| 34 | Se | | 7 K | 13 GPa |
| 35 | Br | | 1.4 K | 150 GPa |
| 38 | Sr | | 4 K | 50 GPa |
| 39 | Y | | 2.8 K | 15 GPa |
| 40 | Zr | 0.6 K | 11 K | 30 GPa |
| 41 | Nb | 9.25 K | 9.7 K | 4.5 GPa |
| 42 | Mo | 0.92 K | | |
| 43 | Tc | 7.2 K | | |
| 44 | Ru | 0.5 K | | |
| 45 | Rh | 35 μK | | |
| 46 | Pd | | 3.2 K | irradiated |
| 48 | Cd | 0.52 K | | |
| 49 | In | 3.4 K | | film |
| 50 | Sn | 3.7 K | 4.2 K / 4.7 K | film |
| 51 | Sb | | 3.6 K | 8.5 GPa |
| 52 | Te | | 7.4 K | 35 GPa |
| 53 | I | | 1.2 K | 25 GPa |
| 55 | Cs | | 1.66 K | 8 GPa |
| 56 | Ba | | 5 K | 20 GPa |
| 57 | La | 6 K | 12.8 K | 20 GPa |
| 72 | Hf | 0.38 K | | |
| 73 | Ta | 4.4 K | 4.5 K | 40 GPa |
| 74 | W | 0.01 K | 5.5 K | film |
| 75 | Re | 1.7 K | | |
| 76 | Os | 0.7 K | | |
| 77 | Ir | 0.1 K | | |
| 80 | Hg | 4.15 K | | |
| 81 | Tl | 2.4 K | | |
| 82 | Pb | 7.2 K | | |
| 83 | Bi | | 8.7 K | 9 GPa |
| 58 | Ce | | 1.75 K | 5 GPa |
| 71 | Lu | 0.1 K | 1.2 K | 18 GPa |
| 90 | Th | 1.4 K | | |
| 91 | Pa | 1.4 K | | |
| 92 | U | 1.3 K | 2.2 K | 1 GPa |
| 95 | Am | 1 K | | |

Table 2.1.1, Periodic Table of Superconducting Elements, (Buzea and Robbie 2005)

## 2.2 High Temperature Superconductors.

A major breakthrough in the field of superconductivity came with the discovery of the so-called "High Temperature" or type II superconductors, which exhibited superconductivity at much higher temperatures than the elemental low temperature superconductors. Prior to this discovery extensive research had been undertaken to find superconductors that possessed higher critical temperatures, yet the highest achieved was with a Niobium-Germanium metallic alloy which achieved transition at a critical temperature of 23.2K (Testardi 1974).

The first high temperature superconductor to be discovered was a Lanthanum Barium Copper Oxide compound, (LaBaCuO) which demonstrated superconductivity at 35K (Bednorz and Muller 1986). It was found that replacing the barium with strontium to create LaSrCuO produced a critical temperature of 48.6K (Wu et al 1987). This provided a significant increase in critical temperature from the type I superconductors, but this temperature could still only be reached through cooling with liquid helium.

## 2.2.1 Superconductivity above 77K.

LaBaCuO has a perovskite structure (Kittel 1996) and it was found that by applying pressure to the compound that its critical temperature could be raised to 57K. It was found that this effect of increased critical temperature through pressurisation could be replicated by substituting the large Lanthanum ion with the smaller Yttrium ion. This change applied chemical pressure to the compound, instead of physical pressure, and produced YBCO (Hor et al 1987). YBCO, a Yttrium Barium Copper Oxide alloy, is a commonly used high temperature superconductor, and possesses a critical temperature of 92.5K.

Crucially this was the first superconductor to have a transition temperature above the boiling point of liquid nitrogen (77K). Nitrogen is readily available in the atmosphere and inexpensive to liquefy, unlike helium which has to be mined due to its scarcity in the atmosphere. The discovery of YBCO sparked new interest in superconductors with a view to developing a room temperature superconductor. Currently the record for the highest

temperature at which superconductivity has occurred was measured in a $HgBa_2Ca_2Cu_3O_{8+x}$ compound, which has a critical temperature of 133K (Reissner 1997). Applying a pressure of 26 GPa to the compound increased the transition to 156K (Tristan Jover et al 1994). However due of the increased difficulty of production, the hazardous nature of the mercury content, and liquid nitrogen remaining the preferred cryogen, YBCO is used for most superconducting levitation applications.

With the discovery of the high temperature superconductors, superconductivity was hailed as the solution to the energy problem, but without a room temperature superconducting material interest has waned. Nevertheless low temperature liquid helium cooled superconducting electromagnets are still used in MRI scanners as they can be formed into long wires to produce superconducting electromagnets capable of creating the very strong magnetic fields required.

2.3 BCS theory

When an electric current is passed through a standard conductor power is dissipated according to equation;

$$P = I^2 R \qquad (2.2)\,(\text{Ohm } 1827)$$

Where P is the power dissipated, I is the current passed through the conductor, and R is the resistance of the conductor. If the current passing through a conductor of a given resistance is doubled then the resulting dissipated power will quadruple. The resistance of a conductor increases as the length of the conductor increases, and as the cross sectional area of the conductor decreases. Consequently this is a problem in long distance power transmission where large distances must be covered and weight and cost are paramount. Electrical resistance is caused by the collisions between the free current carrying electrons and the imperfections in the lattice structure of the conductor. These collisions cause the current carrying electrons to pass on their energy to the lattice structure of the conductors, causing the electrons to decelerate as they lose energy. These collisions cause the temperature of the conductor to increase as the energy of the lattice increases, this causes the lattice structure

to vibrate more rapidly which in turn increases the number of collisions between the electrons and the lattice, increasing the resistance of the conductor.

Superconductivity is explained by the BCS theory, named after Bardeen, Cooper, and Schrieffer, (Bardeen et al 1957). BCS theory centres on Cooper pairs, which are electrons that pair up in the superconducting matrix and move together through the material. Normally, the electrons would repel each other, but when the superconductor is cooled below its transition temperature, they overcome their repulsion due to a combination of two events. The first is the "screening" effect resulting from the motion of other electrons that reduces the repulsion between the Cooper pair. The second more dominant effect is the creation of a charge distortion called a "phonon", as shown in figure 2.3.1.
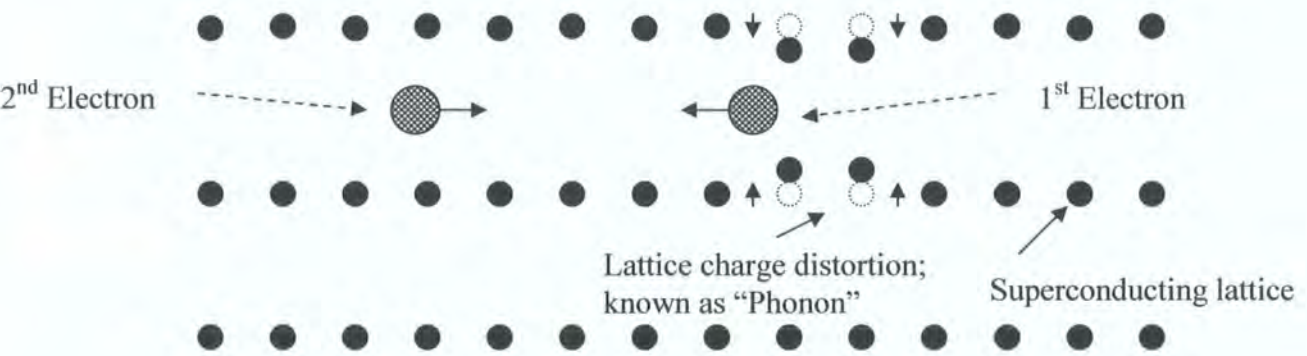


Figure 2.3.1, Electron/Phonon Interaction in the superconducting lattice.

The charge distortion occurs when the first electron of the Cooper pair shifts the position of the ions in the lattice structure of the superconductor and also other electrons as it passes them causing a ripple effect that creates an instantaneous pocket of positive charge. The second electron is then attracted to this concentration of positive charge. Because the electrons are moving at relativistic speeds, far faster than the phonons, by the time the second electron arrives at the site of positive charge, the first electron is far enough ahead that they do not repel each other. The paired electrons can interact by exchanging phonons and have their momentum and spin vectors antialigned. The attraction between the electrons is very weak yet the superconducting phase transition occurs because the

electrons close to the Fermi energy have a net attraction. At a temperature just below the transition temperature in a superconducting material a small energy band develops where there no states. The energy gap is caused by the binding energy due to the formation of Cooper pairs. The formation of Cooper pairs is hindered by the thermal excitation of electrons; as the temperature is lowered the number of electrons that can cross the energy gap is significantly reduced resulting in a greater number of Cooper pairs forming causing the energy gap to become larger. Therefore the collisions of the electrons with imperfections in the lattice in a superconductor do not generate enough energy to cross the energy gap and therefore the electrons remain paired and there is no resistance to the flow of current (Rohlf 1994).

## 2.4 The Meissner Effect

When a superconducting material is cooled below its critical temperature and becomes superconducting, it will exhibit the Meissner effect; this is when the material will expel any magnetic fields impinging on its volume (Meissner and Ochsenfeld 1933) as shown in figure 2.4.1. This state holds as long as the magnetic field does not exceed the materials critical field strength, which when exceeded causes superconductivity to completely break down. When a changing magnetic field acts on a conducting material, it induces eddy currents to form which oppose the movement of the magnetic field, these eddy currents quickly die away because of the resistance of the conductor. However because a superconductor has no resistance to electrical flow the eddy currents do not die away. The currents form the exact opposite magnetic field to the one applied, repelling the external field.
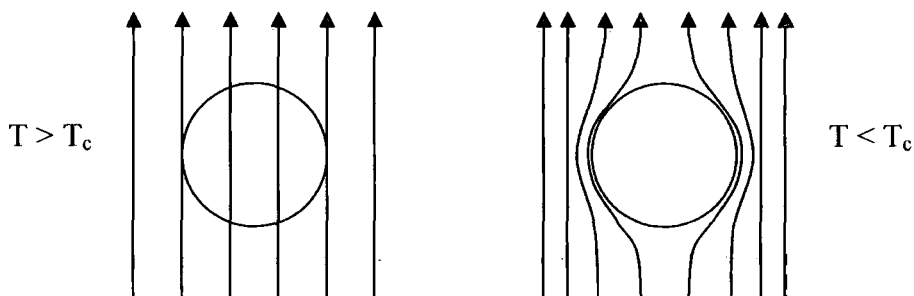
Figure 2.4.1, The Meissner Effect, in a conventional superconductor.

When the magnetic field acting on a superconductor is less than the materials critical magnetic field strength, the magnetic field induced in a superconductor is equal and opposite to the external magnetic field. The critical magnetic field for a type I superconductor is very small and superconductivity breaks down when only a small current is passed through it. For this reason there are very few applications for type I superconductors. However, the critical field strength for a type II superconductor can be several hundred times larger than that of a type I superconductor, and thus type II superconductors are used more extensively.

When a magnetic field is introduced to both type I and type II superconductors that have already been cooled below their critical temperatures, both types of superconductors will display the complete Meissner effect, as long as the magnetic field strength is below the critical field strength of the superconducting material. However once the critical field strength has been exceeded the superconductors behave in different ways. Figure 2.4.2 shows how Type I and Type II superconductors behave when an increasing magnetic field is applied.
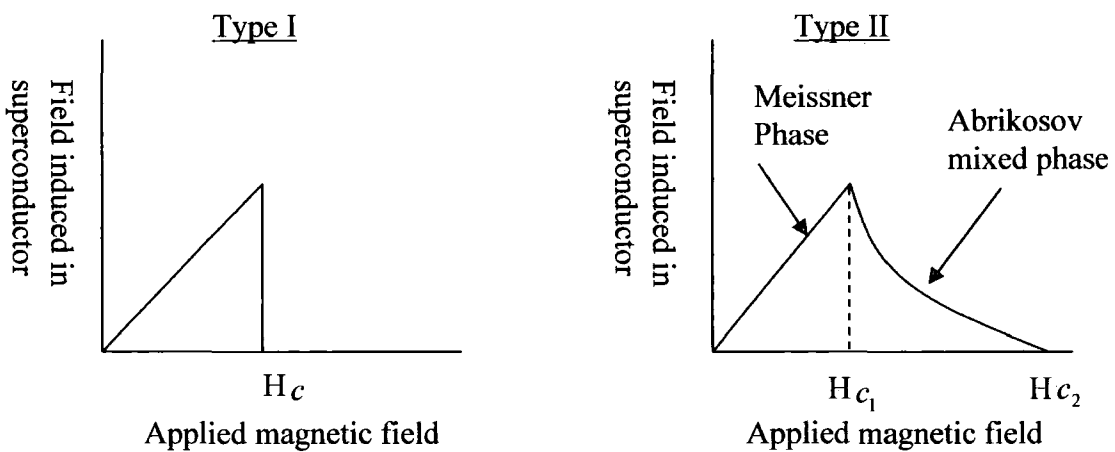
Figure 2.4.2, Effects of magnetic fields on Type I and II superconductors

There is no difference in the process of superconductivity in type I and type II superconductors. Both types have similar thermal properties at the superconductor-normal transition in a zero magnetic field. Type I superconductors exhibit the complete Meissner effect; up to the critical field strength $H_c$, the induced field is equal and opposite to the applied field. When the applied field exceeds $H_c$, the induced field drops to zero and the material ceases to be superconducting (Kittel 1996). There are two other factors that delineate superconductivity; the critical temperature and the critical current density. These three factors form an envelope, as shown in figure 2.4.3, if the limits of the envelope are exceeded in any direction the material ceases to be superconducting.
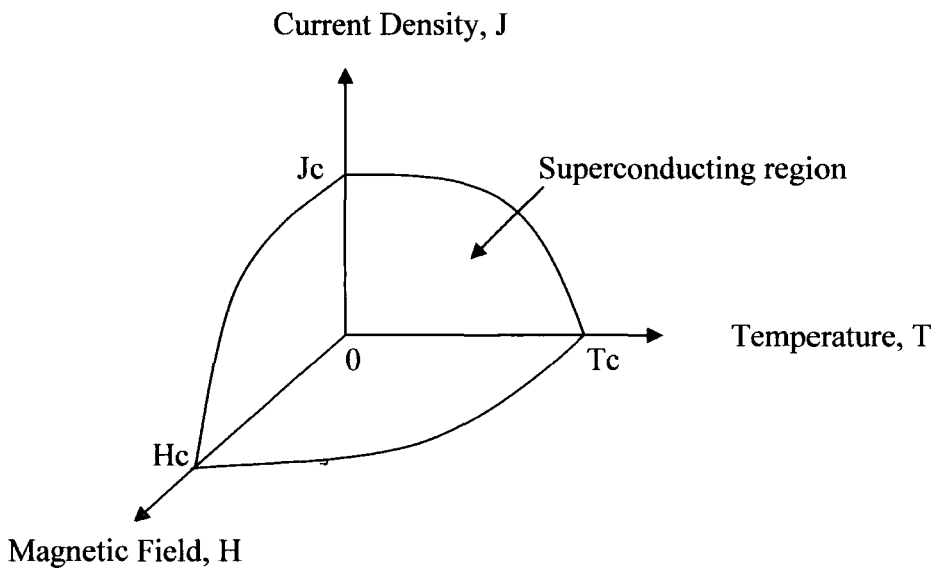
Figure 2.4.3, Critical Surface Phase diagram

Type II superconductors exhibit a partial Meissner effect. Type II superconductors follow the Meissner effect up to the material's first critical magnetic field strength $H_{c_1}$. Once the applied field exceeds this strength, the induced field decreases exponentially as the applied field is increased, until the applied field is equal to the second critical field strength $H_{c_2}$ at which point the induced field is zero. While the applied field is between $H_{c_1}$ and $H_{c_2}$, the material is still partially superconducting; this state is known as the Abrikosov mixed phase. When the field exceeds $H_{c_2}$ the material entirely ceases to be superconducting. Up to the first critical field strength the sample completely excludes the magnetic field. Once

$H_{c1}$ has been reached the sample only partially excludes the magnetic field but remains superconducting. This is known as flux trapping or flux pinning. When the magnetic field strength is between $H_{c1}$ and $H_{c2}$, the superconductor is said to be in the vortex state (Taoufik 2002).

## 2.5, The Vortex State.

A superconductor will completely repel any magnetic field that impinges on its volume, up to the critical field strength for the material. When a magnet is brought close to a superconductor, the Meissner effect occurs, which is also known as the "mirror effect". Currents are induced in the superconductor which produce the exact opposite field to the magnet and the magnet is repelled. Figure 2.5.1 shows the mirror effect.
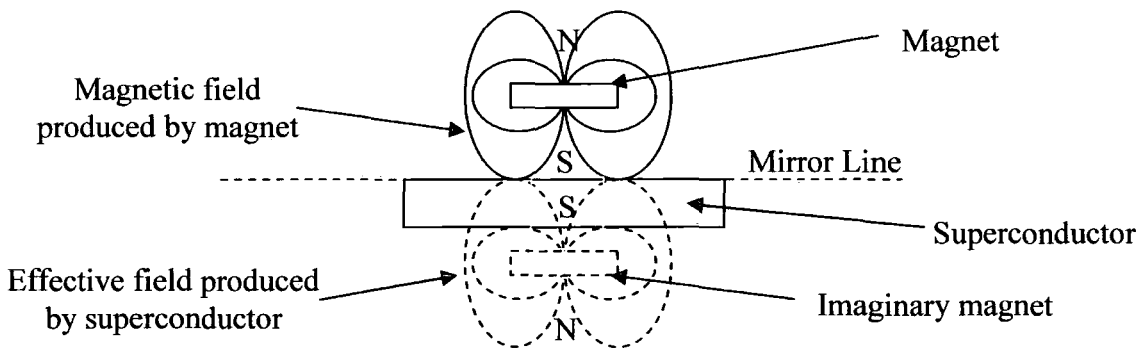


Figure 2.5.1, The Meissner Effect

If the dimensions of the magnet are considerably smaller than the superconductor, it will stably levitate, as the magnetic field generated by the superconductor will instantaneously follow any move the magnet makes because the superconductor has zero resistance to the flow of current. However, if the magnet has similar dimensions to the superconductor, it will not levitate stably because as the magnet moves horizontally it will go beyond the physical limits of the superconductor and will no longer be supported. In order for a magnet to levitate stably over a superconductor of similar size flux trapping must occur. Flux trapping occurs when the superconductor is in the vortex state.

The term 'vortex state' describes the circulation of superconducting currents in vortices throughout the bulk specimen. In the vortex state, when the external magnetic field is greater than the second critical field strength of the material it will penetrate the regions of the superconductor that are no longer superconducting as a result of the external field. The magnetic flux will also partially penetrate the regions that are superconducting; superconductors do not entirely exclude an external magnetic field; the field enters the superconductor up to a penetration depth $\lambda$, 20nm – 40nm, decreasing in strength down to zero at the penetration depth. The magnetic flux of the permanent magnet becomes trapped or pinned within the bulk HTS microstructure in the form of individual flux quanta, each of which is surrounded by a current vortex at sites of imperfection, such as second (211 or $Y_2BaCuO_5$) phase inclusions, in the superconducting matrix, (Feng et al 2001). There are no physical differences between the normal and superconducting regions in the vortex state. Figure 2.5.2 shows a cross section of the penetration of the magnetic field in a type II superconductor in the vortex state, figure 2.5.3 shows the vortices of supercurrent. This is also known as flux trapping. Vortex core size for a YBCO superconductor is ~ 60 Å (6nm) (Sonier 2004) depending on magnetic field strength.
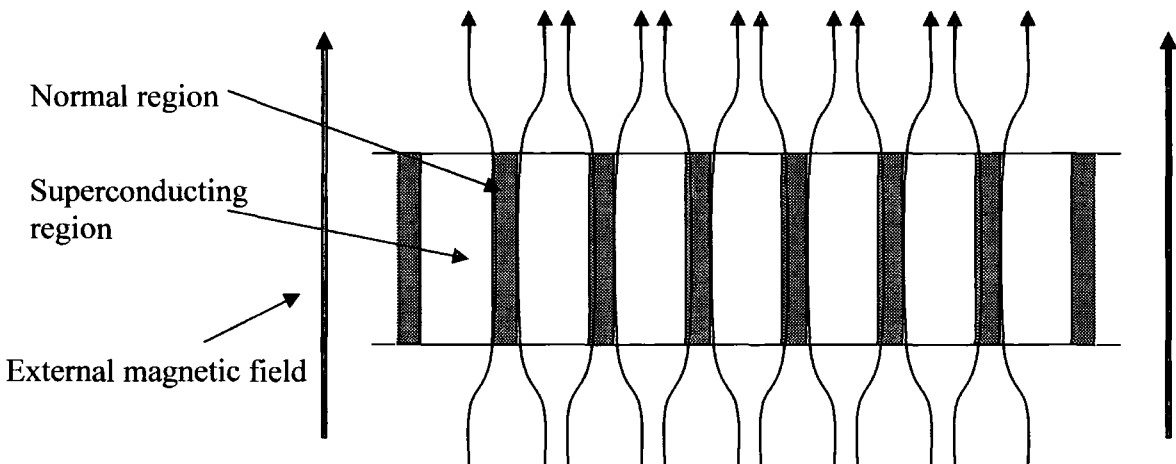


Figure 2.5.2, Magnetic field penetration in a homogeneous bulk structure in the vortex state (Ketterson and Song 1999)
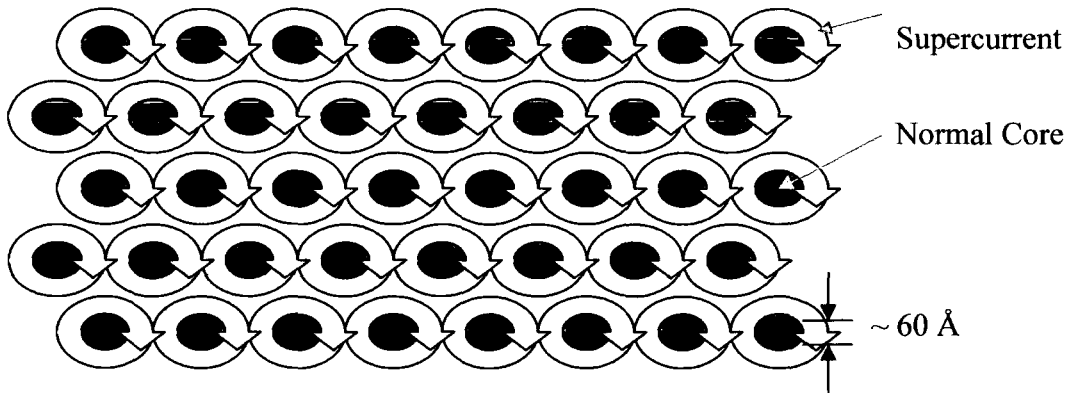
Figure 2.5.3, Vortices formed in a mixed state superconductor

Figure 2.5.2 and figure 2.5.3 show the transition in a superconducting material as it changes from the pure Meissner state to the mixed vortex state. As the external magnetic field acting on the superconducting material exceeds the first critical field strength, the field begins to penetrate through cores of the material no longer in the superconducting state. These cores are surrounded by superconducting current vortices. An increase in temperature or magnetic field towards the limits of superconductivity causes the normal state cores to increase in size and the superconducting currents to decrease until the normal cores overlap and all superconductivity ceases.

The structure of the superconducting material is crucial to the formation and prolongation of the vortices. Movement of the vortices create electrical resistance, imperfections in the crystal lattice, such as inclusions, act to pin the vortices and prevent movement of the magnetic field. The creation of regular artificial imperfections in the crystal lattice either through doping or the creation of microdots in superconducting materials allows the continuation of superconductivity at higher temperatures and higher field strengths. Yang et al (1998) discuss the influence of doping on critical current density in YBCO. The vortex state can also be induced by cooling a type II superconductor below its critical temperature in the presence of a magnetic field that exceeds its first critical field strength but is less than the second critical field strenght. In this case it does not expel all the magnetic field impinging on its volume; instead it traps the magnetic flux and resists any movement of the magnetic field. This is known as field cooling in type II superconductors (Li 2003).

## 2.6, Yttrium Barium Copper Oxide.

The superconducting material used throughout this project was a Yttrium Barium Copper Oxide alloy, which is one of a family of alloys of rare-earth metals and copper oxide, all of which possess high transition temperatures. Their chemical compositions and transition temperatures are shown below.

$BaPb_{0.75}Bi_{0.25}O_3$      : $T_c = 12$ K    [BPCO]

$La_{2-x}Ba_xCuO_4$      : $T_c = 36$ K    [LBCO]    $(x = 0.15)$

$YBa_2Cu_3O_7$      : $T_c = 92.5$ K [YBCO]

$Tl_2Ba_2Ca_2Cu_3O_{10}$      : $T_c = 120$ K   [TBCO]

$Hg_{0.8}Tl_{0.2}Ba_2Ca_2Cu_3O_{8.33}$      : $T_c = 133$ K
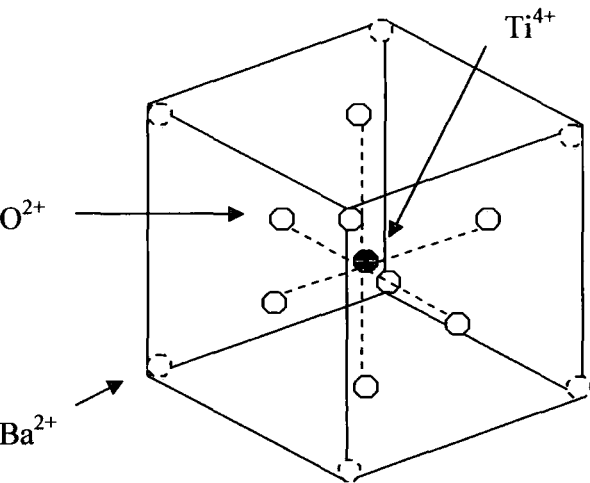


The crystal structures of these compounds are oxygen-defect modifications of the perovskite structure: about one-third of the oxygen positions in the lattice are vacant. Figure 2.6.1 shows the lattice arrangement of barium titanate, an example of the perovskite crystal structure. Barium titanate is cubic with $Ba^{2+}$ ions at the cube corners, $O^{2-}$ ions at the face centres and a $Ti^{4+}$ ion at the body centre.

Figure 2.6.1, Perovskite Crystal Structure (Kittel 1996)

The primitive cell of YBCO is developed from that of a tetragonal perovskite crystal structure tripled along the c axis, as shown in figure 2.6.1. All of the high temperature superconductors with critical temperatures greater than 40 K have parallel layers of $CuO_2$ as part of their structure. In figure 2.6.2 there are three $CuO_2$ planes in a primitive cell of the orthorhombic structure. The two $CuO_2$ planes that run through the interior of the cell are the dominant conductive pathways. However, the $CuO_2$ planes are not superconducting on

their own and require the rest of the structure to act as a charge reservoir (Shimura et al 1994).
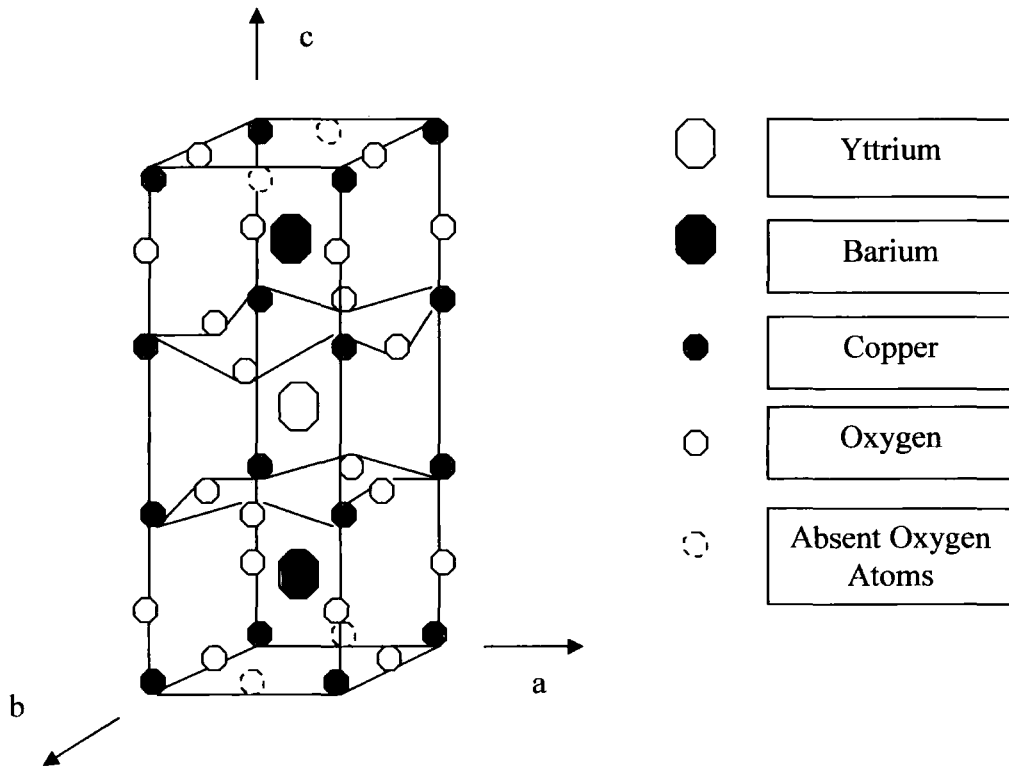


Figure 2.6.2, Crystal Structure of Yttrium Barium Copper Oxide (Kittel 1996)

## 2.7 YBCO Production

There are several methods of producing Yttrium Barium Copper Oxide superconductors; sintering is commonly used in ceramic processing as it has many advantages in preparing precise formed shapes for practical applications. Sintered samples are prepared from powders of high purity $Y_2O_3$, $BaCO_3$ and $CuO$. The powders are mixed well and calcined at 850-950°C for up to 24 hours, the resulting pellet is pulverised and the process repeated to improve the quality of the powder. However while sintered YBCO can be formed into any shape it does not produce samples with high critical current densities, which are essential for levitation applications. These low critical current densities are due to the presence of weak links at the grain boundaries of the YBCO structure. Whilst not suitable for use as levitators, such superconductors with low critical current density can be used for current

limiter applications. A small section of an electric circuit is replaced with a superconductor with properties matched to the circuit so that the maximum safe current is the current limit of the superconductor. Once the current limit of the superconductor is reached the material reverts to its normal insulating state, breaking the circuit (Murakami, 1992).

The properties of the superconductors can be improved through the melt textured growth of YBCO which reduces the weak links in the superconductor. This process involves melting and then slowly cooling sintered YBCO. Melt processing techniques are based on the peritectic reaction that occurs in the YBCO system at around 1015°C. Figure 2.7.1 shows how $YBa_2Cu_3O_{7-\delta}$ melts incongruently at this temperature forming a mixture of solid $Y_2BaCuO_5$ and liquid BaCuO phases. The required 123 ($YBa_2Cu_3O_{7-\delta}$) phase forms as the mixture is cooled slowly in the presence of a temperature gradient through the peritectic temperature according to equation 2.7.1 (Campbell and Cardwell, 1997).

$$Y_2BaCuO_5 \text{ (S)} + Ba_3Cu_5O_{6.72} \text{ (L)} + 0.42O_2 \text{ (G)} \longrightarrow 2YBa_2Cu_3O_{6.28} \text{ (S)} \quad (2.7.1)$$
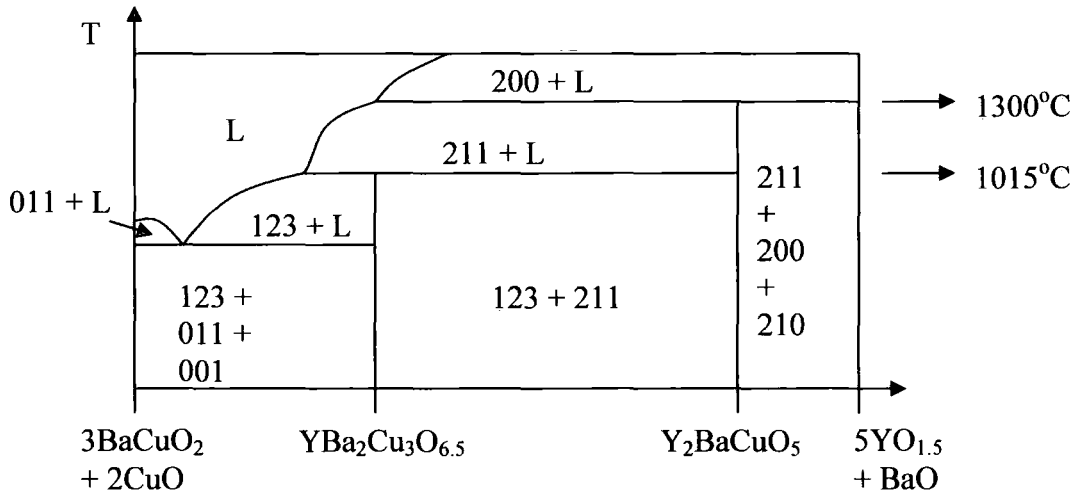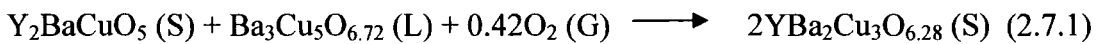


Figure 2.7.1, Phase diagram for the YBCO system (Campbell and Cardwell 1997).

In order to increase the flux pinning centres up to 40% excess 211 ($Y_2BaCuO_5$) phase material is added to the stoichiometric 123 material prior to melt processing. 211 phase inclusions in the superconductor increase the critical current density by generating a fine array of flux pinning centres, and also promote larger grain growth in the superconductor.

The addition of small concentrations of platinum or rhodium to the precursor powder also increases the number of flux pinning centres by inhibiting the growth of the 211 ($Y_2BaCuO_5$) phase (Ogawa et al, 1991), and can triple the critical current density. The platinum or rhodium added to the powder inhibits the growth of the 211 phase by causing considerable numbers of nucleation sites to occur at an early stage of the sintering. No one crystal can grow to a larger size because of the all the other crystals that occur simultaneously. In an undoped sample there are only a few nucleation sites which results in small numbers of large crystal 211 phases limiting the maximum critical current density that can be obtained.

The addition of a seed crystal to the sintered pellets during the melt processing of the superconductors improves the quality of the sample by initiating the nucleation and further growth of the desired Y123 phase, which then solidifies into a single grain during the cooling of the pellet (Reddy et al 2005, Diko et al 2003). The size and the shape of the seed crystal affects the growth of the grains within the bulk. To prepare a sample a mixture of $Y_2O_3$, $BaCuO_2$, and CuO, powders doped with platinum are pressed into pellets of the required size under high pressure. The pellets are then seeded with a chemically and structurally compatible seed crystal such as MgO, SmBCO, or NdBCO, which possess a higher melting point than the YBCO preform powder. The pellets are then heated to around $1050^{\circ}C$, then cooled to the peritectic temperature of the Y123 phase, $1010^{\circ}C$, then cooled more slowly to allow grain formation to occur. At the peritectic temperature the pellet consists of a mixture of solid $Y_2BaCuO_5$ and liquid $Ba_3Cu_5O_{6.72}$ phases (Campbell and Cardwell 1997). The seed crystal instigates the nucleation and subsequent epitaxial growth of the Y123 phase in the pellet, which solidifies into a single grain. The superconductors used in this project were composed of a Yttrium Barium Copper Oxide alloy, prepared in bulk samples with diameters of 42-44mm and a height of 13mm. Each superconductor's structure is a single crystal prepared from powder by the top-seeded melt growth process.

## 2.8 Permanent Magnets

The first magnetic material that was discovered was magnetite ore $Fe_3O_4$, known as lodestone, which was commonly used in compasses for navigation purposes. Every

material has electrons that surround the nucleus of the atoms it contains, which are arranged in shells. Each electron revolves on its axis as it orbits the nucleus; this is termed "spin". Each electron has a magnetic field and an electric field. The number of electrons spinning in the same direction in a material determines the strength of its magnetic field. In a non-magnetic material, an equal number of electrons are spinning in opposite directions and so the magnetic field produced by each electron is cancelled out. In a magnetic material, the majority of the electrons spin in the same direction and so the material develops a magnetic field. Figure 2.8.1 shows the electron shells in an iron atom.
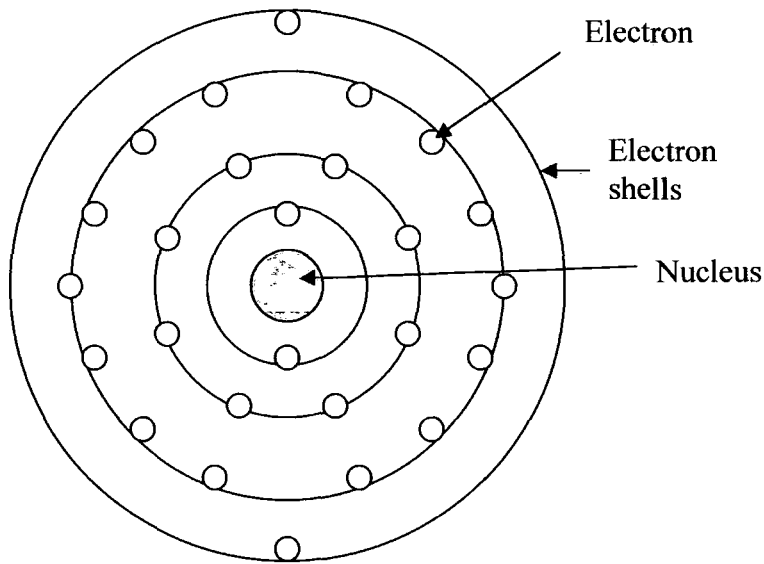


Figure 2.8.1, Free atom of iron, (Hadfield, 1962)

The most commonly used magnets are ferrite magnets, composed of either Barium Iron Oxide, $BaFe_{12}O_{19}$, or Strontium Iron Oxide, $SrFe_{12}O_{19}$. Despite only possessing a low magnetisation value, they are widely used due their low cost and reliability. Cobalt magnet steels such as AlNiCo alloy possess higher magnetic fields than ferrite magnets and also have a higher Curie point. The Curie point is the temperature at which magnetism breaks down within a magnetic material, ferrite magnets have a Curie point of ~500°C, whereas AlNiCo magnets keep their magnetism up to 800°C and as such are used when high operating temperatures are required.

## 2.8.1, Rare-Earth Permanent Magnets

Samarium-Cobalt was the first rare-earth magnet that was developed in the form of $SmCo_5$. Further development led to the samarium cobalt magnet, $Sm_2Co_{17}$, that possessed a magnetic field considerably stronger than both $SmCo_5$, and AlNiCo. These high power magnets were used wherever strong and lightweight magnets were required, such as in stepper motors. High cobalt prices led to a search for high power magnetic materials that did not require the use of cobalt. Neodymium is more abundant in the earths crust than Cobalt or Samarium and also possesses a higher magnetic moment than both elements. The first Neodymium magnet developed had a composition of $Nd_{15}Fe_{77}B_8$. The principal magnetic phase of this compound was later found to be $Nd_2Fe_{14}B$ which possesses the highest magnetic field of all the permanent magnets (Coey 1995). NdFeB magnets are now used extensively in applications where high magnetic fields and light weights are essential. Table 2.8.1 compares the magnetic qualities of permanent magnets.

| Characteristic / Material | $B_r$ (T) | $J_S$ (T) | $_jH_c$ (kAm$^{-1}$) | $_BH_c$ (kAm$^{-1}$) | $(BH)_{max}$ (kJm$^{-3}$) |
|---|---|---|---|---|---|
| $Nd_2Fe_{14}B$ | 1.28 | 1.54 | 1000 | 900 | 300 |
| $Sm_2Co_{17}$ | 1.08 | 1.15 | 800 | 800 | 220 |
| $SmCo_5$ | 0.88 | 0.95 | 1700 | 660 | 150 |
| AlNiCo | 1.25 | 1.40 | 54 | 52 | 43 |
| $SrFe_{12}O_{19}$ | 0.41 | 0.47 | 275 | 265 | 34 |

Table 2.8.1, Magnetic materials and their properties (Coey 2002).

$Nd_2Fe_{14}B$ possesses the highest value of magnetic flux, $B_r$, which is the maximum magnetic flux produced under closed circuit conditions. AlNiCo has a similar value of $B_r$, however $Nd_2Fe_{14}B$ has much higher values of both normal coercivity ($_BH_c$) and intrinsic coercivity ($_jH_c$). Where $_BH_c$ is the applied field intensity required to bring the magnetisation of the material to zero and $_jH_c$ is the applied field intensity required to reverse the direction of the materials magnetisation. The most important parameter is the maximum energy product, $BH_{max}$, which a measure of the useful work that a magnet can produce at a distance from its volume. Despite AlNiCo having a high value of $B_r$, its low values of coercivity result in a

low energy product. $Nd_2Fe_{14}B$ has by far the highest value of $BH_{max}$, showing that is has the highest magnetic field strength to weight ratio. The units of $BH_{max}$ are $kJm^{-3}$, giving a value of energy per unit volume.
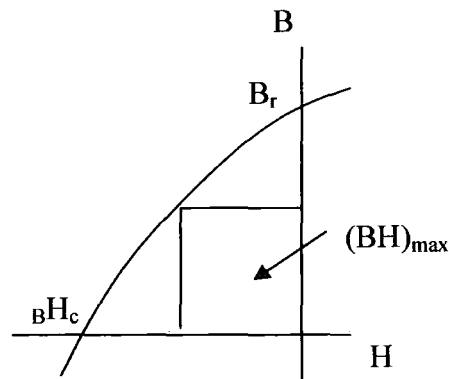


Figure 2.8.2, Demagnetisation curve for a permanent magnet.

Magnetic field strength to weight ratio is the most important property of a magnet if it is to be used for levitation applications. Conventional ferrite magnets do not have a sufficiently high field strength to weight ratio to be levitated, and cannot even support their own weight. As shown in table 2.8.1 Neodymium Iron Boron rare-earth magnets have maximum energy products nearly ten times larger than standard ferrite magnets (Coey 2002), this can be accounted for by the electron shells in the element. Iron has an atomic number of 26, whereas neodymium has an atomic number of 60. The extra 14 electrons in the f shell of each neodymium atom can all be aligned together and accordingly produce a large magnetic moment. For this reason rare-earth magnets were used in this project. It would have not have been feasible to conduct the project without them.

2.9 Earnshaw's Theorem

Earnshaw's theorem states that: A charged body placed in an electrostatic field cannot be maintained in stable equilibrium under the influences of the electric forces alone (Earnshaw 1842). The electrostatic potential of a point charge obeys Laplace's equation; therefore the total potential $\phi$ of a set of point charges must also obey Laplace's equation.

$$\nabla^2 \varphi = 0 \qquad\qquad (2.9.1)$$

$$\frac{\partial^2 \varphi}{\partial x^2} + \frac{\partial^2 \varphi}{\partial y^2} + \frac{\partial^2 \varphi}{\partial z^2} = 0$$

A continuous distribution of charge can be modelled as a set of point charges so that Laplace's equation holds in a charge free region. If φ were to have a minimum at a point then for any change in x, y, or z, φ must increase, as shown in figure 2.9.1. The second order differential $\dfrac{\partial^2 \varphi}{\partial x^2}$ must then be positive, as shown in figure 2.9.3. For a minima to exist this must hold for x, y, and z, therefore $\dfrac{\partial^2 \varphi}{\partial x^2}$, $\dfrac{\partial^2 \varphi}{\partial y^2}$, and $\dfrac{\partial^2 \varphi}{\partial z^2}$ would all be positive which would then mean Laplace's equation did not hold and so it is not possible for a minima to exist.



$$\varphi = x^2 + A$$
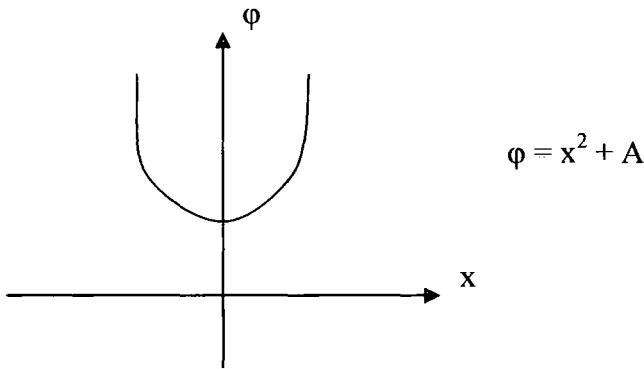
Figure 2.9.1, Graph of φ against x for stable levitation.



$$\frac{\partial \varphi}{\partial x} = 2x$$
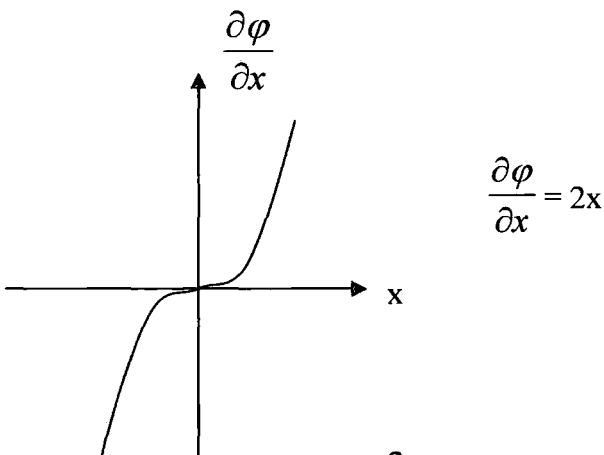
Figure 2.9.2, First order differential, $\dfrac{\partial \varphi}{\partial x}$ .

$$\frac{\partial^2 \varphi}{\partial x^2}$$

$$\frac{\partial^2 \varphi}{\partial x^2} = 2$$

x
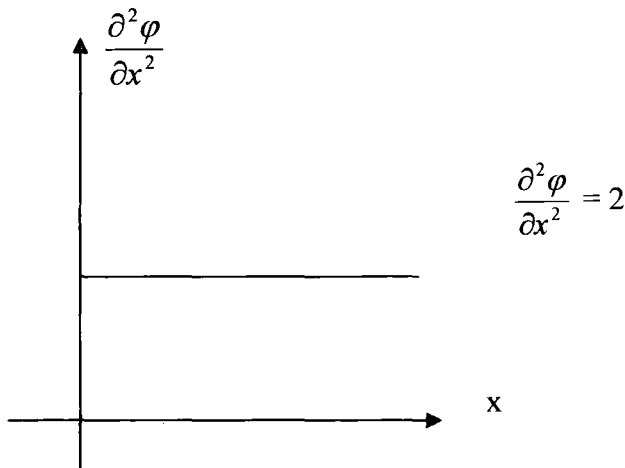
Figure 2.9.3, Second order differential, $\dfrac{\partial^2 \varphi}{\partial x^2}$.

For a charged body the electrostatic energy of an element of charge on or in that body must obey Laplace's equation because the electrostatic potential describing the applied field also obeys Laplace's equation. If the body is moved parallel to itself the position of a point charge can be specified by the position of the body's centre of gravity; the electrostatic energy of the point charge will obey Laplace's equation when regarded as a function of position of the centre of gravity. This will hold for every element of charge in the charged body, therefore the total electrostatic energy of the body φ will obey Laplace's equation. If the charged body is in stable equilibrium and then displaced in a small direction parallel to itself, then no matter the direction of the displacement, φ must increase. Therefore $\dfrac{\partial^2 \varphi}{\partial x^2}$,

$\dfrac{\partial^2 \varphi}{\partial y^2}$, and $\dfrac{\partial^2 \varphi}{\partial z^2}$ must all be negative, but this is not possible as it does not agree with

Laplace's equation and therefore the original assumption of stable equilibrium must be false. For a case where the charges in a body are free to move, any displacement parallel to the original position will result in a situation where φ decreases as the distribution of charge on any conductor is always to minimise the electrostatic potential, (Jones 1980). This indicates that any system of static permanent magnets or electromagnets with constant current will not be able to stably levitate another magnet.

However Milgrom (1998) suggests that while Earnshaw's theorem holds for point charges or a single dipole, that it is possible to suspend point bodies of finite charge, or extended test-charge bodies. This suggests that three or more dipoles connected by stiff links and each supported by a separate set of static magnetic fields should be able to achieve stable levitation. This may provide a method of producing stable levitation without the need for superconductors.

Earnshaw's theorem relies on the linearity of the Laplace operator, and so will not apply to non-linear systems, such as superconductors. This also allows the stable suspension of neutral dipolar bodies with a constant magnitude, as long as the dipole is forced to remain aligned with the potential supporting it. This principle is used in the construction of magnetic traps for atoms, and is also the principle behind the Levitron.

## 2.9.1, The Levitron

The Levitron is an example of stable levitation achieved using only permanent magnets, the Levitron consists of a ring shaped permanent magnet base, and a small disc shaped magnet that levitates over the ring as shown in figure 2.9.4. The Levitron achieves stability through the spinning motion of the top; the gyroscopic force produced allows the top to balance on the magnetic field produced by the base, (Gov et al, 1999, Dullin and Easton, 1999). When the levitating disc magnet is not spinning the Levitron is stable in four degrees of freedom, and unstable in pitch and roll. The spinning motion stabilises the top on pitch and roll and levitation is sustained until the top slows down.
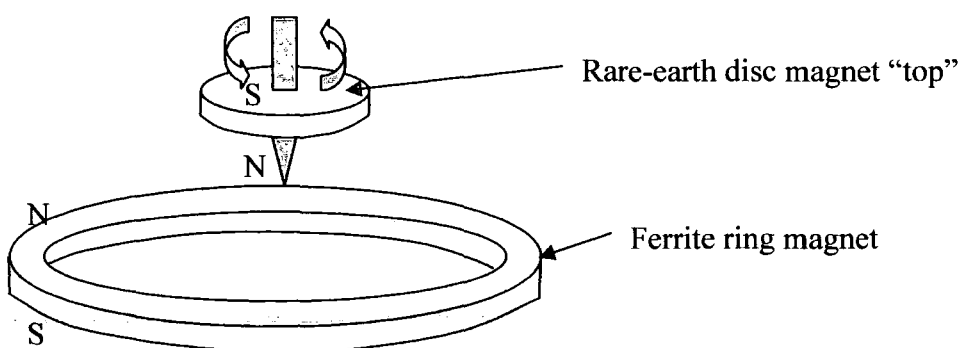
Figure 2.9.4, The Levitron.

Earnshaw's theorem does not apply to the superconducting levitation used in this project as levitation with a superconductor occurs in the vortex or mixed state. The magnetic field of the levitating magnet enters the superconductors' volume and the magnetic flux is trapped in superconducting current vortices, resisting any movement of the magnet. The current vortices are pinned in position at inclusions or defects in the crystal lattice of the superconductor (Taoufik 2002), allowing stable levitation to occur. Milgrom (1998) suggests that is may be possible to construct a series of permanent magnet only levitation devices that could be used to bolster the superconducting levitation.

## 3. Analysis and Testing of the Superconducting Pod for Levitation

3.1 Introduction

This chapter describes the analysis and testing of the "Superconducting Pod" and its use for levitation applications. The superconducting pod formed the basis for the Superconducting Magnetic Levitation System and utilised one superconducting bulk. Electromagnetic Finite Element Analysis that was used to model the interactions between the electromagnets, the levitating magnets and the superconductors used in this project is also covered. The MEGA software (MEGA 2000) was used to optimise the design of the electromagnets used in the system to provide the most efficacious horizontal restoring force to act against the wind force applied to the levitating magnets. Finally the construction of a larger superconducting system is detailed; a system that employed three superconducting pods was then designed, built, and tested against destabilising forces acting in the direction of the airflow.

3.2 Superconducting Levitation and the Superconducting Pod

When a superconductor is cooled below the critical temperature at which it becomes superconducting, it will exhibit the Meissner effect. The Meissner effect is one of the hallmarks of superconductivity in which a superconducting material will expel any magnetic flux impinging on its volume. A magnet will levitate over a superconductor in the Meissner state as long as the diameter of the superconductor is several orders of magnitude larger than the diameter of the magnet. The superconductor creates a mirror image of the magnetic fields produced by the levitating magnet. Because the superconducting material has no resistance the mirror image of the levitating magnet moves instantaneously, matching any movement of the levitating magnet, thereby keeping it supported at all times. However this cannot occur if the levitating magnet is of a similar size to the superconductor. In this case movement of the magnet causes it to move beyond the boundary of the superconductor and as such it can no longer support it.

Levitation of a magnet over a superconductor of comparable dimensions can only occur when the superconductor is in the mixed or vortex state. In this state the superconducting

44

material is a mixture of superconducting regions and normal state sections. The magnetic flux penetrates the volume of the superconductor throughout the normal state regions, and is pinned in place by vortices of supercurrent which surround the normal state sectors at defects within the superconducting lattice. The movement of the magnetic flux is resisted by the vortices of supercurrent, and consequently so is any movement of the magnet, thus allowing stable levitation to occur; this is known as flux pinning. This mechanism is the main principle behind the stable levitation of the superconducting pod that was designed and tested, as shown in figure 3.2.3, figure 3.2.4, and figure 3.2.5.
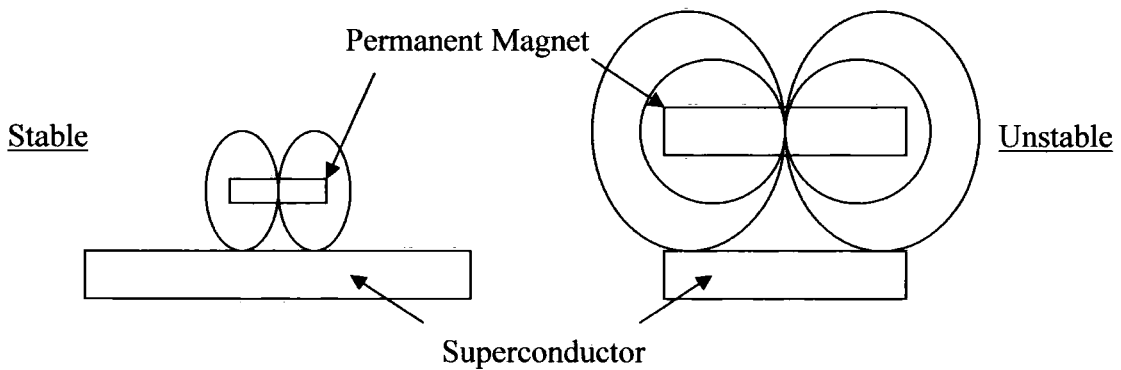


Figure 3.2.1, Stable and unstable levitation with superconductors in the Meissner state.

The superconducting pod was developed as part of the author's previous work (Muscroft 2002). Initially the superconducting levitation was tested whilst restricted to two degrees of freedom. A neodymium-iron-boron magnet with dimensions 50mm x 50mm x 6mm was mounted on a 1 metre long non-ferrous arm that was attached to a gimbal to restrict the motion of the magnet to two degrees of freedom, as shown in figure 3.2.2. The long arm reduced the displacement of the magnet towards the gimbal when moved from its central position. A melt textured YBCO superconducting bulk with a diameter of 44mm was mounted in a resin sealed polystyrene cryostat. Two electromagnets were used, one positioned either side of the cryostat, and each electromagnet had 400 turns and drew 5A. The height of the neodymium magnet was set using a non-ferrous spacer between the superconductor and the magnet. Various sizes of spacers were used to vary the levitation height. The superconductor was then cooled with liquid nitrogen and the spacer removed; this is known as flux pinning by field cooling. The position of the levitating magnet could be controlled by changing the current in the electromagnets; increasing the current in the

electromagnet on the left hand side of the magnet caused the levitating magnet to move to the right and vice versa.
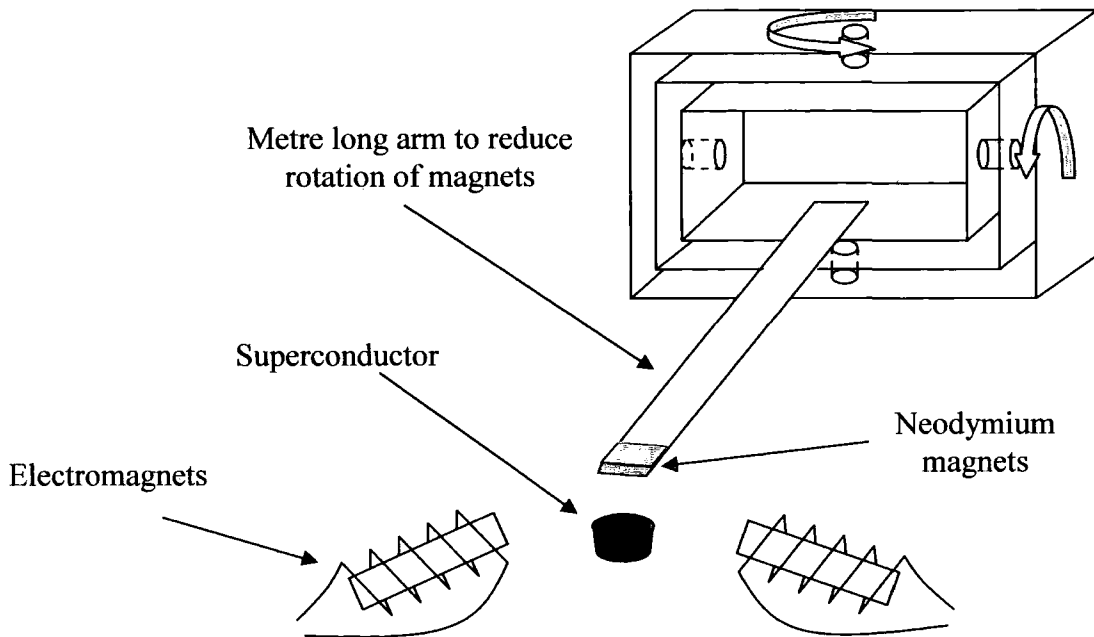


Figure 3.2.2, Two Degree of Freedom Testing

The system was then extended to six degrees of freedom by adding another set of electromagnets at 90° to the existing electromagnets and removing the gimbal and arm. The superconducting bulk was mounted in an aluminium casing, which was located by means of a central mounting pin attached to an aluminium base plate that formed the floor of the cryostat. The main body of the cryostat was formed out of polystyrene which was sealed with resin in order to make it impermeable to the liquid nitrogen. The cryostat was positioned at the outlet of one of the Durham wind tunnels with a jet of 457mm x 457mm square. An aluminium floor was installed to cover the cryostat and represent the floor of a wind tunnel. The main cryostat was joined to a second feeder cryostat, positioned outside of the jet of the wind tunnel, which was raised above the level of the main cryostat to allow the gravity fed flow of liquid nitrogen to cool the superconductor once the aluminium floor was in place. Four electromagnets positioned equidistant from each other around the cryostat were used to provide a restoring force to the levitating magnet to resist the horizontal force acting on them produced by the airflow, as shown in figure 3.2.4.

Before the wind tunnel was turned on the levitation height of the magnets were set by the use of a non-ferrous spacer placed between the magnets and the YBCO superconducting bulk. The superconductor was then field cooled by the addition of a liquid nitrogen bath and the spacer removed. The four electromagnets each had 400 turns and prior to the tunnel being turned on each electromagnet was drawing 2.5A. As the speed of the wind tunnel was ramped up the air applied a force to the levitating magnets, forcing them backwards away from their central point. This movement was countered by reducing the current being supplied to the front two electromagnets which caused the magnets to become centred again. The position of the levitating magnets could be controlled by changing the current in the electromagnets. The superconducting pod was proved to be stable at a wind speed of 20ms$^{-1}$, which was the limit of the wind tunnel being used for testing.

The test was initially performed with just the levitating magnets in the air flow, as shown in figure 3.2.3. In order to test the limits of the system the levitating magnets were then encased in modelling foam to increase the drag of the magnets and act as a bluff body to subject the system to unsteady air fluctuations as shown in figure 3.2.5 and figure 3.2.6. The modelling foam body was cylindrical and had a diameter of 100mm and a height of 50mm. With the aluminium floor in place and the addition of the bluff body to the levitating magnets the superconducting pod proved to be stable at 20ms$^{-1}$, which was the maximum speed of the wind tunnel. Despite the wind tunnel operating at its maximum speed the levitating magnets remained centred and stationary suggesting that the system was capable of operation at higher wind speeds.
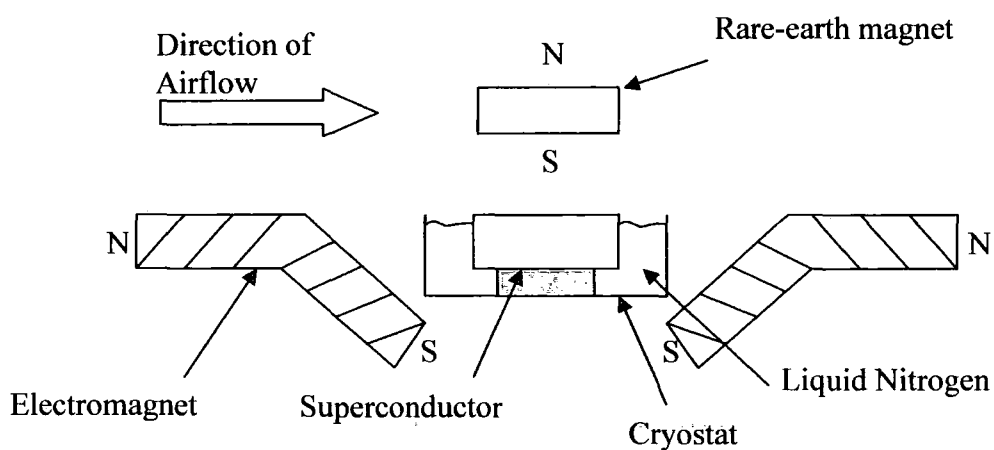


Figure 3.2.3, Schematic of the Superconducting Pod.
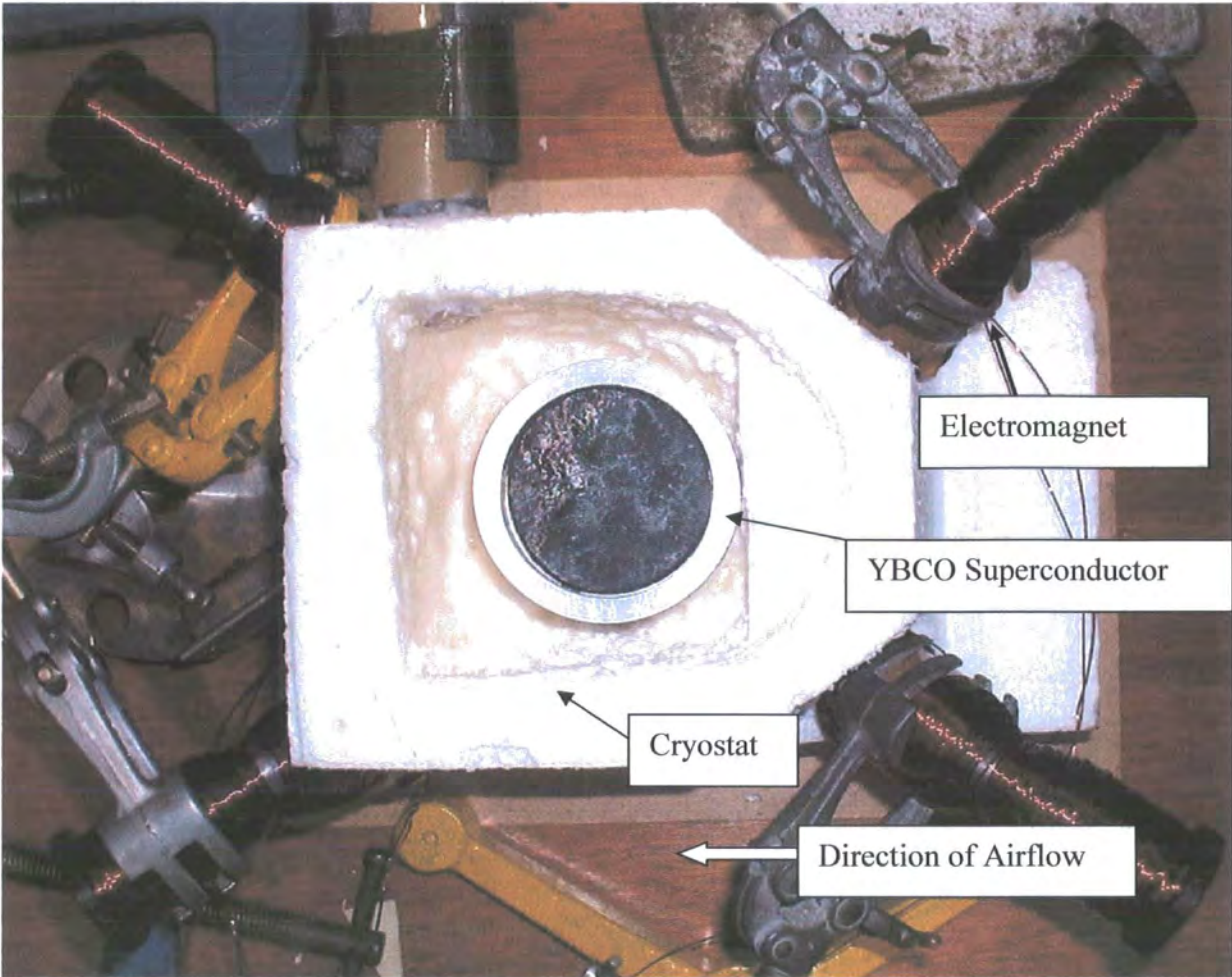
Figure 3.2.4, Layout of the Superconducting Pod
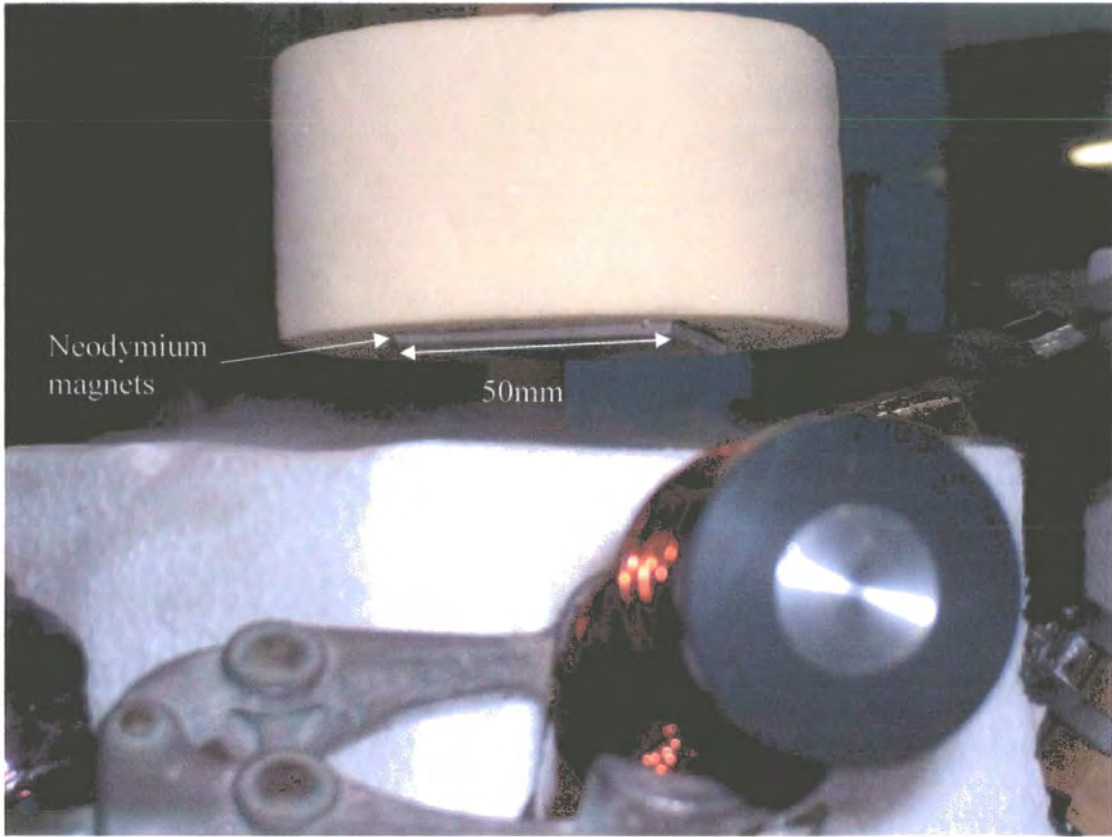
Figure 3.2.5, The Superconducting Pod Levitating
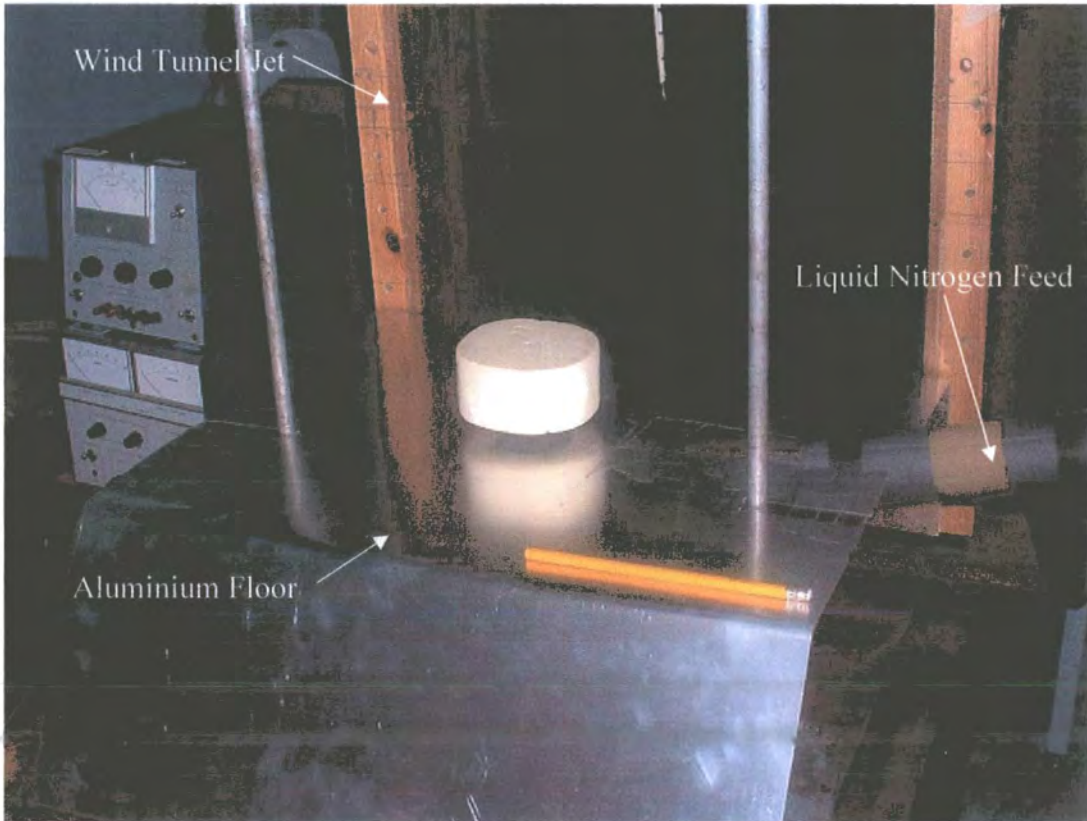


Figure 3.2.6, The Superconducting Pod Levitating with Aluminium Floor in Place.

## 3.3, Superconductor Crystal Quality and Domain Size

The levitation force that is produced by a magnet positioned over a superconductor, that has been cooled below its critical temperature, is proportional to the diameter of the superconducting current that is induced in the superconducting sample by the magnetic field of the magnet. The larger the diameter of the superconducting current produced, the greater the resulting levitation force. The size of the supercurrent is dependant upon the quality of a superconducting sample which itself is defined by the crystal structure of the superconducting bulk. The maximum levitation force is produced if the supercurrent can circulate throughout the entirety of the superconducting bulk; for this to happen the structure of the superconductor must be composed of a single grain crystal. Several factors can cause the production of samples consisting of multiple grains during manufacture. These factors can include polycrystal seed crystals, edge nucleation, or misorientation within a domain where c-axis misalignments occur between adjacent sub domains, (Sengupta et al 1998). All these manufacturing flaws prevent the flow of the supercurrent between the adjacent grains and reduce the size of the supercurrent loop. Physical cracks within the superconductor bulk can of course also reduce the domain size. These are all macroscopic factors which can affect the domain size unlike the microscopic imperfections introduced to the crystal structure as sites for flux pinning which do not disrupt the flow of the supercurrent.

## 3.3.1, Measurement of Trapped Magnetic Flux

Three of the Yttrium-Barium-Copper Oxide superconducting samples that were used for levitation purposes in this project were examined. All three samples displayed small cracks on their surface, but one sample exhibited a crack running across half its width. A visual examination is not capable of revealing the extent of the cracks to assess whether the fractures run deep enough to disrupt the flow of current and alter the domain size of the samples. Yang et al (2002) investigated the effect of domain size on levitation force. It was found that the larger the domain size of the superconductor, the greater the levitation force the superconducting sample could produce. However the relationship between domain diameter and levitation force is not linear. The levitation force of a superconducting sample

of a given size consisting of a single domain is considerably greater than the sum of the levitation force produced by two superconducting samples of half the size or that of a sample of the same size but with a physical crack throughout the sample dividing the domain into two. The levitation force that a sample can produce is inversely proportional to the perimeter of the grain boundaries in the sample (Yang et al 2001), cutting a sample in half increases the grain boundaries by four times the radius of the sample. The trapped magnetic flux in a single domain sample is at a maximum at the centre and decreases towards the edge of the sample as shown in figure 3.3.5 and figure 3.3.6. A crack in the sample, as shown in figure 3.3.3 creates an extra boundary at which the trapped magnetic flux is reduced, resulting in decreased levitation force as shown in figure 3.3.8. Maximising the area in which the supercurrent loop can form produces the largest levitation force. Therefore for a given area over which superconductors are to provide levitation, the maximum force will be gained using superconducting samples with the largest diameter available whilst still consisting of a single domain and possessing the shortest grain boundary achievable.

The three superconducting samples were then tested to ascertain the size and number of domains contained within each. Domain sizes were determined by measuring the trapped flux in each sample using a Hall probe. The superconducting samples were cooled below their critical temperature by means of liquid nitrogen, and then a magnetic field was introduced, and then subsequently removed. To exceed the first critical field strength of the YBCO superconductors a stack of four 50mm x 50mm x 6mm neodymium-iron-boron magnets was used. The magnets were forced towards the superconductor causing the magnetic flux to be compressed between the superconductor and magnet and thereby exceeding the first critical field strength of the magnet, before being removed. The strength of the magnetic field trapped within the superconducting bulk was then measured by a Hall probe mounted on a non-ferrous arm connected to a traverse gear. A three axis traverse gear was used to position the Hall probe. The stepper motors were RS 440-458 12V 0.6A units with a step resolution of 1.8°. The Hall probe measured the trapped field emanating from each superconductor at a height of 2mm above the surface of the samples. The results are shown below.
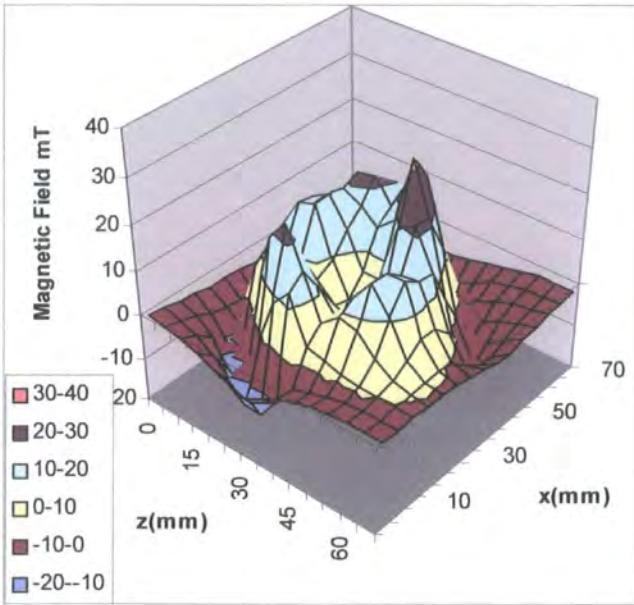
Figure 3.3.3, Trapped flux pattern in sample 1.    Figure 3.3.4, Superconducting sample 1.
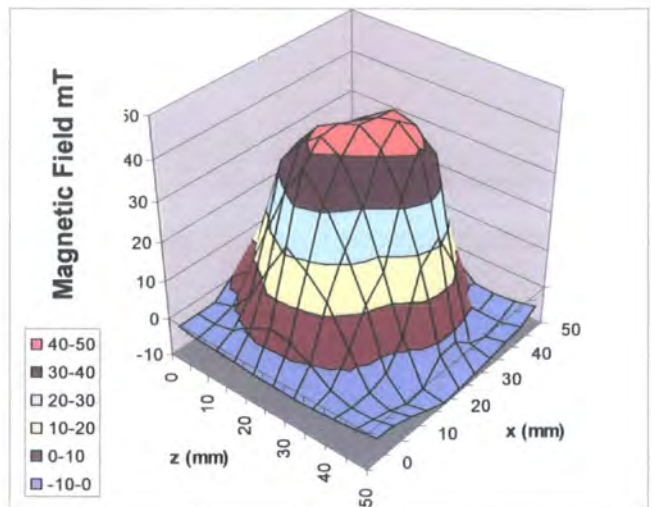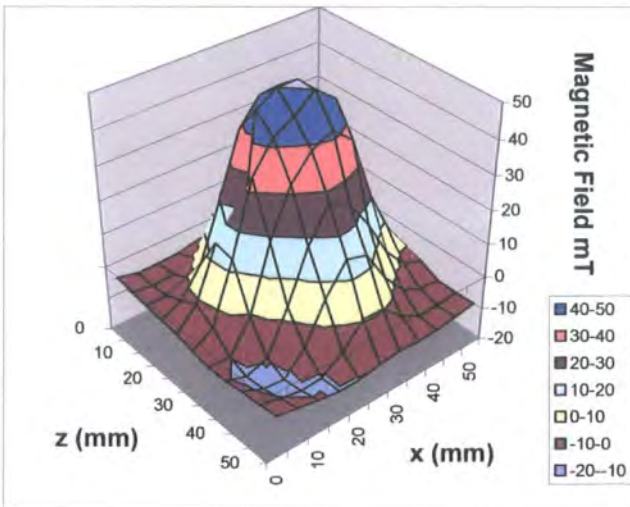


Figure 3.3.5, Trapped flux pattern in sample 2.    Figure 3.3.6, Trapped flux in sample 3.

Figure 3.3.3 shows the trapped flux in superconducting sample 1. Visual examination of sample 1 shows a crack running from the middle of the sample to its edge, as shown in figure 3.3.4. The graph of the trapped magnetic flux in the sample shows that the crack runs at least to the depth that the magnetic field penetrated into the crystal, this crack disrupts the flow of the supercurrent and produces the uneven flux distributions seen in the graph in figure 3.3.3. The crack does not extend across the entire width of sample 1 so it still has only one domain. However the crack severely reduces the diameter of the supercurrent loop

that the superconductor can produce. This also results in the effective domain size of the sample being reduced considerably, and the perimeter of the grain boundary is increased; hence it would be expected to significantly reduce the levitation force that it can produce. Figures 3.3.5 and 3.3.6 show that while the other two samples were shown to have small cracks on their surface, the cracks do not penetrate through the thickness of the samples. Leblond et al (1999) showed that the levitation force that a superconducting sample produces increases with the thickness of the sample up to a thickness of 6mm above which point no further increase in levitation force is achieved. Levitation force is proportional to the superconducting volume up to the point at which the magnetic field from the permanent magnets cannot penetrate any further into the superconductor. The superconducting samples that were tested were 12mm thick. Single domain superconducting samples allow the supercurrent loop to form with a diameter comparable to the diameter of the sample. The conical shapes of the graphs of the trapped magnetic flux show that both samples have only one domain and that the domain size is comparable with the size of the samples.

3.3.2, Levitation Forces Produced by Superconducting Samples

The levitating force that each sample could produce was then measured. Each superconducting sample was placed within a cryostat and mounted on to a six component force balance. The force balance consisted of two plates connected by six thin links. The links were directly attached to one plate and connected to the other plate through six strain gauge load cells positioned to measure the axial force in each link. The force balance was designed to isolate the load cells from out of plane forces. A directly applied vertical force would load links 1, 2, and 3, as a thin rod is axially stiff, but because a thin rod is relatively flexible in bending and torsion the load on links 4, 5, and 6 would be negligible. The resulting loads would be measured by the six strain gauge load cells. The load cells were manufactured by Graham and White Instruments with a full scale load of ±60N, and full scale deflection of 0.6mm. The links were manufactured from 1.6mm diameter steel rods, the plates and all other components of the balance were made from aluminium (Docton 1997).
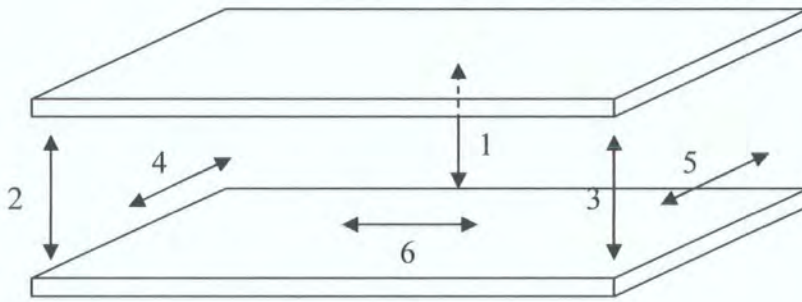
Figure 3.3.7, Schematic of the Six Component Force Balance

Three neodymium-iron-boron rare earth magnets with dimensions of 50mm x 50mm x 6mm were attached to the traverse gear via a non-ferrous arm. The superconducting samples were cooled below their critical temperatures in liquid nitrogen and the rare-earth magnets were lowered from directly over the samples from a height of 100mm. Figure 3.3.8 shows the levitation force produced by each superconducting sample interacting with the rare-earth magnets. To account for the weight of liquid nitrogen that boiled off during the measurements a run was performed without any permanent magnets and the readings subtracted from the force measurements.
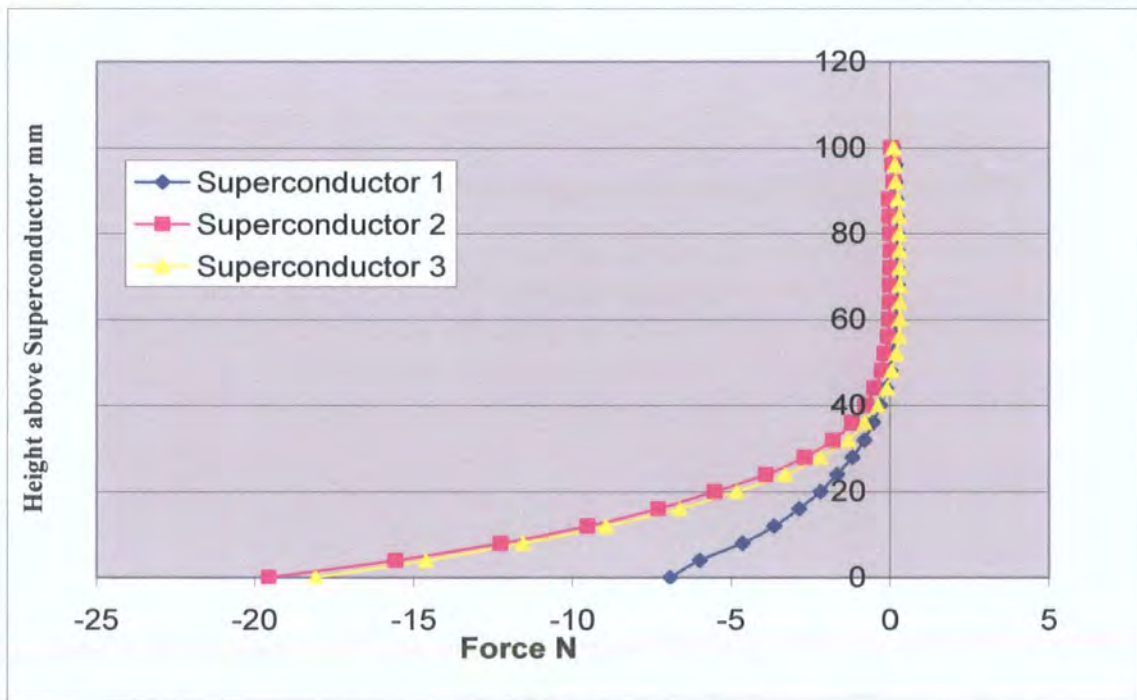


Figure 3.3.8, Levitation force produced by superconducting samples and rare-earth magnets.

The results of the levitation force traverses shown in figure 3.3.8 show good correlation with the results of the flux trapping measurements. The flawed sample 1 only produced a maximum levitation force of around 7N, whereas samples 2 and 3 both produced a maximum levitation force of around 20N. The samples without any cracks, and hence larger domain sizes, produced significantly larger levitation forces than the cracked sample, despite the cracked sample still possessing only one domain. Where possible throughout this project only single grain superconductors were used.

The maximum levitation force that a superconducting sample can generate is determined by the magnetic field strength that the levitating magnets produce. The stronger the magnetic field that is produced by the magnets, the greater the levitation force that is produced. This relationship is followed up until the point at which the magnetic field acting at the surface of the superconducting sample exceeds the upper critical field strength of the superconducting bulk; at which point superconductivity within the sample breaks down. Teshima et al (1997) investigated the relationship between the diameter of magnet used and the levitation force produced. It was found that the effective maximum levitation force was produced when the levitating magnet had a diameter which was marginally smaller than that of the superconductor; this was found to be approximately 90% of the diameter of the superconducting bulk. The use of a levitating magnet with a larger diameter than this will result in a greater levitation force being produced, however the extra levitation force is less than that required to compensate for the extra weight of the magnetic material and as such reduces the effective levitation force.

The magnetic field acting on the superconductor can also be increased using magnets of increased thickness or by stacking the levitating magnets on top of each other. Adding subsequent magnets will increase the resulting magnetic field but, as with the width of the magnets, there is a limit where the extra magnet will not provide a sufficient increase in levitation force to compensate for the extra weight that it adds, thereby decreasing the levitation potential of the system. To ascertain the ideal number of magnets to stack to produce the maximum levitation force a superconducting bulk was mounted in a cryostat on a six component force balance and a varying number of magnets were mounted to a traverse gear via a non-ferrous arm. Figure 3.3.9 shows the relationship between levitation

force produced by a superconducting bulk and number of levitating magnets being used. To ensure the results are not affected by the liquid nitrogen boiling off a dry run was performed and the measurements subtracted from the force readings.
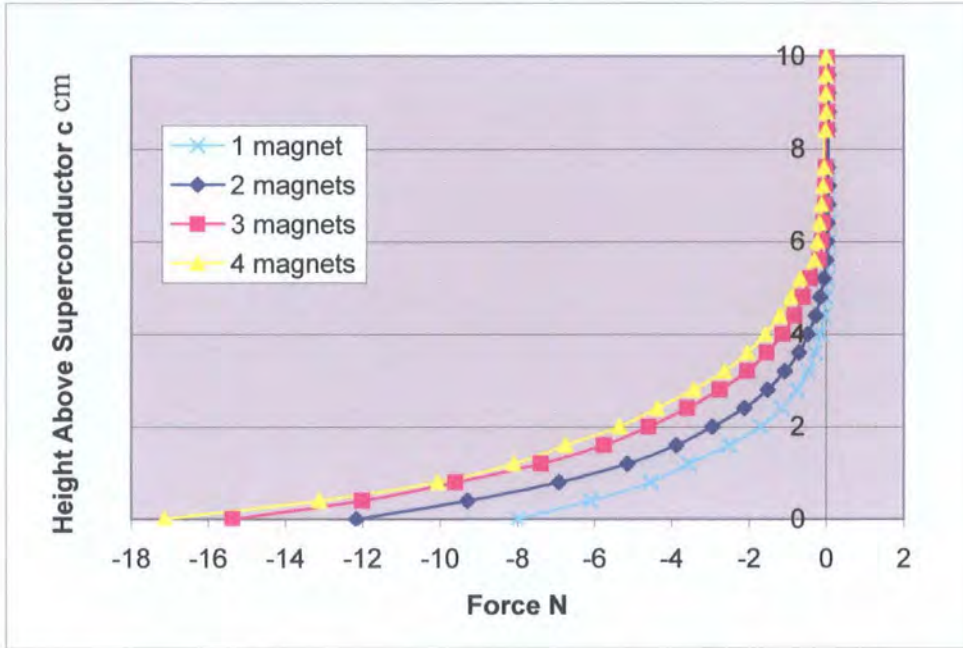


Figure 3.3.9 Effect on levitation force of increasing the number of magnets.

Figure 3.3.9 shows a marked increase in the levitation force produced by increasing the number of magnets from one to two, and a similar increase resulted from the addition of a third magnet. However the addition of a fourth magnet produced only a minor increase in the resulting levitation force. The increase in levitation force engendered was not sufficient to compensate for the extra weight that the magnet added. At a height of 2cm above the superconducting bulk a fourth magnet produced an extra levitation force of 0.5N. However in order to compensate merely for its own weight the extra magnet would have to have produced an additional levitation force of 0.91N. Therefore the result of the addition of a fourth magnet would be to actually reduce the levitation height of the magnets.

When a rare-earth magnet is levitating over a superconducting bulk in the vortex state, the superconductor is capable of resisting large forces in the vertical direction; however the superconductor can resist only relatively small horizontal forces, therefore requiring the use of the electromagnets to hold the magnets in position. In the authors previous work

(Muscroft 2002) it was considered whether the superconductors could provide more horizontal restoring force by placing them at an angle towards the direction of the airflow. To test this theory a YBCO superconducting bulk was mounted in a cryostat at increasing angles, from horizontal to $30^o$ in increments of $10^o$, as shown in figure 3.3.10. A neodymium-iron-boron rare-earth magnet was mounted to a traverse gear on a non-ferrous arm and force plots were taken over an area from 100mm above the superconductor to 80mm horizontally from the centre of the superconductor. The results are shown in figures 3.3.11, 3.3.12, 3.3.13, 3.3.14. With the superconductor parallel to the magnet the maximum force produced was 3.55N. Changing the angle of the superconductor by $10^o$ reduces the maximum force produced to 2.13N. Increasing the angle to $20^o$ again further reduces the maximum levitation force produced to 1.65N. Increasing the angle to $30^o$ causes a reduction in levitation force to just 0.36N. These results show that any gain in horizontal restoring force by changing the angle of the superconductor is considerably outweighed by such a dramatic loss of levitation force. This effect was due to the average distance between the superconductor and levitating magnets being considerably increased as the highest point of the superconductor had to be below the effective floor level. Therefore this is not a beneficial configuration when horizontal restoring force is produced considerably more effectively through the use of electromagnets. Figure 3.3.11 shows that the superconductor produces significant levitation force even though the magnet is not directly over the superconductor. This means that although the space for levitating magnets will be constrained by the size and shape of the vehicle to be levitated, extra levitation force can be achieved by positioning superconductors beyond the boundaries of the vehicle.
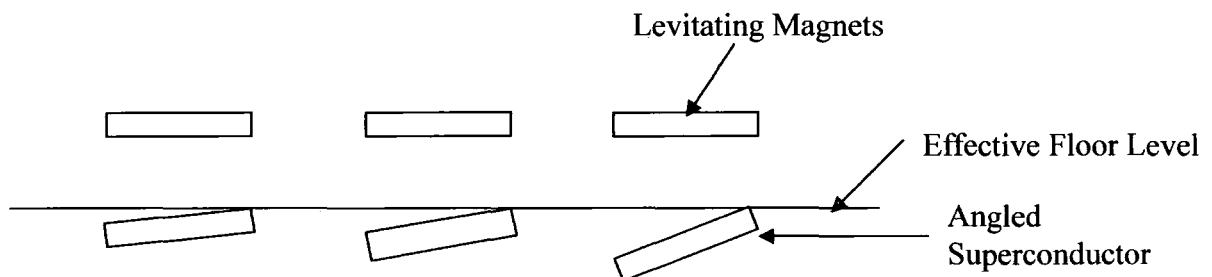


Figure 3.3.10, Increasing the angle of incidence between levitating magnets and superconductors.
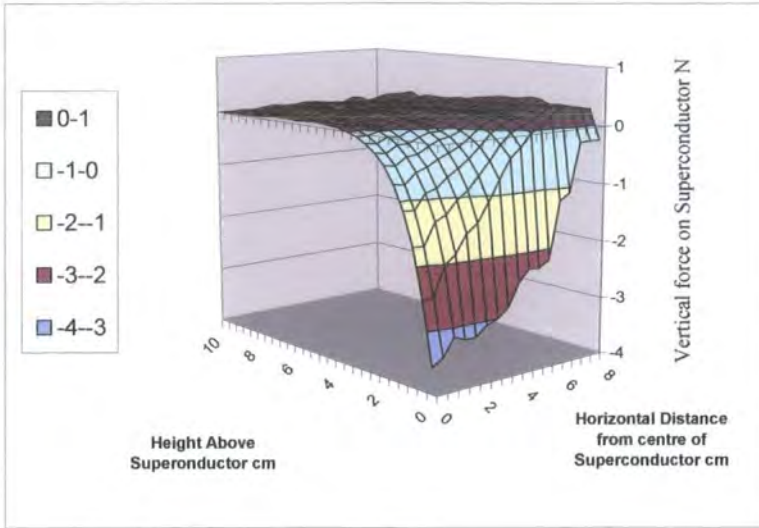
Figure 3.3.11, Force produced at 0°.
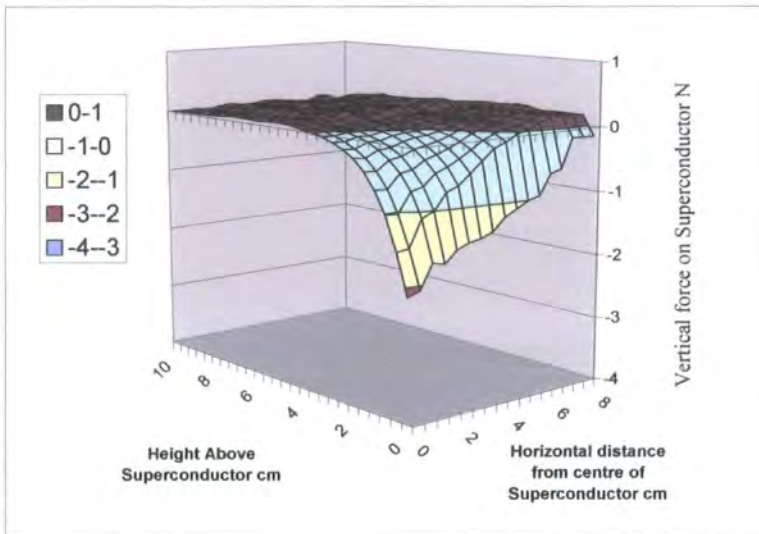


Figure 3.3.12, Force produced at 10°.
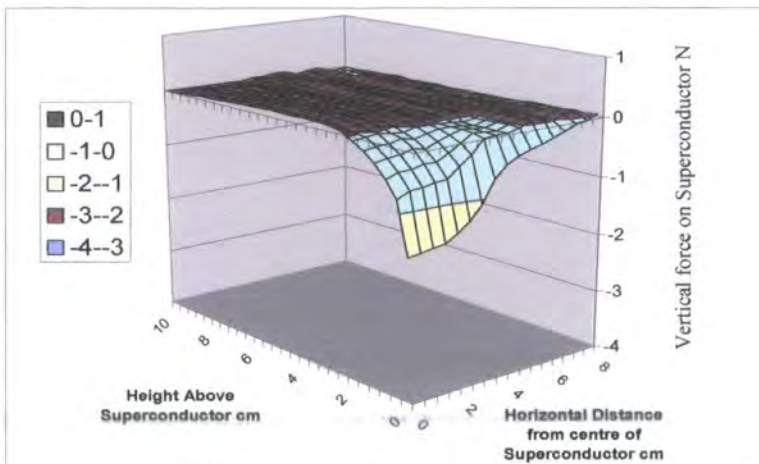


Figure 3.3.13, Force produced at 20°.
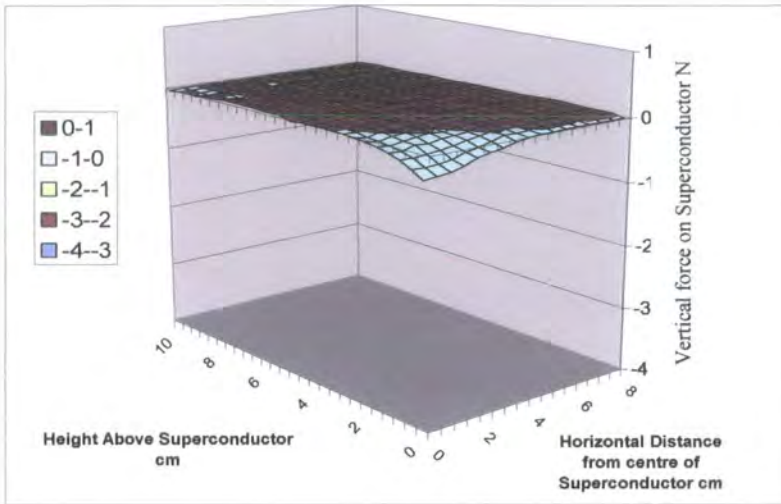
Figure 3.3.14, Force produced at 30°.

## 3.4 Electromagnetic Finite Element Analysis

### 3.4.1 E.F.E.A. Method

MEGA is an electromagnetic finite element analysis package developed at the University of Bath (Mega 2000). MEGA solves the low frequency subset of Maxwell's equations using the finite element method. MEGA is based on four fundamental field equations:

$$\nabla . \vec{B} = 0 \qquad (3.1)$$

$$\nabla \times \vec{E} + \frac{\partial \vec{B}}{\partial t} = 0 \qquad (3.2)$$

$$\nabla . \vec{D} = \rho \qquad (3.3)$$

$$\nabla \times \vec{H} + \frac{\partial \vec{D}}{\partial t} = \vec{J} \qquad (3.4)$$

Where $\vec{H}$ is the magnetic field strength, $\vec{J}$ is the current density, $\vec{E}$ is the electric field, $\vec{B}$ is the magnetic field, $\vec{D}$ is the electric displacement field, $\rho$ is charge density, and t is time (Monk, 2003).

The Finite Element Method is employed to model a system numerically in order to assess its properties without the need to physically build it. The test configuration is modelled in the finite element program and values are attributed to the components. The model is solved by breaking it down into small elements. The model is divided into a sufficiently fine mesh, and then the governing equations are then solved for each small element, as defined by the set boundary conditions. The size and shape of the mesh and the elements that it is divided into are regulated by a trade off between accuracy and processing power. The smaller the elements and the more complex the mesh, the more accurate the result will be. However, a very fine mesh will consume a lot of processing power, considerably increasing the time taken for the program to solve the problem; for a complicated model the solving time can run into weeks. As a result the design of the mesh is of great importance.

In any design of a system that is to be modelled there will be areas in which either there are large force gradients, or where there are large electrical gradients. These areas occur around features such as stress concentrators or points of high load. In order to produce an accurate solution for the regions incorporating the steepest gradients the mesh must be structured to be sufficiently fine to capture the small detail. However structuring the entire mesh in this fashion causes processing power to be wasted on areas containing only moderate or low gradients. Instead the mesh is structured to be gradated so that it is fine in areas where there is a large amount of detail to be captured and coarse in areas far from the point of interest. This approach allows detailed analysis of points of interest whilst minimising the run time taken for the program to solve each mesh, careful design of the mesh is important to optimise this trade off without missing any fine detail. Computer modelling is a useful tool to reduce the time required to investigate the behaviour of electromagnetic circuits, or where it is either impractical or financially unfeasible to build multiple variations of the actual circuits. MEGA (2000) was the FEA package that was used for all of the computer simulation covered in this report. Meshes in MEGA could be constructed using a combination of quadrilateral and triangular elements.

3.4.2 Scope of the Analysis

The role of the electromagnets used in this research was to provide a restoring force opposing the destabilising horizontal aerodynamic force of the air flow acting on the model in the wind tunnel. Finding the optimal orientation of the electromagnets experimentally would have required the manufacture of all the electromagnets that were under consideration and taken considerable time to test all the potential variations. Computer simulation significantly cut the time taken to explore the possibilities and removed the need for the costly manufacture of multiple designs of electromagnets.

The layouts of the simulations were based on a single superconducting pod. The pod consisted of a superconducting bulk, a levitating permanent magnet, and two electromagnets modelled in 2D. In MEGA 2D models are modelled as a cross section through the centre point of a 1m long 3D model so that end effects are far enough away so that they do not impinge upon the test section. This configuration is a good approximation

of the superconducting pod as the electromagnets are designed to resist a force in one plane and forces acting in other planes will be opposed by a separate set of electromagnets. All the components of the superconducting pod system that are designed to resist the wind force acting in one direction lie in one plane, therefore all the simulations of the superconducting pod system were performed in 2D. Whilst the 3D effects are significant this approach will provide a good indication as to the most effective configuration of the electromagnets.

### 3.4.3 Modelling of Permanent Magnets

The MEGA software was capable of modelling an allocated area as permanent magnet material with an ascribable field strength and direction; however the MEGA program cannot calculate the force that one permanent magnet is applying to either another permanent magnet or an electromagnet. The MEGA software calculates the force acting on an element by multiplying the current density by the magnetic field and integrating over the area specified (MEGA 2000), therefore as areas specified as permanent magnets have no current density no forces can be calculated. Therefore in order to allow forces to be measured the permanent magnet models simulated were created as electromagnets so that there would be a current density to measure. As the models were tested in 2D, opposite current densities were assigned to either side of the permanent magnets in the models to produce the required magnetic fields. The current densities for the electromagnetic representation of the permanent magnets were chosen by meshing a magnet and assigning it as a permanent magnet and measuring the magnetic field it produced. An electromagnet of the same dimensions was then meshed and the current densities varied until the magnetic field it produced was the same as the permanent magnet model.

### 3.4.4 Modelling of the Vortex State

The Meissner state, in which a superconducting material expels any magnetic flux impinging on its volume, can be modelled by applying a boundary condition of tangential flux at the perimeter of the area to be designated as a superconductor. This condition holds as long as the magnetic field acting on the material is below the first critical field strength

of the material. However when the magnetic field strength at the surface of a type II high temperature superconductor, such as the Yttrium, Barium, Copper Oxide alloy that was used in this research, exceeds the first critical field strength of the material, the superconductor can no longer expel all of the magnetic flux, and some of the flux enters its volume. This is known as the mixed or Vortex state. The MEGA finite element analysis package is not capable of modelling the processes that occur within the superconductors in the vortex state that were used in this project.

The principal objective of modelling the electromagnet, superconductor, and levitating magnet system was to measure the forces produced by the interaction between the electromagnets and the levitating magnet. The purpose of the electromagnets in the system is to oppose the destabilising horizontal wind force acting on the levitating magnets. The interactions between the fields produced by the levitating magnets and the electromagnets are a significant distance away from the superconductor and as such are not appreciably affected by the superconductor. In the Vortex state caused by field cooling of the superconductor the shape of the magnetic field differs only slightly from the Meissner state as the field dips into the volume of the superconductor. Modelling the system with the superconductor assumed to be in the Meissner state is a reasonable approximation in order to allow the effect of the electromagnets to be assessed.

## 3.4.5 Mesh Resolution

The mesh size used for the models was determined by running the simulations and refining the mesh between each run until comparison of the results showed the difference between refinements was negligible. The mesh used for Model 1, as shown in figure 3.5.3, consisted of 10472 cells. This mesh was chosen as it was shown that quadrupling the number of elements used from 2500 to 10000 resulted in a change in the magnet field of 0.5%, whilst a further quadrupling of the number of cells to over 40000 cells resulted in a change in the magnetic field of less than 0.2%, as shown in figure 3.4.1.
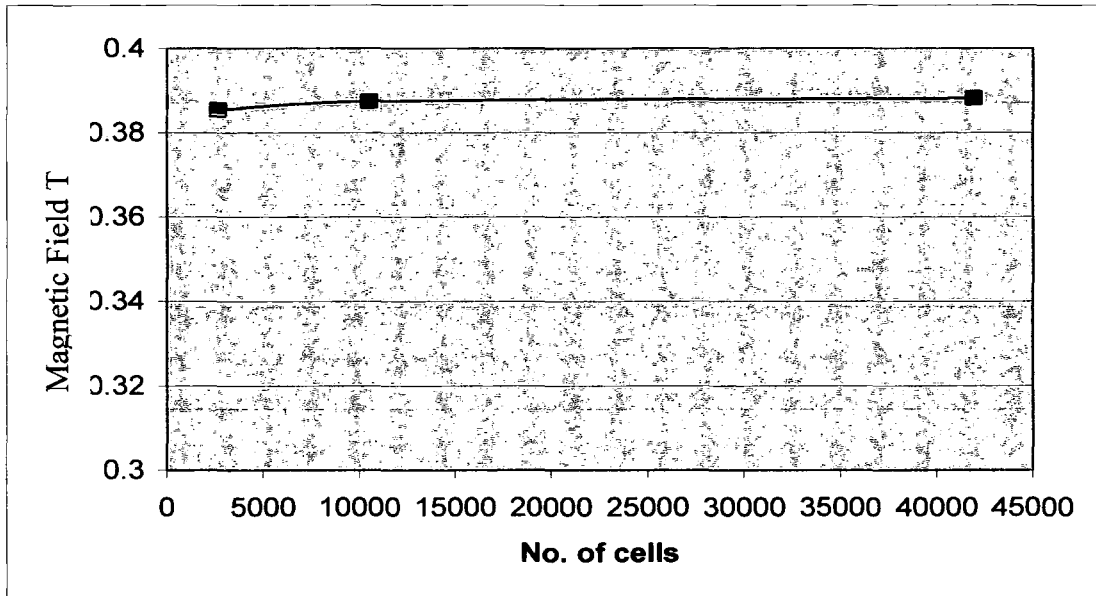
Figure 3.4.1, Graph of Cell Number against Magnetic Field.

## 3.5 Electromagnetic Finite Element Analysis Results

In order to find the optimum shape of electromagnet to produce the maximum horizontal force a standard arrangement of the superconductor and levitating permanent magnet was chosen. A superconductor and magnet of equal size were positioned directly over each other at a fixed height as shown in figure 3.5.1, with a boundary condition of tangential magnetic flux applied to the superconductor. For each simulation the electromagnets being tested were meshed to lie on either side of the superconductor, all lying below the line where the floor of the wind tunnel would be. The horizontal forces acting on the levitating magnet were then calculated. The models were then re-meshed to move the levitating magnet 2mm horizontally as shown in figure 3.5.2, and the new model solved to find the horizontal forces acting on the levitating magnets to ascertain whether the force was either a restoring force or a destabilising force.

The first simulation that was investigated was a 2D representation of the superconducting pod. Curved electromagnets were used in this system as previous experimental results (Muscroft 2002) suggested that they provided a more stable repulsion force, (Figure 3.5.3). Several other shapes of electromagnets were simulated including straight and curved electromagnets with a range of angles (Figures 3.5.4 - 3.5.8). The forces acting on each

element of the levitating magnet were calculated by MEGA and the forces written out to a text file. A datum reading of the levitating magnet on its own was deducted from the readings to only show the forces being produced by the perturbation.
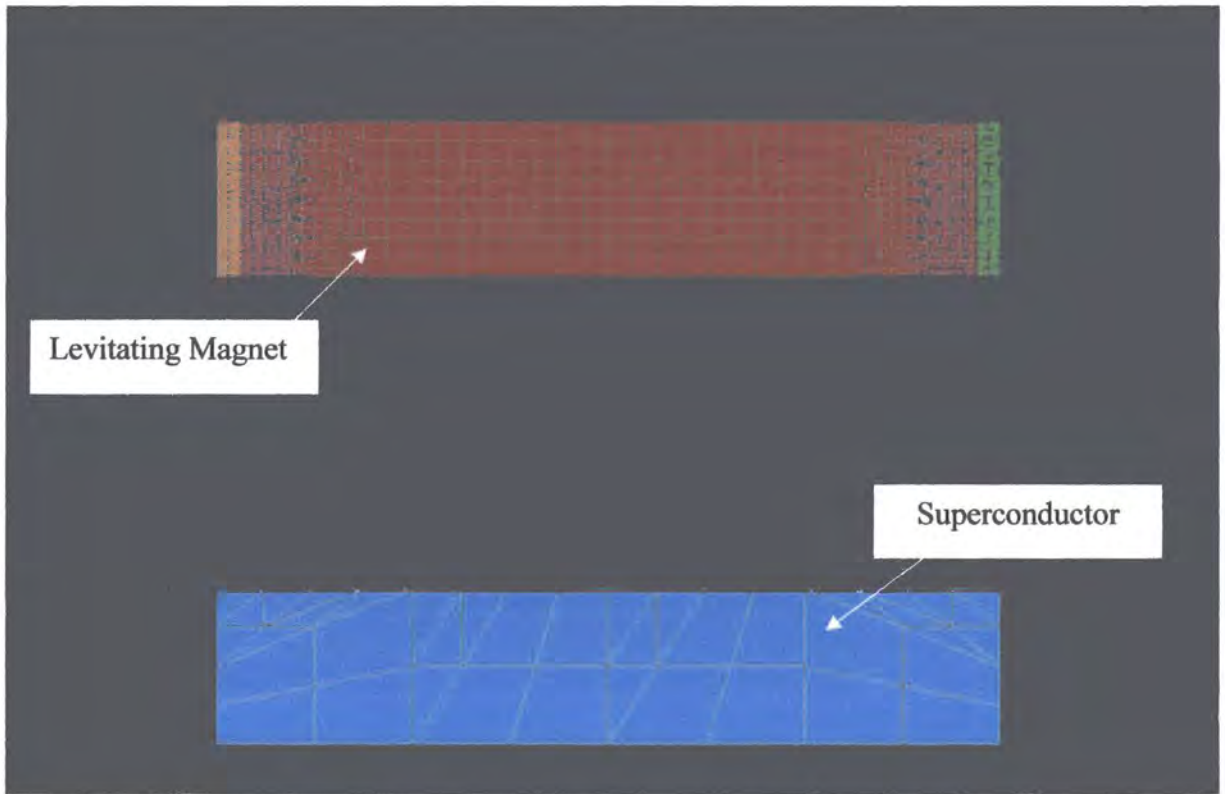


Figure 3.5.1, Arrangement of magnet and superconductor and element distribution.
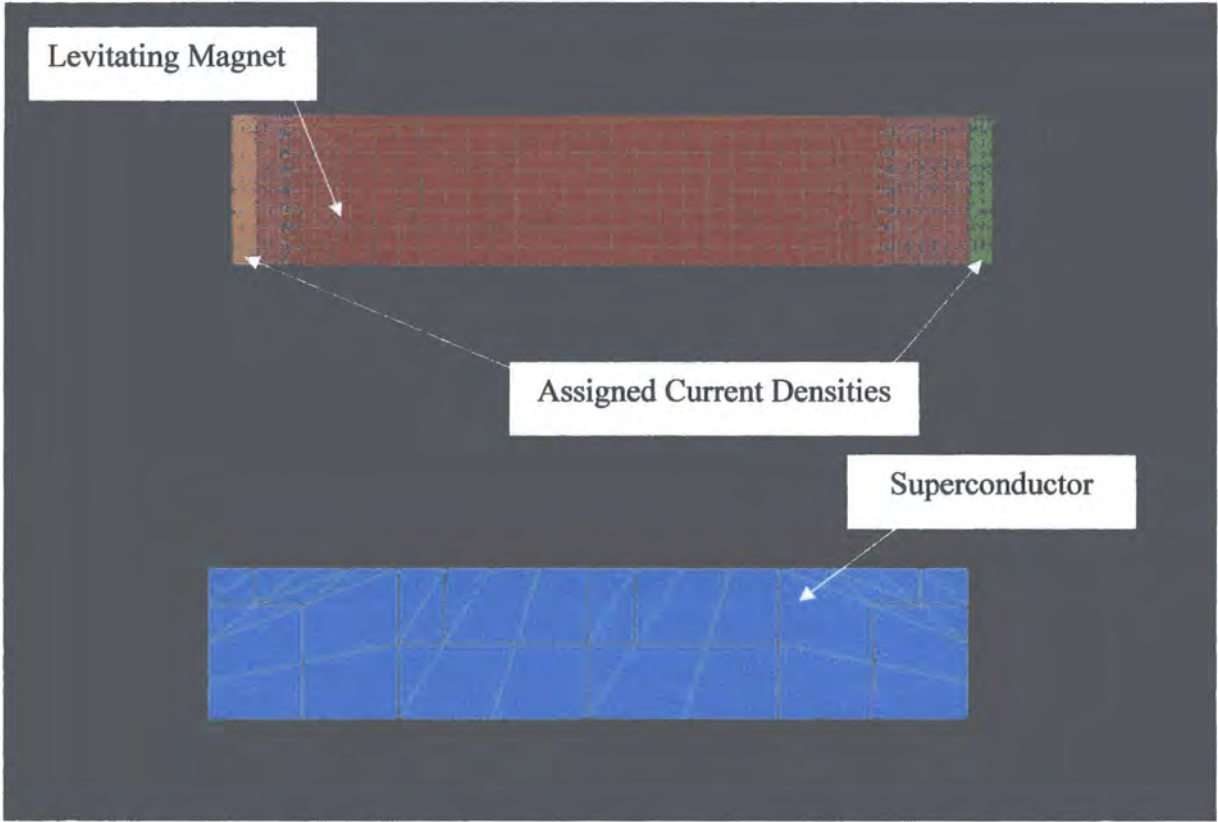
Figure 3.5.2, Configuration with 2mm horizontal displacement of the magnet.
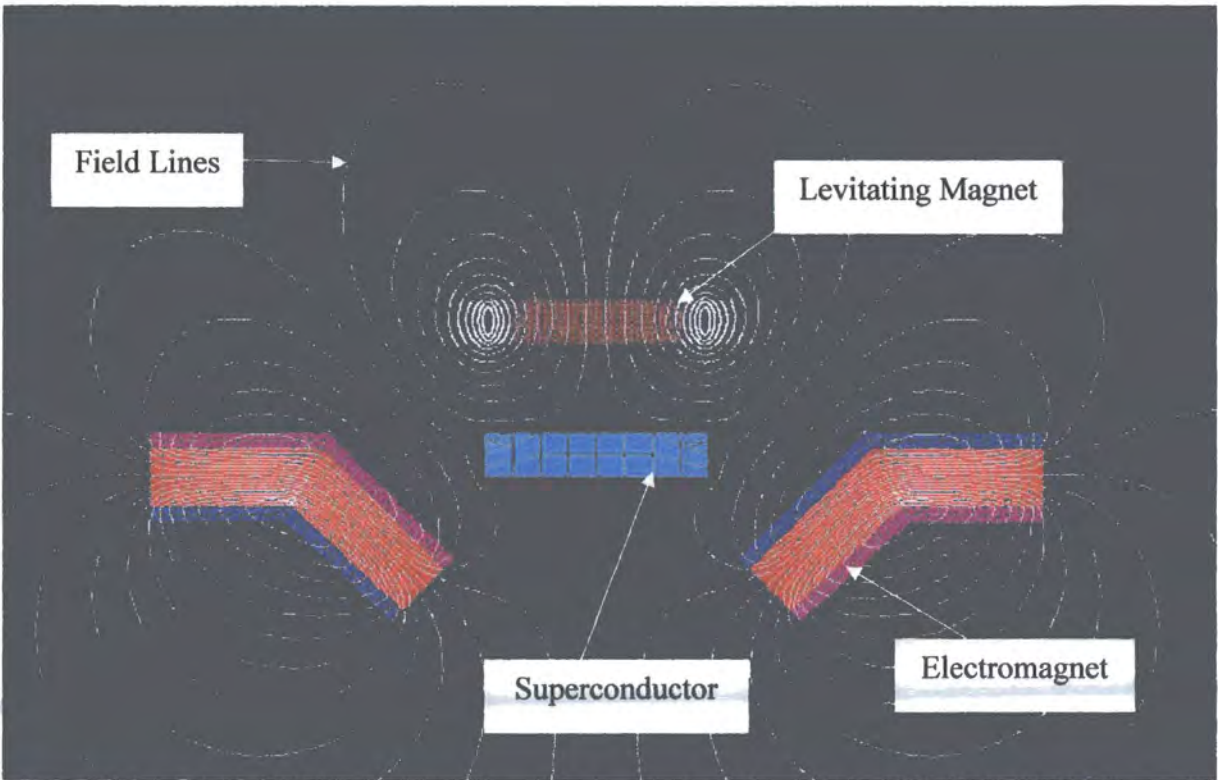


Figure 3.5.3: Model 1, $45^0$ Electromagnets.
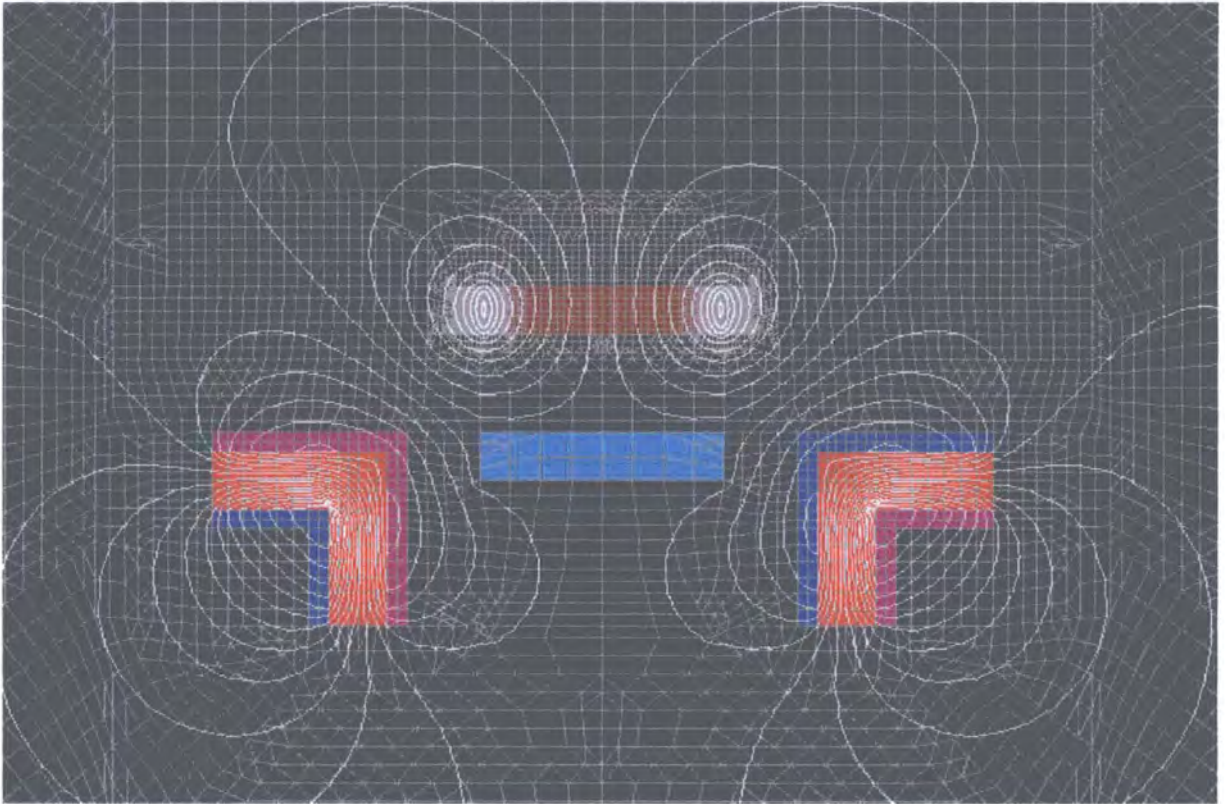
Figure 3.5.4: Model 2, $90^0$ Electromagnets.
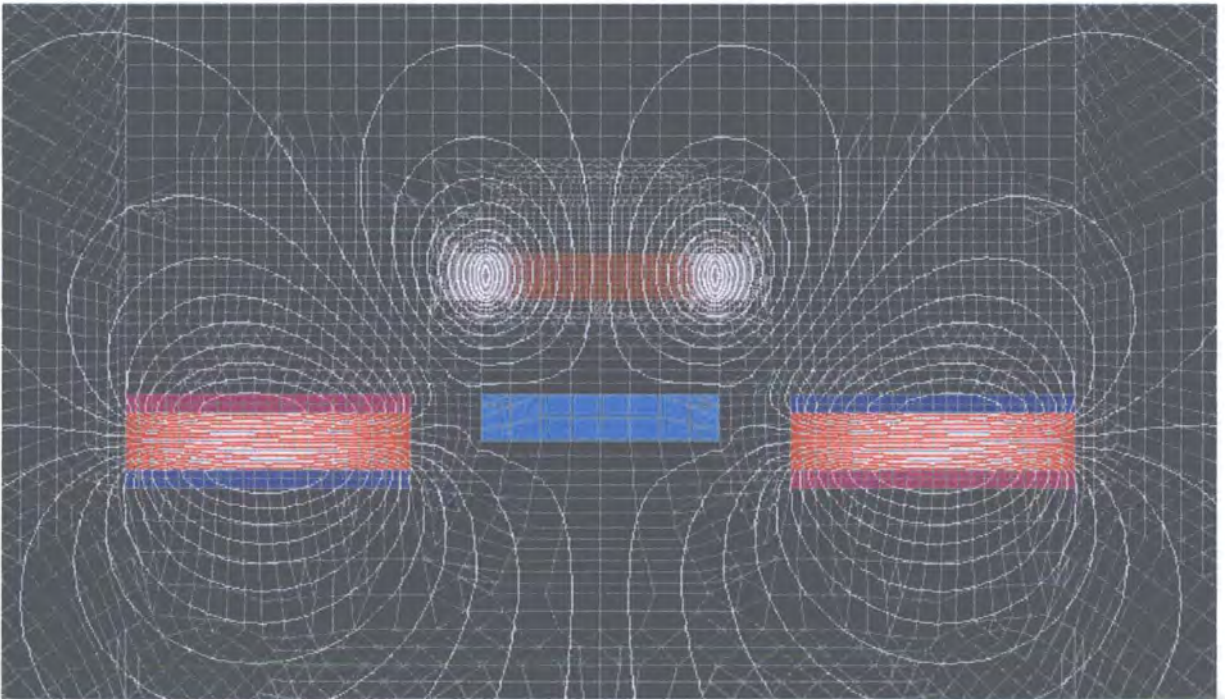


Figure 3.5.5: Model 3, Horizontal Electromagnets.
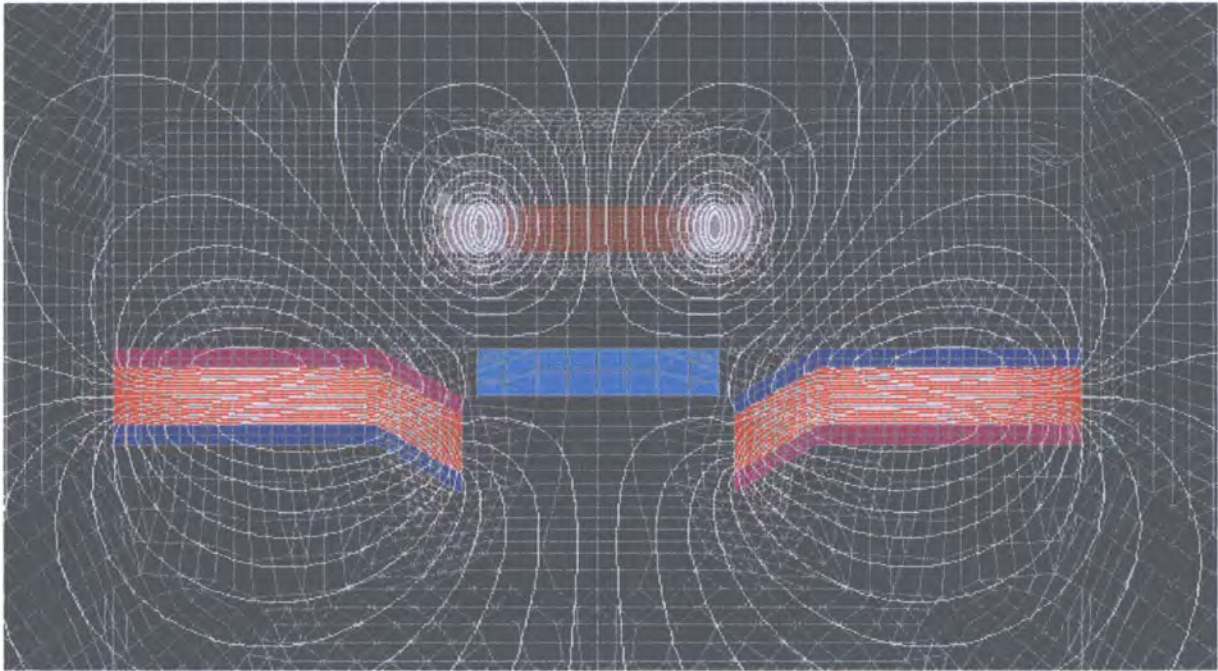
Figure 3.5.6: Model 4, $30^0$ Electromagnets.
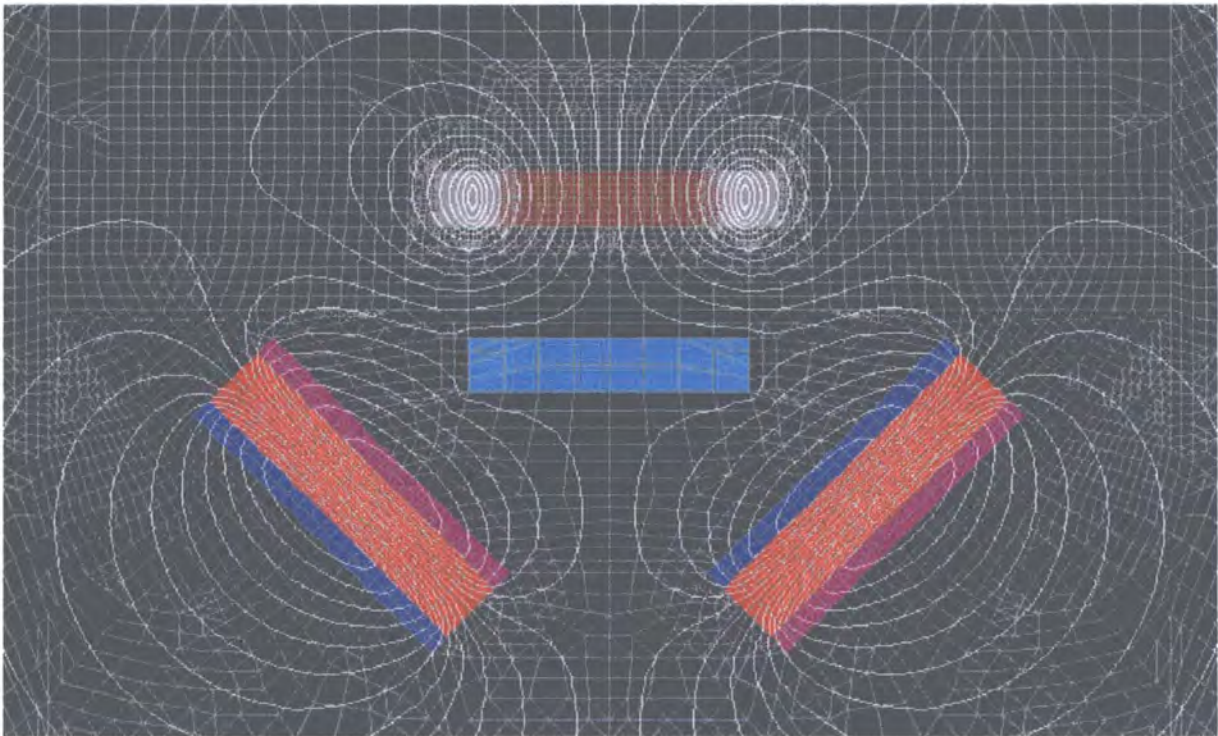


Figure 3.5.7: Model 5, Electromagnets at $45^0$ angle.
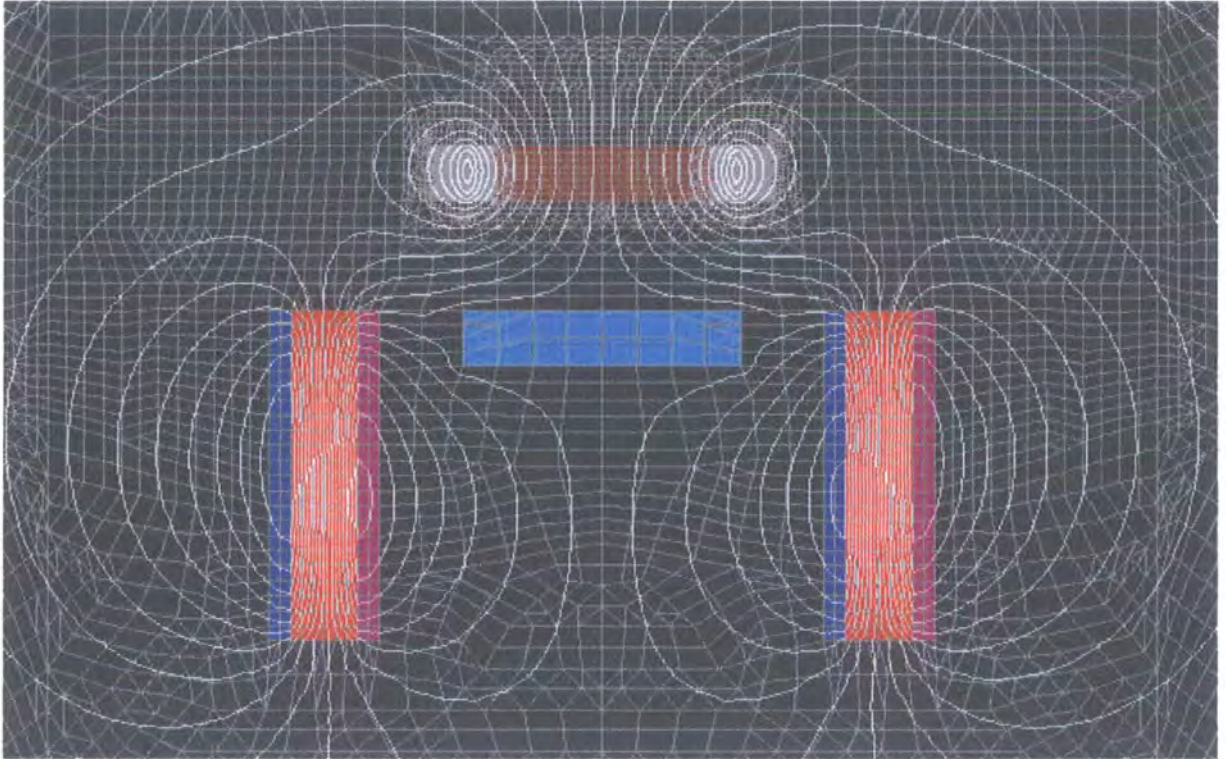
Figure 3.5.8: Model 6, Vertical electromagnets.

For the purposes of analysis the simulations were split into two families; one of straight electromagnets aligned horizontally and another group of angled electromagnets.

| Straight electromagnets | | Angled Electromagnets | |
|---|---|---|---|
| Model 3 | Horizontal | Model 3 | 0° |
| Model 5 | 45° | Model 4 | 30° |
| Model 6 | Vertical | Model 1 | 45° |
| | | Model 2 | 90° |

Table 3.5.1, Electromagnet groupings.
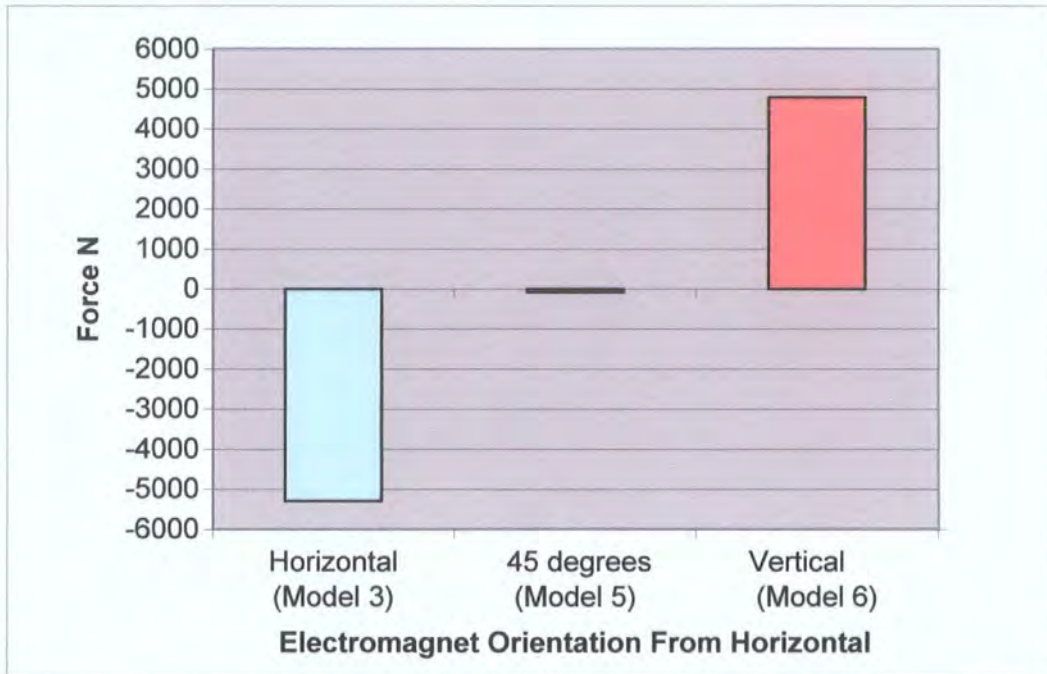
Figure 3.5.9, Horizontal restoring force acting on the levitating magnets from the straight electromagnets from a 2mm horizontal displacement.

The results shown in Figure 3.5.9 shows that the straight horizontal electromagnet (model 3) produces the largest restoring force, (negative forces being in the desired direction). The straight electromagnet angled at $45^\circ$ (model 5) produced very little restoring force and the straight vertical electromagnets (model 6) actually produced a destabilising force. The forces produced are very large due to the way 2D models are simulated in MEGA; a 2D model is considered a cross section of a 1m long 3D model. This result correlates with the angle of the flux lines produced by each of the simulations. The flux lines are steepest in figure 3.5.5 showing that they produce the greatest horizontal force on the levitating magnet.
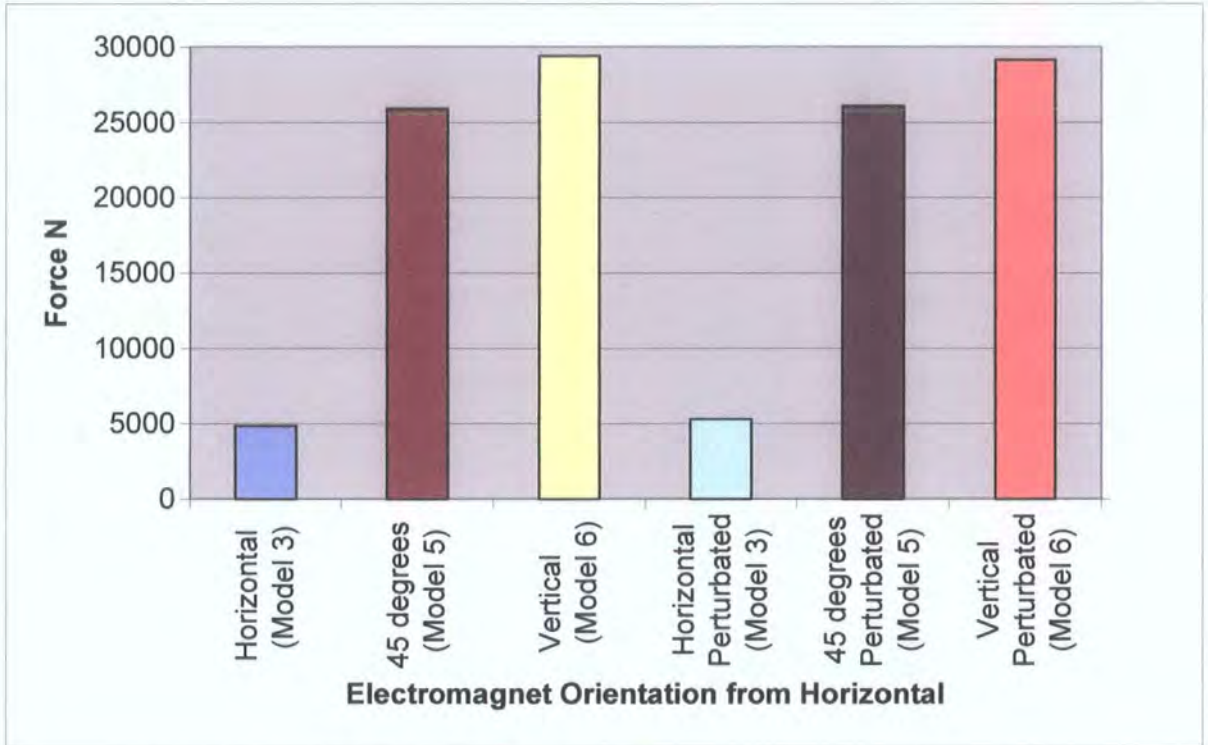
Figure 3.5.10, Total vertical forces acting on the levitating magnets with the straight electromagnets before and after applied horizontal perturbation.

The change in the vertical forces acting on the levitating magnet before and after a 2mm horizontal perturbation is applied to it are shown in figure 3.5.10. The vertical electromagnets produced the largest vertical force, the horizontal electromagnets produced the smallest vertical force, and the 45° electromagnets were between the two. This is due to the orientation of the poles of the electromagnets. When the electromagnets are vertical their south poles are directly opposed to the south pole of the levitating magnet and therefore produce the greatest vertical force. As the south poles of the electromagnets are turned away from the levitating magnet the vertical force is reduced. The changes in the vertical force when the displacement is applied for each of the models is small, as correspondingly are the turning moments produced on the levitating magnet as shown in figure 3.5.11. The smallest turning moment was produced by the straight horizontal electromagnets.
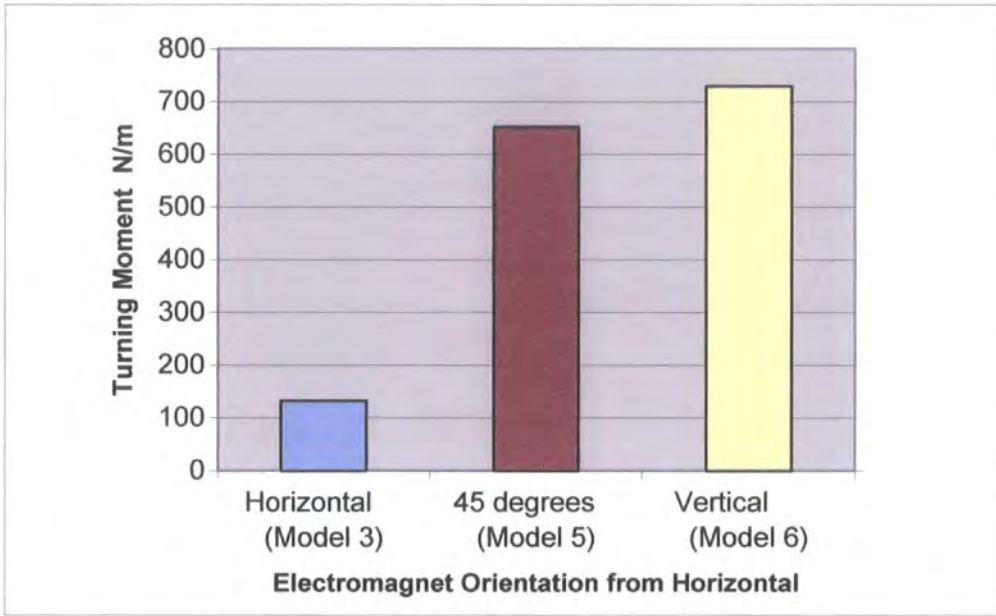
Figure 3.5.11, Turning moment acting on levitating magnet from the straight electromagnets.
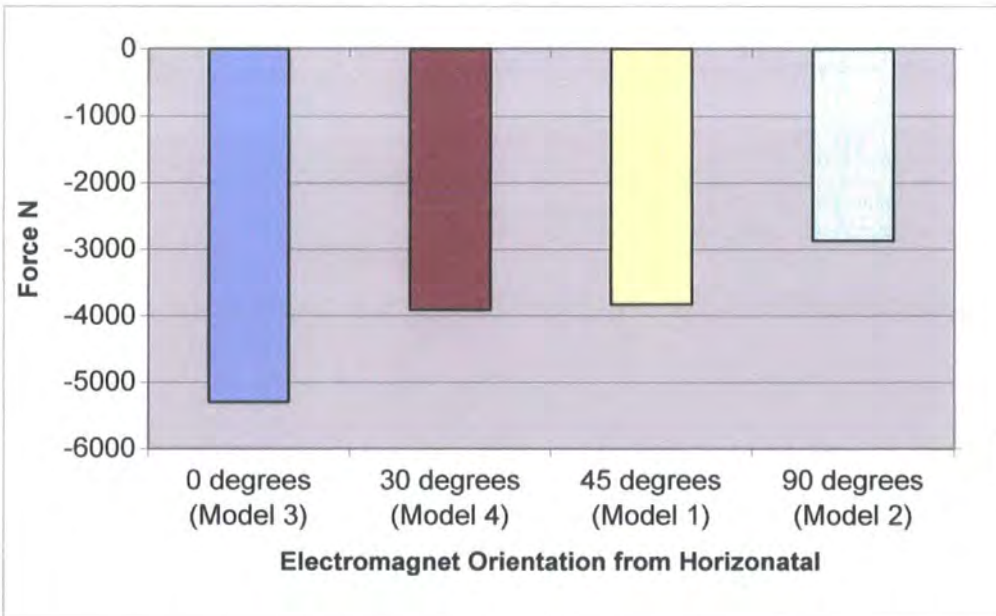


Figure 3.5.12, Horizontal restoring force acting on the levitating magnets from the angled electromagnets.

The horizontal restoring forces produced by an electromagnet with an increasing angle of bend are shown in figure 3.5.12. The largest restoring force was produced by model 3, the

electromagnets with the $0^o$ bend. Increasing the angle of the bend in the electromagnets caused the horizontal restoring force to be reduced.
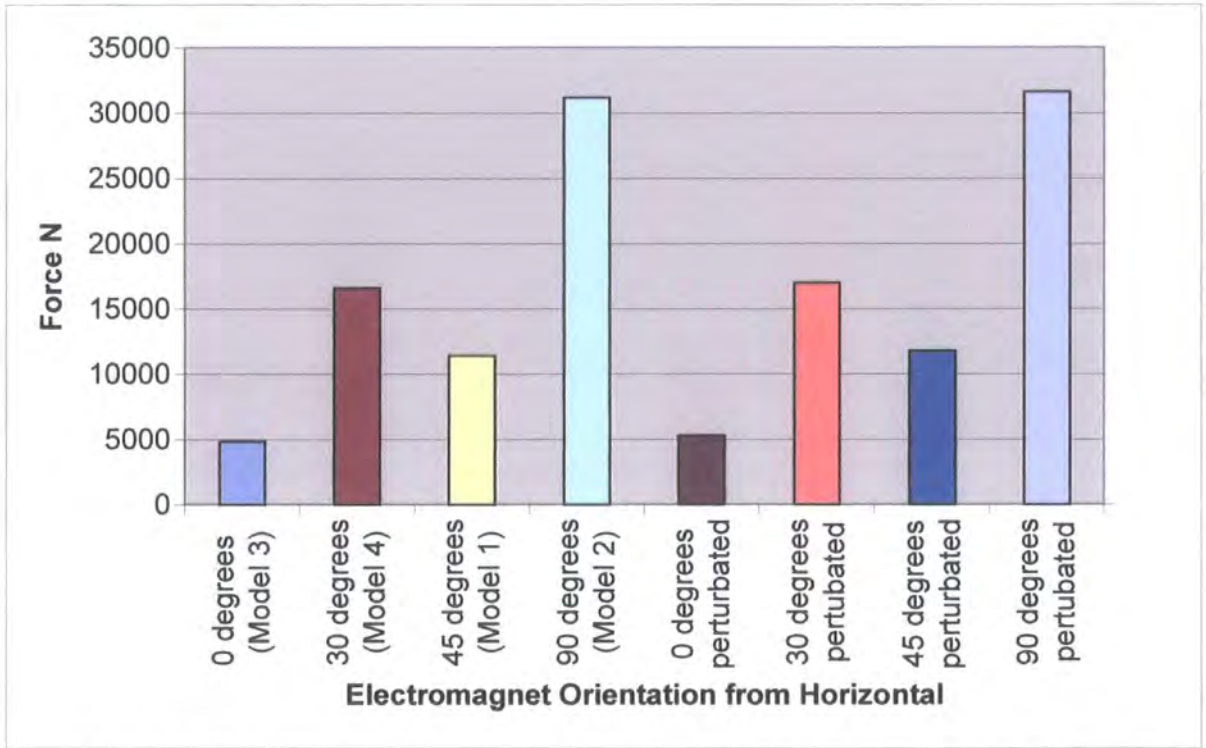


Figure 3.5.13, Total vertical forces acting on the levitating magnets from the angled electromagnets before and after applied horizontal perturbation.

The vertical forces for the angled electromagnets before and after a 2mm horizontal perturbation was applied are shown in figure 3.5.13. As with the straight electromagnets there was only a small change in the vertical force which was also reflected in the turning moments acting on the levitating magnets as shown in figure 3.5.14. As with the non-angled electromagnets the electromagnet with a $0^o$ degree bend (model 3) produced the smallest turning moment on the levitating magnet.
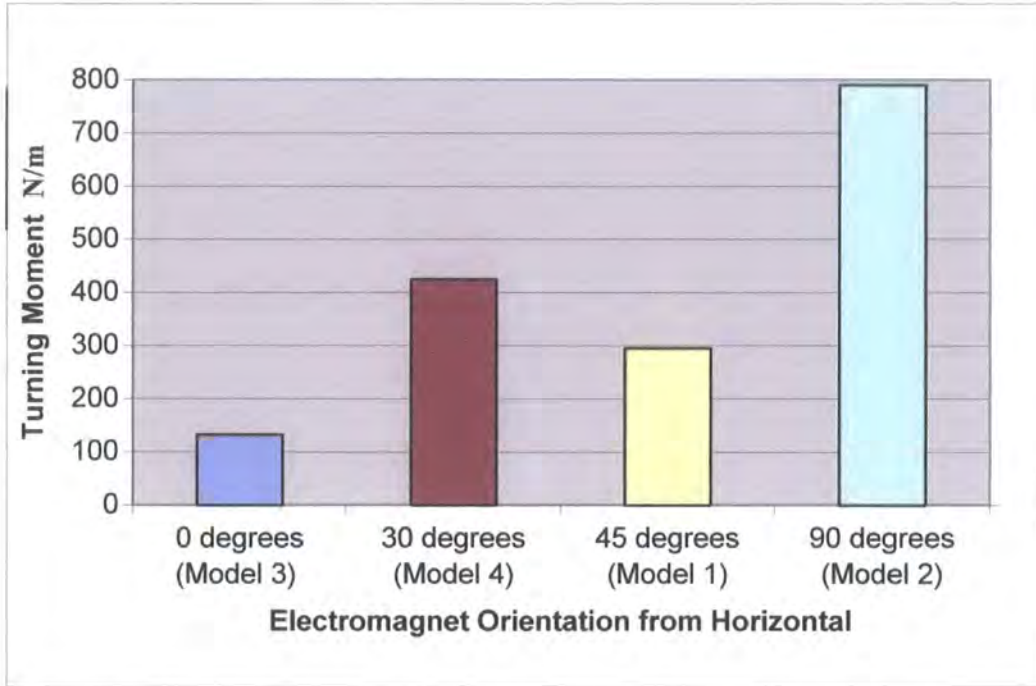
Figure 3.5.14, Turning moment acting on levitating magnet from angled electromagnets.

These results show that the most effective way of applying restoring force to the levitating magnets is through the use of straight horizontal electromagnets, model 3 as shown in figure 3.5.5, as these electromagnets produced the largest horizontal force. The horizontal electromagnets produced very little vertical force but changing the orientation to provide more vertical force results in a significant decrease in the horizontal restoring force. Vertical force is more easily produced through the use of permanent magnet levitation as will be discussed in chapter four. Therefore the electromagnets shown in figure 3.5.5 (model 3) were used to provide restoring force against the drag force produced by the air flow acting on the model.

Further simulations were then performed on model 1 and model 3, the electromagnets with 45° and 0° bends as shown in figure 3.5.3 and figure 3.5.5 respectively, to assess the effect of raising the height of the magnet by 10mm, from 20mm to 30mm. Figure 3.5.15 shows the results before and after the magnets were raised. The restoring force produced decreases as the height increases; this is due to the increased distance between the electromagnets and the levitating magnets. The ratios of the forces produced by the two simulations remains the same.
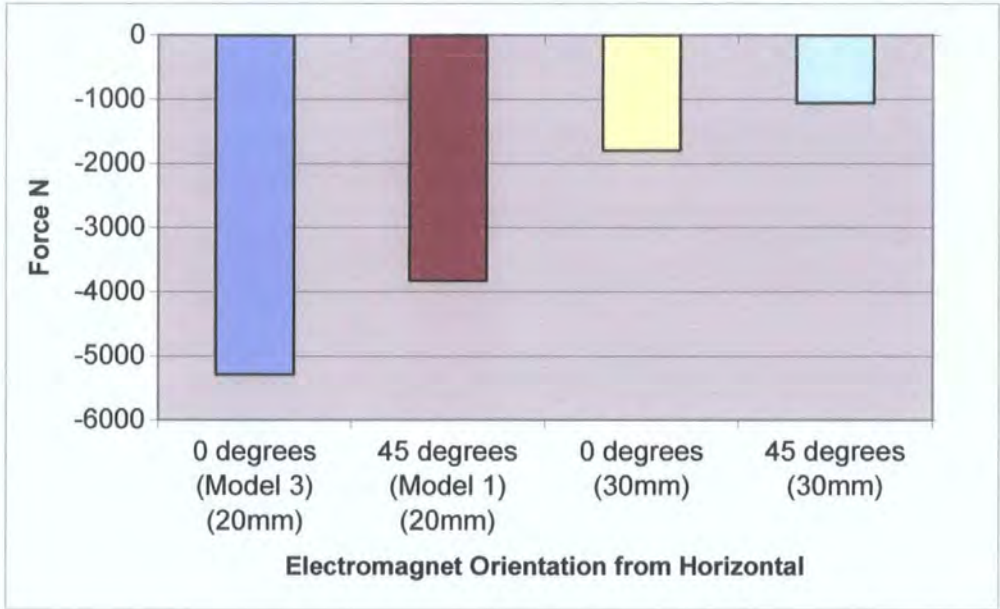
Figure 3.5.15 Restoring force acting on the levitating magnets at different heights.

3.6 Force Testing of the Superconducting Pod

Tests were then performed on the superconducting pod to measure the forces acting on the levitating magnets produced by the electromagnets and the superconductor. Different configurations were tested with the levitating magnets at a range of heights and the electromagnets at varying currents. The first set of tests was performed on a superconducting pod with four electromagnets equally spaced around the central cryostat as shown in figure 3.6.1. Each electromagnet had 400 turns.
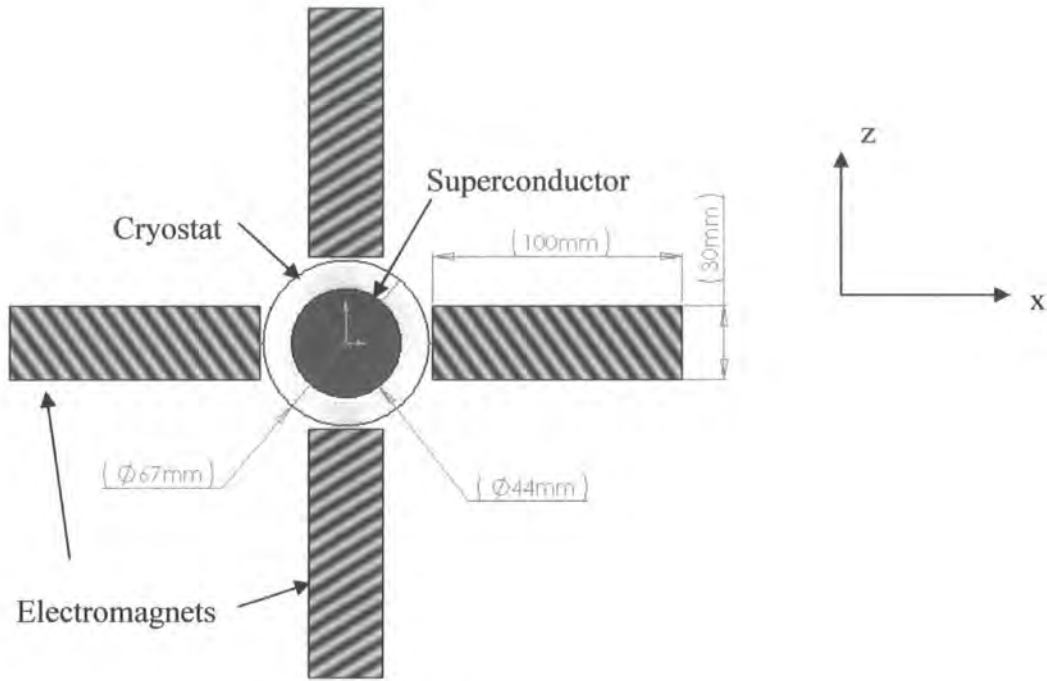
Figure 3.6.1, Layout of the Superconducting Pod

The superconductor, cryostat, and the electromagnets were then mounted on the six component force balance. Three neodymium-iron-boron permanents magnets, each with dimensions of 50mm x 50mm x 6mm, were mounted onto the traverse gear via a non-ferrous arm. The height between the superconductor and the magnets were set at 10mm, 15mm, 20mm, and 25mm. Liquid Nitrogen was added to the cryostat to field cool the superconductor and then the magnets were traversed 10mm in the x direction and the horizontal forces measured. For each height setting of the magnets five tests were performed with different currents applied to the electromagnets from 0A to 4A in 1A increments. Figure 3.6.2 through figure 3.6.5 shows the horizontal forces acting on the system
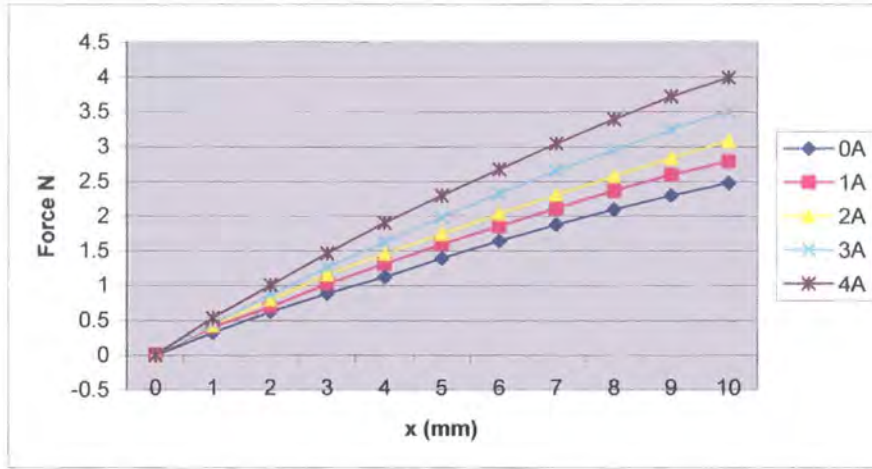
Figure 3.6.2, Horizontal forces at an air gap of 10mm
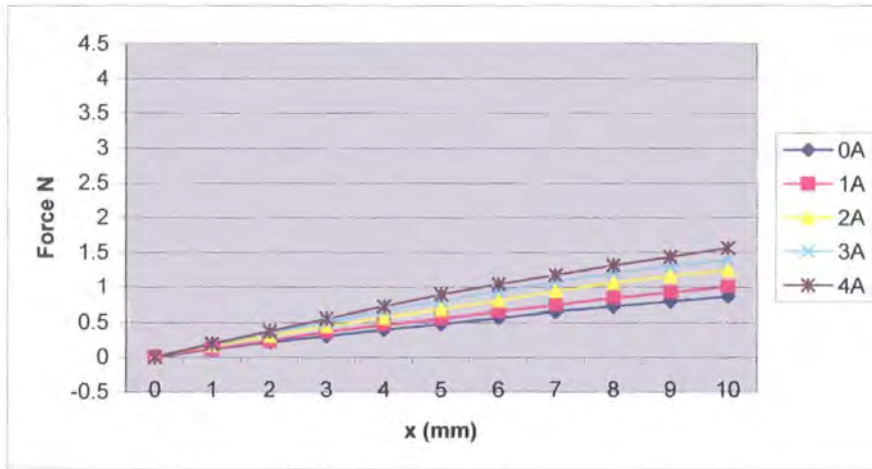


Figure 3.6.3, Horizontal forces at an air gap of 15mm
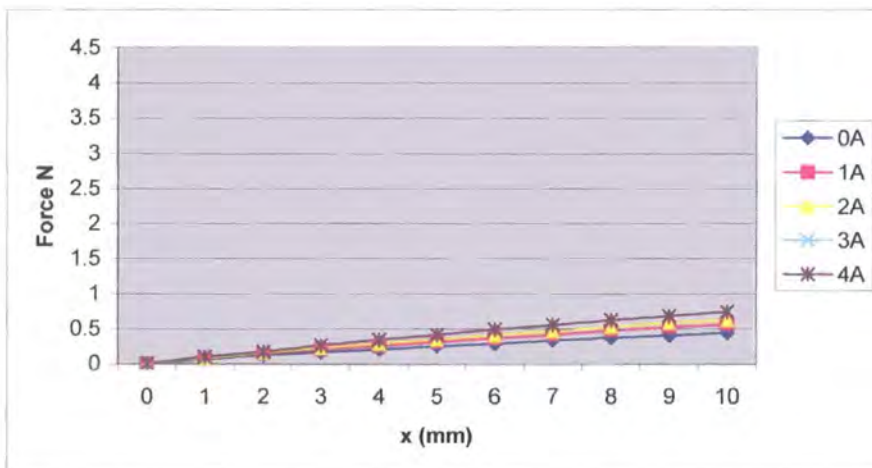


Figure 3.6.4, Horizontal forces at an air gap of 20mm.
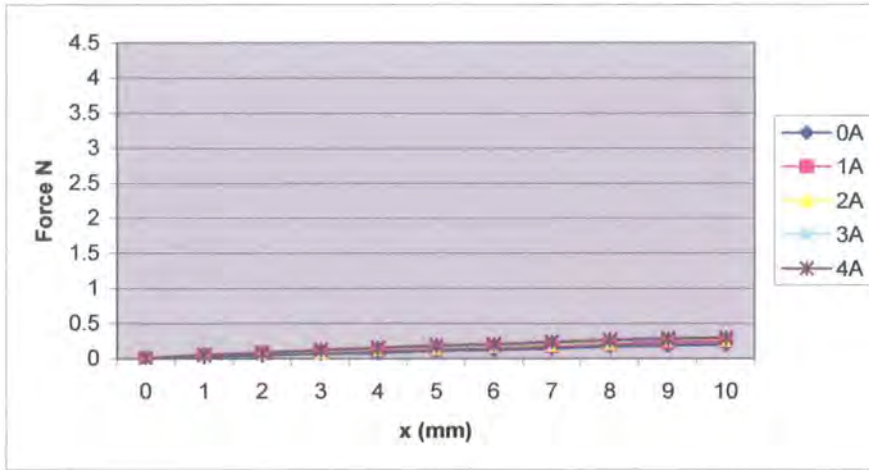
Figure 3.6.5, Horizontal forces at an air gap of 25mm.

Figure 3.6.2 shows that the superconductor on its own produces a significant horizontal restoring force when the magnets are moved from their central position with an air gap of 10mm. Increasing the current in the electromagnets increased the restoring force as expected. When the air gap of the system is increased the horizontal restoring force produced by both the superconductor and the electromagnets decreases. As the air gap increases the quantity of magnetic flux that encroaches into the volume of the superconductor during field cooling is reduced, reducing the flux pinning that occurs and therefore also the resistance to movement. As the air gap increases the horizontal restoring force produced by the electromagnets decreases because of the angle of interaction between their respective magnetic fields, and the resulting force acts in an increasingly vertical direction. The increased separation between the magnets also causes the forces between them to decrease.

This result is also shown in the results from the Electromagnet Finite Element Analysis of the superconducting pod in fig 3.5.5. The restoring force produced by the electromagnets was also being reduced by the effect of the other electromagnets. The opposing electromagnets work against each other by applying forces to opposite sides of the levitating magnets. In order to produce the maximum restoring force from the electromagnets, the test was repeated using only two electromagnets with an angle of 45 degrees between them equidistantly spaced either side of the x axis. The configuration of the new superconducting pod is shown in figure 3.6.6.
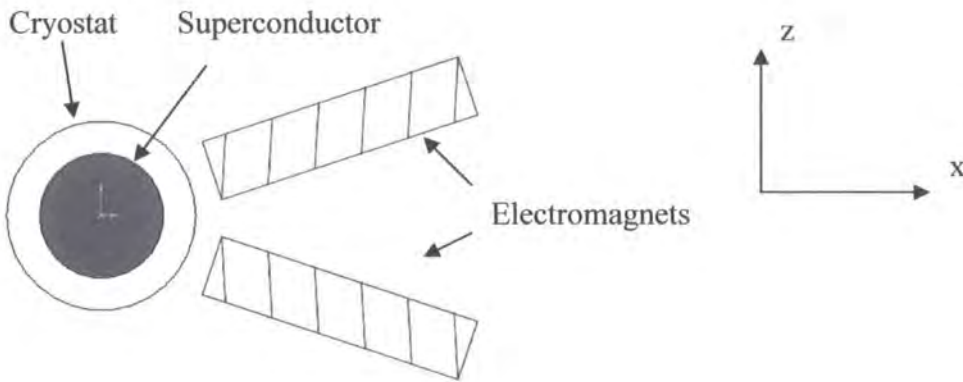
Figure 3.6.6, Configuration of Superconducting Pod for Maximum Restoring Force

Tests were performed with the air gap between the magnets and the superconductors at 10mm, and 30mm. The magnets were centred over the superconductor and liquid nitrogen added to the cryostat to field cool the superconductor. Each electromagnet had 100 turns and drew 4A. The magnets were then traversed 10mm in the x direction and the forces produced measured. The results are shown in figure 3.6.7.
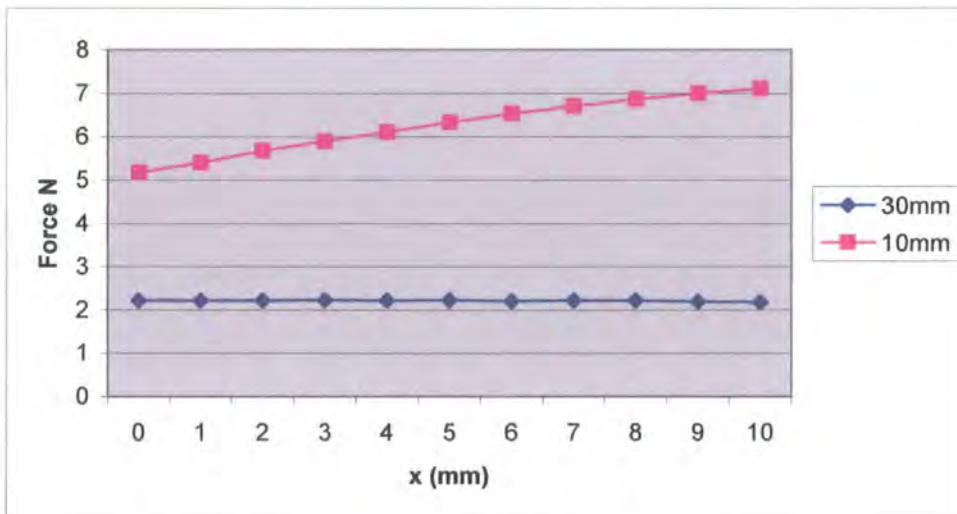


Figure 3.6.7, Horizontal Restoring Forces.

The results show a similar trend to the previous results with the restoring force produced being reduced as the height increases, however without the influence of the opposing electromagnets greater restoring force is achieved. These results show that the most efficacious way to provide restoring force is not to surround the levitating magnets with

electromagnets but to position electromagnets to provide restoring force in the opposite direction of the force applied by the air flow. This result corresponds with the results from the wind tunnel testing of single superconducting pod which had four evenly spaced electromagnets as shown in fig 3.2.3. With no air flow all the electromagnets were magnetised and the levitating magnets stayed stationary and centred. As the wind speed was increased and the magnets started to move backwards, the current in the front electromagnets was reduced allowing the magnetic fields from the rear electromagnets to push the magnets back to their central position. By positioning electromagnets around the levitating magnets the location of the magnets can be controlled by changing the currents in the required electromagnets so as not to have them opposing each other.

3.7 Three Pod Superconducting Levitation System

The superconducting pod described at the beginning of this chapter was tested in a wind tunnel at a wind speed of $20ms^{-1}$. The speed at which it was tested was not limited by the superconducting levitation system, but was the maximum speed at which the wind tunnel was capable of operating. The levitating magnets were encased in modelling foam to act as a bluff body to increase the drag acting on the superconducting levitation system, as the magnets on their own did not produce sufficient drag to test the limits of the system. Even so the size of the block of modelling foam that could be used to increase drag was not limited by the amount of horizontal restoring force that the system could supply, but by the amount of turning moment that the system could supply. The force acting on the levitating magnets was applied at a point higher than the central point of the magnets causing the magnets to pitch nose up. This turning of the levitating magnets was opposed by the electromagnets arranged around the system, but whilst the electromagnets could supply more than enough horizontal restoring force, they could not produce sufficient turning moment to oppose the force applied by the air flow.

This problem was rectified by expanding the superconducting levitation system to use three superconducting pods in its design. This resulted in an aspect ratio of the three pod system that was considerably greater than that of the single superconducting pod system. This change meant that the turning moment caused by the wind force acting on the levitating

magnets was opposed by the increased lever arm of the system. This acts to greatly reduce the effect of any pitching or rolling moment acting on the system, considerably increasing its stability. The three pod system was built and tested on the bench; figure 3.7.1 shows the arrangement of the superconductors and electromagnets. Figure 3.7.2 shows the three pod system in operation. Optical benches were used to support the system as they incorporated slots on the top and sides to which platforms to support the cryostats and electromagnets could be mounted. The optical benches were also constructed out of aluminium and as such were suitable for use in applications involving strong magnetic fields. The three superconducting bulks were mounted in separate double insulated cryostats supported by aluminium brackets attached to the optical benches. Each cryostat was fed from a main central cryostat situated to the side of the system to allow operation of the system with an aluminium floor in place. The electromagnets were mounted to the rails running along the top of the optical benches using adjustable aluminium brackets. Figure 3.7.1 shows the layout of the three pod system.
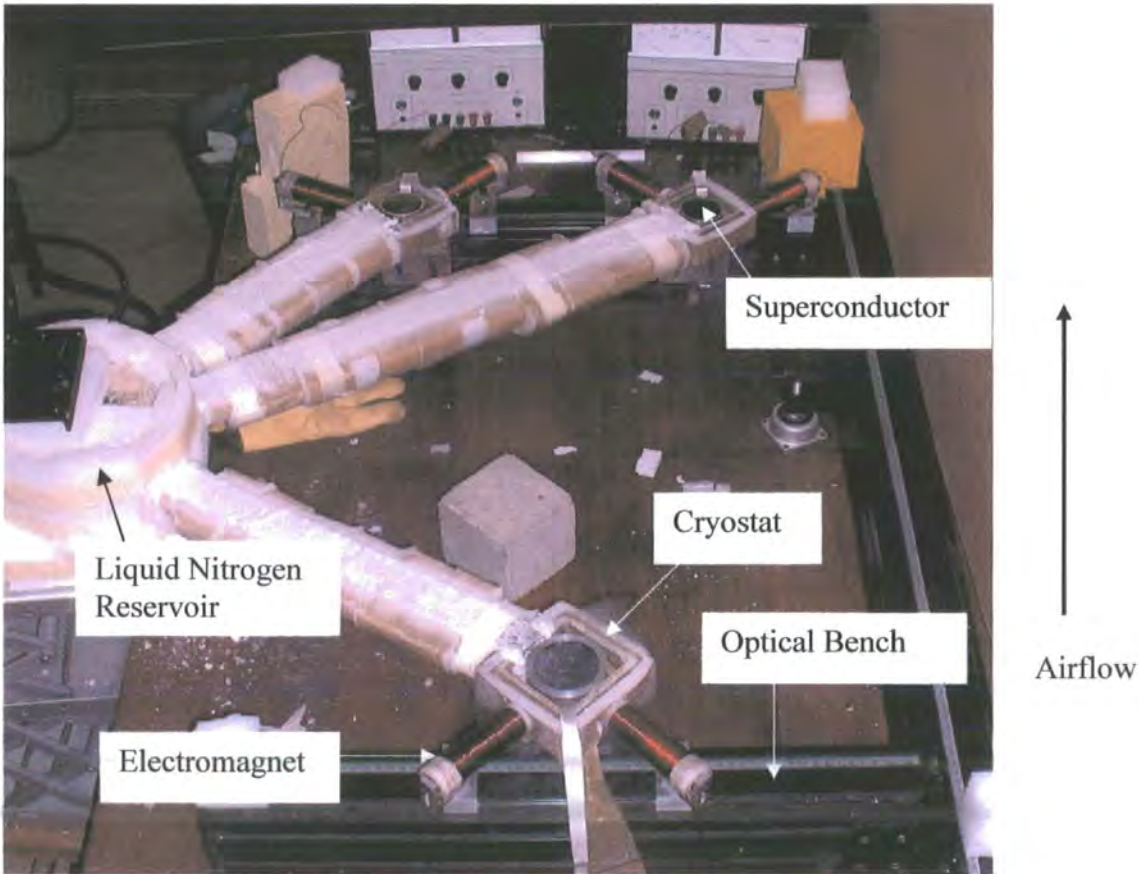


Figure 3.7.1, The three pod system layout.

A frame to support the levitating magnets was constructed out of three L section aluminium bars. The bars were connected by bolts on top of the mounting brackets for the neodymium-iron boron magnets, as shown in figure 3.7.2. Nine neodymuium-iron-boron magnets were used, three for each superconducting pod, with dimensions of 50mm x 50mm x 6mm.
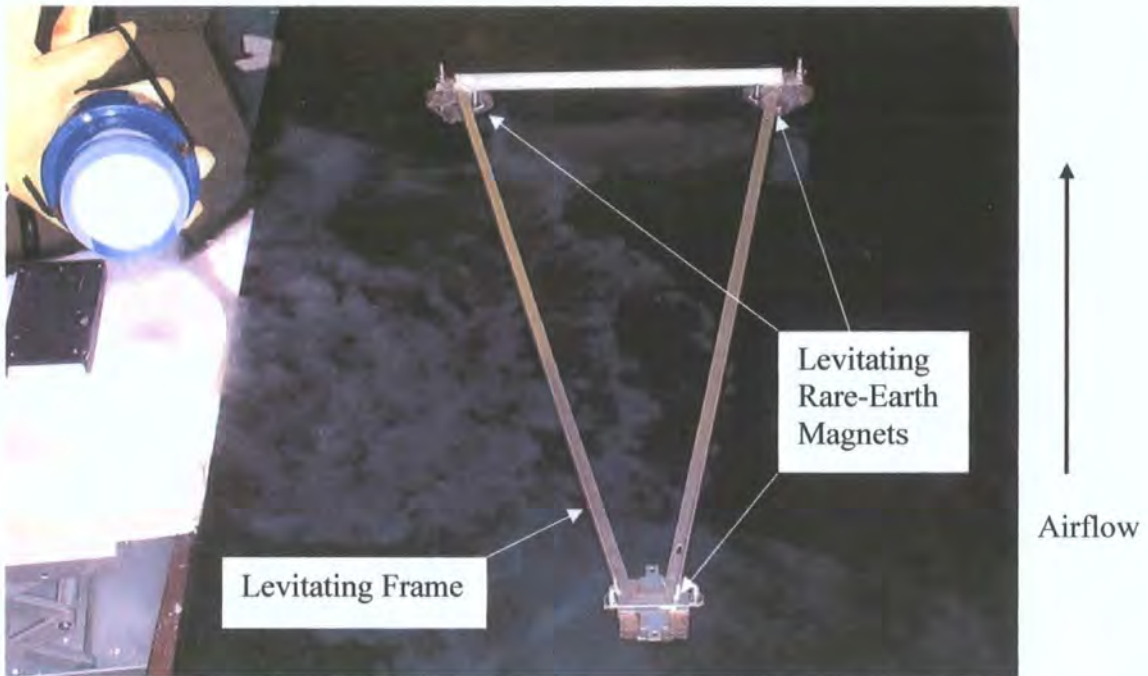


Figure 3.7.2 Three pod system levitating with aluminium floor in place.

Stable levitation was achieved with the three pod system; figure 3.7.2 shows the frame and the rare-earth magnets levitating. Also shown is the anodised black aluminium sheet placed between the superconducting pods and the levitating frame to act as the floor of a wind tunnel. Figure 3.7.2 also shows liquid nitrogen being added to the main feeder cryostat to keep the superconductors cooled below their transition temperature. As with the small scale system the position of the floating magnets could be controlled by changing the current in the electromagnets that surrounded each pod. Due, however, to the considerably increased aspect ratio of the three pod system the changing currents in the electromagnets did not cause the levitating frame to pitch, and the movement of the frame was solely in the horizontal plane.

Six electromagnets were used in the three pod prototype, two for each superconducting pod, as shown in figure 3.7.1. Each electromagnet was initially positioned at $\pm 45^0$ to the

direction of the air flow to allow for maximum stability of the levitating model. This configuration meant that any movement of the frame brought it closer to a set of the electromagnets which caused the force acting on the frame to increase, pushing the frame back to its central position. The four electromagnets at the back of the test rig were connected to a separate power supply to the two electromagnets at the front to allow independent control of the current in the electromagnets. Tests were carried out to show that increasing the current to the rear electromagnets and reducing the current to the forward electromagnets caused the frame to move forward and vice versa. The rear electromagnets were then rewired to have both left facing electromagnets connected to one supply and both right facing electromagnet connected to the other supply. The levitating frame could then be moved side to side by controlling the current in the electromagnets. The only limit to the accuracy of this movement is the limit of the fine adjustment of the current output of the power supplies. During these tests the levitating frame remained level at all time, any turning moment acting on levitating magnets from the electromagnets was resisted by the large aspect ratio of the system. Further tests on the three pod system were carried out to determine the drag force that the system could withstand. It was found that there was a linear relationship between the current through the electromagnets and the resisting force. In these tests the maximum drag force that the system could resist was limited by the number of turns in the electromagnets and the maximum current that the power supplies were able to produce. The frame was field cooled at an air gap of 20mm and each of the electromagnets at the rear of the system had 400 turns and drew 4.5A. With this configuration the system was able to withstand 7.5N of drag force before moving from its central position.

## 3.7.1 Large Scale Superconducting Levitation System

Figure 3.7.3 shows a potential configuration for a large scale superconducting levitation system. The layout is based on an extended version of the three pod system described above. The central section of the system is tiled with YBCO superconducting bulks which would correspond to an equivalent number of rare-earth magnets mounted inside the vehicle to be supported. Electromagnets would be placed around the central superconducting section to allow positional control of the vehicle and oppose the

destabilising force of the air flow acting on the model at a range of yaw angles. However such a system would be limited in the maximum ground clearances that it could operate at due to the air gap between the rare-earth magnets and superconductors at which flux pinning can occur.
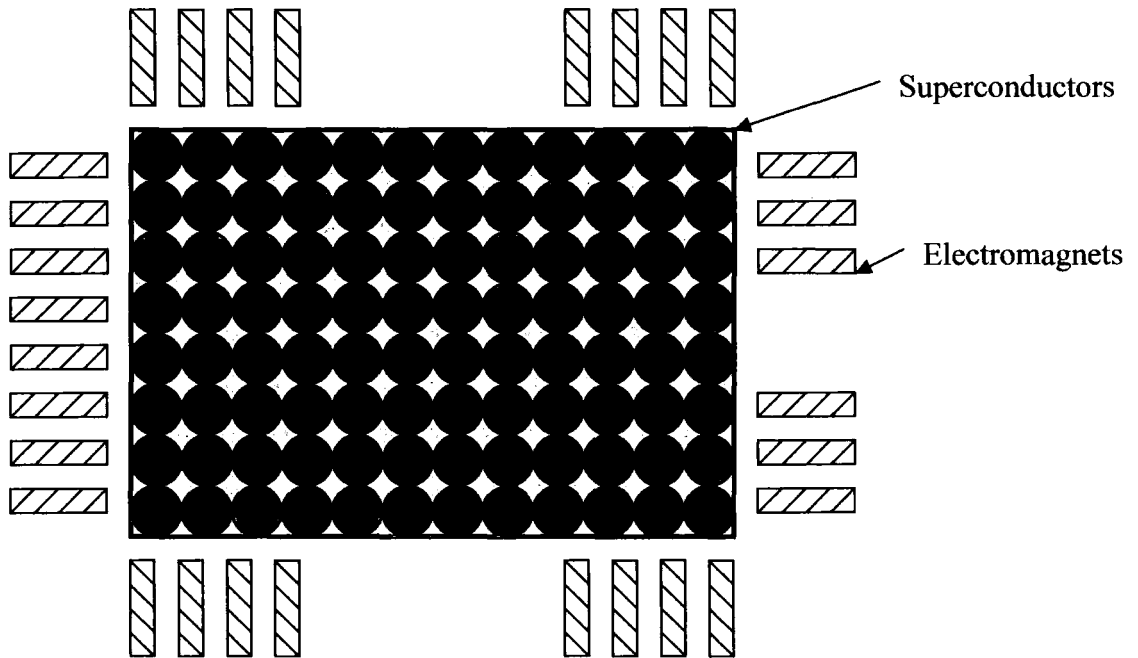


Figure 3.7.3, Potential configuration for a large scale superconducting levitation system.

## 4. Design and Development of Magnetic Reinforcement

4.1 Introduction

This chapter details the invention and analysis of the magnetic "rail" system that was utilised to provide permanent magnet levitation to augment the superconducting levitation. The magnetic "rail" increases the usefulness of permanent magnet levitation by reducing its destabilising influence. A considerable number of different magnetic "rail" configurations were constructed and tested using a six component force balance and a traverse gear. Ring magnets were also tested to ascertain their usefulness in a levitation application. The "Levitron", a permanent magnet system that achieves stable levitation using a ring magnet base and a spinning levitating disc magnet, was analysed to assess its potential for levitation applications.

4.2 Magnetic Reinforcement of Superconducting Levitation

A scaled up version of the three pod system, that was designed and tested using only superconductors for levitation as discussed in chapter 3, would be capable of supporting a 40% scale Formula 1 car for aerodynamic testing operating at corresponding levels of lift and drag. However such a system would place limitations on the maximum ride height of the model that could be achieved; superconducting levitation can only operate at a limited ground clearance that is determined by the strength of the magnetic field produced by the levitating magnets. The mirror effect of the superconductor, as discussed in chapter 2, means that the levitating magnet experiences a force as if from another opposing magnet that is twice as far away as the superconductor. If the levitating magnet is a similar size to that of the superconductor then it experiences a force as if from an opposing magnet that is smaller than itself as only part of the magnetic flux from the magnet is "mirrored" in the superconductor as the flux extends beyond the diameter of the superconductor.

Two neodymium rare-earth magnets are capable of repelling each other with considerably more force than that produced by a rare-earth magnet and a superconductor, and at a much greater air gap between the two. This is because instead of the levitating magnet

experiencing a force akin to that of a smaller opposing magnet twice the distance away, as in superconducting levitation, the levitating magnet will experience a force from a larger magnet acting from floor level. This means that augmentation of the superconducting levitation system with magnet on magnet levitation would extend the air gap over which the system would be able to operate and also increase the downforce that the system can support, considerably increasing the usefulness of the levitation system.

When two permanent magnets are positioned directly over each other with like magnetic poles facing so that they repel, they are in a state of unstable equilibrium. Any deviation from this stable point, other than directly towards or away from each magnet, will result in a net force which acts to further destabilise the magnets. Earnshaw's theorem (Earnshaw 1842) describes how a point charge cannot be stably levitated using any combination of static electric charges. The use of one permanent magnet levitating over another permanent magnet to bolster the system's ability to compensate for downforce will introduce instability. This instability will reduce the ability of the system to compensate for the force acting on it due to the air flow. The more magnet only levitation that is used the more unstable the system will become. Milgrom (1998) suggests that, while Earnshaw's theorem applies to point charges or a dipole, it may be possible to suspend point bodies of finite charge, or extended test-charge bodies where the large aspect ratio of linked dipoles stabilises the levitating system in pitch and roll. The Levitron is an example of stable levitation achieved using solely permanent magnets, (Gov et al, 1999, Dullin and Easton, 1999).

Reducing the instability of the magnet-only levitation would improve the useful range of the levitating system as the extra instability introduced reduces the amount of useful damping intrinsic to the superconducting levitation that could be used to counter the force acting on the levitating magnets due to the air-flow. Reducing the instability of permanent magnet levitation would also increase the load-bearing capability of the system as destabilising forces between two magnets increase as the force acting between them also increases.

## 4.3 The Magnetic "Well"

The electromagnets that were used to compensate for the force of the airflow acting on the levitating magnets in the prototype superconducting pod were designed to create a magnetic "well" in one plane. This "well" supported the levitating magnets against the destabilising force of the air-flow, with the superconductor plugging the hole in the bottom of the "well" and stabilising the levitating magnets in pitch and roll. Extrapolation of this system suggested that bringing the electromagnets closer together should allow stable levitation in two degrees of freedom without the need for the superconductor. In order to test this scenario a rare-earth magnet was attached to a gimbal via a 1m long non-ferrous arm restricting it to two degrees of freedom and positioned over two electromagnets in close proximity of each other as shown in figure 4.3.1. The levitating magnet should be able to balance on the magnetic fields produced by the electromagnets as shown in figure 4.3.2.
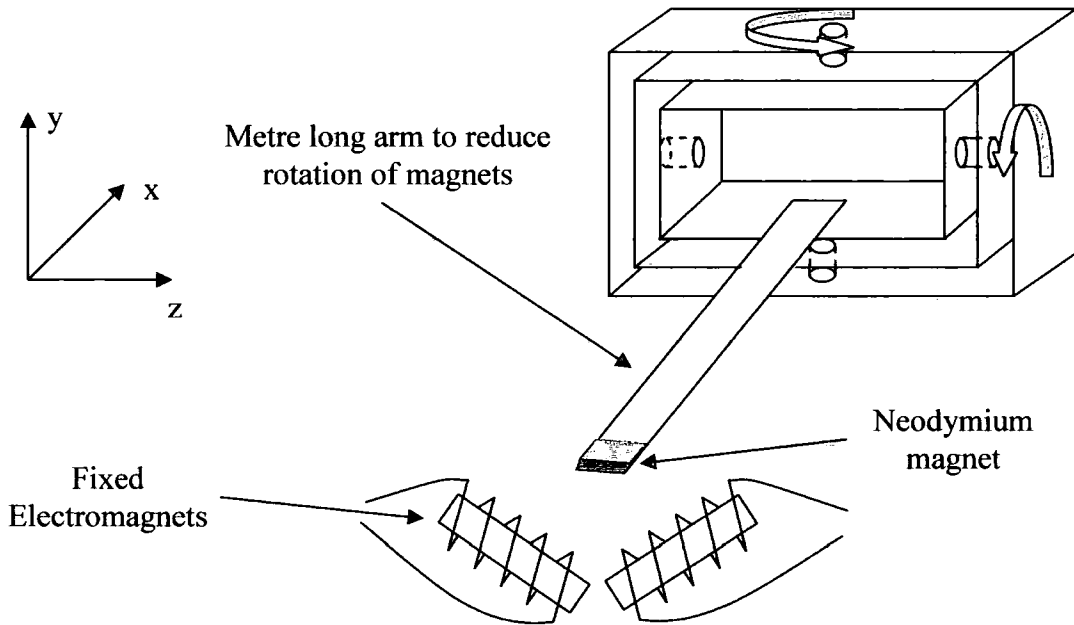


Figure 4.3.1, Levitation with electromagnets restricted to two degrees of freedom.
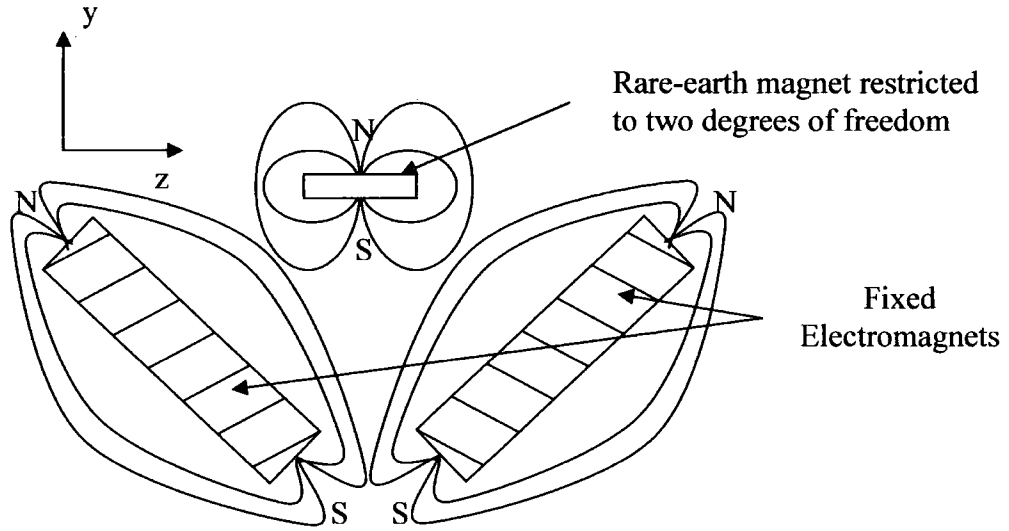
Figure 4.3.2, Magnetic fields for the two degrees of freedom configuration.

However when the configuration shown in figure 4.3.2 was tested it was found that the available power supplies were not strong enough to magnetise the electromagnets sufficiently to prevent the rare-earth magnet from being attracted to the steel cores of the electromagnets. This was due to the low coercivity of the electromagnets. The same experiment was then tried using only rare-earth magnets, although instead of having the two fixed magnets at an angle as with the electromagnets, they were laid flat as shown in figure 4.3.3. This arrangement proved to be stable and capable of supporting a range of loads. The configuration of the three magnet system produces an arrangement that was stable in both the y and z direction but that is unstable in the x direction and in pitch and roll, and neutrally stable in yaw.
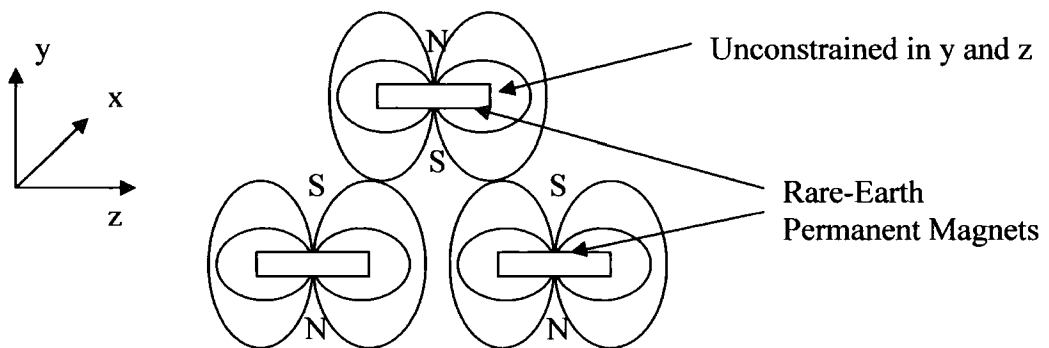


Figure 4.3.3, Two degree of freedom levitation with permanent magnets

The height above the fixed magnets at which the magnets attached to the gimbal were in equilibrium could be varied by changing the size of the gap between the two fixed magnets. By making the gap between the two fixed magnets smaller, the height at which the magnets attached to the gimbal were in stable equilibrium was increased. Conversely, increasing the gap between the two fixed magnets decreased the height at which stable equilibrium of the magnets on the gimbal was achieved. For a given number of magnets on the gimbal there is a limit to the range of spacing between the two fixed magnets that allow the system to be stable. If the two fixed magnets are positioned too close together then the magnets on the gimbal will become unstable and are pushed to one side by the fixed magnets. If the two fixed magnets are placed too far apart they are no longer able to support the weight of the magnets on the gimbal and the magnets will fall down.

4.3.1, Stability of the three magnet system.

Measurements of the load bearing capability of the three magnet system were then taken. The configuration of the magnets was the same as in figure 4.3.3. The two lower magnets were fixed, while the levitating magnet was attached to a gimbal restricting it to movement in two degrees of freedom. The distance in the z direction between the fixed base magnets was varied, and a range of loads were added to the levitating magnet, and for each permutation the height at which stable equilibrium was achieved was measured. The results are shown in table 4.3.1. Three Neodymium-Iron-Boron permanent magnets were used, each having dimensions of 50mm x 50mm x 6mm. The levitating magnet was attached to a gimbal via a 1m long non-ferrous arm to minimise the rotation of the magnet caused by any displacement. The gimbal was counterbalanced to negate the effect of the weight of the arm. Weights were added directly over the levitating magnet using a non-ferrous spacer to prevent any interference effects.

The results show a stable region where the magnet on the gimbal is in stable equilibrium. The stable zone is a compromise between stability and the load that the system can support. When the fixed base magnets are positioned closer together, the magnets can support more load at a given height. However this also causes the system to become less stable, as the

magnetic fields produced by the magnets are squashed together reducing the size of the "well" in which the magnet on the gimbal can sit.

| Distance between fixed magnets (mm) | | 5 | 10 | 15 | 20 | 25 | 30 | 35 |
|---|---|---|---|---|---|---|---|---|
| Vertical Force on arm (N) | Levitation height (mm) | | | | | | | |
| 0 | | Unstable | Unstable | Unstable | Unstable | 53 | 48 | 0 |
| 0.5 | | Unstable | Unstable | Unstable | 55 | 49 | 38 | 0 |
| 1.0 | | Unstable | Unstable | Unstable | 50 | 44 | 0 | 0 |
| 1.5 | | Unstable | Unstable | Unstable | 45 | 39 | 0 | 0 |
| 2.0 | | Unstable | Unstable | Unstable | 42 | 32 | 0 | 0 |
| 2.5 | | Unstable | Unstable | Unstable | 38 | 27 | 0 | 0 |
| 3.0 | | Unstable | Unstable | Unstable | 35 | 0 | 0 | 0 |
| 3.5 | | Unstable | Unstable | 43 | 33 | 0 | 0 | 0 |
| 4.0 | | Unstable | Unstable | 37 | 28 | 0 | 0 | 0 |
| 4.5 | | Unstable | Unstable | 35 | 25 | 0 | 0 | 0 |
| 5.0 | | Unstable | Unstable | 33 | 22 | 0 | 0 | 0 |

Table 4.3.1, Stable regions of the three magnet system

The forces produced by the three magnet system were then mapped by mounting the two base magnets onto a six component force balance and mounting the third magnet on a traverse gear via a non-ferrous arm. The force balance and traverse gear are described in chapter 3. The magnets were mounted to the traverse gear via a rigid non-ferrous arm.

4.4 Force measurements of the Magnetic "Rail"

Several force testing arrangements of the magnetic rail were tested, based on the three magnet layout shown below in figure 4.4.1. Rails of different constituent magnets were tested, using magnets of varying sizes, the different compositions of each test are listed below in table 4.4.1.
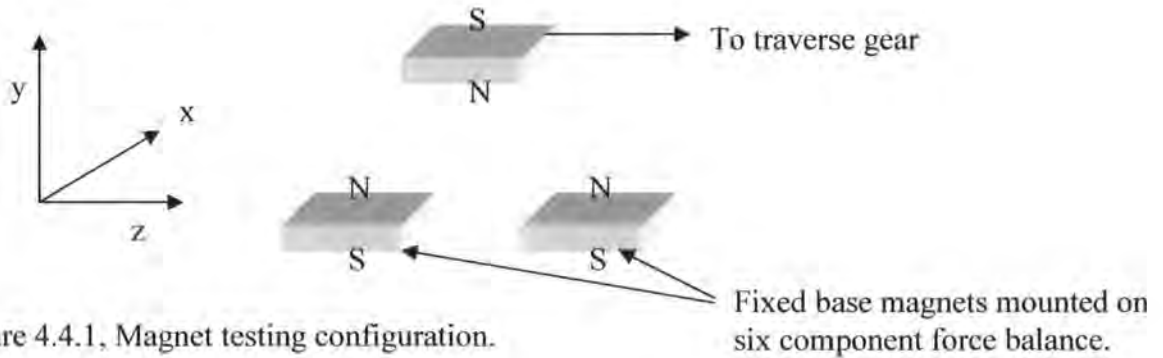


Figure 4.4.1, Magnet testing configuration.

Fixed base magnets mounted on six component force balance.

| Rail | Dimensions of fixed base magnets (mm). | Dimensions of levitating magnet (mm). | Gap between fixed magnets (mm). |
|---|---|---|---|
| 1 | 50 x 50 x 6, 50 x 50 x 6. | 50 x 50 x 6. | 20 |
| 2 | 50 x 50 x 6, 50 x 50 x 6. | 12 x 30 x 5. | 16 |
| 3 | 50 x 50 x 6, 50 x 50 x 6. | 12 x 30 x 5. | 14 |
| 4 | 50 x 50 x 6, 50 x 50 x 6. | 12 x 30 x 5. | 12 |
| 5 | 50 x 50 x 12, 50 x 50 x 12. | 12 x 30 x 5. | 16 |
| 6 | 50 x 50 x 6, 50 x 50 x 6. | 12 x 30 x 10. | 16 |
| 7 | 50 x 50 x 6, 50 x 50 x 6. | 12 x 30 x 10. | 18 |

Table 4.4.1, Magnetic rail testing configurations.

For each configuration a 50mm by 50mm horizontal grid was traversed in 2mm height increments from a height of 20mm to 40mm around the centre point of the fixed magnets. The forces acting on the magnets at each position were measured. The results are shown below.

4.4.1, Force testing on rail configuration 1.

Forces in the x direction for rail configuration 1;
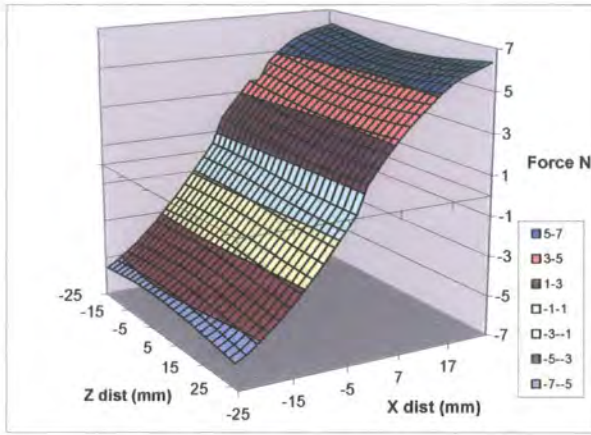


Figure 4.4.2; Force in x at 20mm height
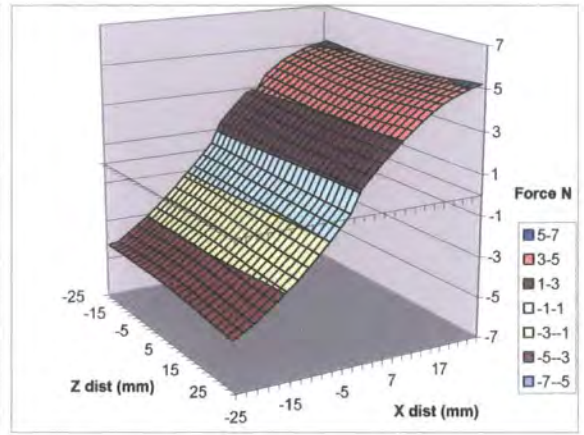


Figure 4.4.3; Force in x at 24mm height
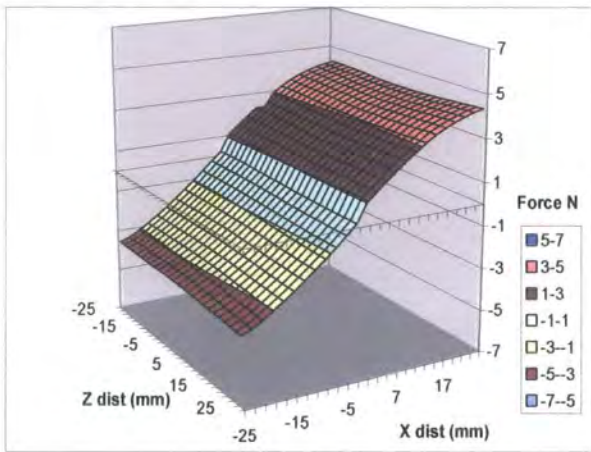


Figure 4.4.4; Force in x at 28mm height
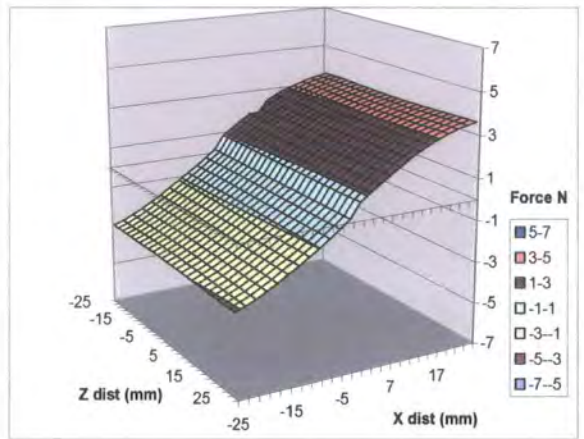


Figure 4.4.5; Force in x at 32mm height
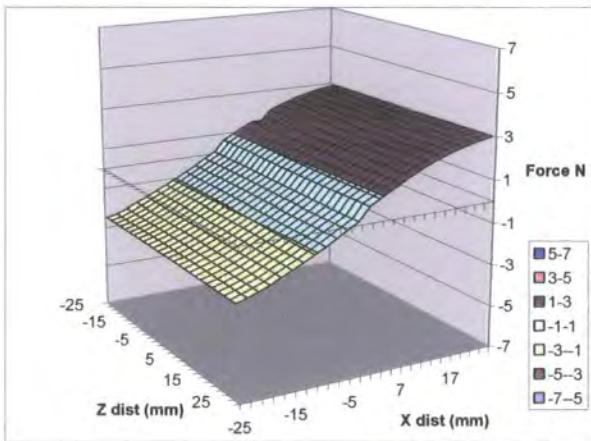


Figure 4.4.6; Force in x at 36mm height
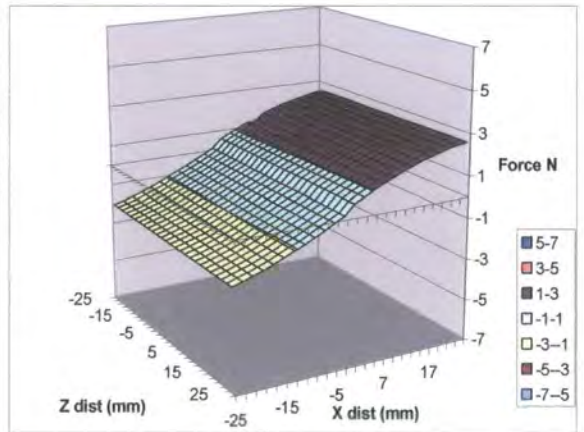


Figure 4.4.7; Force in x at 40mm height

Forces in the y direction for rail configuration 1;
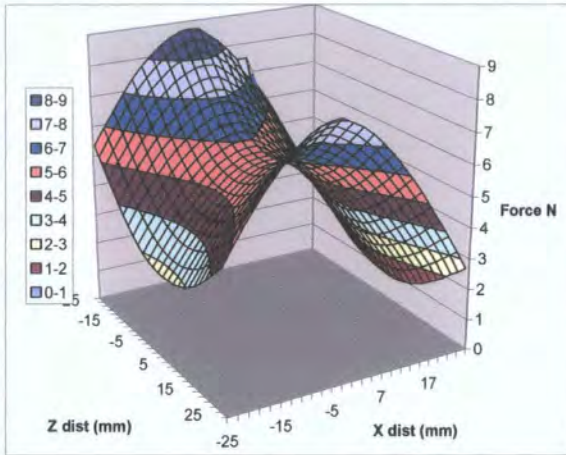


Figure 4.4.8; Force in y at 20mm
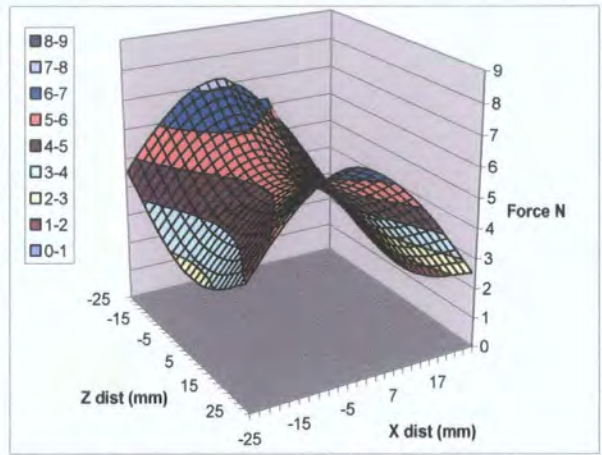


Figure 4.4.9; Force in y at 24mm
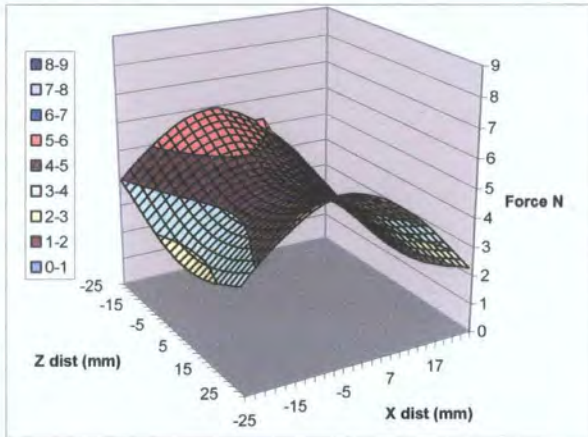


Figure 4.4.10; Force in y at 28mm
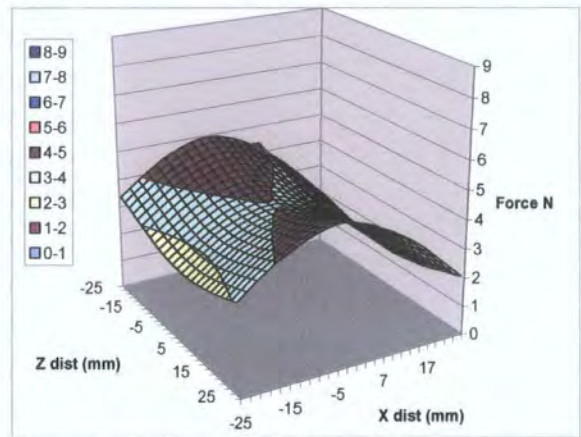


Figure 4.4.11; Force in y at 32mm
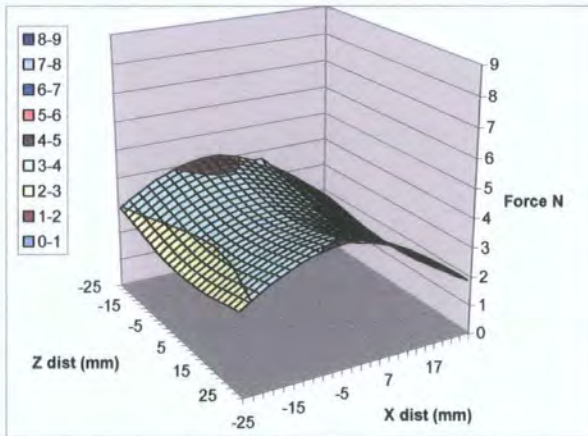


Figure 4.4.12; Force in y at 36mm
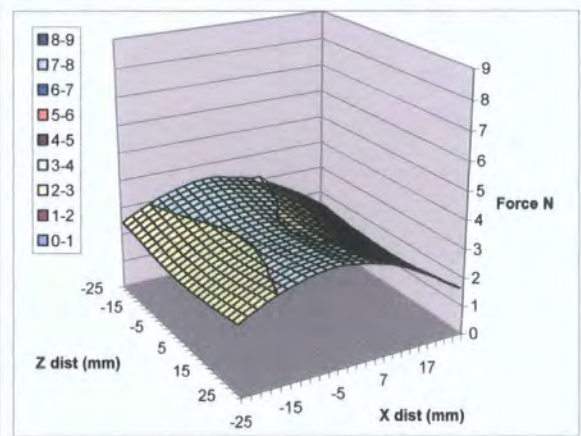


Figure 4.4.13; Force in y at 40mm

Forces in the z direction for rail configuration 1;
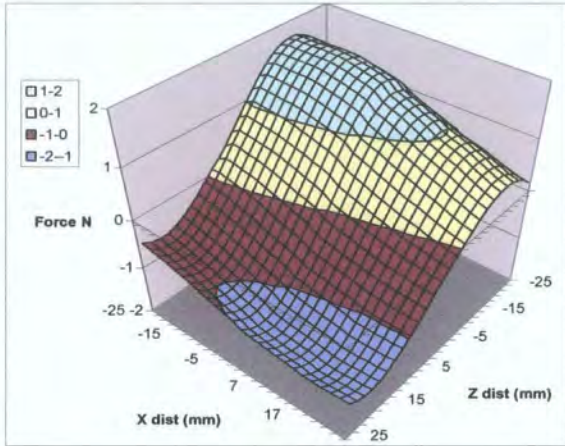


Figure 4.4.14; Force in z at 20mm
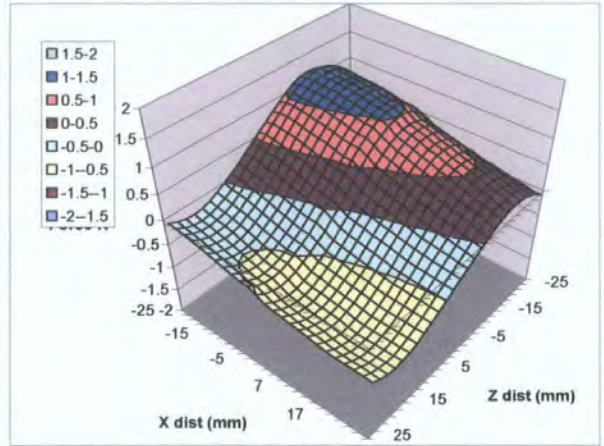


Figure 4.4.15; Force in z at 24mm
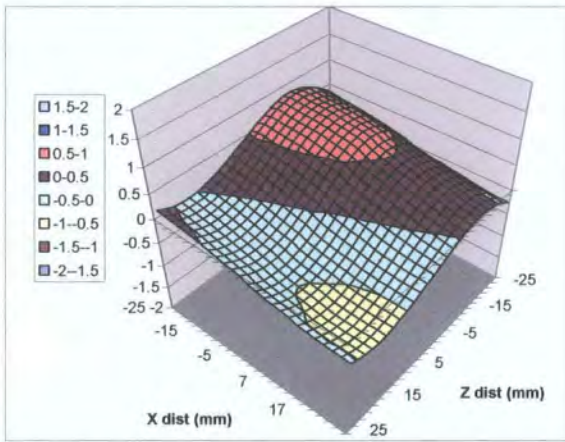


Figure 4.4.16; Force in z at 28mm
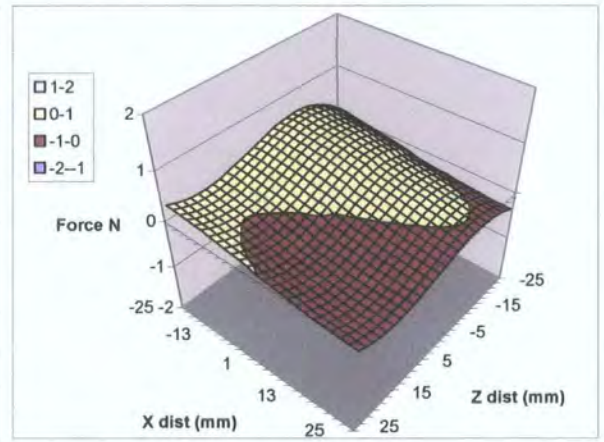


Figure 4.4.17; Force in z at 32mm
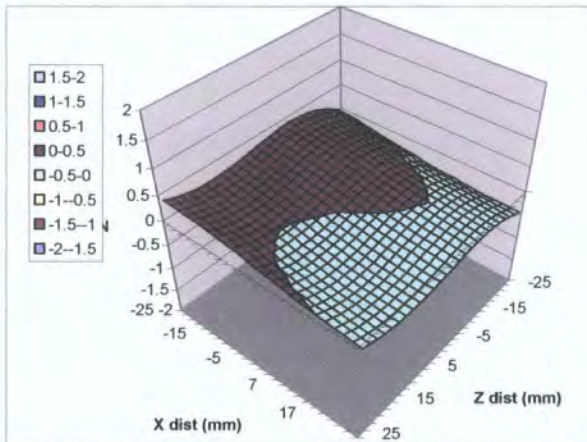


Figure 4.4.18; Force in z at 36mm
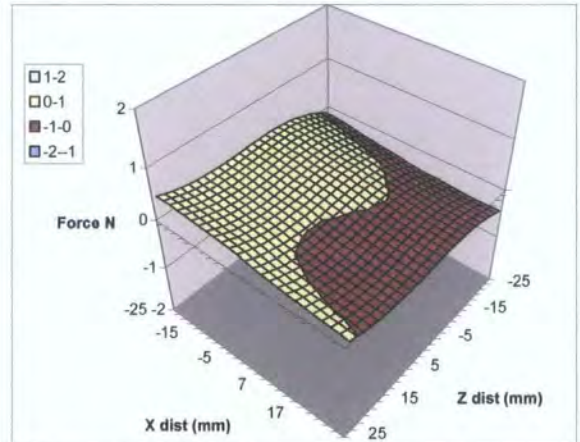


Figure 4.4.19; Force in z at 40mm
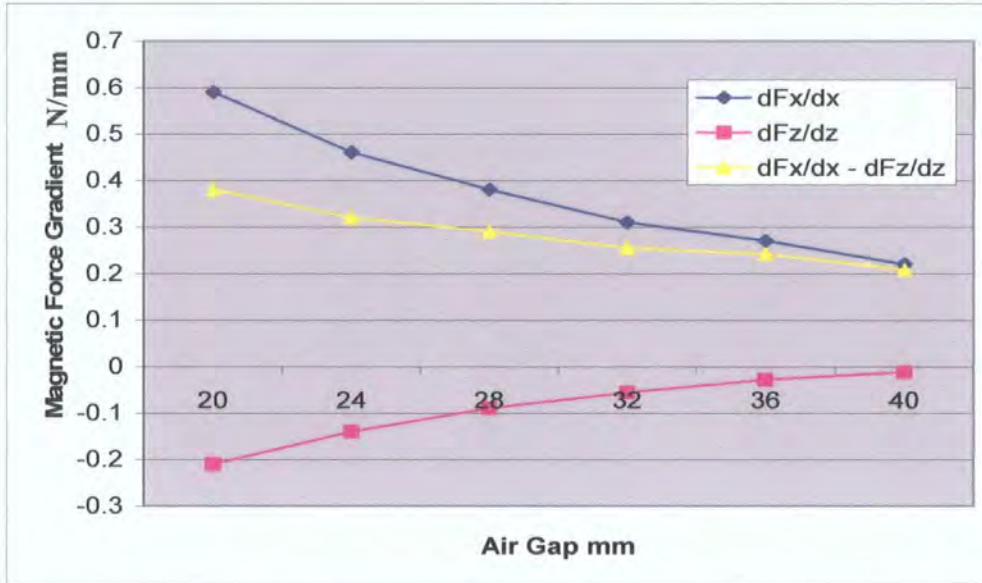
Figure 4.4.20, Graph of the gradients of the forces for rail configuration 1.

Figure 4.4.2 through figure 4.4.7 show the forces in the x direction acting on the system of magnets shown in figure 4.4.1. Figure 4.4.14 through figure 4.4.19 show the forces in the z direction. The graphs of the forces in the x and z direction show a primarily linear relationship between force and movement. As is to be expected at the centre point of the x axis the force acting in the x direction is zero as the forces are in equilibrium. Movement of the magnet on the traverse gear either side of this central point results in a force acting to further move the magnet away from its central neutral point, further increasing the destabilising force acting on the system. This of course only applies to a region close to the fixed magnets, past a certain point the destabilising force in the x direction will start to decrease as the distance between the "levitating" magnet and the fixed magnets increases. As the height of the magnet above the base increases, the destabilising force acting on it steadily decreases, this is also due the increased distance between the magnets. At a height of 40mm the destabilising forces are approximately half that of which they are at a height of 20mm. This is also shown in the gradients of the destabilising force in the x direction as shown in table 4.4.20 which are measured from the central linear section of the graph. The gradient of the destabilising force decreases from -0.59 Nmm$^{-1}$ at a height of 20mm, to -0.22 Nmm$^{-1}$ at a height of 40mm. Doubling the height between the magnets decreases the instability in the x direction of the magnets by nearly 60%. This is due to the increased distance between the fixed magnets and the "levitating" magnet.

Figure 4.4.8 through figure 4.4.13 show the forces in the y direction acting on the system shown in figure 4.4.1. A saddle shaped graph is produced, the peaks of maximum force corresponding to the points at which the centre point of the magnet on the traverse gear is closest to the centre point of either one of the fixed magnets, as this is where the greatest overlap of the magnets occur. Unlike the force acting in the x direction, deviation from the centre point of the graph in the x direction causes the force in the y direction to decrease, whereas deviation from the centre point of the graph in the z direction causes the force in the y direction to increase.

Figure 4.4.14 through figure 4.4.19 show the forces in the z direction acting on the system shown in figure 4.4.1. The results are similar to the forces acting in the x direction, although unlike the destabilising forces in the x direction, a movement away from the central position results in a restoring force acting on the magnet connected to the traverse gear. Increasing the height between the magnets leads to a reduction in the restoring force that results from a movement of the magnet in the z direction. The gradient of the restoring force decreases from 0.21 N/mm at a height of 20mm to 0.012 N/mm at a height of 40mm. While the central section of the graphs show a linear relationship similar to the linear shape of the graphs showing the force in the x direction, the graph takes on an s shaped profile towards its edges. This is caused by the varying distance between the magnet attached to the traverse gear and the fixed magnets. As the upper magnet moves closer to the centre point of one of the fixed magnets it initially causes a restoring force to act on the magnet, however once the upper magnet approaches the centre point of one of the fixed magnets the restoring force starts to decrease, as the angle of interaction between the magnetic flux of each magnet increases until the "levitating" magnet is directly over one of the fixed magnets.

4.5 Reducing Magnetic Levitation Instability

The graphs of the forces acting in the magnetic system shown in figure 4.4.1 and the graph of the gradients of the magnetic forces shown in figure 4.4.20 show that the destabilising forces acting in the x direction are considerably larger than the restoring forces acting in the z direction. Therefore any stability advantage a levitation system gained in the z direction is

more than negated by the instability in the x direction. The three magnet system is only stable in two degrees of freedom, but can be made stable in pitch, roll, and yaw by using multiple three magnet systems. A system could be built that would be stable in five degrees of freedom. Four of these three magnet systems spaced at suitable intervals from each other and all aligned in the same direction would result in a configuration that would only require restraint in one degree of freedom.

The instability of the system stable in five degrees of freedom means that it still requires an element of active control to stay in total equilibrium. This instability could be reduced by extending the length of the two fixed magnets to infinity in the x direction. This would create two rails over which multiple magnets of finite size would be positioned. As the length of the rails increased the instability of the system would decrease. This would result in a system that would be neutrally stable in the x direction. This would allow the creation of a system consisting of two rails and four levitating magnets that would be stable in five degrees of freedom, and neutrally stable in one degree of freedom, as shown in figure 4.5.1
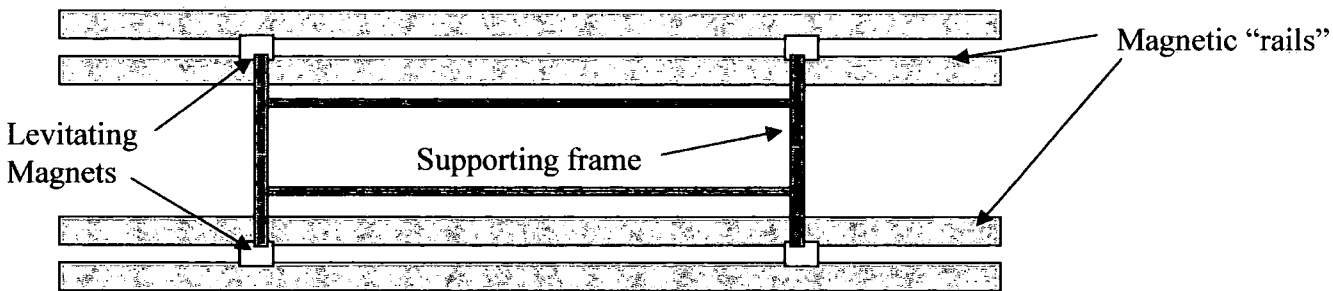


Figure 4.5.1, Neutrally Stable Magnetic Rail System.

In practice extending the magnets to infinity is of course not possible. However increasing the length of the rails will reduce the instability of the system and there will be a point where the fixed magnets have dimensions that are sufficiently greater than the levitating magnet in order that the destabilising force in the x direction will be smaller than the stabilising force in the z direction. This should mean that a system consisting of an even number of such magnet configurations should then be stable. Figure 4.5.2 shows a possible configuration for a stable system.
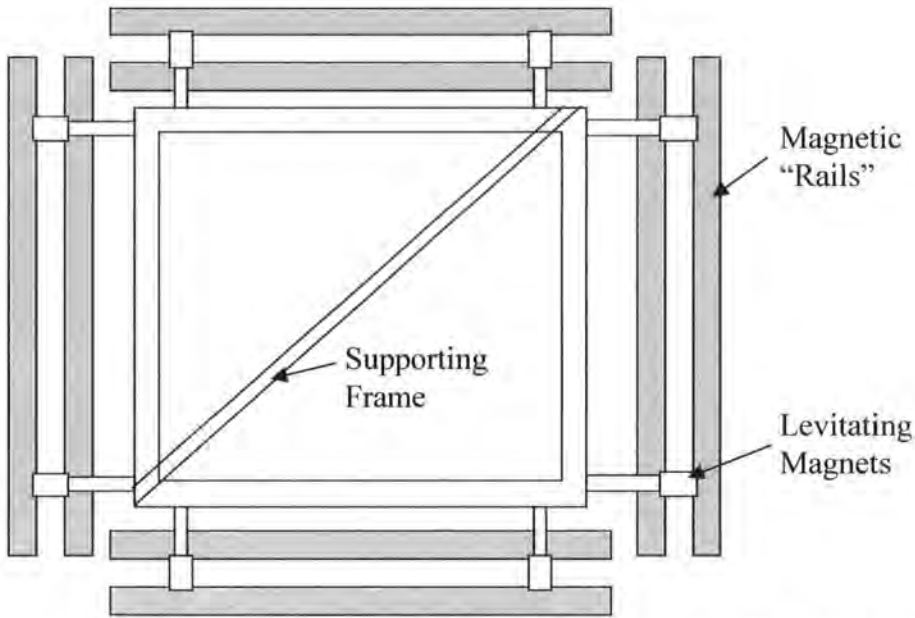
Figure 4.5.2; Potential configuration for a stable magnet only system.

4.5.1, Traverses of the composite magnetic rail

To test this hypothesis, further traverses were performed using four fixed magnets of dimensions 50mm x 50mm x 6mm arranged in "rails" a distance of 20mm apart, and one levitating magnet with dimension 50mm x 50mm x 6mm at a height of 30mm, as shown in figure 4.5.3. The fixed magnets were mounted on to a six component force balance, and the "levitating" magnet mounted on a non-ferrous arm, connected to a traverse gear. The results of the traverses are shown in figures 4.5.4 - 4.5.6.
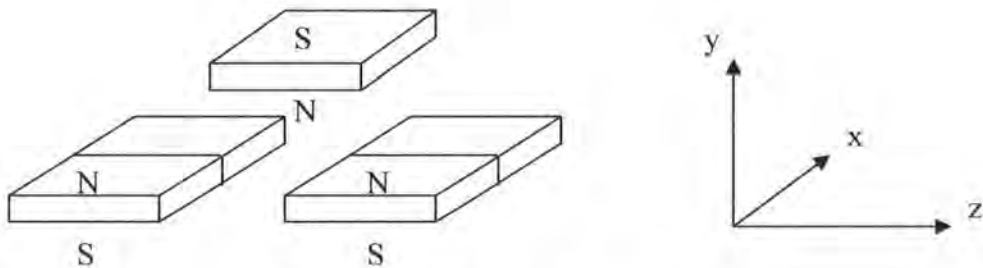


Figure 4.5.3, Testing Configuration with Extra Magnets
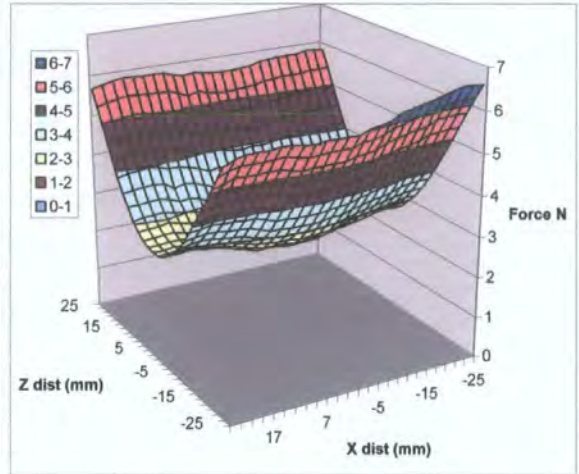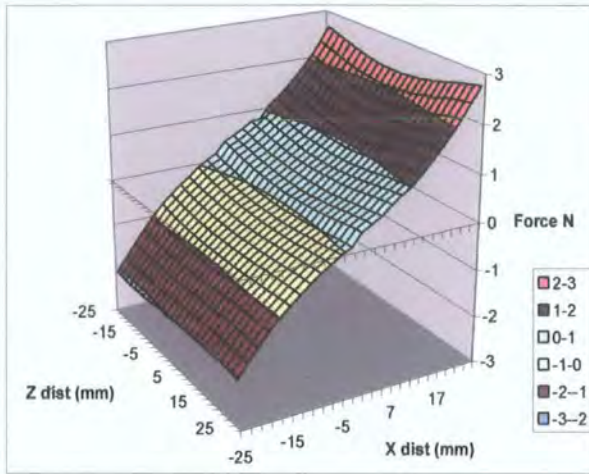
Figure 4.5.4; Force in x direction at 30mm



Figure 4.5.5; Force in y direction at 30mm
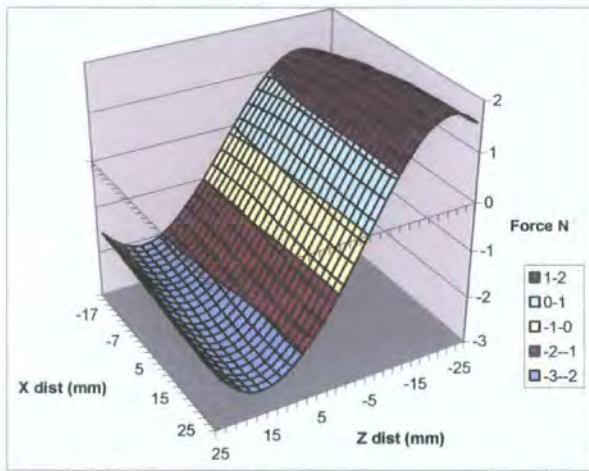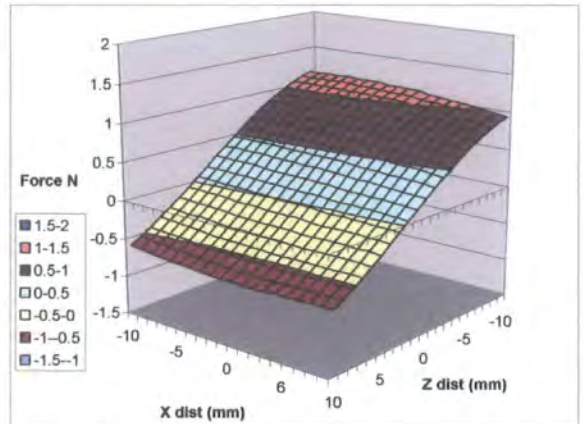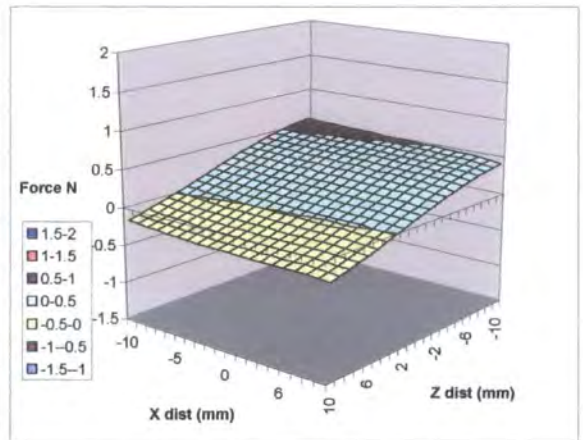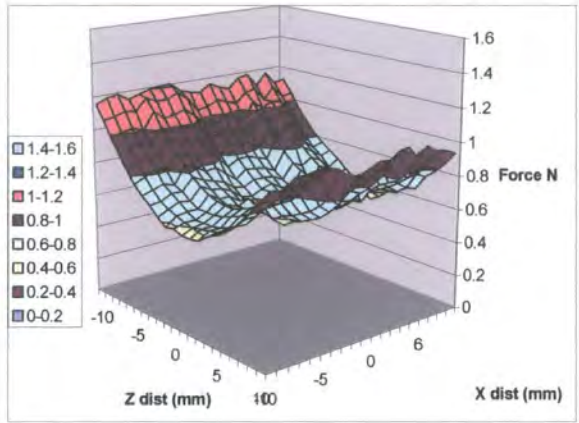


Figure 4.5.6; Force in z direction at 30mm

The shapes of the graphs are similar to those produced from the previous traverses of the three magnet system, although because of the extended "rails" the resulting shapes are more uniform. The force produced in the y direction shown in figure 4.5.5 produced an arch shaped graph, unlike the saddle shaped graph shown in figures 4.4.8 to 4.4.13 where the force produced reduces as the "levitating" magnet moves past the edges of the fixed magnets. The gradient of the central linear section of the graph of the force in the z direction was 0.31 N/mm, and the gradient of the central section of the graph of the force in the x direction was 0.10 N/mm. This indicates that the restoring force in the z direction was greater than the destabilising force in the x direction. It follows that continuing to add more magnets to the fixed ones, creating longer "rails", will further decrease the destabilising force, leading to a situation where the system becomes even more stable.

The arrangement of magnets shown in figure 4.5.3 was then tested experimentally with the "levitating" magnet mounted on a 1 metre long non-ferrous arm connected to a gimbal. It was found that the amount of weight the magnet attached to the gimbal could support had decreased substantially, despite the extra magnets that had been introduced into the system. This was caused by the gap between the magnets affecting the magnetic field and reducing the stable region, even though fixed base magnets were touching.

When two magnets with the same directional polarity are put close together side by side, the magnetic field of each magnet repels the other. As they are brought together the magnetic fields are distorted, resulting in an uneven distribution of magnetic flux at the join. This effect is masked due to the size of the levitating magnet and is not particularly pronounced in figure 4.5.5, as the effect is averaged out due to the area over which the magnets are interacting. However a small reduction of vertical force can be seen at the centre of the graph, despite an increase in force being expected at the centre point due to the maximum area of overlap between the magnets. To ensure that this effect was not due to the "levitating" magnet being directly positioned over the join between the fixed magnets, the experiment was repeated with six fixed magnets to ensure the levitating magnet was not over a join, however the same loss of load bearing capability was observed. The traverses were then repeated using a smaller "levitating" magnet with dimensions 30mm x 25mm x 6mm. Figure 4.5.7 shows the vertical force acting on the system when using the smaller magnet. A more pronounced loss of lift is seen in the central portion of the graph than in the previous graph, and in fact the lift becomes negative and the "levitating" magnet is attracted to the fixed base magnet. For this reason composite rails are not suitable for levitation applications.
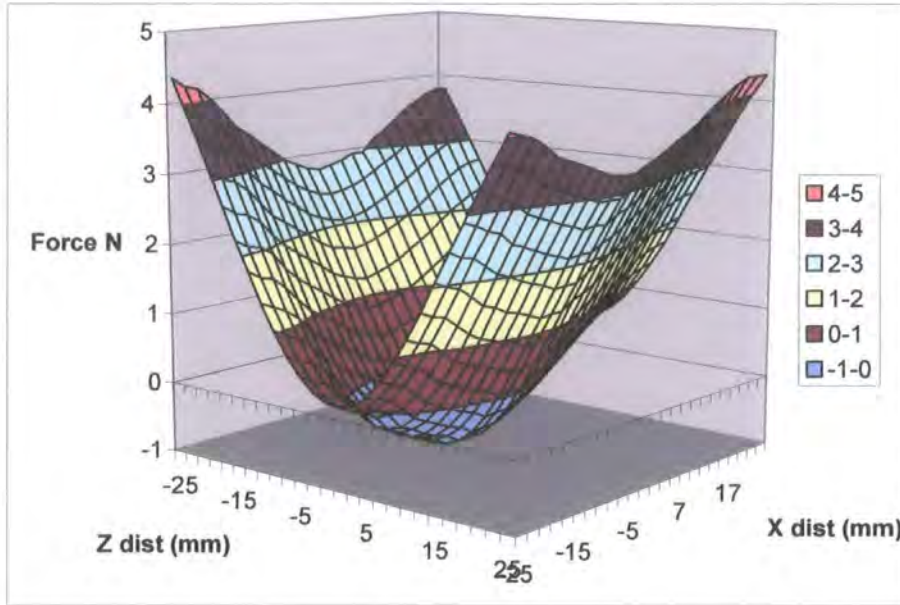
Figure 4.5.7, Force in the y direction at 30mm using a composite rail design.

In order to explain the destabilising effect of the composite magnetic rails, the arrangement was modelled in the electromagnetic finite element analysis package, MEGA. Figure 4.5.8 shows a small magnet positioned over a larger one piece magnet with like poles facing each other. The field lines are clearly separated and show the repulsion between the magnets. Figure 4.5.9 shows a small magnet positioned over two larger magnets, with like poles facing each other, with a very small gap between the two. The field lines from the small magnet can be seen to penetrate through the small gap between the two larger magnets, interacting with the magnetic flux from the underneath of the larger magnets and experiencing an attractive force. Force readings were taken for the split magnet and it was found that reducing the height between the levitating magnet and the fixed magnet by half caused the vertical force on the levitating magnet to decrease by 60%. Despite the magnets being closer together the repulsion force between is actually decreased, this creates the instability experienced in the experimental tests.
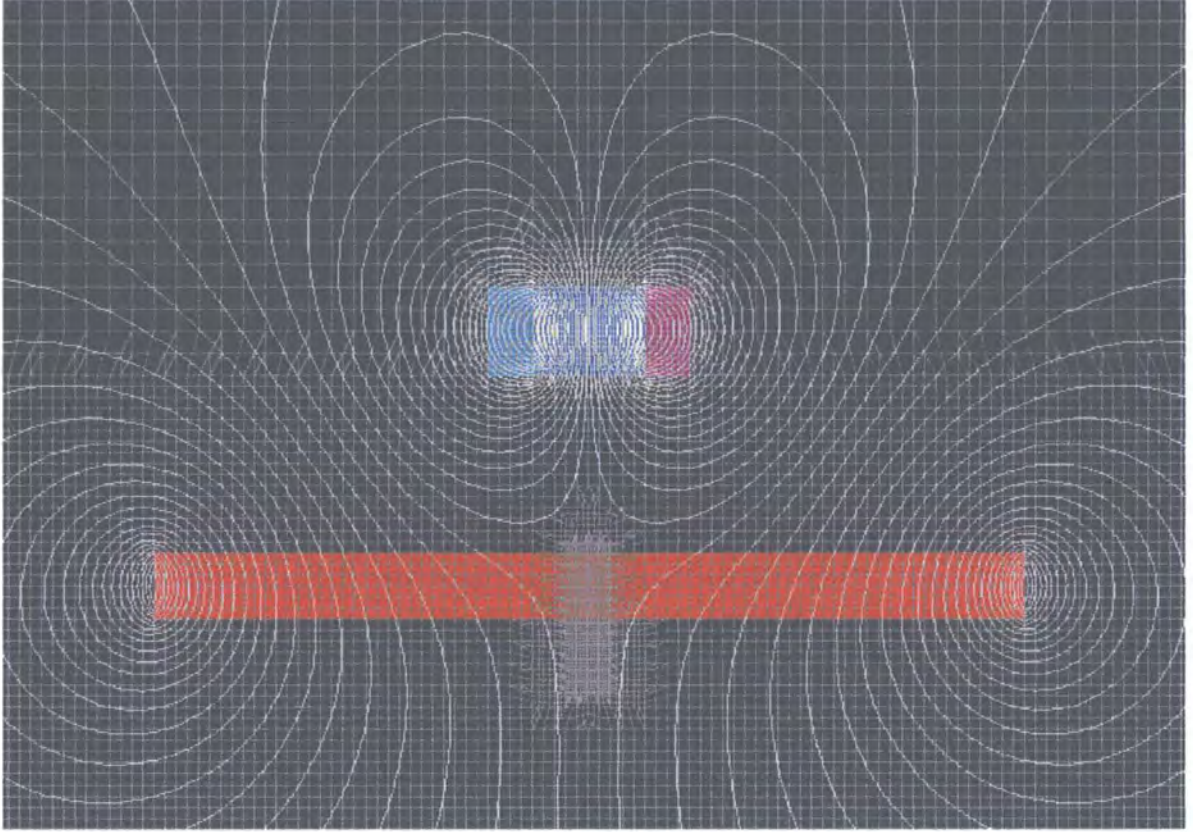
Figure 4.5.8, Small Magnet over Large One Piece Magnet.
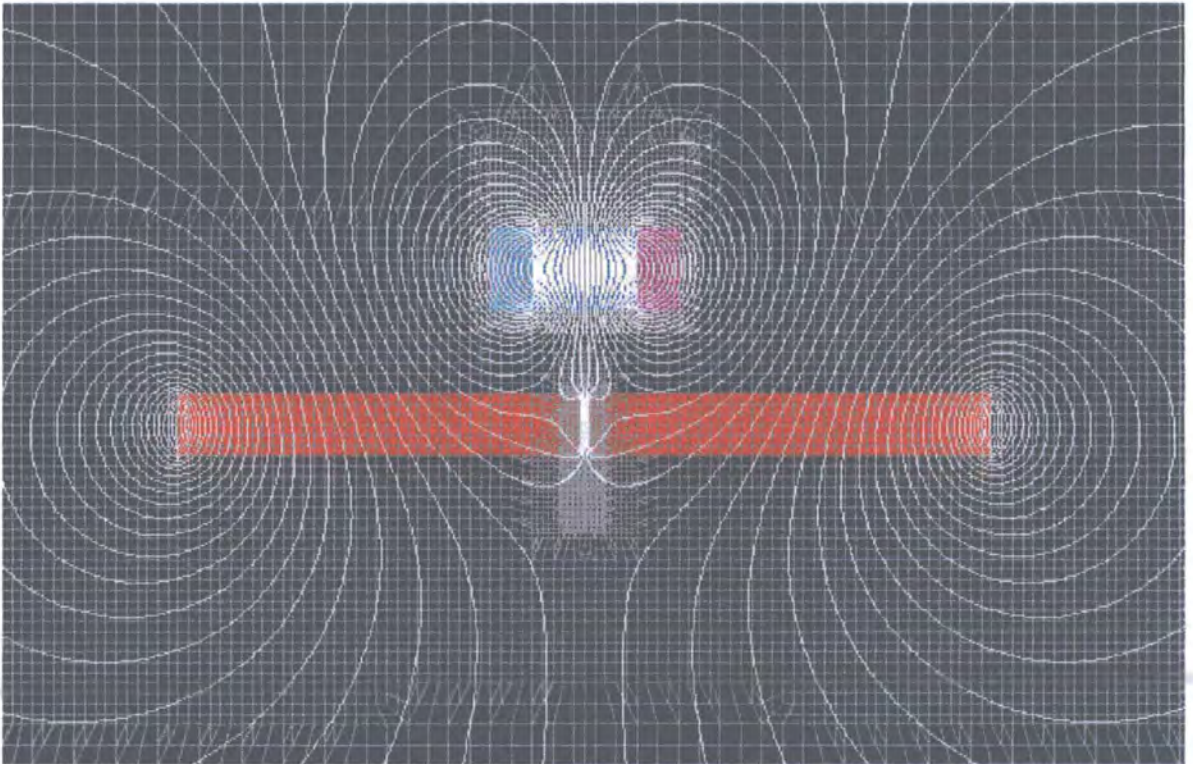


Figure 4.5.9, Small Magnet over Larger Composite Magnet.

4.5.2, Force testing on rail configuration 2.

In order to test the effect of the changing ratios of the length of the fixed base magnets to the length of the "levitating" magnet without using multiple fixed magnets, smaller "levitating" magnets were used. Two fixed neodymium magnets with dimensions 50mm x 50mm x 6mm were traversed using a neodymium magnet with dimensions 12 mm x 30mm x 5mm. This configuration gave a ratio of magnets lengths of 12/50 = 0.24. Traverses were performed with decreasing intervals of 2mm between the fixed magnets. The first run was performed with a gap of 16mm, rail configuration 2, between the fixed base magnets.

Forces in the x direction for rail configuration 2;
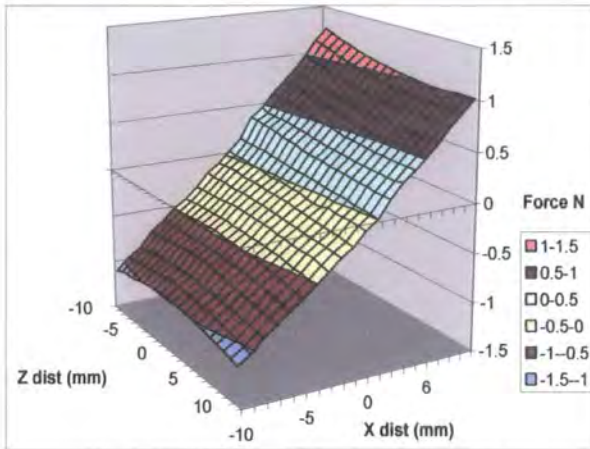


Figure 4.5.2.1, Force in x direction at 20mm
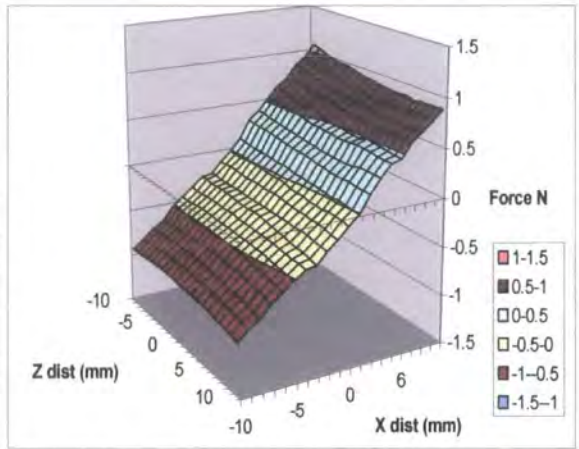


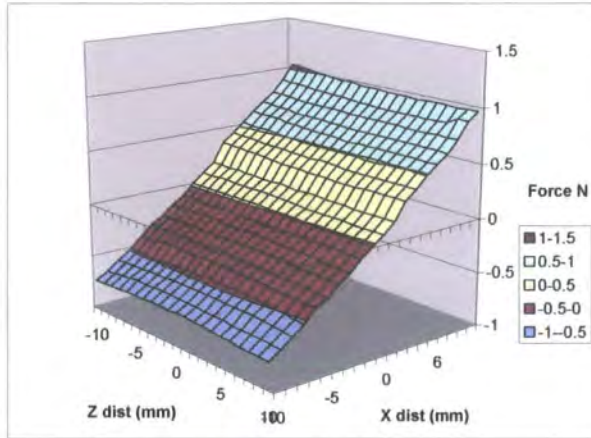Figure 4.5.2.2, Force in x direction at 24mm
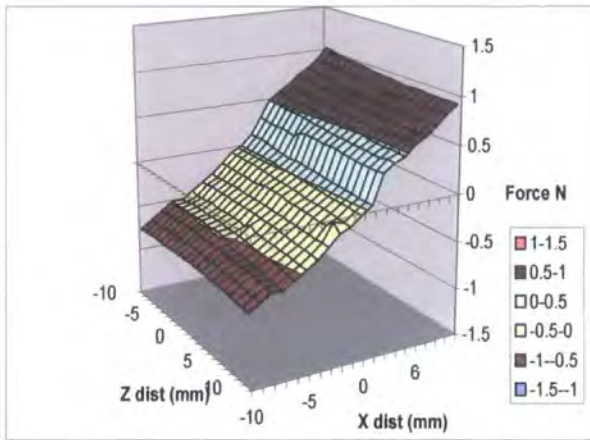

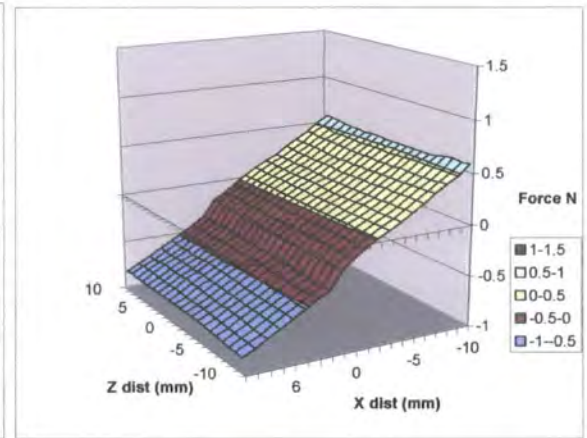
Figure 4.5.2.3, Force in x direction at 28mm
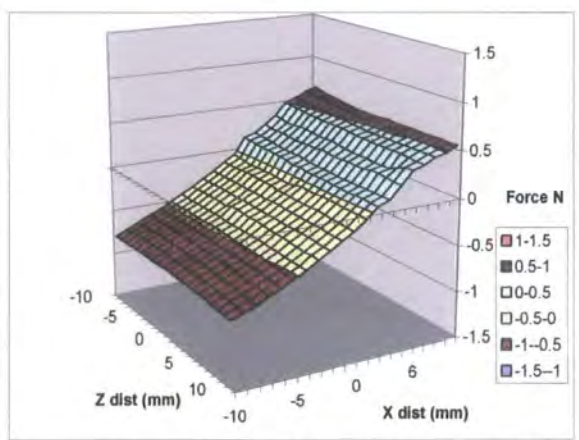


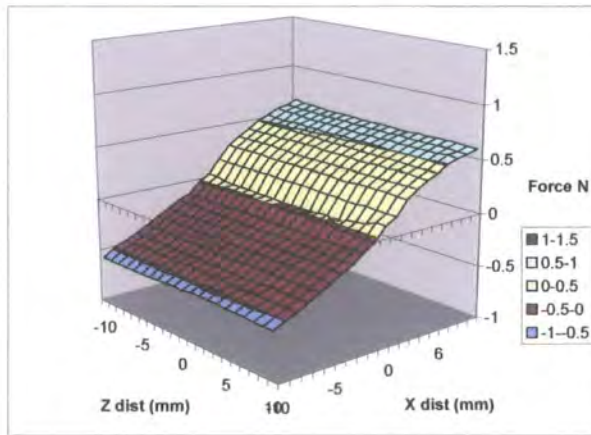Figure 4.5.2.4, Force in x direction at 32mm
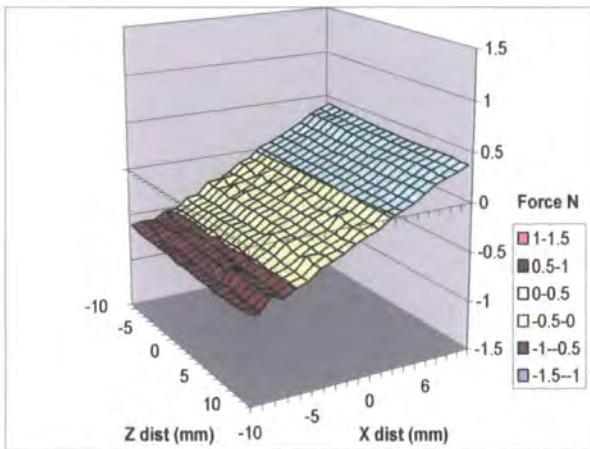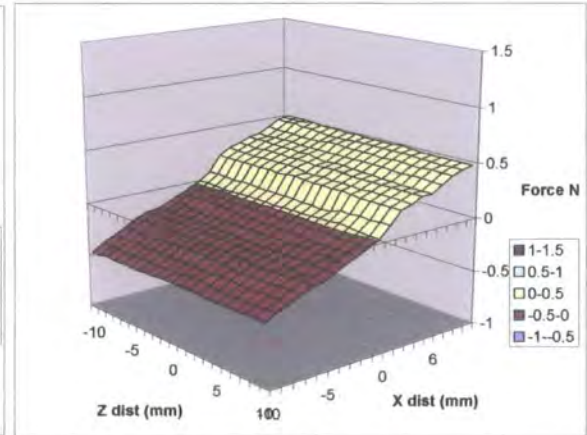


Figure 4.5.2.5, Force in x direction at 36mm
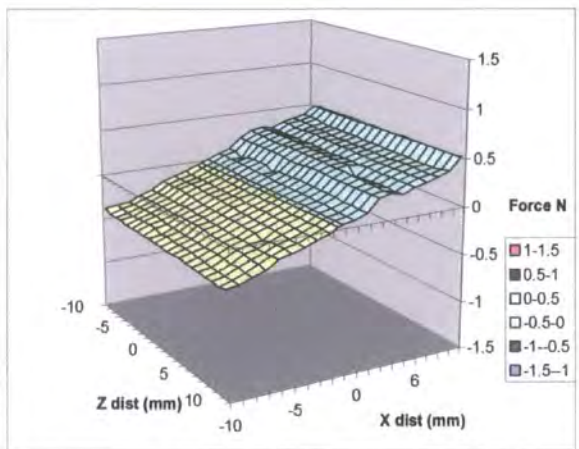


Figure 4.5.2.6, Force in x direction at 40mm

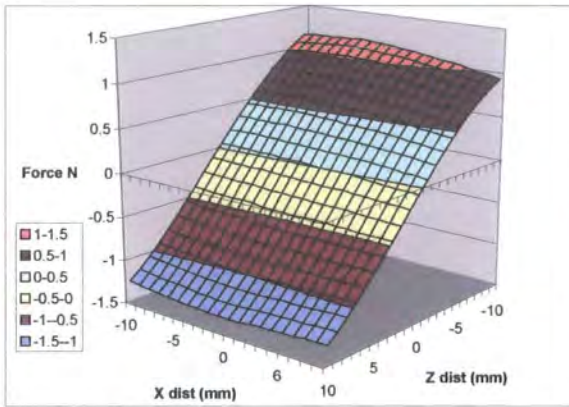Forces in the z direction for rail configuration 2;
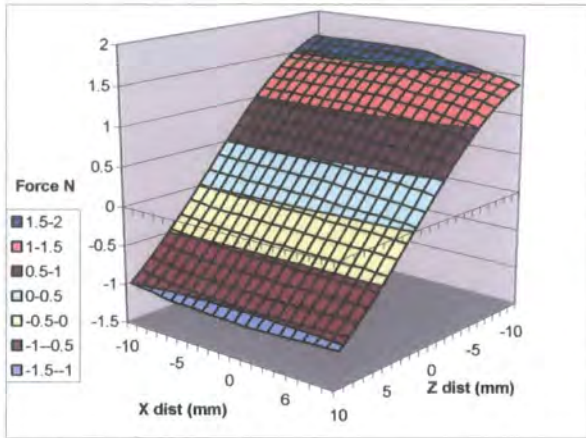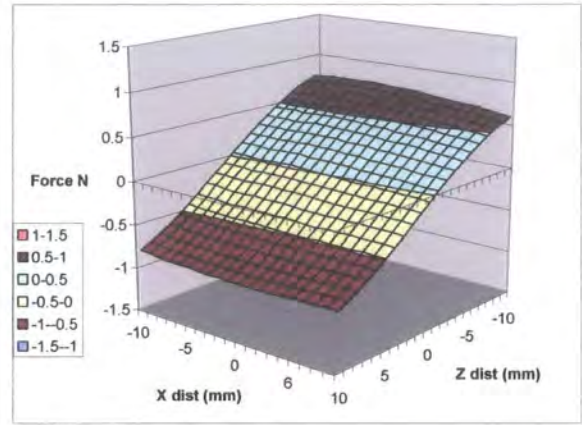


Figure 4.5.2.7, Force in z direction at 20mm



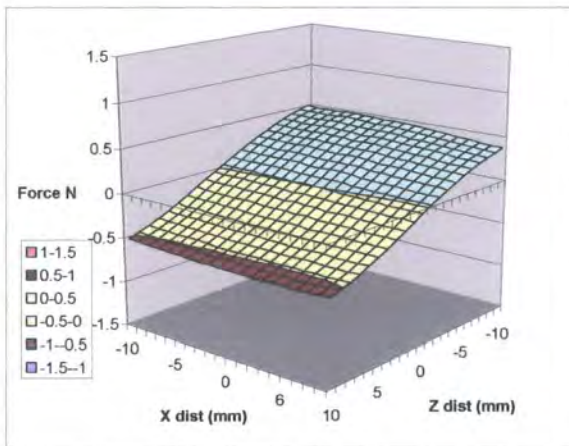Figure 4.5.2.8, Force in z direction at 24mm
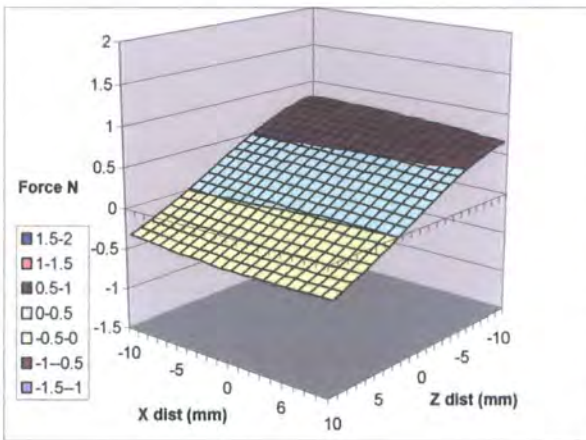


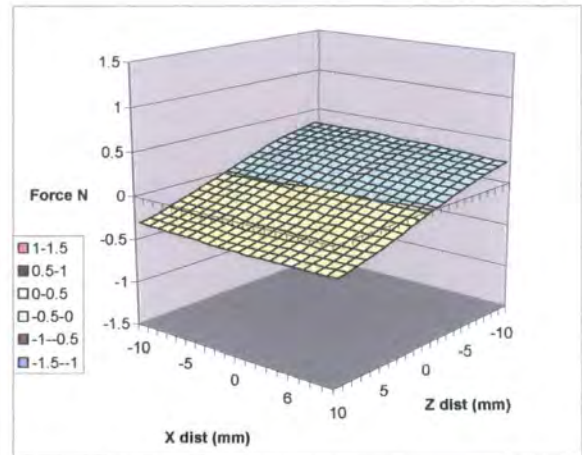Figure 4.5.2.9, Force in z direction at 28mm



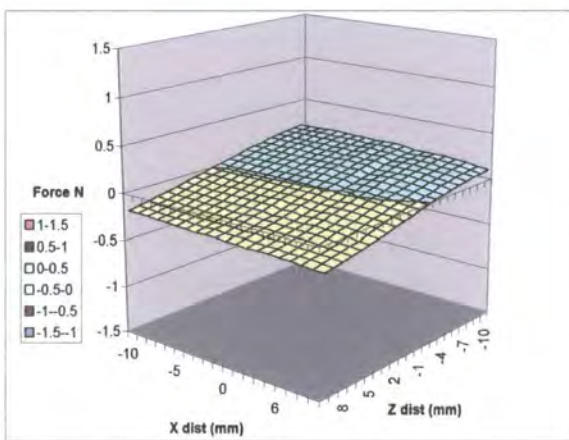Figure 4.5.2.10, Force in z direction at 32mm
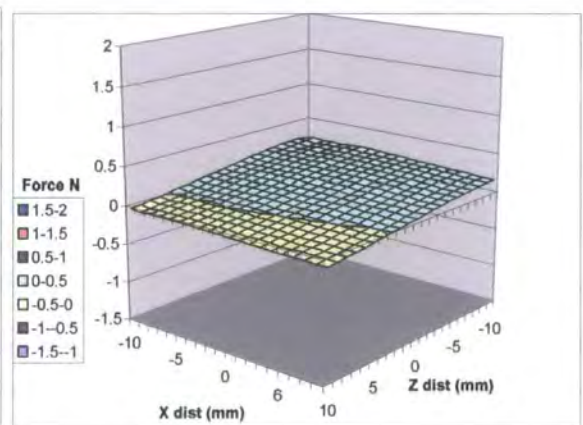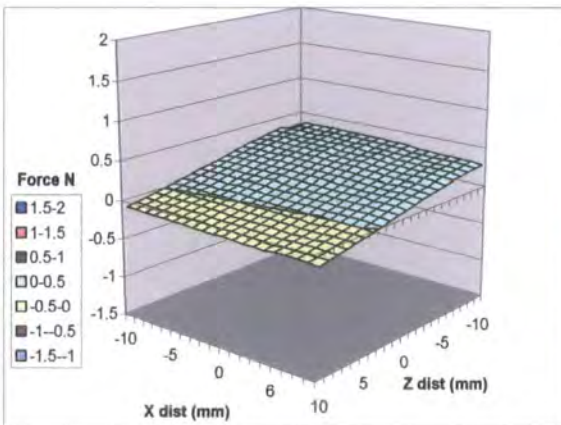


Figure 4.5.2.11, Force in z direction at 36mm
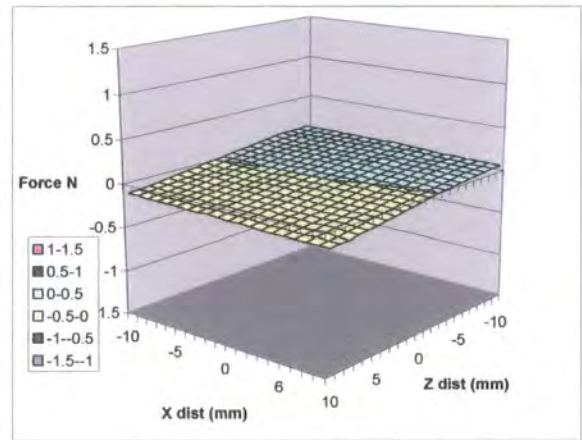


Figure 4.5.2.12, Force in z direction at 40mm
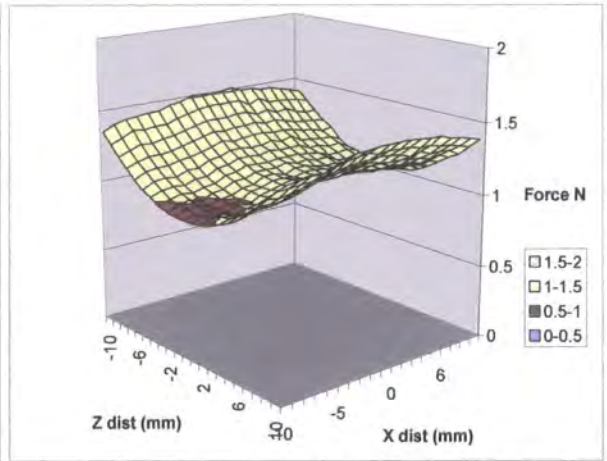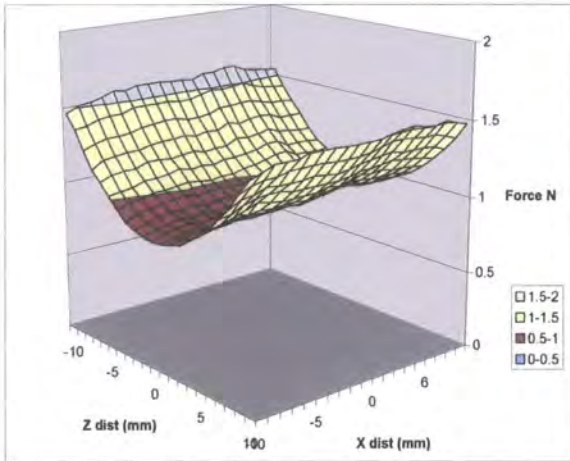
Forces in the y direction for rail configuration 2;
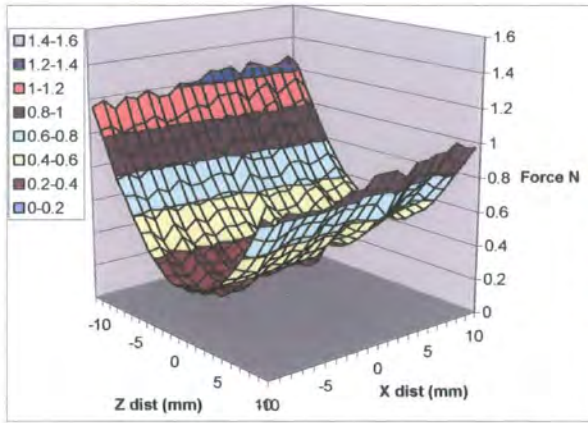


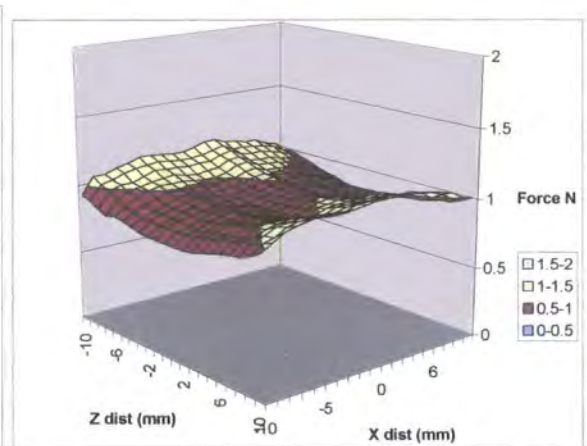Figure 4.5.2.13, Force in y direction at 20mm Figure 4.5.2.14, Force in y direction at 24mm
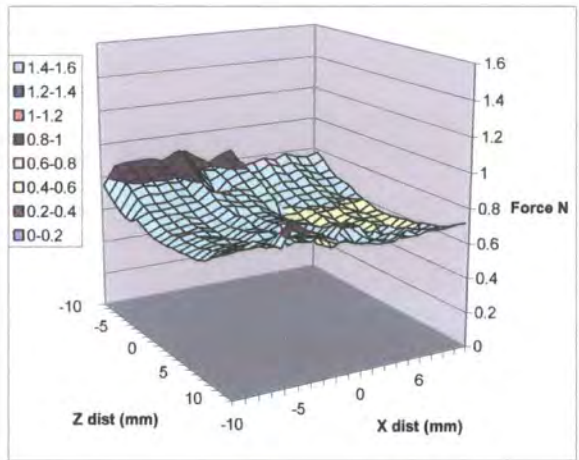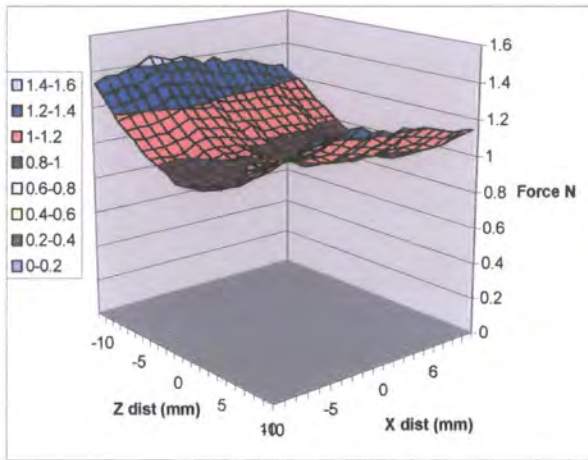

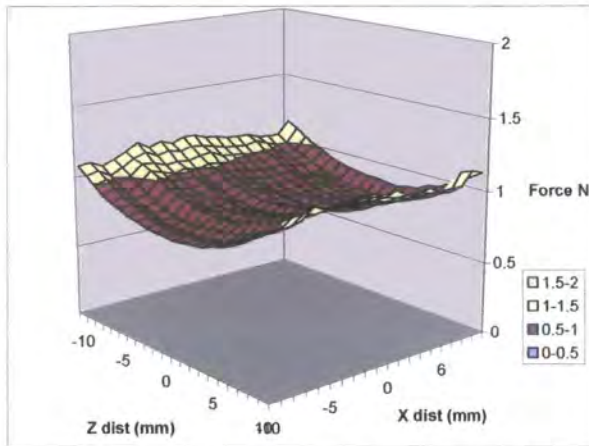
Figure 4.5.2.15, Force in y direction at 28mm Figure 4.5.2.16, Force in y direction at 32mm
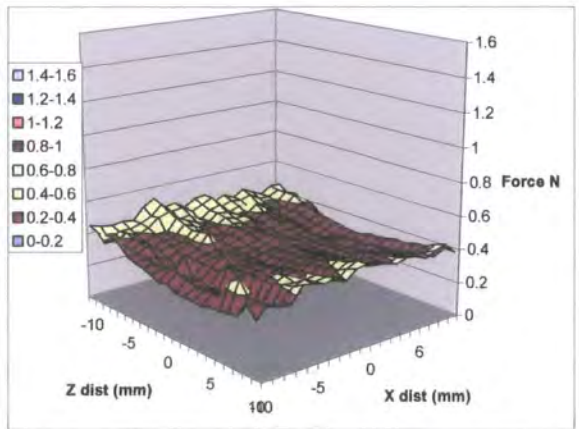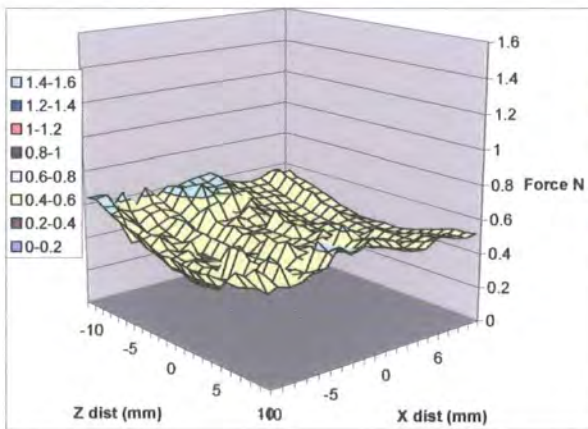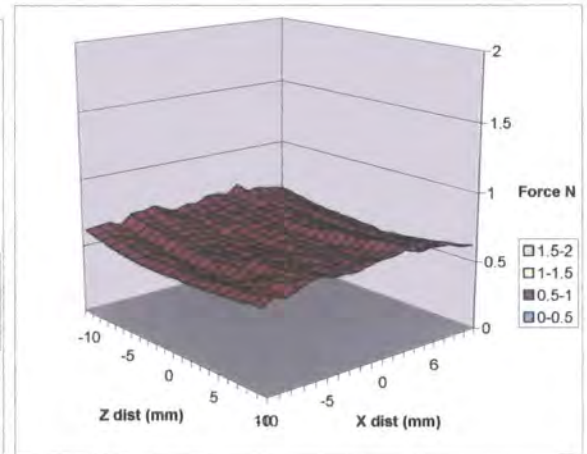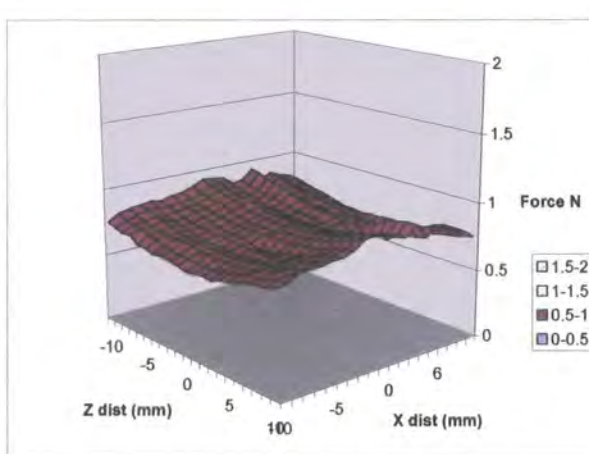


Figure 4.5.2.17, Force in y direction at 36mm Figure 4.5.2.18, Force in y direction at 40mm
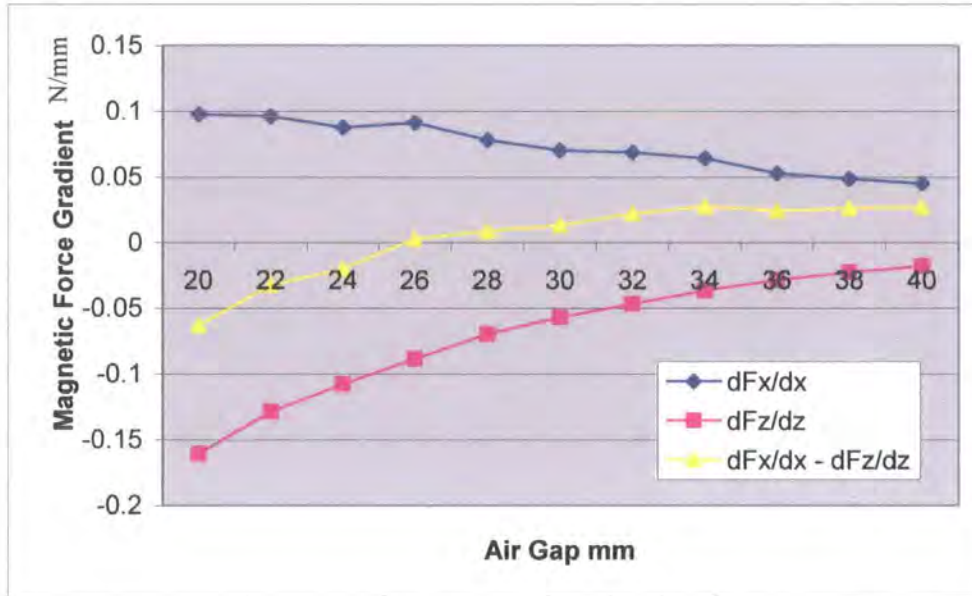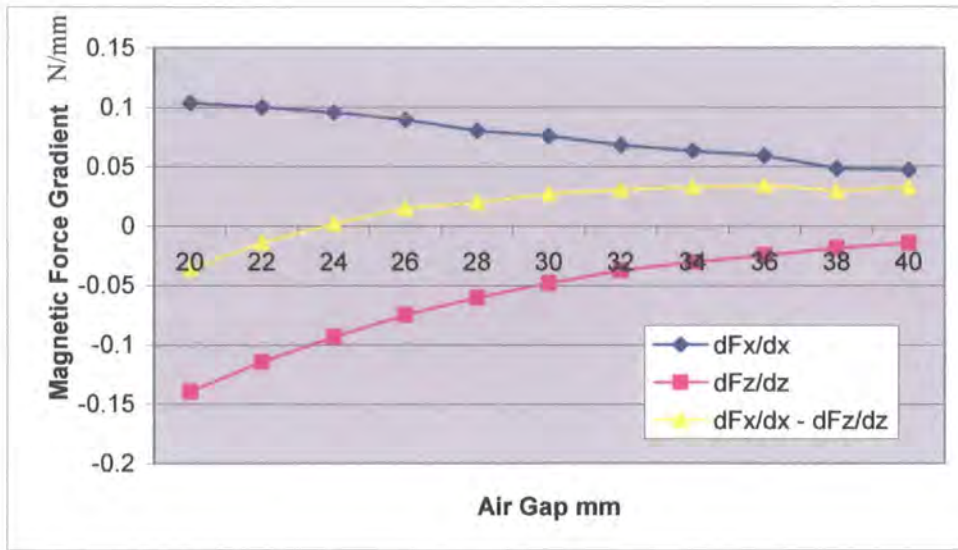
Figure 4.5.2.19, Graph of magnetic force gradients for rail configuration 2.

With the "levitating" magnet below a height of 26mm above the fixed base magnets, in rail configuration 2, the restoring force in the z direction is greater than the destabilising force in the x direction. However at a height of more than 26mm above the fixed base magnets the destabilising force in the z direction becomes greater than the restoring force in the x direction. This is due to the angle of intersection between the fields of the magnets. When the height of the "levitating" magnet is reduced the horizontal component of the force from the fixed base magnets increases. As the height of the "levitating" magnet is increased, the horizontal component of the force from the fixed base magnets decreases as the relative angle between the magnets increases. The restoring force in the z direction decreases faster than the destabilising force in the x direction because the fixed base magnets are opposing each other in the z direction but are working together to destabilise the "levitating" magnet in the x direction.

The vertical force between the "levitating" magnet and the fixed base magnets does not change linearly with the changing height between the magnets. The force at a height of 20mm is less than the force at a height of 24mm, despite the "levitating" magnet being closer to the fixed base magnets. This is due to the changing angle of interaction between the magnetic flux from the magnets. This means that there is a stable zone where levitation can occur which has an upper limit at the point at which the restoring force in the z

direction becomes less than the destabilising force in the x direction, and with a lower limit at the point at which the "levitating" magnet becomes attracted to the magnetic flux from the underside of the fixed magnets. Increasing the size of this stable zone will result in a more stable configuration and ultimately a more effective levitation system. The traverses were then repeated with the gap between the fixed base magnets reduced to 14mm, rail configuration 3, to investigate the effect that this will have on the stable levitation region.

4.5.3, Force testing of rail configuration 3.

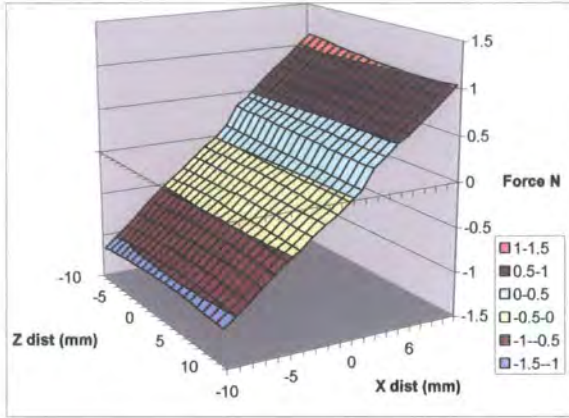Forces in the x direction for rail configuration 3;
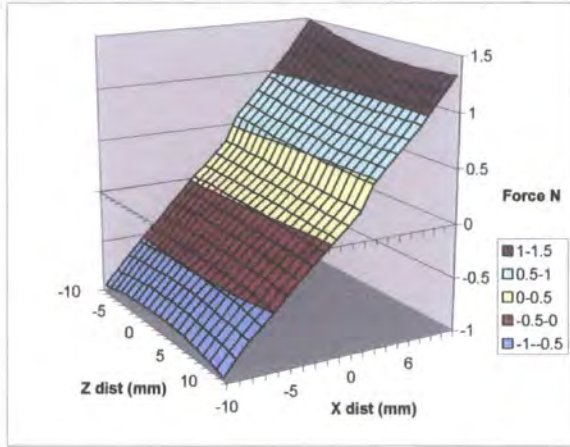


Figure 4.5.3.1, Force in x direction at 20mm
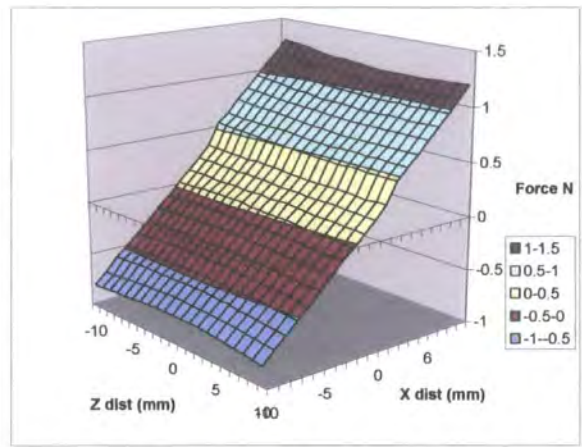


Figure 4.5.3.2, Force in x direction at 24mm



Figure 4.5.3.3, Force in x direction at 28mm



Figure 4.5.3.4, Force in x direction at 32mm



Figure 4.5.3.5, Force in x direction at 36mm



Figure 4.5.3.6, Force in x direction at 40mm

Forces in the z direction for rail configuration 3;



Figure 4.5.3.7, Force in z direction at 20mm

Figure 4.5.3.8, Force in z direction at 24mm

Figure 4.5.3.9, Force in z direction at 28mm

Figure 4.5.3.10, Force in z direction at 32mm

Figure 4.5.3.11, Force in z direction at 36mm Figure 4.5.3.12, Force in z direction at 40mm

Forces in the y direction for rail configuration 3;
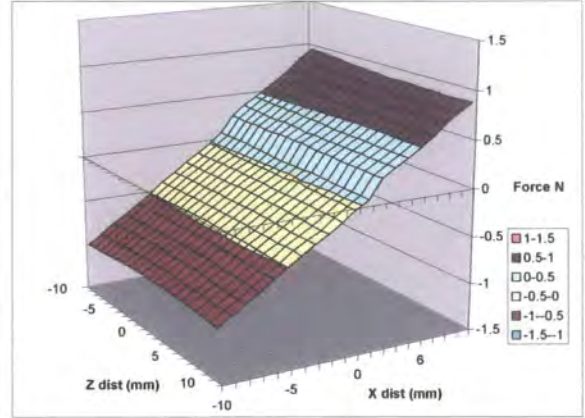


Figure 4.5.3.13, Force in y direction at 20mm Figure 4.5.3.14, Force in y direction at 24mm
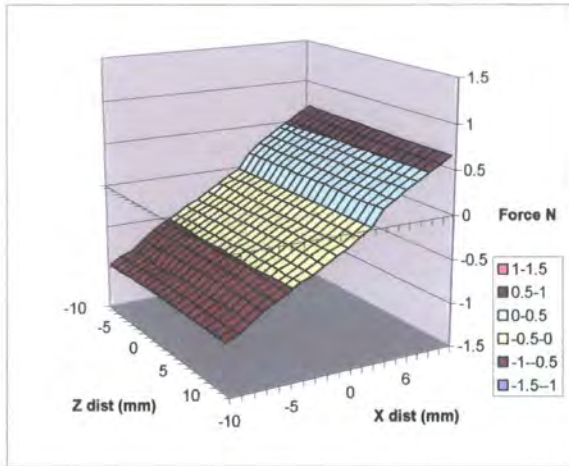


Figure 4.5.3.15, Force in y direction at 28mm Figure 4.5.3.16, Force in y direction at 32mm



Figure 4.5.3.17, Force in y direction at 36mm Figure 4.5.3.18, Force in y direction at 40mm

Figure 4.5.3.19, Graph of magnetic field gradients for rail configuration 3.

The graph of the magnetic field gradients shows that when the gap between the fixed base magnets is reduced the size of the stable levitation region decreases. With the gap between the fixed base magnets at 16mm, in rail configuration 2, the three magnet configuration proved to be stable to a height of 26mm. However with the gap between the magnets set at 14mm, in rail configuration 3, the stable levitation region only extends to a height of 24mm. This result shows that reducing the distance between the fixed base magnets causes the three magnet system to become more unstable. This is caused by the angle at which the magnetic fluxes from the magnets interact; when the gap between the fixed base magnets are reduced, the angle at which the flux they produce interacts with the flux from the levitating magnet increases. This causes the horizontal component of the force between the magnets to decrease, therefore reducing the restoring force applied to the levitating magnet. However this also causes the vertical component of the force to increase, and as a result the vertical force acting on the system is almost doubled. The traverses were then repeated with the gap between the fixed base magnets reduced to 12mm, rail configuration 4, to further investigate the effect that changing the layout of the three magnet has on the stable levitation zone.

4.5.4, Force testing of rail configuration 4.

Forces in the x direction for rail configuration 4;



Figure 4.5.4.1, Force in x direction at 20mm



Figure 4.5.4.2, Force in x direction at 24mm



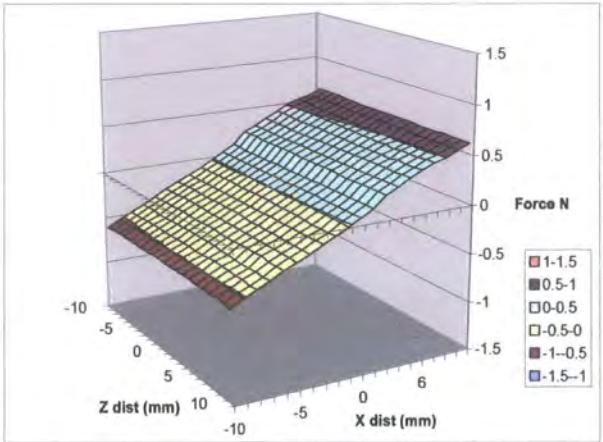Figure 4.5.4.3, Force in x direction at 28mm
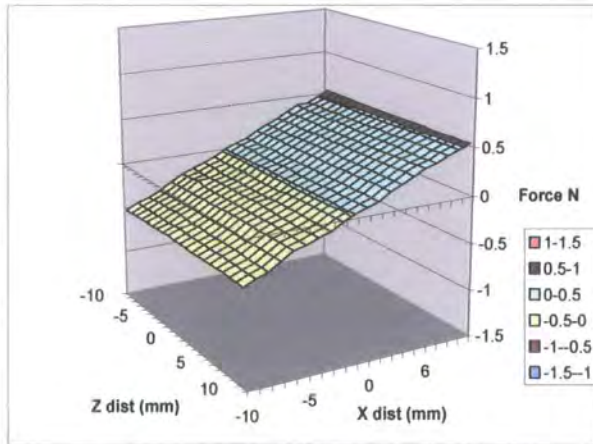


Figure 4.5.4.4, Force in x direction at 32mm



Figure 4.5.4.5, Force in x direction at 36mm



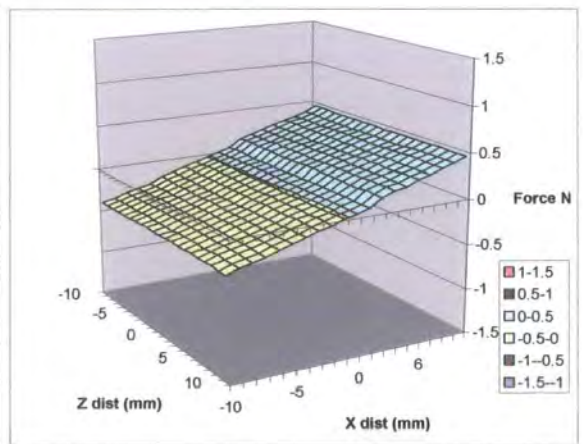Figure 4.5.4.6, Force in x direction at 40mm
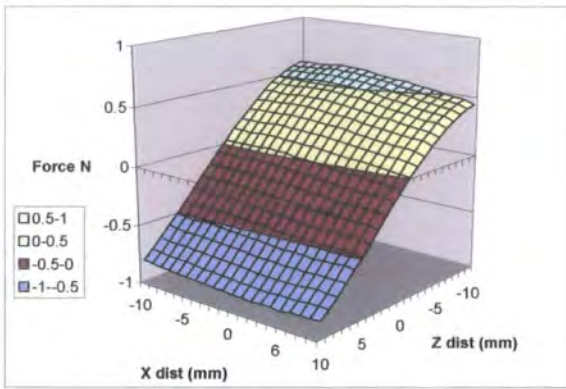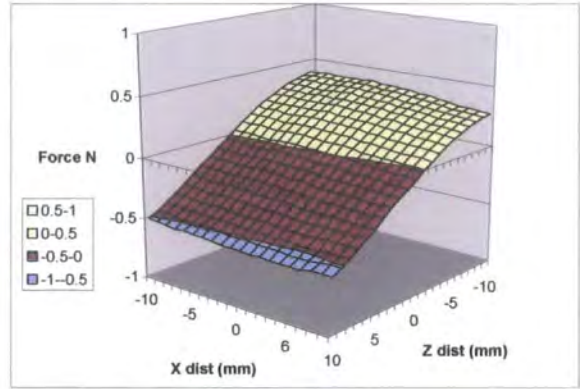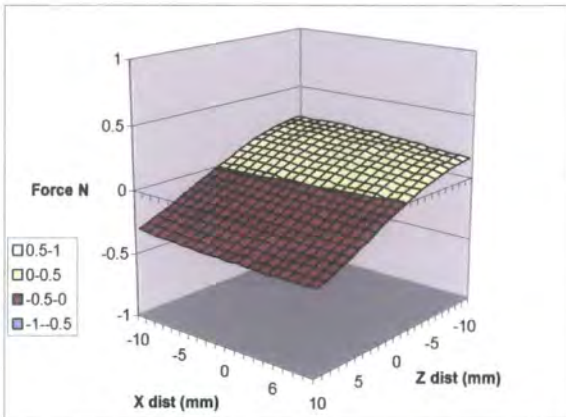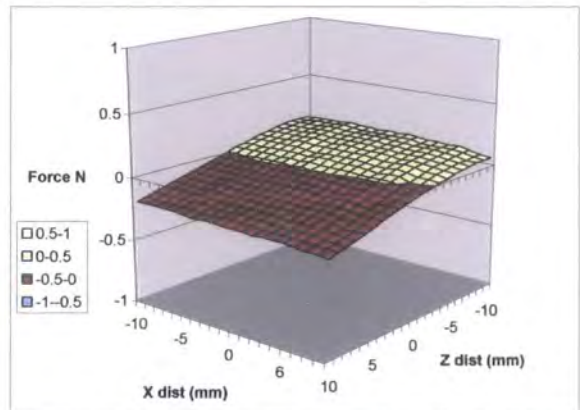
Forces in the z direction for rail configuration 4;



Figure 4.5.4.7, Force in z direction at 20mm



Figure 4.5.4.8, Force in z direction at 24mm



Figure 4.5.4.9, Force in z direction at 28mm



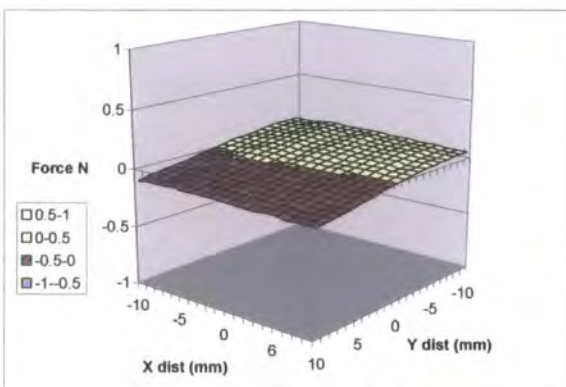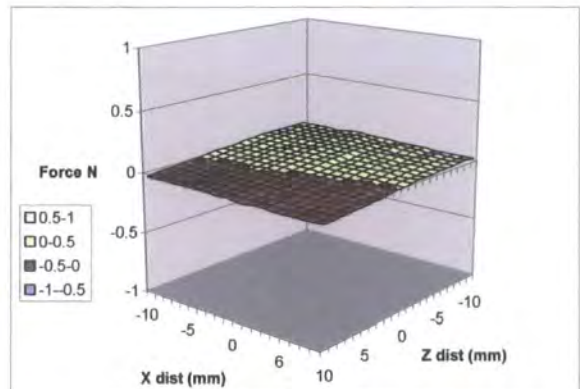Figure 4.5.4.10, Force in z direction at 32mm



Figure 4.5.4.11, Force in z direction at 36mm



Figure 4.5.4.12, Force in z direction at 40mm

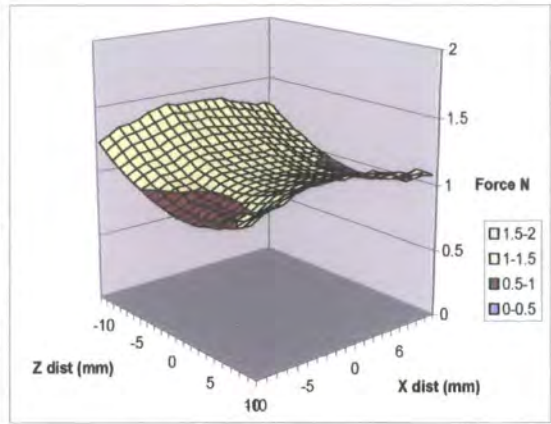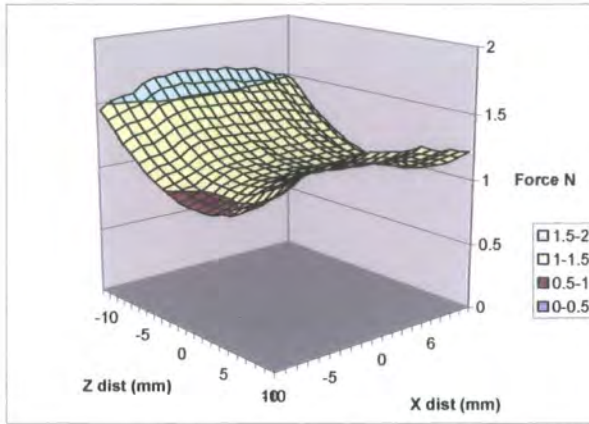Forces in the y direction for rail configuration 4;



Figure 4.5.4.13, Force in y direction at 20mm Figure 4.5.4.14, Force in y direction at 24mm
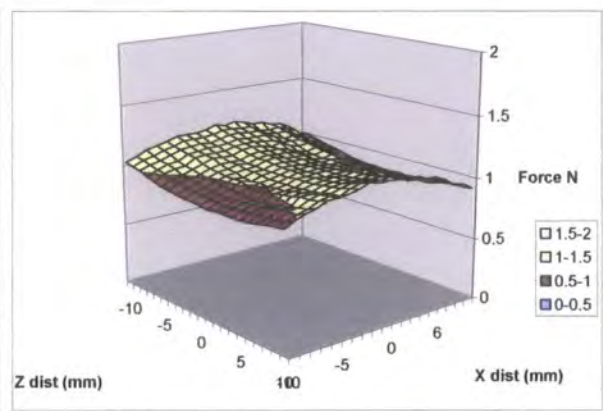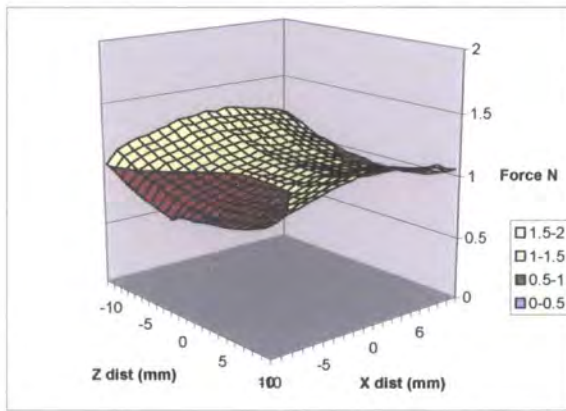


Figure 4.5.4.15, Force in y direction at 28mm Figure 4.5.4.16, Force in y direction at 32mm
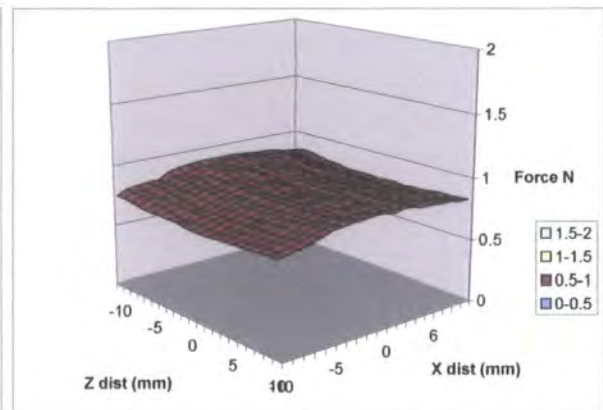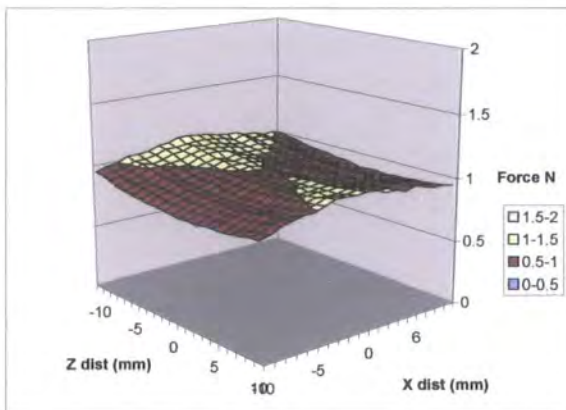


Figure 4.5.4.17, Force in y direction at 36mm Figure 4.5.4.18, Force in y direction at 40mm
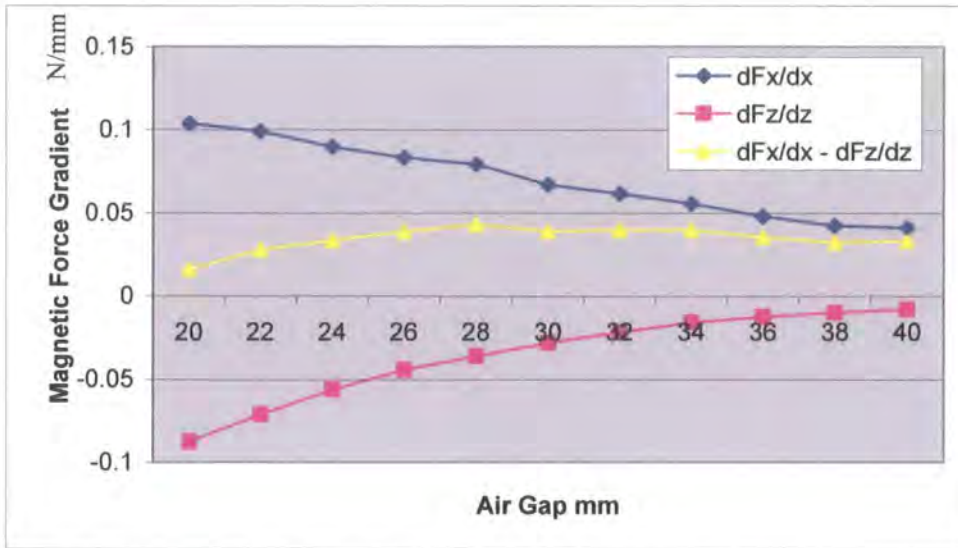
Figure 4.5.4.19, Graph of magnetic field gradients for rail configuration 4.

With the gap between the fixed base magnets reduced to 12mm, in rail configuration 4, there is no point above an air gap of 20mm at which the configuration is more stable than unstable. The graph of the magnetic gradients shows that this configuration would be likely to become stable below a height of 18mm. As with the previous set of results this is due to the horizontal component of the forces between the magnets being reduced as the angle of interaction of the magnetic flux decreases. Again the vertical force acting on the levitating magnet is increased as there is more overlap between the dimensions of the fixed base magnets and the levitating magnet. The results produced from theses traverses show how the configuration of the three pod system affects the size of the stable levitating region. Increasing the gap between the fixed base magnets results in a more stable system and the lower the height at which the levitation occurs, the more stable the levitation becomes. Decreasing the gap between the fixed base magnets increases the load bearing capability of the three magnet system as this increase the overlap between the "levitating" magnet and the fixed base magnets. However this also decreases the stability of the three magnet system and reduces the height at which stable levitation can occur.

The traverses were then repeated with a 16mm gap, rail configuration 5, between the fixed base magnets, and two extra magnets were added so that each base magnet consisted of a stack of two magnets to assess their effect on the stable levitation region and the vertical forces acting on the magnets.

4.5.5, Force testing of rail configuration 5.

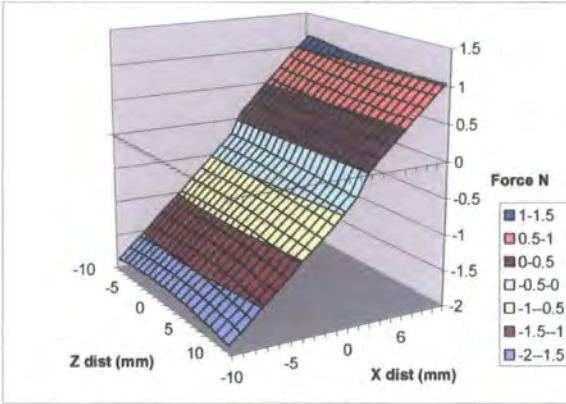Forces in the x direction for rail configuration 5;



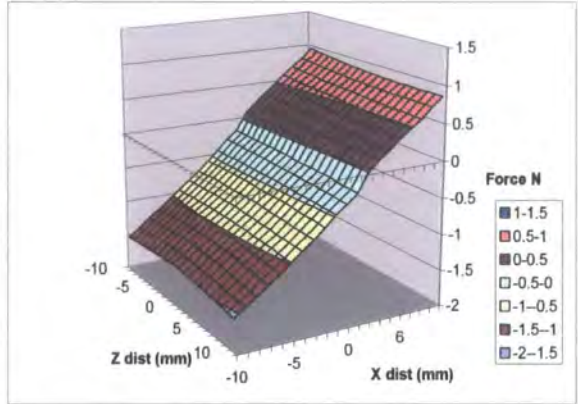Figure 4.5.5.1, Force in x direction at 20mm



Figure 4.5.5.2, Force in x direction at 24mm



Figure 4.5.5.3, Force in x direction at 28mm



Figure 4.5.5.4, Force in x direction at 32mm



Figure 4.5.5.5, Force in x direction at 36mm



Figure 4.5.5.6, Force in x direction at 40mm

Forces in the z direction for rail configuration 5;



Figure 4.5.5.7, Force in z direction at 20mm



Figure 4.5.5.8, Force in z direction at 24mm



Figure 4.5.5.9, Force in z direction at 28mm



Figure 4.5.5.10, Force in z direction at 32mm



Figure 4.5.5.11, Force in z direction at 36mm



Figure 4.5.5.12, Force in z direction at 40mm

Forces in the y direction for rail configuration 5;



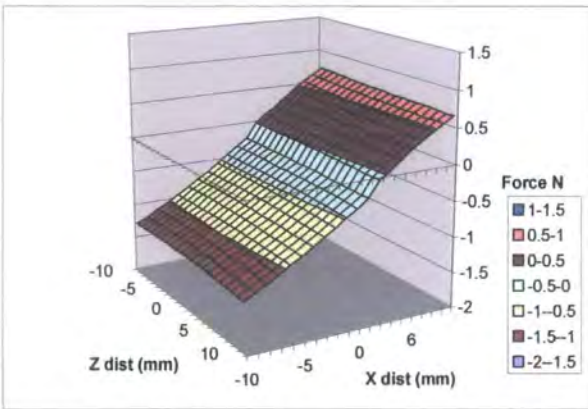Figure 4.5.5.13, Force in y direction at 20mm Figure 4.5.5.14, Force in y direction at 24mm



Figure 4.5.5.15, Force in y direction at 28mm Figure 4.5.5.16, Force in y direction at 32mm



Figure 4.5.5.17 Force in y direction at 36mm Figure 4.5.5.18, Force in y direction at 40mm

Figure 4.5.5.19, Graph of Magnetic Field Gradients for rail configuration 5.

Doubling the thickness of the fixed base magnets with a 16mm gap between them, as in rail configuration 5, increased the instability of the system and resulted in the configuration of magnets being unstable above a height of 18mm between the magnets. However the vertical force acting on the "levitating" magnets was significantly increased compared to the configuration with single fixed base magnets with a 16mm gap. The traverses were then repeated with rail configuration 6 where the thickness of the "levitating" magnet was doubled, and the thickness of the base magnets reduced back to their original thickness.

4.5.6, Force testing of rail configuration 6.

Forces in the x direction for rail configuration 6;



Figure 4.5.6.1, Force in x direction at 20mm



Figure 4.5.6.2, Force in x direction at 24mm
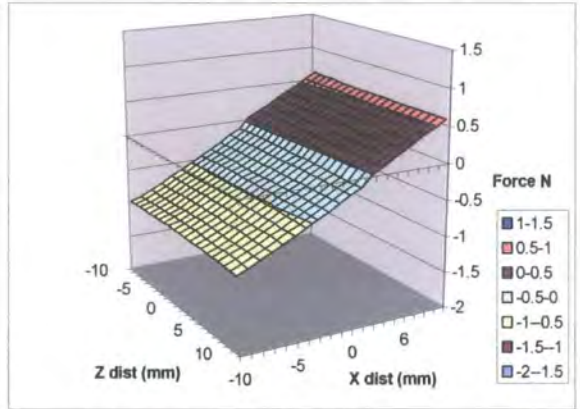


Figure 4.5.6.3, Force in x direction at 28mm
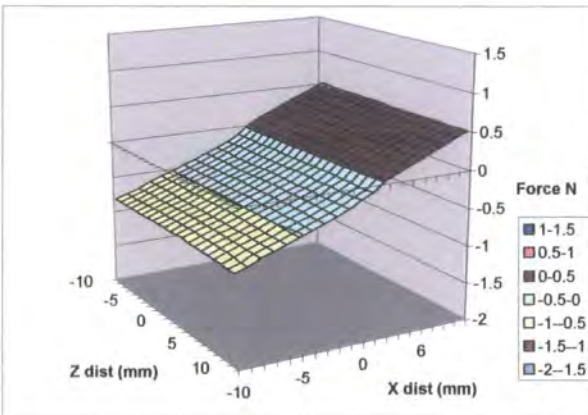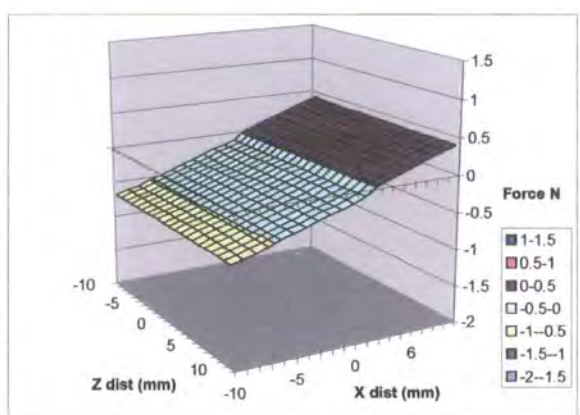


Figure 4.5.6.4, Force in x direction at 32mm



Figure 4.5.6.5, Force in x direction at 36mm



Figure 4.5.6.6, Force in x direction at 40mm
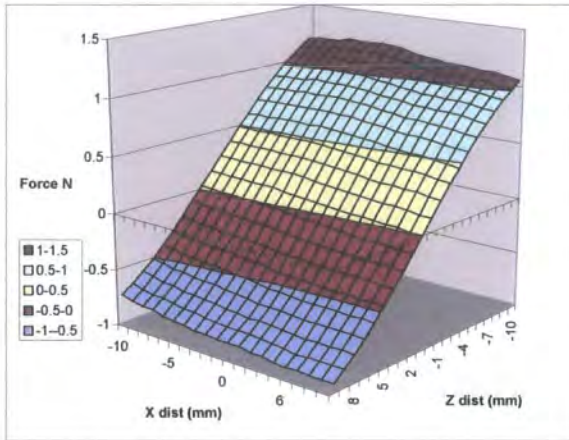
Forces in the z direction for rail configuration 6;

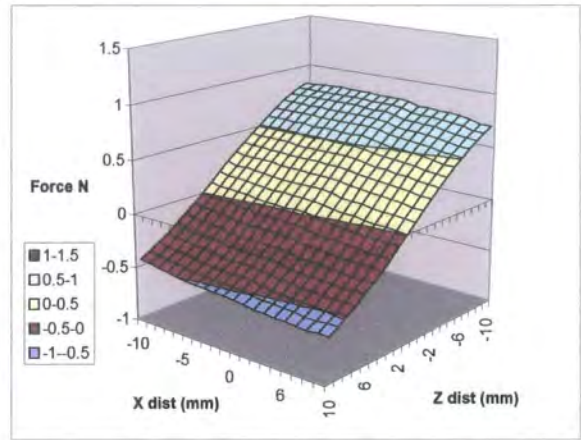

Figure 4.5.6.7, Force in z direction at 20mm



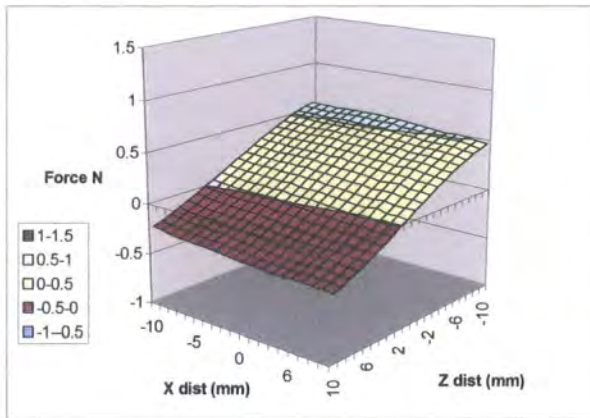Figure 4.5.6.8, Force in z direction at 24mm



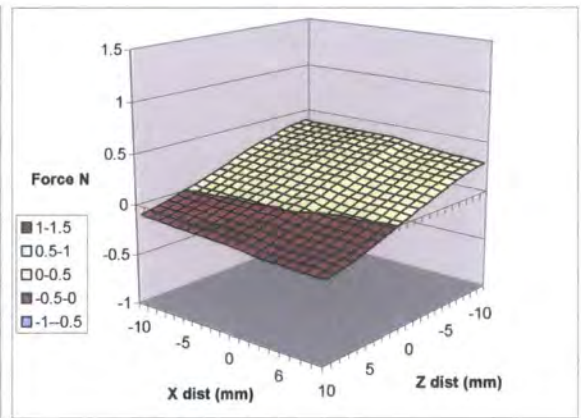Figure 4.5.6.9, Force in z direction at 28mm



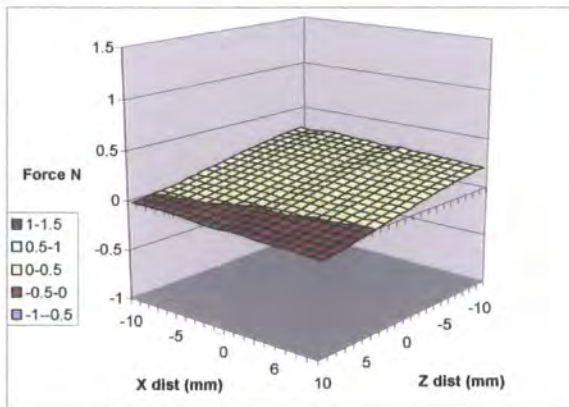Figure 4.5.6.10, Force in z direction at 32mm
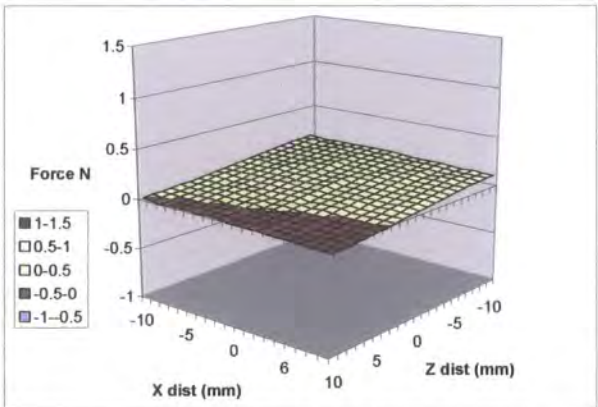


Figure 4.5.6.11, Force in z direction at 36mm



Figure 4.5.6.12, Force in z direction at 40mm
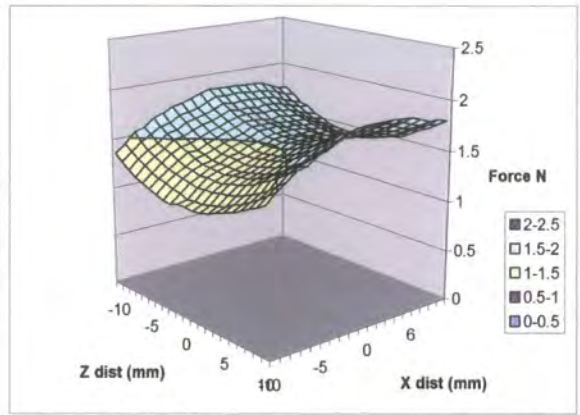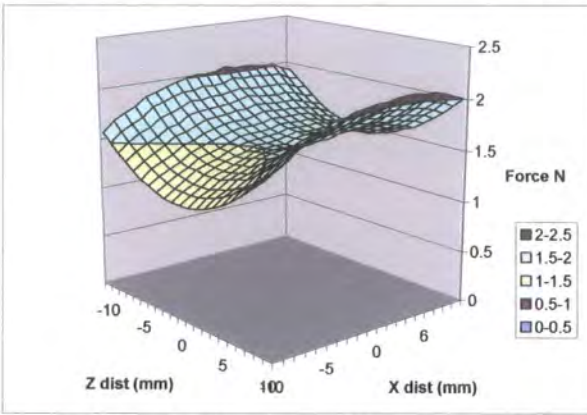
Forces in the y direction for rail configuration 6;
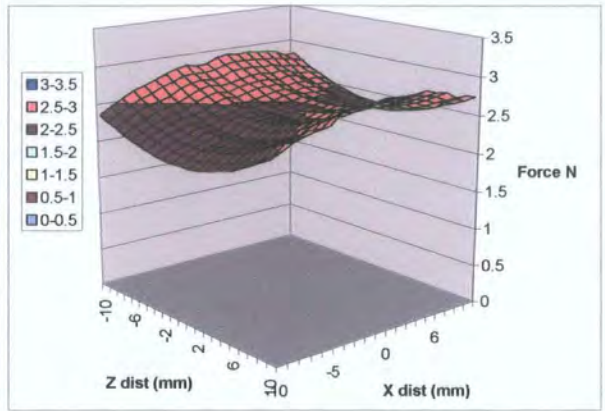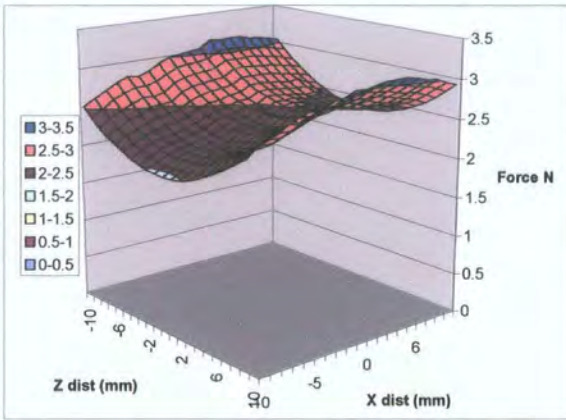


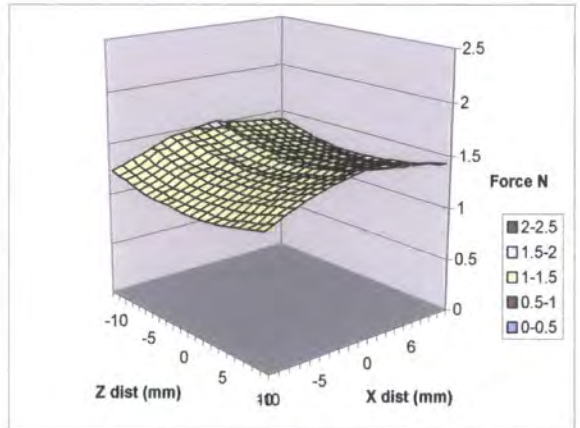Figure 4.5.6.13, Force in y direction at 20mm Figure 4.5.6.14, Force in y direction at 24mm
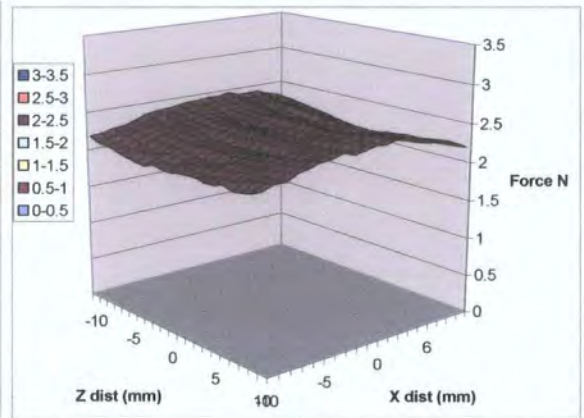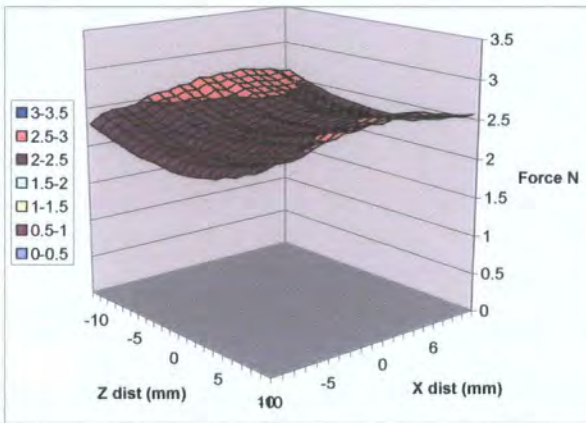

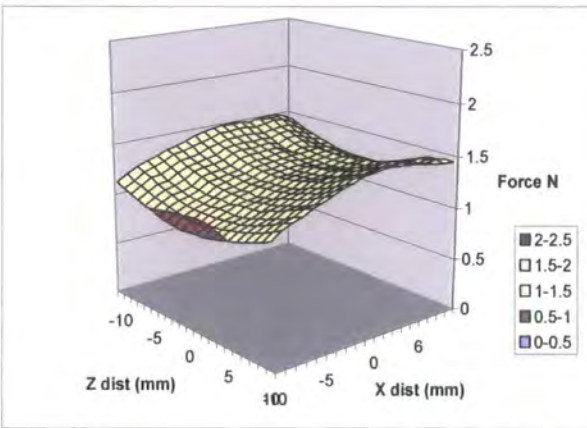
Figure 4.5.6.15, Force in y direction at 28mm Figure 4.5.6.16, Force in y direction at 32mm
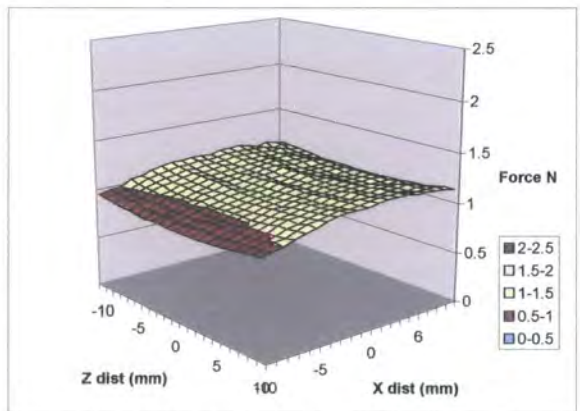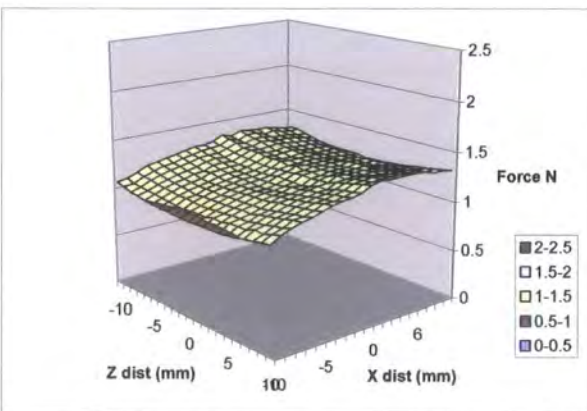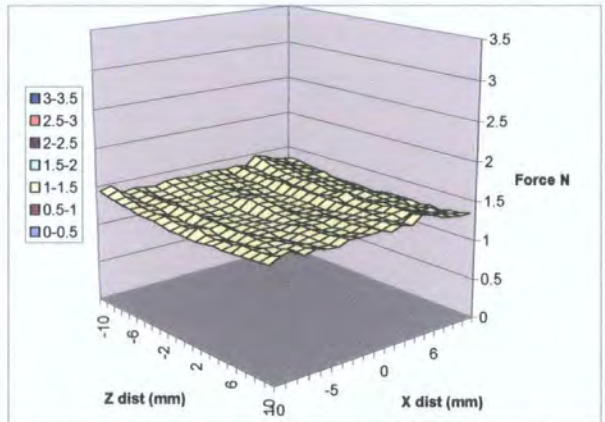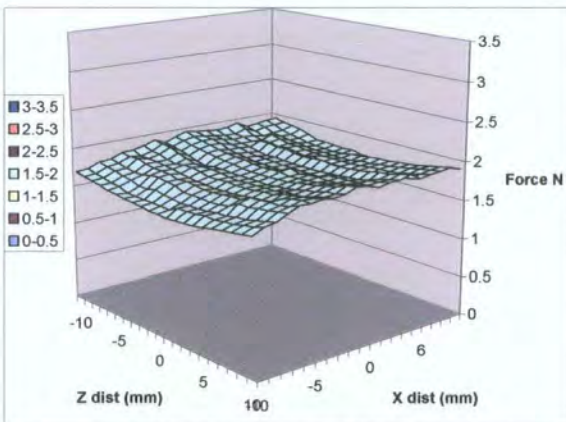


Figure 4.5.6.17, Force in y direction at 36mm Figure 4.5.6.18, Force in y direction at 40mm
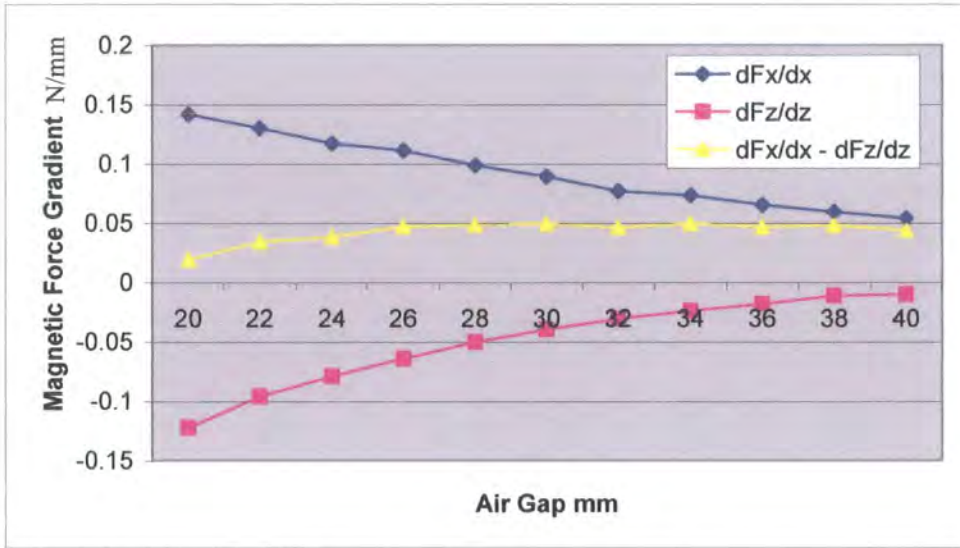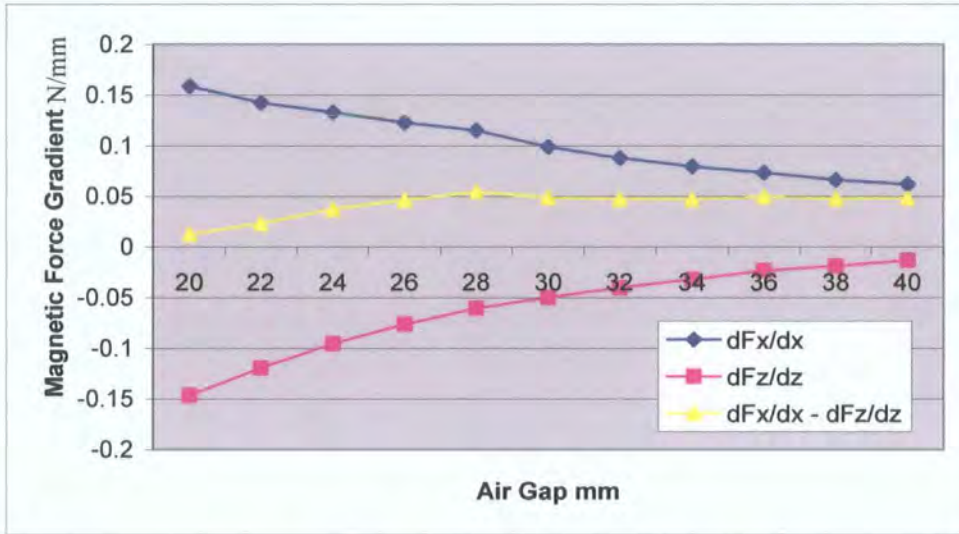
Figure 4.5.6.19, Graph of Magnetic Field Gradients for rail configuration 6.

4.5.7 Effect of Magnet Stacking

Doubling the "levitating" magnet, as in rail configuration 6, has a similar effect on the gradients of the magnetic fields as doubling the fixed base magnets, as in rail configuration 5, in increasing the instability of the system. The system became unstable above a levitation height of 18mm. However the increase in vertical force acting on the three magnet configuration was significantly greater than the increase that occurred when the fixed base magnets were doubled. This effect is due to the shape of the magnetic fields produced by the magnets. In order to show the effects of additional magnets on the magnetic fields produced by a small magnet positioned over a larger magnet the formation was modelled in MEGA (2000), the meshed magnets were assigned as permanent magnets with opposing field directions. Figure 4.5.7.1 shows the magnetic fields produced by a small magnet positioned over a large magnet. Figure 4.5.7.2 shows the magnetic fields produced by stacking two small magnets over the initial large magnet. Figure 4.5.7.3 shows the magnetic fields produced by stacking two large magnets below the initial small magnet.

The addition of a second small magnet results in a stronger field which mainly acts within the boundaries of the larger magnet, thereby maximising the interaction between the flux lines of both magnets. However when a second large magnet is added to the original system the result is an increased magnetic field of which only part interacts with the small magnet.

The addition of a second large magnet increases the levitation force but not as much as the addition of a second small magnet because of the way the additional magnetic flux is distributed.
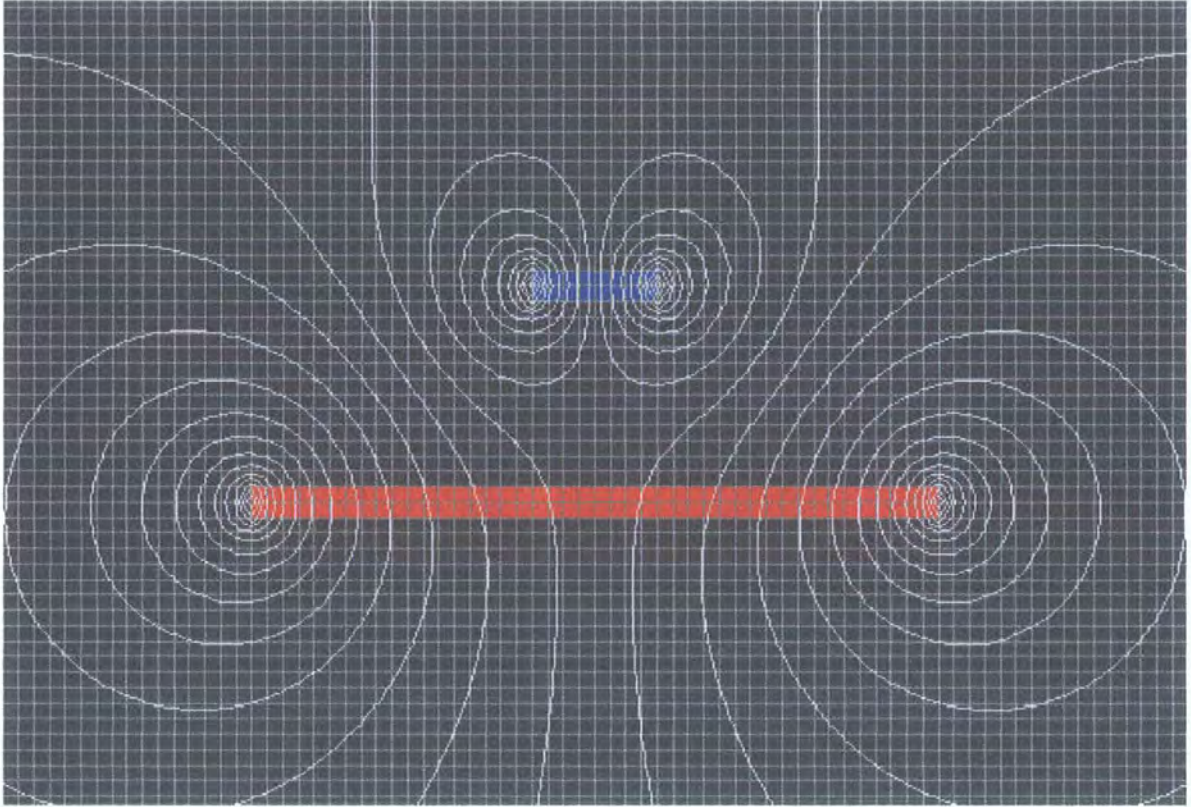


Figure 4.5.7.1, Small Magnet over Larger Magnet of Identical Thickness
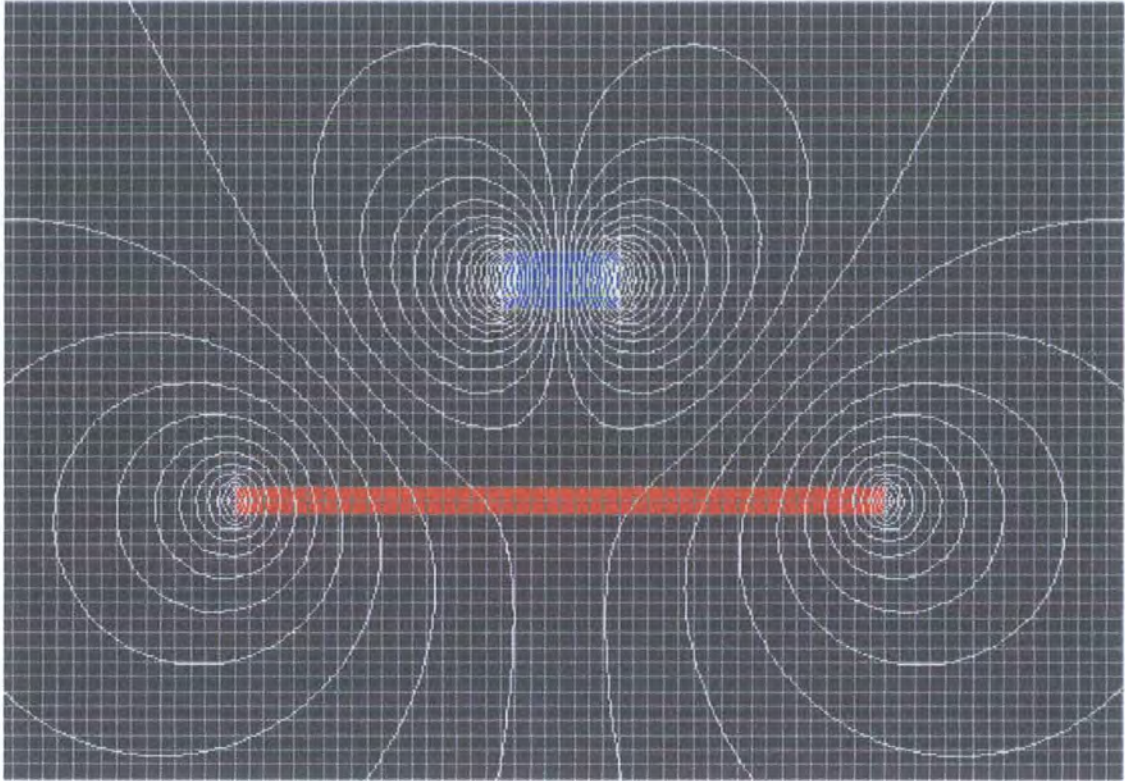
Figure 4.5.7.2, Double Thickness Small Magnet over Large Magnet
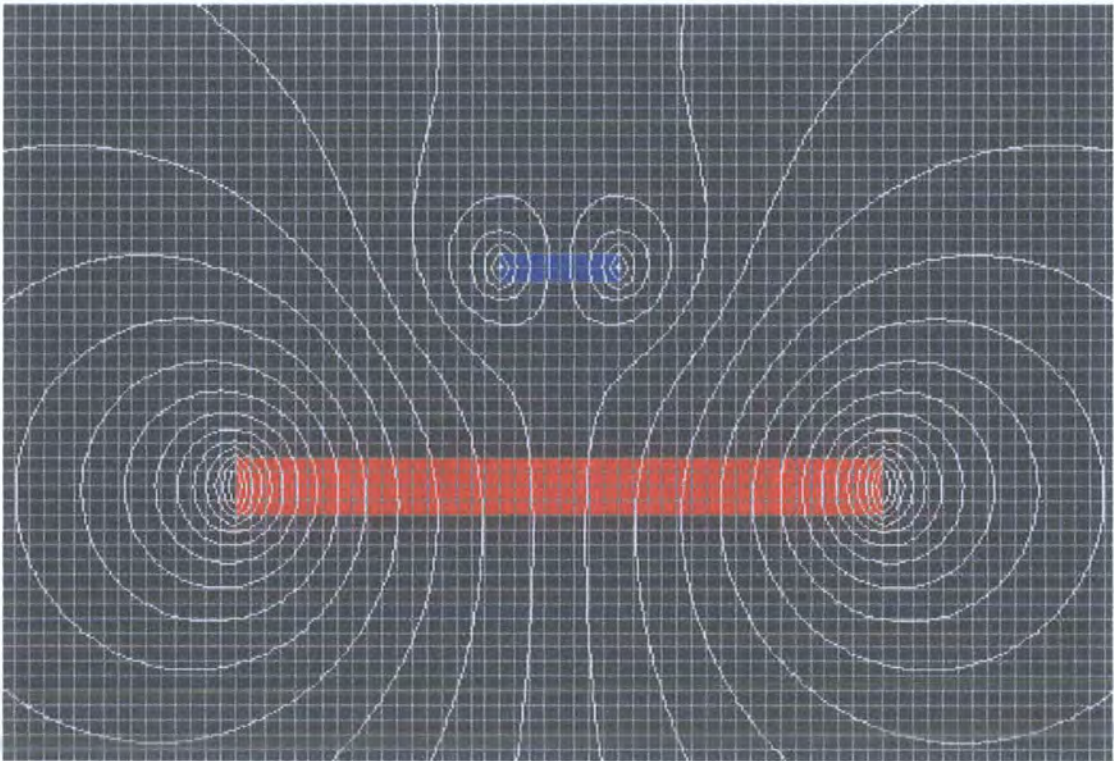


Figure 4.5.7.3, Small Magnet over Double Thickness Large Magnet

4.5.8, Force testing of rail configuration 7.

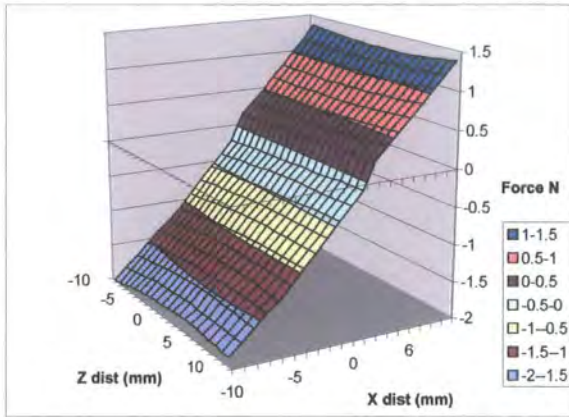Forces in the x direction for rail configuration 7;
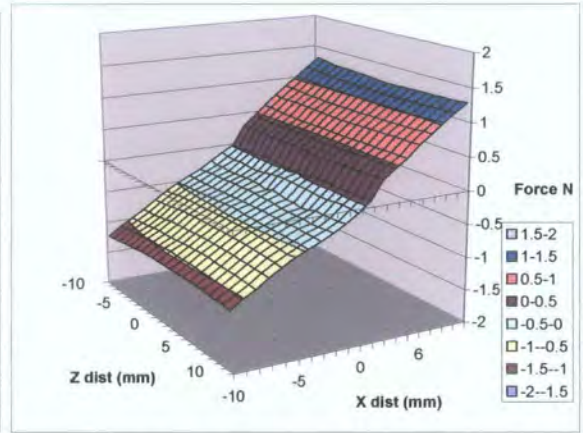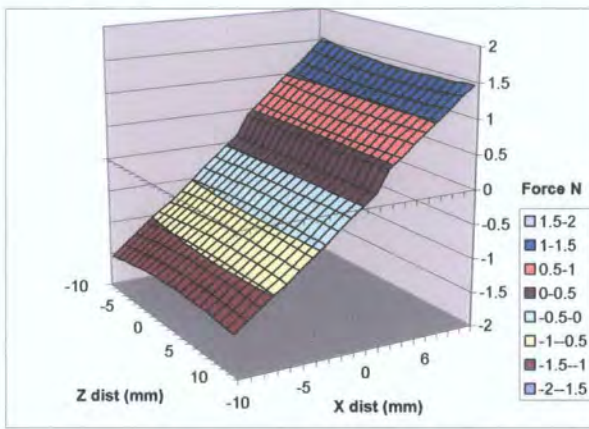


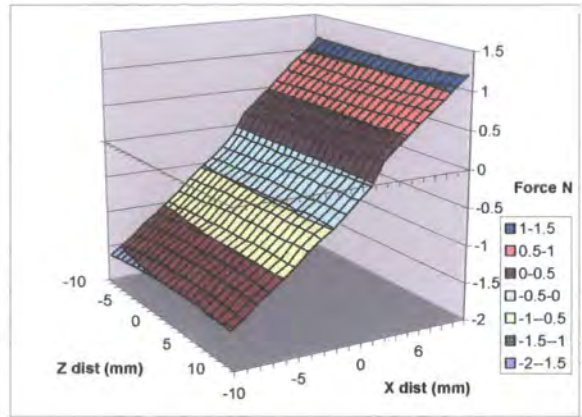Figure 4.5.8.1, Force in x direction at 20mm



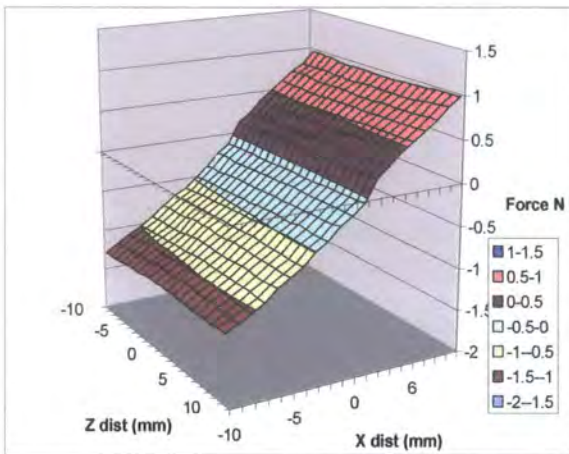Figure 4.5.8.2, Force in x direction at 24mm



Figure 4.5.8.3, Force in x direction at 28mm



Figure 4.5.8.4, Force in x direction at 32mm
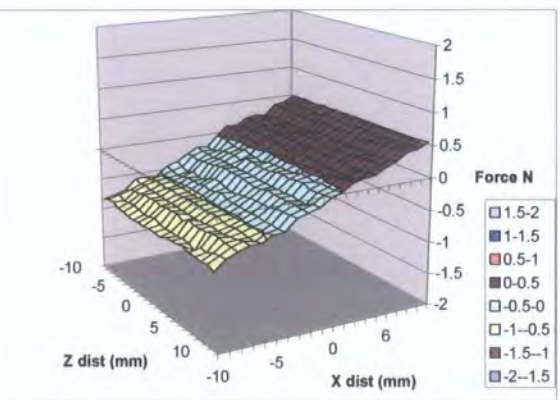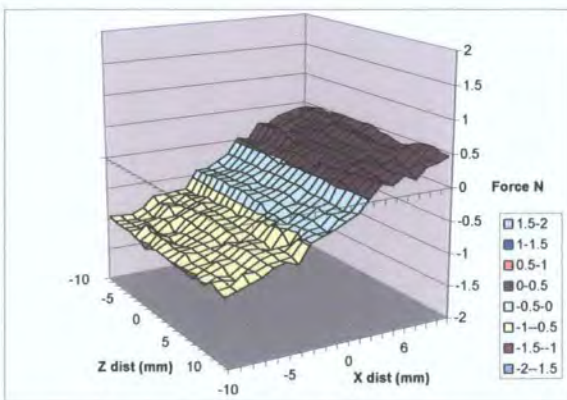


Figure 4.5.8.5, Force in x direction at 36mm



Figure 4.5.8.6, Force in x direction at 40mm

127

Forces in the z direction for rail configuration 7;
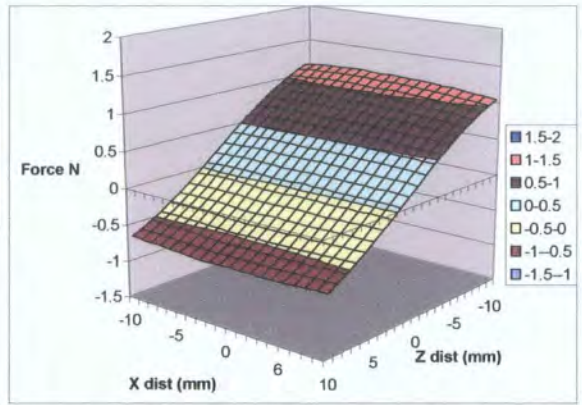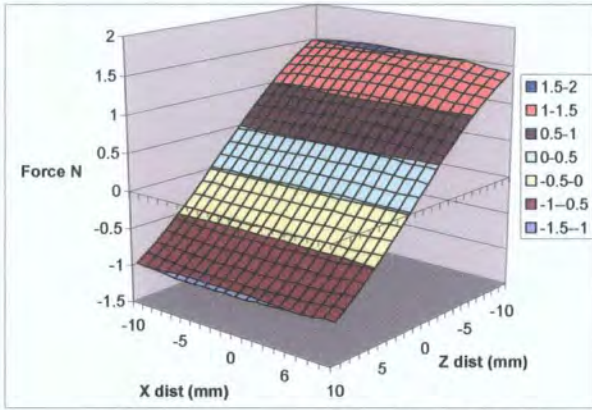


Figure 4.5.8.7, Force in z direction at 20mm



Figure 4.5.8.8, Force in z direction at 24mm
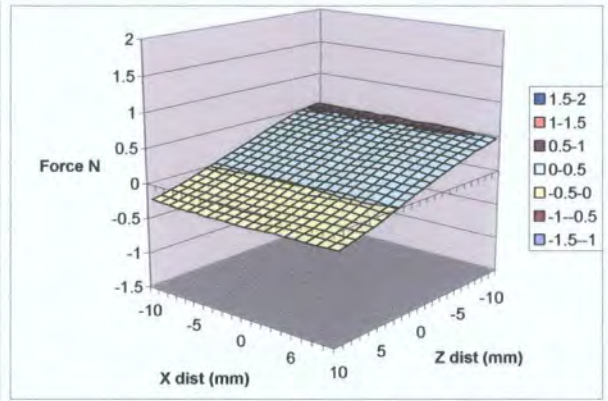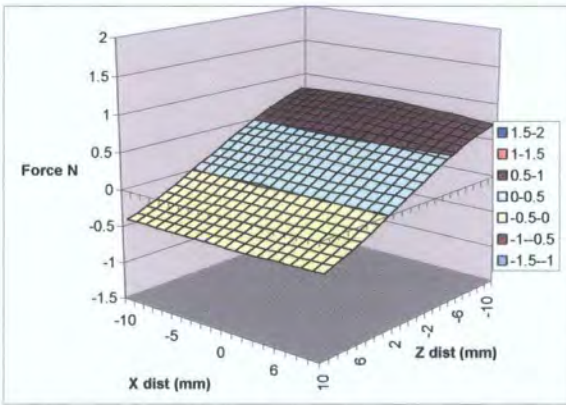


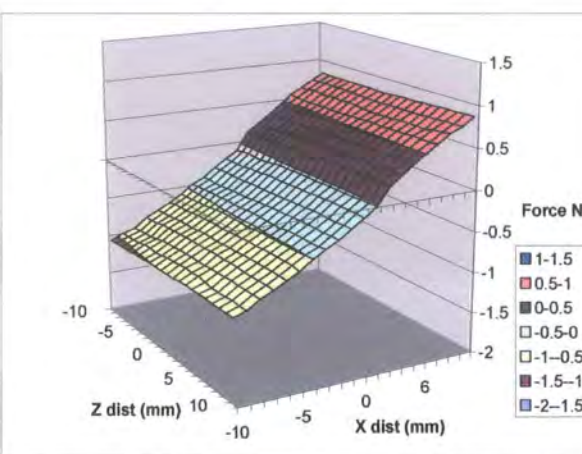Figure 4.5.8.9, Force in z direction at 28mm



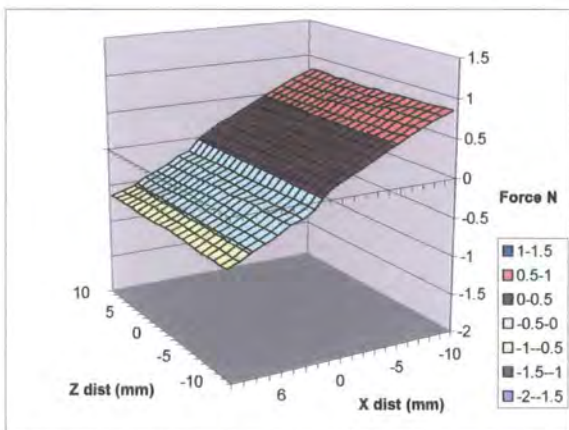Figure 4.5.8.10, Force in z direction at 32mm
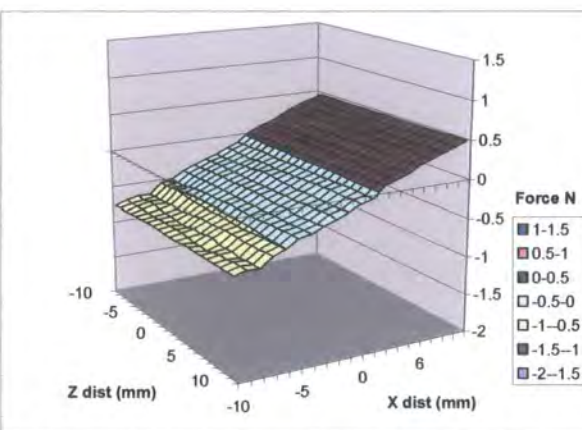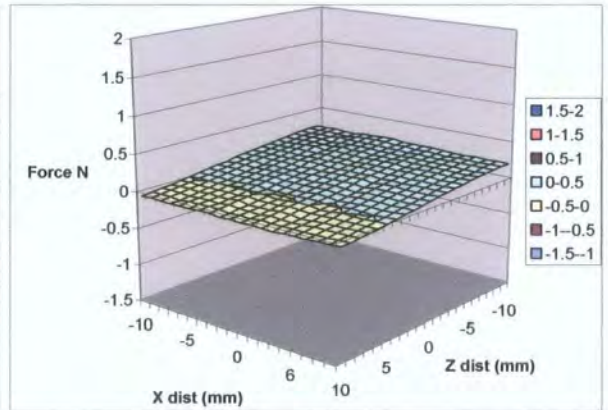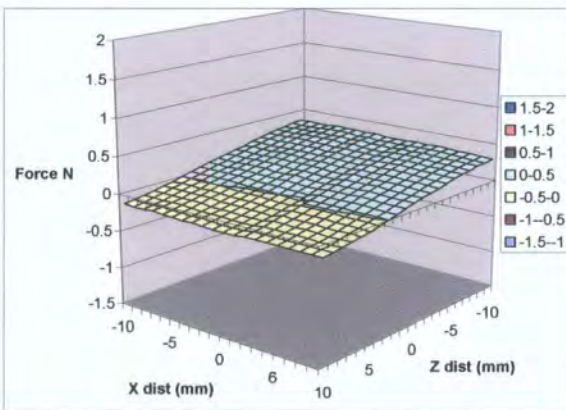


Figure 4.5.8.11, Force in z direction at 36mm



Figure 4.5.8.12, Force in z direction at 40mm
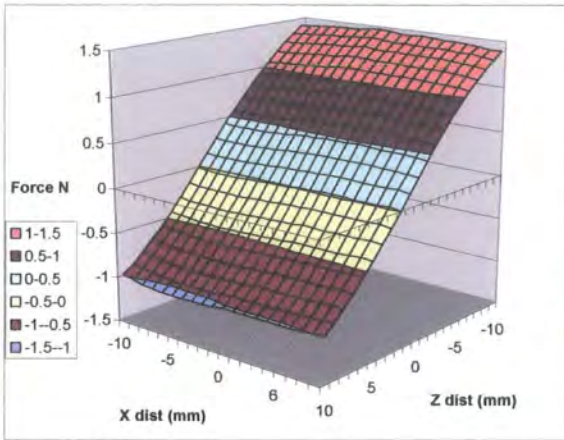
Forces in the y direction for rail configuration 7;
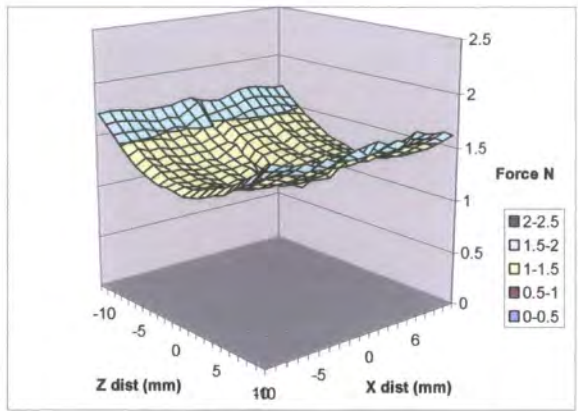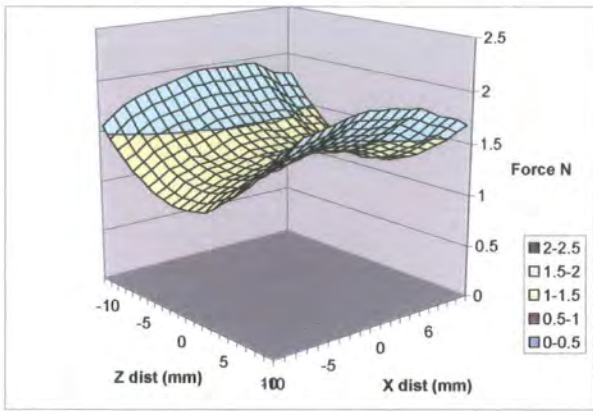


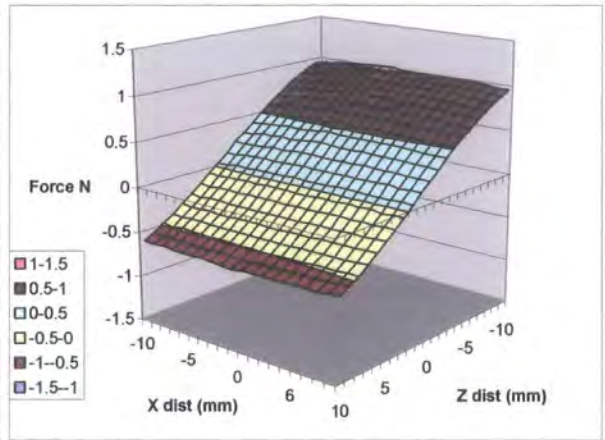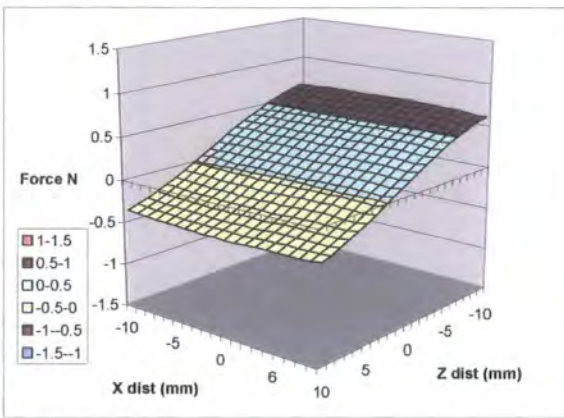Figure 4.5.8.13, Force in y direction at 20mm Figure 4.5.8.14, Force in y direction at 24mm
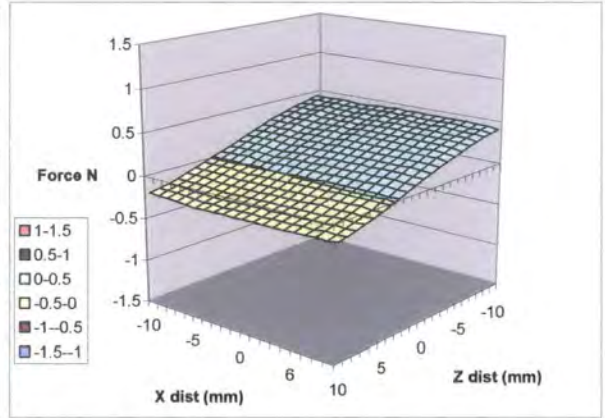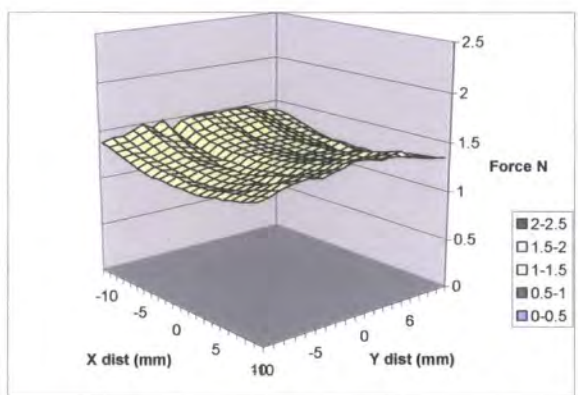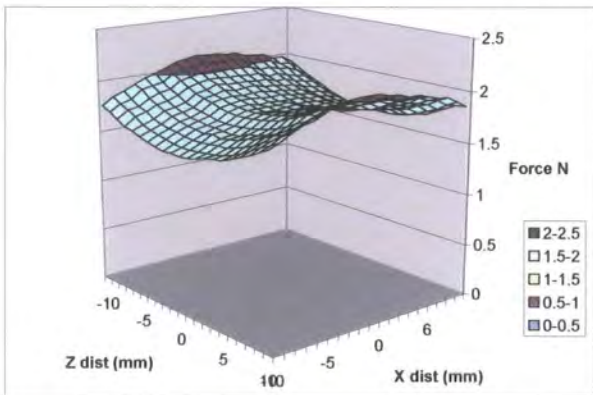


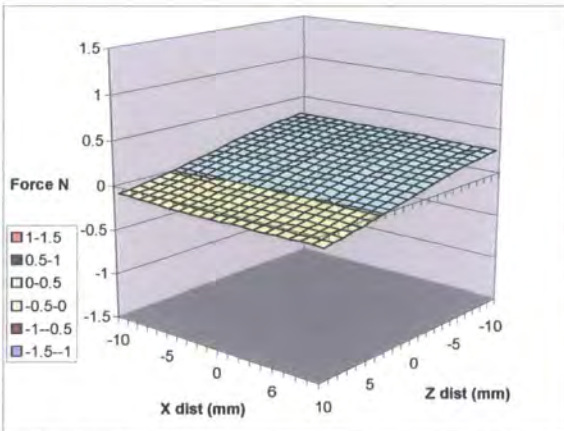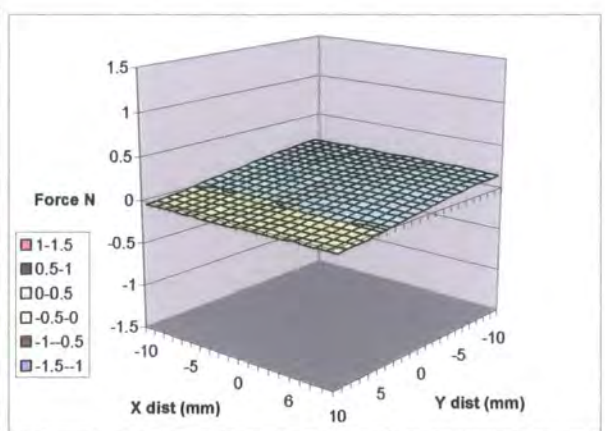Figure 4.5.8.15, Force in y direction at 28mm Figure 4.5.8.16, Force in y direction at 32mm
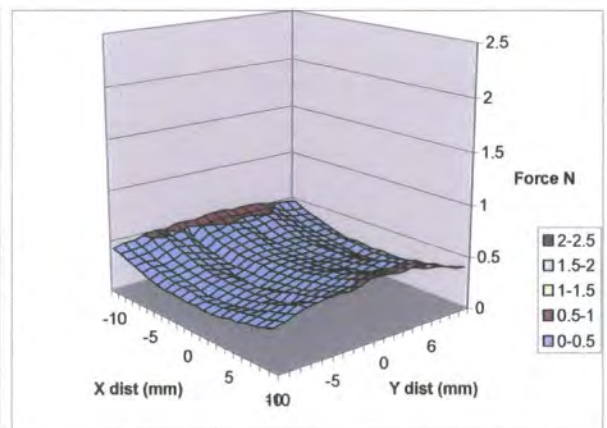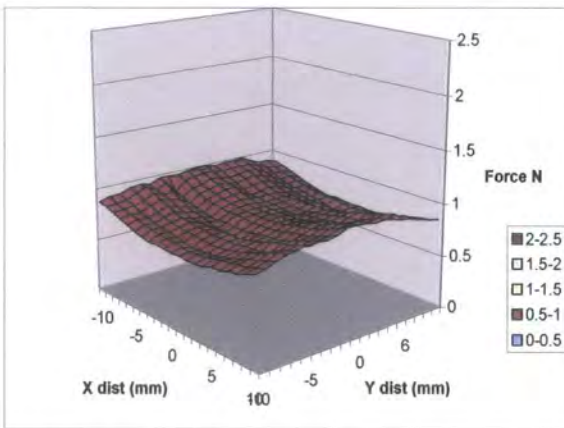


Figure 4.5.8.17, Force in y direction at 36mm Figure 4.5.8.18, Force in y direction at 40mm
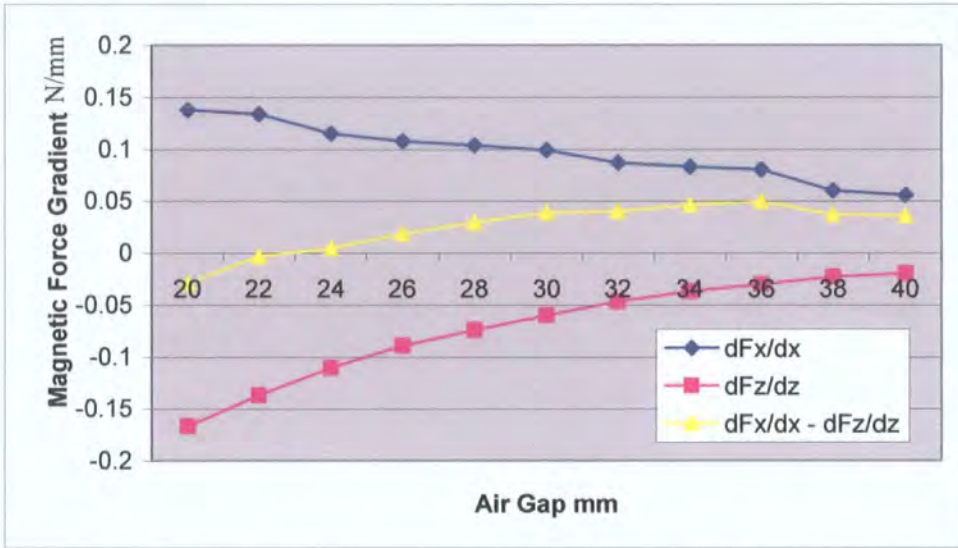
Figure 4.5.8.19, Graph of Magnetic Field Gradients for rail configuration 7.

As expected from the results of the previous traverses, it was found that increasing the gap between the fixed base magnets to 18mm reduces the instability in the x direction, and increases the restoring force in the z direction. As a result the height at which the three magnet system is stable is also increased; below a height of 23mm the system is more stable than unstable. In line with previous results the vertical force produced by the system is also reduced.

4.6, The Levitron

A more elegant and compact solution than an infinitely long magnetic "rail" would be to turn the system into a closed loop by the use of a ring magnet and a cylindrical levitating magnet. By effectively joining either end of the ends of the fixed magnetic base described previously the destabilising force should be eliminated leaving a system that is only unstable in pitch and roll, although due to the symmetry of such a system they can be treated as instability in one degree of freedom only. A system based on such principles is the Levitron (Dullin 1999) the configuration of which is shown in figure 4.6.1.

Rare-earth disc magnet "top"

Ferrite ring magnet
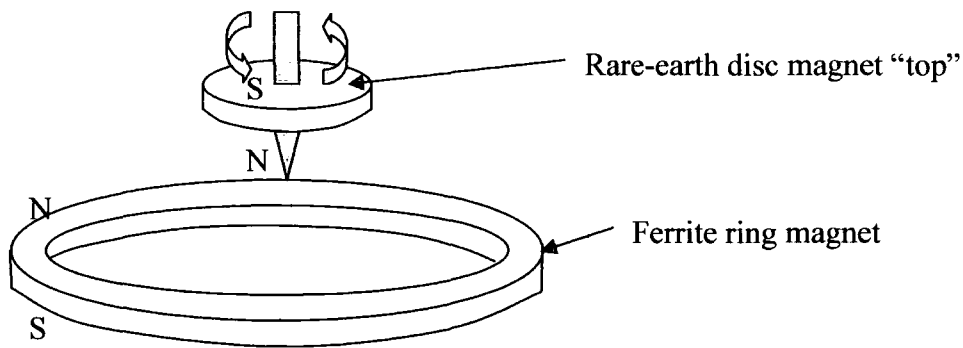
Figure 4.6.1; The Levitron

The Levitron consists of a ferrite ring magnet encased in the plastic base of the Levitron and a spinning top that is made of a rare-earth magnet mounted in a plastic "top" with the like poles of the magnets opposing each other. The Levitron works in a similar way to the magnetic "rails" described previously; a small stable region exists above the ring magnet where the repulsion of the two magnets is equal to the gravitation pull on the top, and any horizontal displacement of the levitating magnet is opposed by the ring magnet. The gyroscopic effect of the spinning top keeps it stable in pitch and roll preventing the top from flipping over.

Three Levitrons spaced at a suitable distance apart with the tops connected together by a stiff frame should, in theory, be able to achieve stable levitation without the need for the stabilising gyroscopic force that the spinning motion of the top provides. However in practice this is unlikely. The Levitron has several drawbacks, it has an extremely small stable region and constantly requires fine adjustment of its weight, and each Levitron comes with a selection of washers to allow adjustment of the weight by as little as 0.5 g. Small changes in the ambient temperature affect the magnetic field produced by the magnet which requires the weight of the top to be changed in order to remain balanced.

The spinning top experiences a restoring force when it is moved away from its central position. The restoring force decreases with increasing height as the horizontal component of the force between the two magnets decrease as the angle of the interaction between the

131

magnetic flux increases, as shown in figure 4.6.2. When the spinning top is a long distance away from the ring magnet it experiences a primarily vertical force, as it approaches the ring magnet the vertical repulsion force it feels becomes less as lines of magnetic flux that are interacting between the magnets become more vertical than horizontal and the forces acting on the top in the horizontal plane increases. The lower the spinning top is the greater the horizontal stability the Levitron possesses, but the vertical force it produces is decreased, as shown in figures 4.6.3 - 4.6.13.
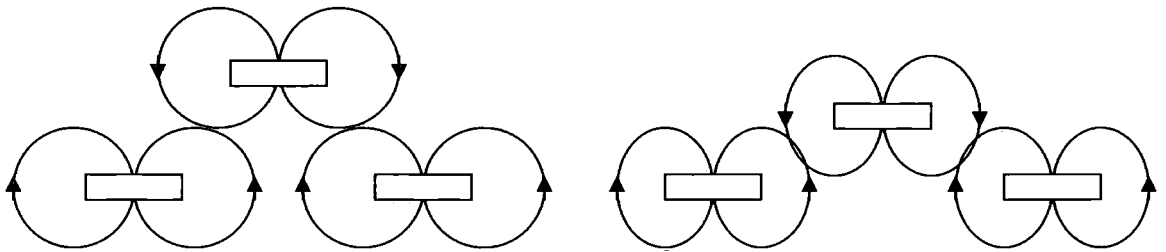


Figure 4.6.2, Magnetic Field Interactions of the Levitron

When the vertical repulsion force acting on the top becomes less than the weight of the spinning top, levitation breaks down. There is only a small region where the repulsion force keeping the magnet levitating is greater than the weight of the top, and the horizontal restoring force is strong enough to prevent the lateral movement of the magnet. Figure 4.6.3 through figure 4.6.7 show the rapid decrease in the horizontal restoring force acting on the top as the levitation height increases. Figure 4.6.8 through figure 4.6.13 show how the vertical forces acting on the top change as the levitation height increases.

Radial forces acting on the spinning top of the Levitron;
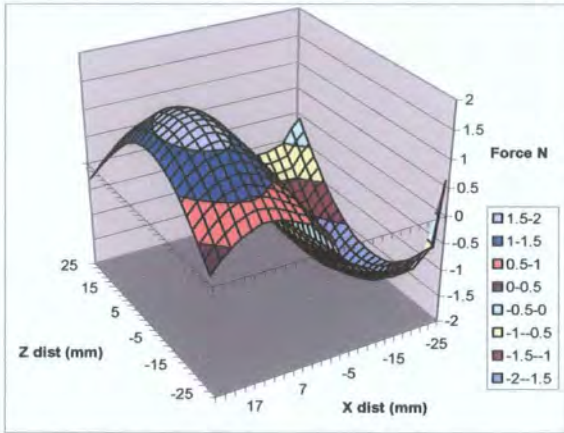


Figure 4.6.3; Force in x direction at 25mm    Figure 4.6.4; Force in x direction at 29mm
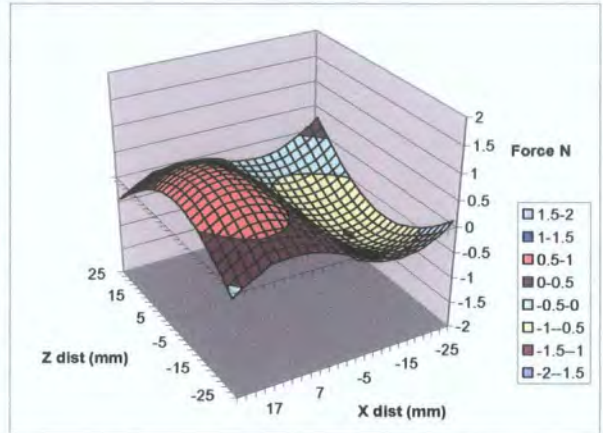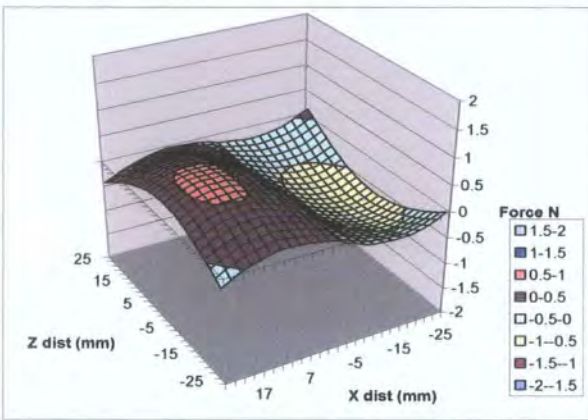


Figure 4.6.5; Force in x direction at 33mm    Figure 4.6.6; Force in x direction at 37mm
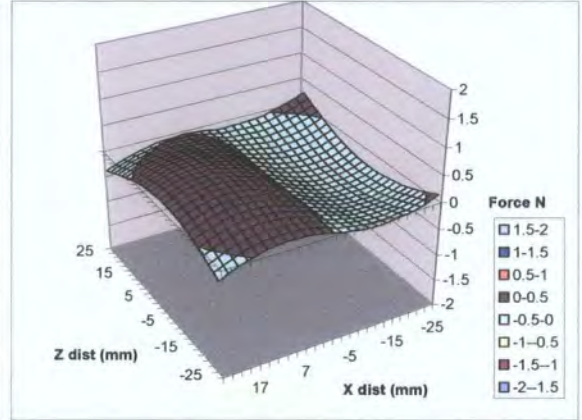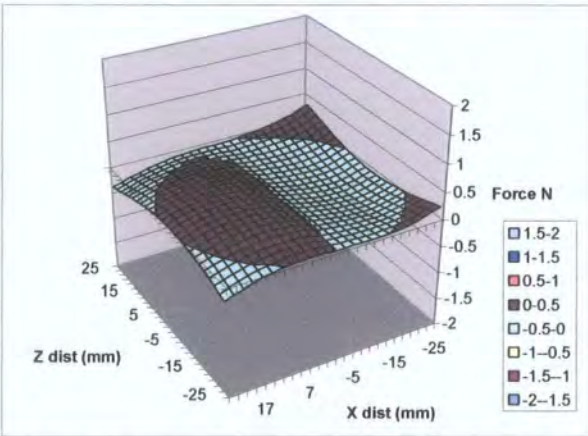


Figure 4.6.7; Force in x direction at 41mm    Figure 4.6.8; Force in x direction at 45mm
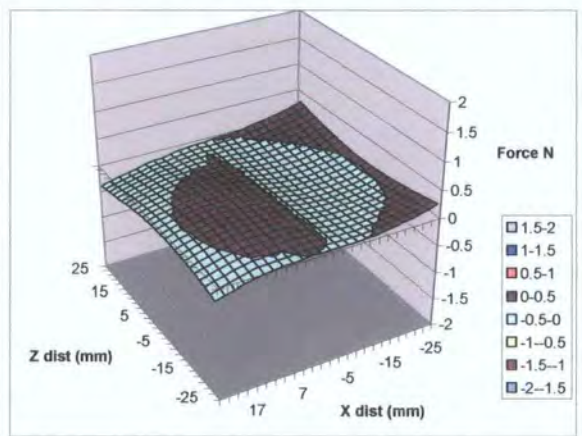
Vertical forces acting on the spinning top of the Levitron;
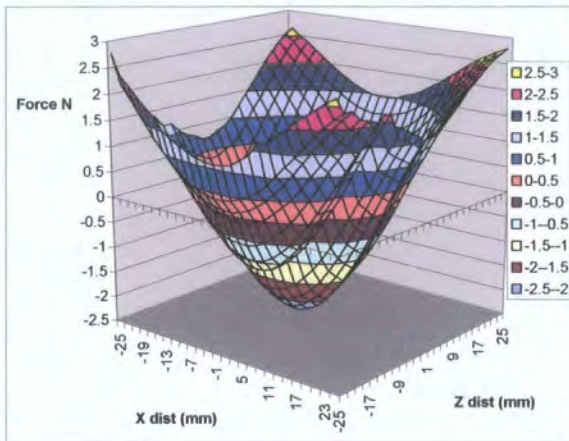


Figure 4.6.9; Force in y direction at 25mm
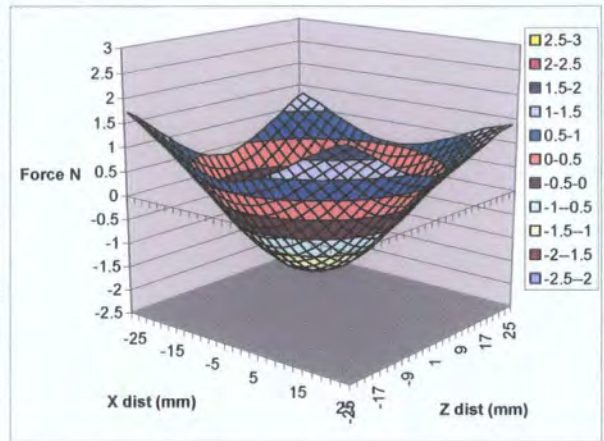


Figure 4.6.10; Force in y direction at 29mm
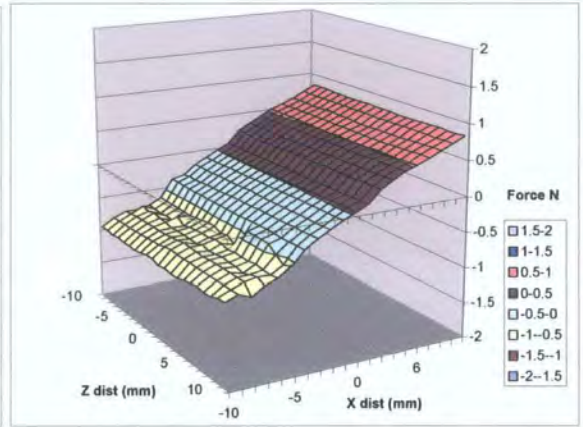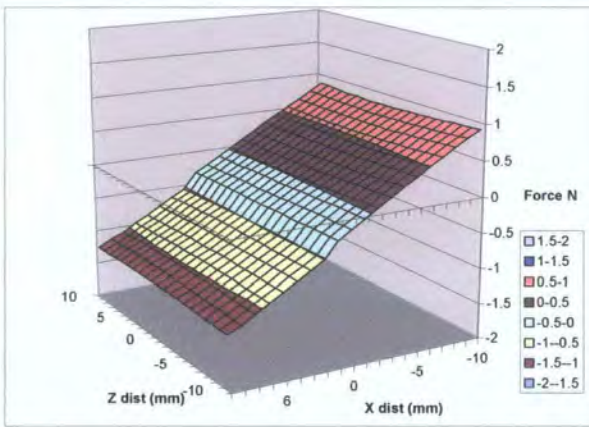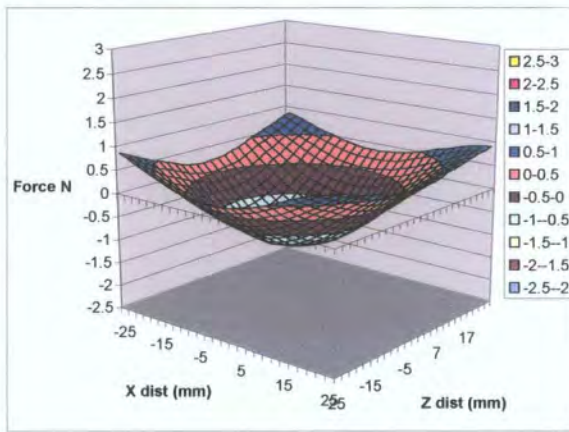


Figure 4.6.11: Force in y direction at 33mm
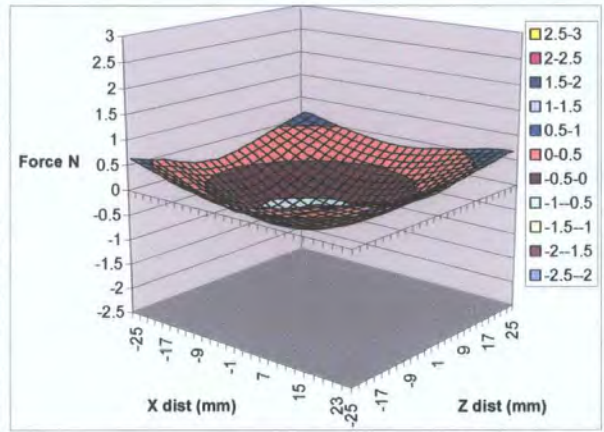


Figure 4.6.12: Force in y direction at 37mm
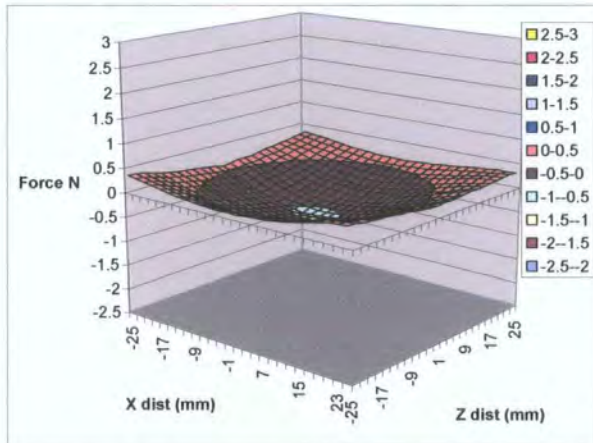


Figure 4.6.13; Force in y direction at 41mm
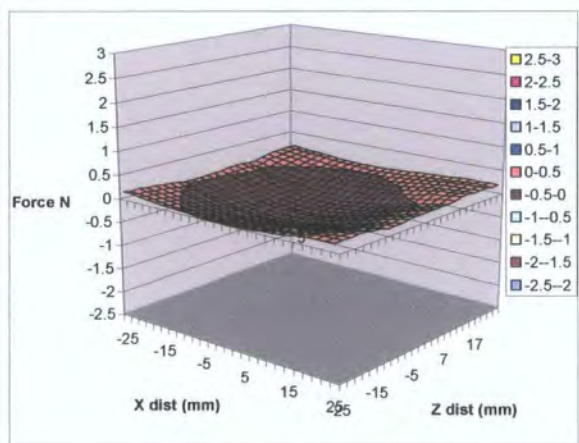


Figure 4.6.14; Force in y direction at 45mm
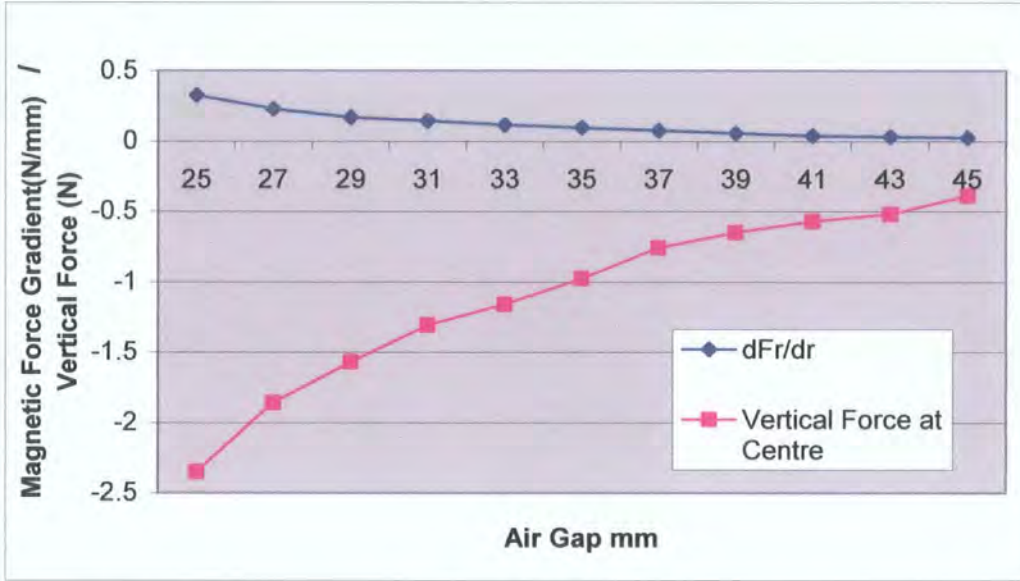
Figure 4.6.15: Magnetic field gradients and vertical force produced by the Levitron.

Figure 4.6.15 shows the gradients of the magnetic fields as the magnets are moved radially from their central position and the vertical forces at the centre of the Levitron. At a height of 25mm above the ring magnet the restoring force to any horizontal movement of the levitating magnet is significant. However as the height of the "levitating" magnet increases the gradient of the restoring force drops dramatically and at the point at which the vertical force becomes positive is approached the restoring forces are very small. As a result the Levitron is only capable of supporting light magnets, and with changing atmospheric conditions affecting the magnetic field strength regular adjustment of the ballast added to the levitating magnet in increments as small as 0.5g are required. As a consequence the Levitron can only resist small horizontal or vertical displacements before stable levitation breaks down.

4.7, Ring Magnets

The Levitron arrangement of a cylindrical magnet levitating over a ring magnet is an attractive solution to the problem of creating stable levitation. The original Levitron used a rare earth levitating magnet and a ferrite base ring magnet, presumably because ferrite magnets are considerably cheaper than Neodymium magnets and ferrite magnets are safer for untrained personnel to handle.

Through the use of a rare earth magnet as the base magnet in a similar arrangement to the Levitron it should be possible to achieve greater levitation height and greater load bearing capabilities due to the much greater magnetic field strength of Neodymium-Iron-Boron magnets. Various ring magnets were tested for suitability for levitation, with varying inner and outer diameter. Circular magnets with diameter of 40mm and thickness of 6mm were attached to a gimbal via a 1m long non-ferrous arm to restrict movement to two degrees of freedom. The rare earth ring magnets enabled levitation to occur at a larger air gap; however they still only produced a very small stable region. This was due to the flux distribution around the ring magnet. Although the system with the ring magnets is in essence an extension of the "rail" system shown in figure 4.3.3, the flux distributions are very different due to the geometry of the magnet.



(a)                                        (b)
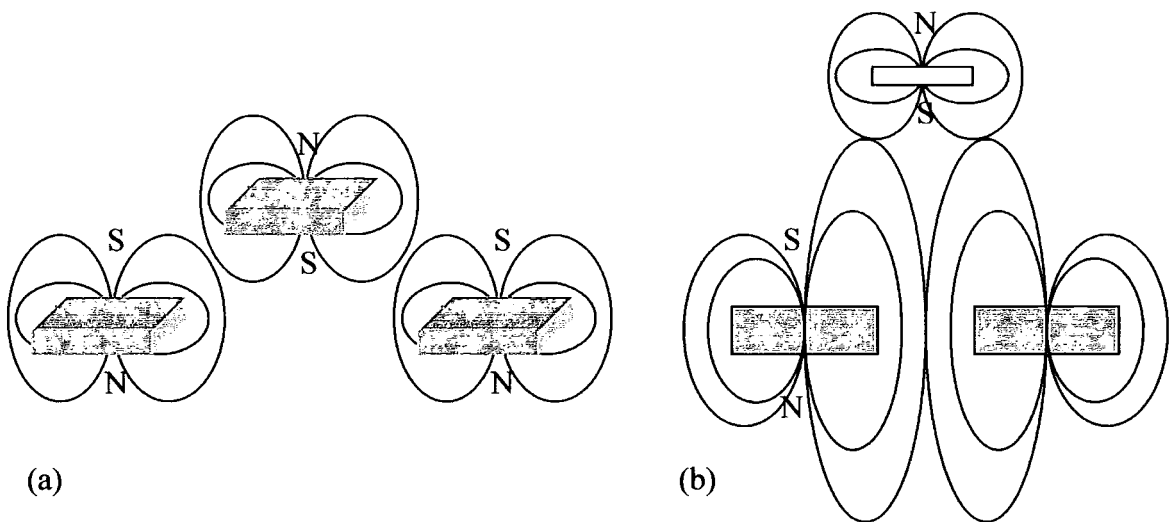
Figure 4.7.1 Magnetic field distributions

Figure 4.7.1 shows the differences in the magnetic field distributions between the magnetic rail system using separate magnets and the Levitron style ring magnet. The magnetic field lines around the rail system shown in figure 4.7.1(a) are gently sloping creating a shallow magnetic well in which the levitating magnet sits. For the ring system shown in figure 4.7.1(b) a similar amount of magnetic flux passes through the centre of the ring as goes around the edge of the ring; as the magnetic flux is forced through a restricted area the field lines are compressed, producing the peak shown. This peak of magnetic flux significantly reduces the size of the stable region. Where the rail system had a large stable zone similar

to the size of the levitating magnet, and could support a large range of weight, the ring system has only a small stable zone and can support a very limited range of weight. A solution to this would be to increase both the inner and outer diameter of the ring magnet. As the diameter of the magnet increased the ratio of the size between the area inside the magnet and the area outside the magnet would increase. Extending this to infinity would result in a situation where there would be no difference between the magnetic flux path inside and outside the magnet. Therefore the larger the diameter of the ring magnet used the more stable such a system should be. However the maximum size of the magnets is limited by the size and power of the electromagnets used to magnetise the precursor material during the production process. The largest commercially available magnets are not large enough to significantly alter the flux patterns to increase the stability.

## 4.8, Summary of Magnetic Rail Results

The results of these traverses in section 4.4 to section 4.5.8 show how the forces produced by the three magnet system, shown in figure 4.3.3, and the extent of the stable zone, change as the characteristics of the system are altered. Reducing the gap between the fixed base magnets reduces the stability of the system but increases the load bearing capability of the system. Conversely increasing the gap between the fixed base magnets increases the stability of the system, but also decreases the amount of weight the system can support. Doubling the number of the fixed base magnets used increases the amount of load that the system can support but also reduces the stability of the system and the maximum height at which the system is stable. Doubling the number of levitating magnets used reduces the instability of the system by a similar amount as when the fixed base magnets were doubled, but because of the resulting change in magnetic field shape the vertical force produced was significantly more. Whilst this is a beneficial result because the levitating magnets used are smaller than the fixed base magnets and only require half the number of magnets, so therefore are considerably cheaper, reducing the overall cost of the system, and are also easier to handle; this also increases the weight that has to be supported. The results of these traverses show that the optimum configuration of the three magnet "rail" system would consist of long fixed base magnets and narrow levitating magnets. The longer that the fixed magnets that make up the rails are, the more stable the three magnet system will be.

The Levitron is a stable magnet only system that is stabilised by the gyroscopic effect of the spinning levitating magnet. However it is not feasible to use it for the support of large weights due to the small stable zone it produces, its small load bearing capacity and the fine weight adjustments required to keep it within the stable zone. Larger versions of the Levitron using more powerful magnets are also unfeasible for large scale levitation applications because of the small stable zone inherent to ring magnets caused by the magnetic flux distributions as shown in figure 4.7.1. Therefore due to the infeasibility of the ring magnets for levitation applications it was decided that the magnetic "rails" are the most suitable solution for augmenting the superconducting levitation.

## 5. Design and Evaluation of the Hybrid Superconducting Levitation System.

### 5.1 Introduction

This chapter describes the design, testing, and analysis of several superconducting magnetic levitation systems. Firstly, the medium scale hybrid system that was designed and constructed to combine the stability of the superconducting levitation with the large ground clearances and increased load bearing capability that permanent magnet levitation can provide. Then the final large scale prototype designed to support a 40% scale Formula 1 car. The Superconducting Magnetic Levitation System is the largest wind tunnel magnetic levitation system in the world, which was built and successfully tested in the Durham 2m wind tunnel.

### 5.2 Hybrid Superconducting Levitation System for 20% Le Mans Style Vehicles

Magnet only levitation systems such as the Magnetic Suspension and Balance System (NASA 1991) can only maintain levitation through the use of a complex active control feedback system and require very high power electromagnets to operate. As previously demonstrated in chapter 3 a stable levitation system can be built using only superconducting levitation, but due to the mirror effect such a system is limited in the maximum air gap at which it can operate, and as such is limited in its applications. A solution to this problem could be achieved by combining the stability inherent to the superconducting levitation with the large air gap capability of the magnet on magnet levitation to produce a hybrid superconducting magnetic levitation system.

The objective of this research was to investigate the feasibility of a system of non-intrusive support primarily for use in the aerodynamic testing of racing cars. Such vehicles tend to have low ground clearance at the front axle and relatively high ground clearance at the rear axle, with this change in height designed to create a diffuser effect to produce downforce. A 40% scale model of a Le Mans type racing car operates with sufficiently low ground clearance at the front axle to allow support through the use of superconducting levitation for the front half of the vehicle. However the high ground clearance at the rear axle means

that the rear half of the model can not be supported in this way, but the ground clearance is well within the operating range of permanent magnet on permanent magnet levitation. By combining the inherently stable superconducting levitation with the magnet on magnet levitation it is possible to create a stable system that is capable of supporting a vehicle with a large range of ground clearances without the need for active control.

A medium scale prototype of the hybrid superconducting magnetic levitation system was then constructed. The system was based on a 20% scale Mercedes Le Mans racing car. Three Yttrium Barium Copper Oxide superconducting bulks were used to provide levitation at the front of the model. The superconductors were mounted in double insulated linked brass cryostats to allow the flow of liquid nitrogen to the superconductors to be controlled by filling only the most accessible cryostat. The cryostats were mounted on aluminium L section supports bolted to aluminium optical benches, as shown in figure 5.2.1. Six electromagnets were used in the design, two for each superconducting pod. Adjustable aluminium mounting brackets were used to affix the electromagnet to the rails on top of the optical benches allowing for five degree of freedom positioning. The electromagnets for the central pod were aligned parallel to the direction of air flow; the electromagnets for the pods on either side were positioned at an angle of 45° to the direction of air flow to provide lateral stability and positional control for the levitating magnets.
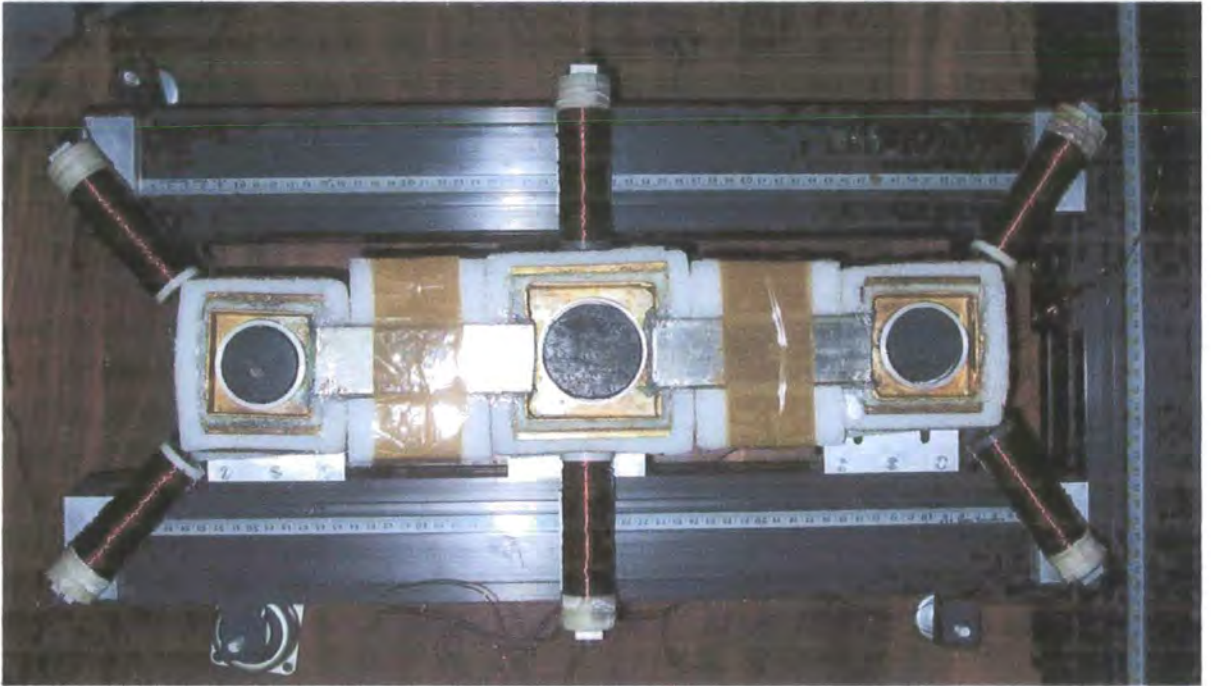
Figure 5.2.1 Superconducting Section of the Hybrid Levitation System.

The levitating magnets were mounted to a frame constructed from lengths of 12mm x 12mm x 1mm aluminium angle section. The frame was rectangular with two crossbraces; the extra crossbrace served as a mounting point for the offset levitating magnets and also balanced the frame side to side; tests with just one crossbrace resulted in one side of the rear of the frame levitating at a lower air gap due to the increased weight on one side. The frame and the attached levitating magnets are shown below in figure 5.2.2.
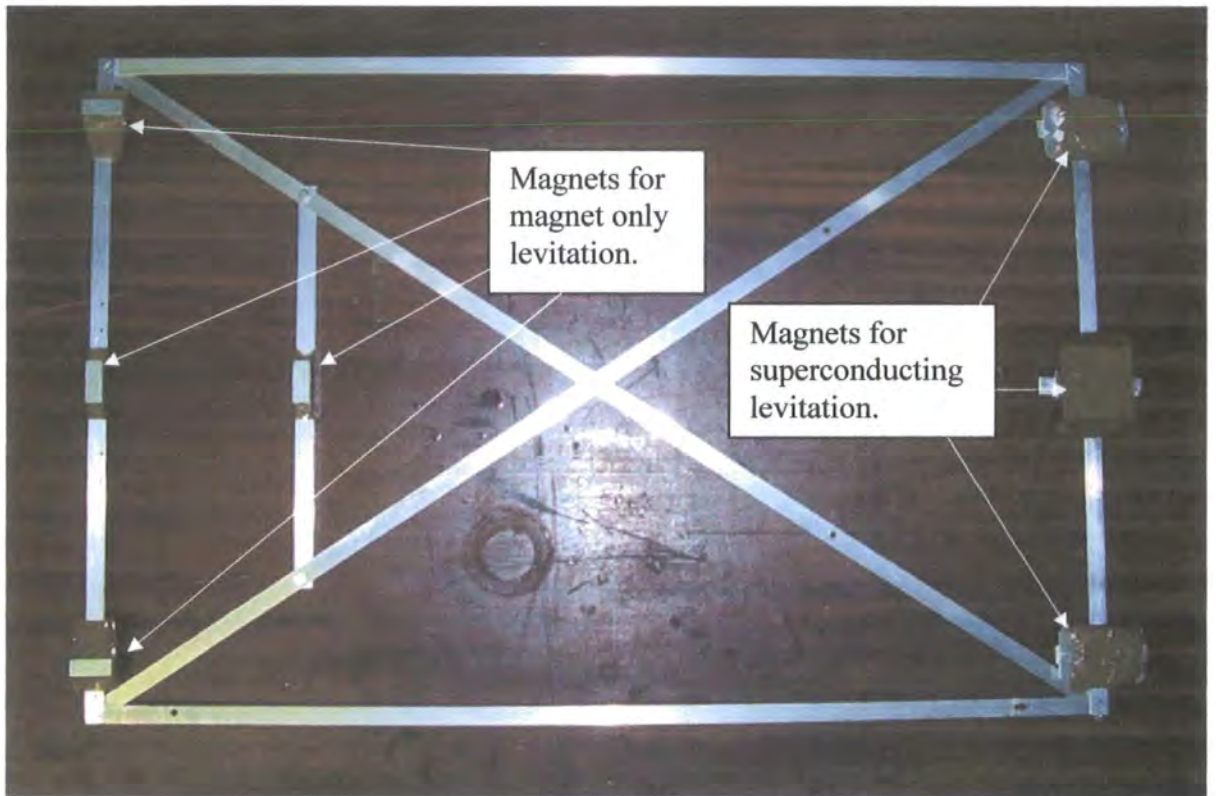
Figure 5.2.2, Frame for levitating magnets

For the rear section of the hybrid superconducting levitation system the magnetic "rail" configuration was employed to reduce the instability inherent to permanent magnet on permanent magnet levitation. The magnetic "rail" configuration, as discussed in chapter four, is stable in one horizontal direction, and unstable in the horizontal direction perpendicular to it. Combinations of several magnetic "rails" can be used to create a system that is either neutrally stable/unstable, or more stable in one direction than another, depending on the desired outcome.

The rear magnet only system used 50mm by 50mm by 6mm Neodymium magnets on the base and levitating Neodymium magnets with dimensions 30mm by 10mm by 5mm. Several combinations of the magnetic "rail", that was used for the rear magnet only section of the system, were evaluated. Figure 5.2.3 shows the different configurations that were assessed for stability.
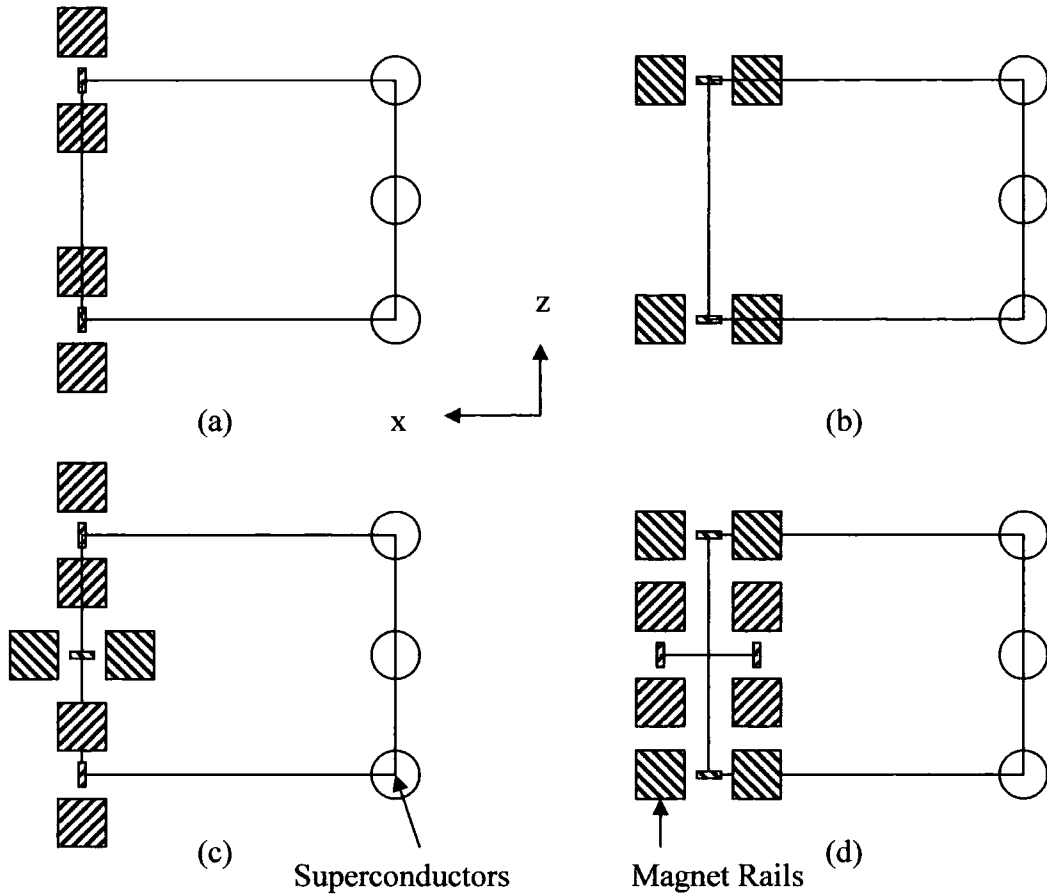
Figure 5.2.3 Hybrid Superconducting Magnetic Levitation "Rail" Configurations.

The first configuration that was tested was comprised of two rails positioned to be stable in the z direction, as shown in figure 5.2.3a. This arrangement was proved to be stable; however due to the orientation of the magnetic rails this setup had limited resistance to force in the x direction. The second configuration that was tested is shown in figure 5.2.3b. The magnetic "rails" were aligned to be stable in the x direction to ascertain if the orientation of the rails affected the stability of the system. This arrangement of the rails was also shown to be stable but could only withstand a significantly smaller displacement from the central position than the configuration shown in figure 5.2.3a. The reason for this reduced stability is the lever arm of the frame over which the destabilising forces of the magnetic rails act. In the arrangement shown in figure 5.2.3a the magnetic rails were unstable in the x direction and applied a uniform force in the x direction to the superconductors that they were capable of resisting. However in the arrangement shown in figure 5.2.3b the magnetic rails were unstable in the z direction, this resulted in the central

143

superconductor acting as a pivot point. The destabilising force of the magnetic rail was multiplied by the lever arm of the aluminium frame resulting in a force too great for the superconductors to resist. This arrangement meant that only two superconductors were able to resist the movement of the frame, with the middle superconductor rendered redundant and unable to resist the destabilising movement. The longer the frame, and consequently the distance between the superconductors and the magnetic rails, the more unstable the system will be.

Despite the reduced instability of the system shown in figure 5.2.3b the magnetic "rails" provided a restoring force in the x direction that would oppose the force acting on the levitating magnets caused by the force of the wind, but as the system has only a small degree of stability it is not particularly useful. The configuration shown in figure 5.2.3c consists of two magnetic "rails" that are unstable in the x direction and another "rail" positioned at right angles so that it is unstable in the z direction. This configuration was designed to provide stability with the two rails unstable in the x direction and some restoring force in the x direction with the rail unstable in the z direction. Testing of this configuration showed it possessed improved stability over the arrangement in figure 5.2.3b. Another magnetic "rail" was then added to the system as shown in figure 5.2.3d. This configuration consisted of four rails; two were unstable in the x direction and two were unstable in the z direction. This configuration was also shown to be stable, because each magnetic "rail" had a counterpart at right angles to itself, any displacement of the levitating magnets was opposed by one set of rails, as a destabilising movement in the x direction for one set of rails resulted in a restoring force from the other set. The magnetic rails in this configuration also cancel out each other in rotation as well. The result of this is the creation of an almost neutrally stable system of magnetic rails. The hybrid superconducting magnetic levitation system is shown in operation in figure 5.2.4.

Figure 5.2.4 Hybrid Superconducting Magnetic Levitation System Levitating.

As shown in chapter 3 the behaviour of the magnetic rails is dictated by the gap between the magnets that form the base of the rails and the number of levitating magnets used. Reducing the gap between the fixed magnets resulted in greater load bearing ability and increased air gap at the expense of stability. The use of multiple rails allows for fine tuning of the system; by increasing or reducing the gap between the rails positioned in either the x or z direction the system can be made to be more stable of unstable in a given direction. In the case of testing of a vehicle at yaw angles the aerodynamic loads act unevenly on the vehicle. By tuning specific rails the system can be configured to apply a restoring force in the required direction when the magnets are displaced.

The addition of a non-ferrous conducting sheet between the levitating magnets and the superconductors and the magnetic rails, as shown in figure 5.2.5, will help to damp any movement of the frame. The levitating magnets induce eddy currents in the conducting sheet, in this case aluminium, which oppose the movement of the magnetic field that created them. Teshima (1997) investigated the effects of eddy current damping in non-ferrous conductors, it was found that a copper sheet provided the most damping, and the thicker the sheet the more damping produced. For levitation applications the rolling road platen would be required to be a non-ferrous sheet, a copper platen would be very expensive therefore an aluminium platen was used in this project.

Figure 5.2.5 Hybrid System Levitating with Aluminium Floor in Place.

5.3 Inherent stability of the Levitating system

Superconducting levitation has a range of air gaps over which it can operate in the vortex state. The closer the magnet is to the superconductor, the greater the volume of the superconductor that is in the vortex state. The greater the proportion of the superconductor in the vortex state, the greater the restoring force that the superconductor provides to a perturbation. Therefore at larger air gaps the amount of restoring force that the superconductor can produce decreases, as a result it is desirable to have a stable as possible system before any wind forces act on the system. The Superconducting Magnetic Levitation System is a modular system which means it is capable of being used for any size and shape of model. Therefore the demands on the system will differ depending upon the application in question. In order to create as stable a system as possible initially the magnetic "rails" will be positioned so that half are stable in the x direction and half are stable in the z direction. The system can then be tuned once the demands on system are known. Until this point the restoring force required for the system to oppose the force of the air flow will be produced through the use of electromagnets as these are capable of producing large forces in any direction.

5.4 Design of Large Scale Hybrid Superconducting Magnetic Levitation System

The most probable application of the Superconducting Magnetic Levitation System would be for the wind tunnel testing of Formula 1 cars. F1 cars run at very low ground clearances making them ideal candidates for the technology, and the manufacturers consider

aerodynamic testing to be the most important aspect of building a fast car. All Formula 1 teams perform aerodynamic testing of their vehicles and several manufacturers run multiple wind tunnels twenty four hours a day, such is the importance of the resulting data. These tests are performed with a moving ground plane to simulate the diffuser effect produced by the low ground clearance of the cars. Therefore the vehicles are supported by large struts and stings from the walls and roof of the tunnel which disrupt the airflow around the car and cause the tests to deviate from on track conditions as discussed in chapter 1. As a result large amounts of time and resources are being expended to produce flawed data.

The varying ground clearance along the chassis of an F1 car dictated the positioning of the superconductors within the model. Figure 5.4.1 shows the changing ground clearance of the Toyota TF103



Figure 5.4.1, the Toyota TF103 (Toyota 2003).

The lowest ground clearance is around the central section of the car. Unlike a Le Mans car which has its lowest ground clearance at the front axle, an F1 car has a raised nose, in accordance to the regulations (F.I.A. 2004), which makes it unsuitable for superconducting levitation. The ground clearance is also greater at the rear axle because of the raised section used to form the diffuser, making it unsuitable for superconducting levitation. Therefore all the magnets used for superconducting levitation for a scale model of an F1 car must be positioned centrally. The larger ground clearances at the front and back of the model are suited to magnet on magnet levitation.

Whilst the nose section operates at too great a height to be suitable for support using superconducting levitation, the front wing runs at a lower ground clearance and as such is a candidate for superconducting levitation. However following consultation with the Toyota F1 it was decided to not place magnets inside the front wing. This was due to the regularity with which the design and components of the front wing were changed, rendering it unfeasible to constantly change the layout of the magnets in the wing and the superconductors beneath the floor of the wind tunnel.

Many of the Formula 1 manufacturers test their vehicles in the wind tunnel at 40% scale so therefore the model used for this project was based upon a 40% scale Formula 1 car. For the 2004 season the FIA regulations stated that a Formula 1 car must fit within a rectangular box that is 4600mm long and 1800mm wide, the same dimensions are still in force for the 2006 season. The body of the car is 1400mm wide at it largest point and the rear wing extends 600mm beyond the rear axle. For a 40% scale model the box becomes 1840mm long and 720mm wide, it was decided to initially build a simplified frame without either wings or wheels on to which the magnets would be mounted. A frame was built from sheet aluminium mesh with 5mm diameter holes to allow the magnets to be easily mounted. The frame was 1600mm long and 560mm wide at the largest point; the shape of the frame was based upon the Ferrari F2004. Figure 5.4.2 shows a plan view of the F2004.



Figure 5.4.2, Plan view of the F2004 (Ferrari 2004).

Figure 5.4.3 shows the frame for the levitating magnets superimposed over the plan view of the F2004. The area of the frame was divided into three sections; sections 1 and 3 are areas of high ground clearance and as such are suitable for support with magnet only levitation, section 2 is an area of low ground clearance and therefore is suitable for support through the use of superconducting levitation. The size and shape of the levitating frame dictates the layout of the superconductors, cryostats, permanent magnets, and electromagnets required to support the levitating magnets.
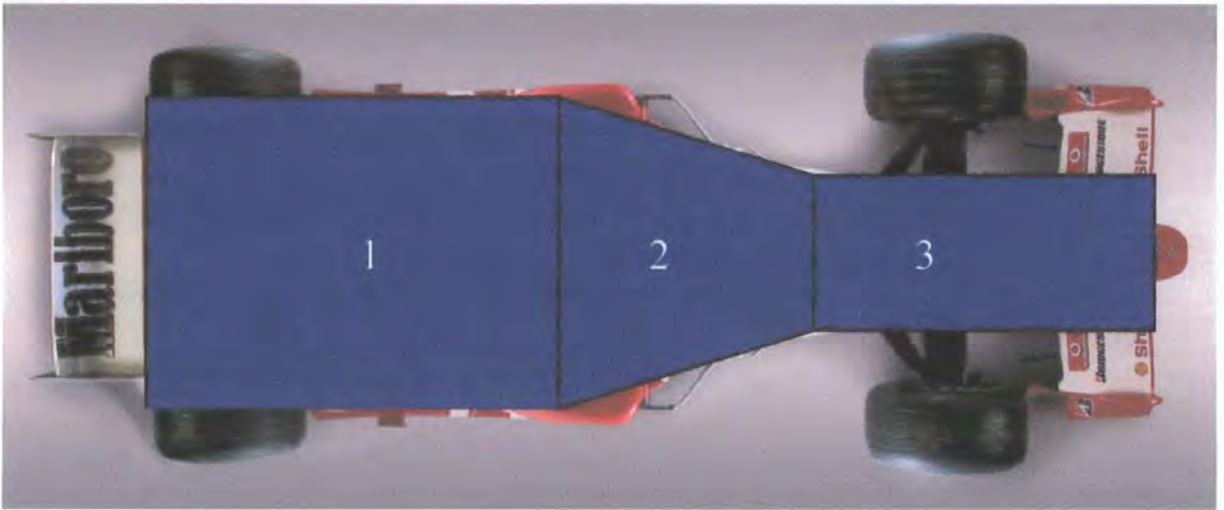


Figure 5.4.3, Frame for levitating magnets superimposed on the F2004.

5.4.1, 150mm Rare-Earth Neodymium Magnets

The magnetic rails become more stable as the ratio of the length of the fixed base magnets to the length of the levitating magnets increase. Therefore the longer the fixed rails are, the more stable a system incorporating them will be. The maximum size for production of the magnets is limited by the method by which they are magnetised. The raw materials that the magnets are composed of can be pressed and sintered into virtually any shape and any size; it is the magnetising of the material that is the limiting factor in the process. In order to produce a magnet with a uniform magnetic field throughout its volume, the electromagnetic coil that is used to magnetise it must be capable of producing at its centre a uniform magnetic field the same size as the resulting magnet. The larger the size of the magnet that is required, the larger the magnetising coil must be in order to magnetise the Nd-Fe-B

powder. At present the largest commercially available magnets are 150mm in length. The magnets that were chosen to be used in this project were rare-earth neodymium-iron-boron magnets with dimensions of 150mm x 50mm x 10mm. Magnets of this size allow fine tuning of the rail system by changing the gap between the fixed magnets and using levitating magnets of varying sizes to change the properties of the system to best augment the superconducting levitation.

5.4.2, Layout of the Large Scale Hybrid Superconducting Magnetic Levitation System

The ideal configuration for the supporting formation would be to have the entire central section of the system tiled with YBCO superconducting bulks to provide maximum levitation force and damping to the system, as shown in figure 5.4.4. The extent of the superconductors extends beyond the area of the levitating frame as a superconductor is capable of producing a vertical levitation force on a magnet that is not positioned directly over it as shown in chapter 3. The front and rear sections of the levitating frame would be supported by multiple magnetic "rails" composed of 150mm long rare-earth magnets. Each rail consisted of two 150mm x 50mm x 10mm Neodymium-Iron-Boron rare-earth magnets; each magnet had two aluminium end caps with an 8mm hole running along the width of the magnets. Stud bar was used to connect the end caps and wing nuts were used to adjust the distance between the magnets. The area of the levitating frame dictated the number of rails that could be used in each section. The available space allowed for the use of four magnetic "rails" to support the front section of the frame, and eight magnetic "rails" to support the rear section of the frame. This configuration is shown in figure 5.4.4.
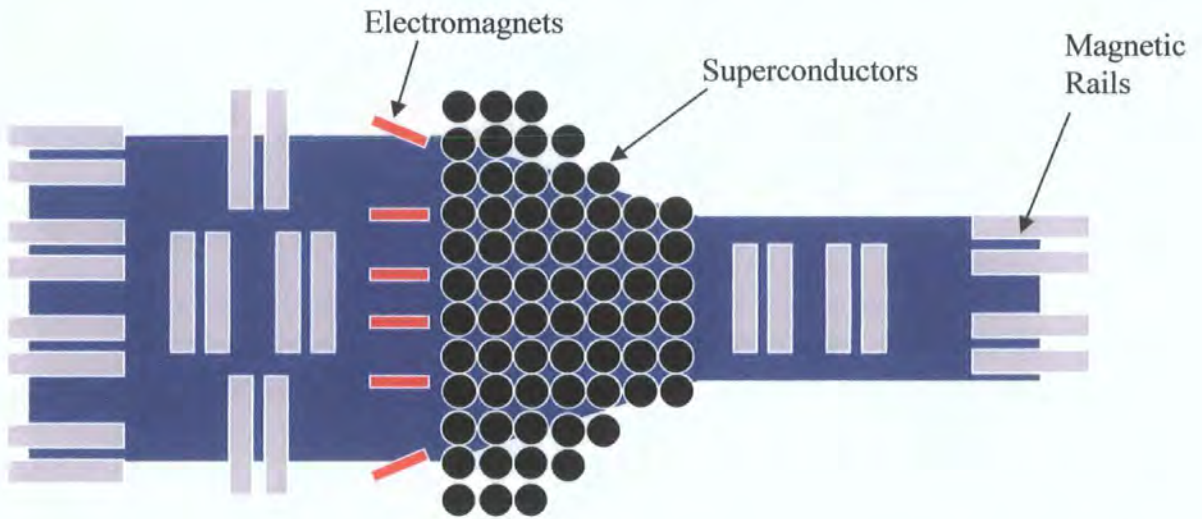
Figure 5.4.4, Original configuration of the Superconducting Magnetic Levitation System.

Unfortunately due to budgetary constraints the project was limited to seventeen 44mm diameter Yttrium Barium Copper Oxide bulks manufactured by THEVA Gmbh (THEVA 2004), rather than the sixty superconductors that would have filled the available space as shown above. The superconductors were evenly spaced around the central section of the system in order to preserve a long lever arm between the superconductors to better allow them to resist any rotation of the system. The superconductors were held in aluminium cases mounted in linked brass cryostats. All the cryostats were fed from a central reservoir situated to the side of the main system, as shown in figure 5.4.5, to allow continuous cooling of the superconductors when a floor was used to cover the system. The cooling system was heavily insulated to reduce the boil-off rate of the liquid nitrogen as much as possible. The cryostats were supported using optical benches that provide multiple mounting points for brackets. Six electromagnets were positioned behind each superconductor in the rearmost row corresponding to the position of the levitating magnets.
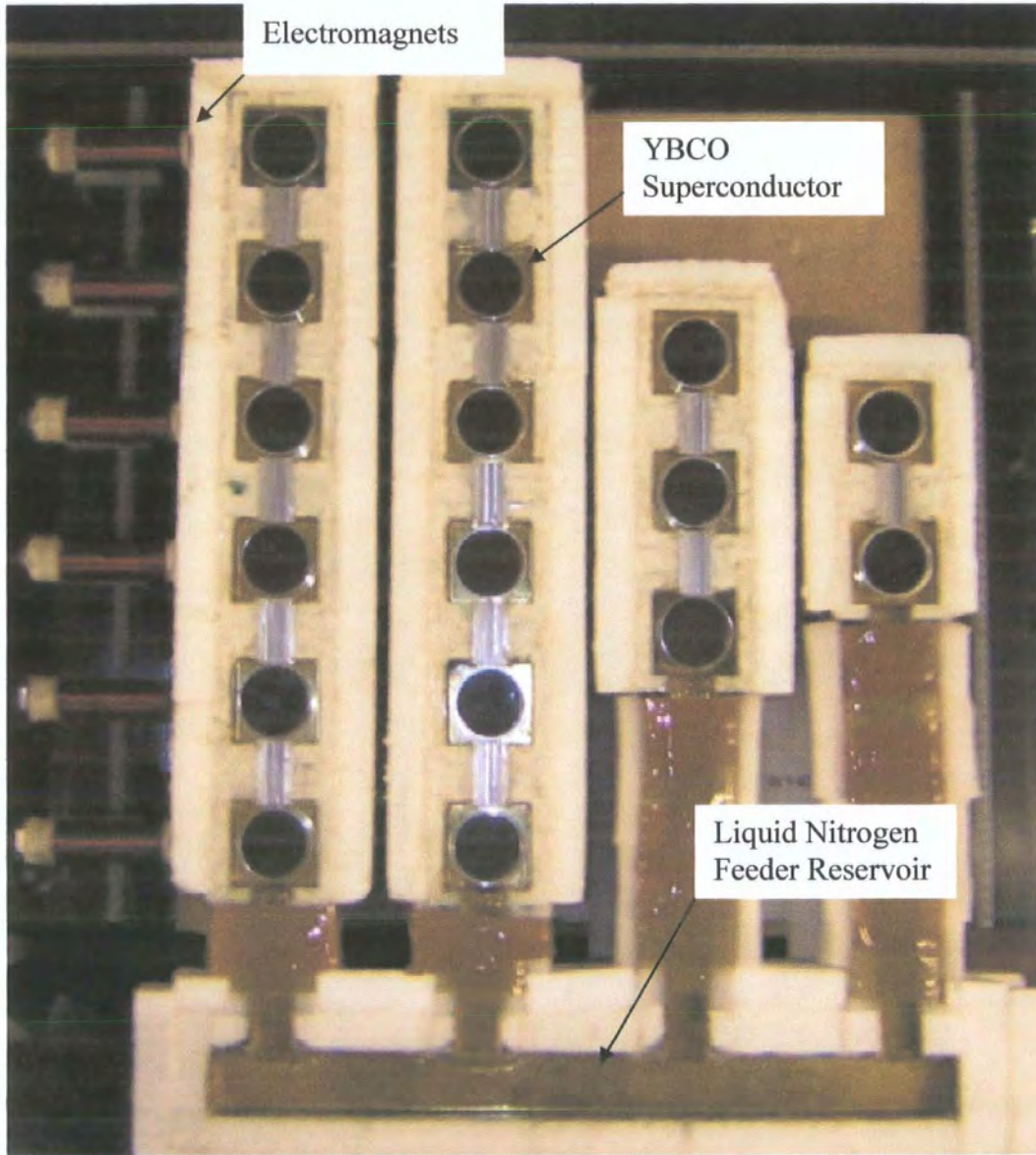
Figure 5.4.5, Layout of the Cryostats and Superconductors.

It was found that the space taken up by the optical benches and the electromagnets meant that space in the rear section of the system was reduced requiring a reduction in the number of magnetic rails from eight to six. Figure 5.4.6 shows the layout of the system. Figure 5.4.7 shows the layout of the Superconducting Magnetic Levitation System on the bench.
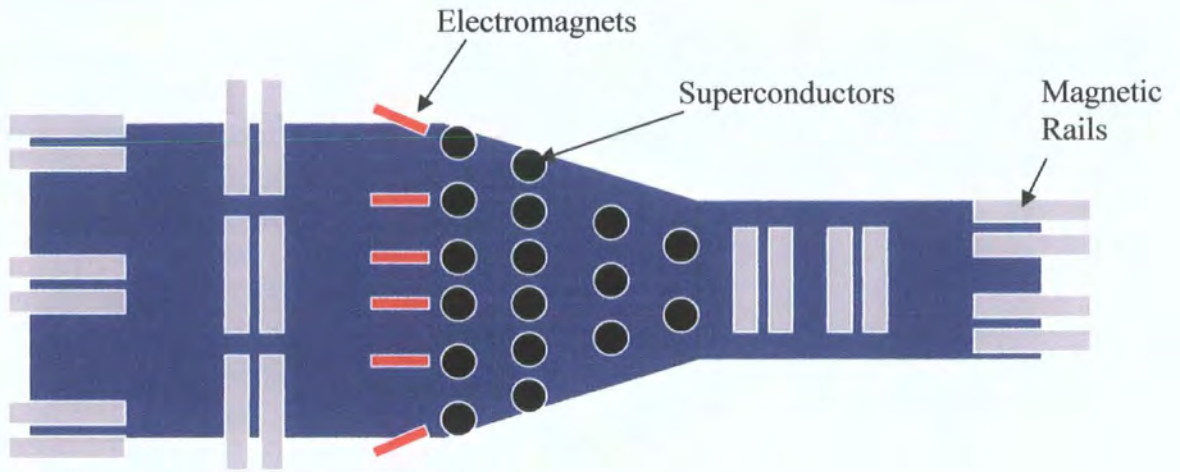
Figure 5.4.6, Actual layout of the System
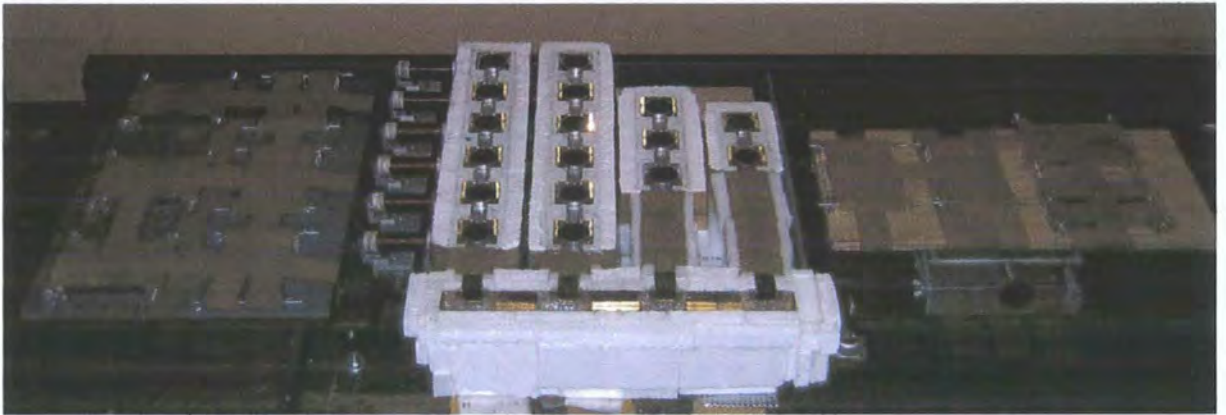


Figure 5.4.7, Prototype of the Superconducting Magnetic Levitation System.

Figure 5.4.7 shows the superconductors within the cryostats attached to the liquid nitrogen feeding system. The magnetic rails are mounted on adjustable scissor platforms in front and behind the superconductors. A row of electromagnets sit behind the superconductors to counteract the wind force applied to the model. Figure 5.4.8 shows the system with the aluminium levitating frame in position.
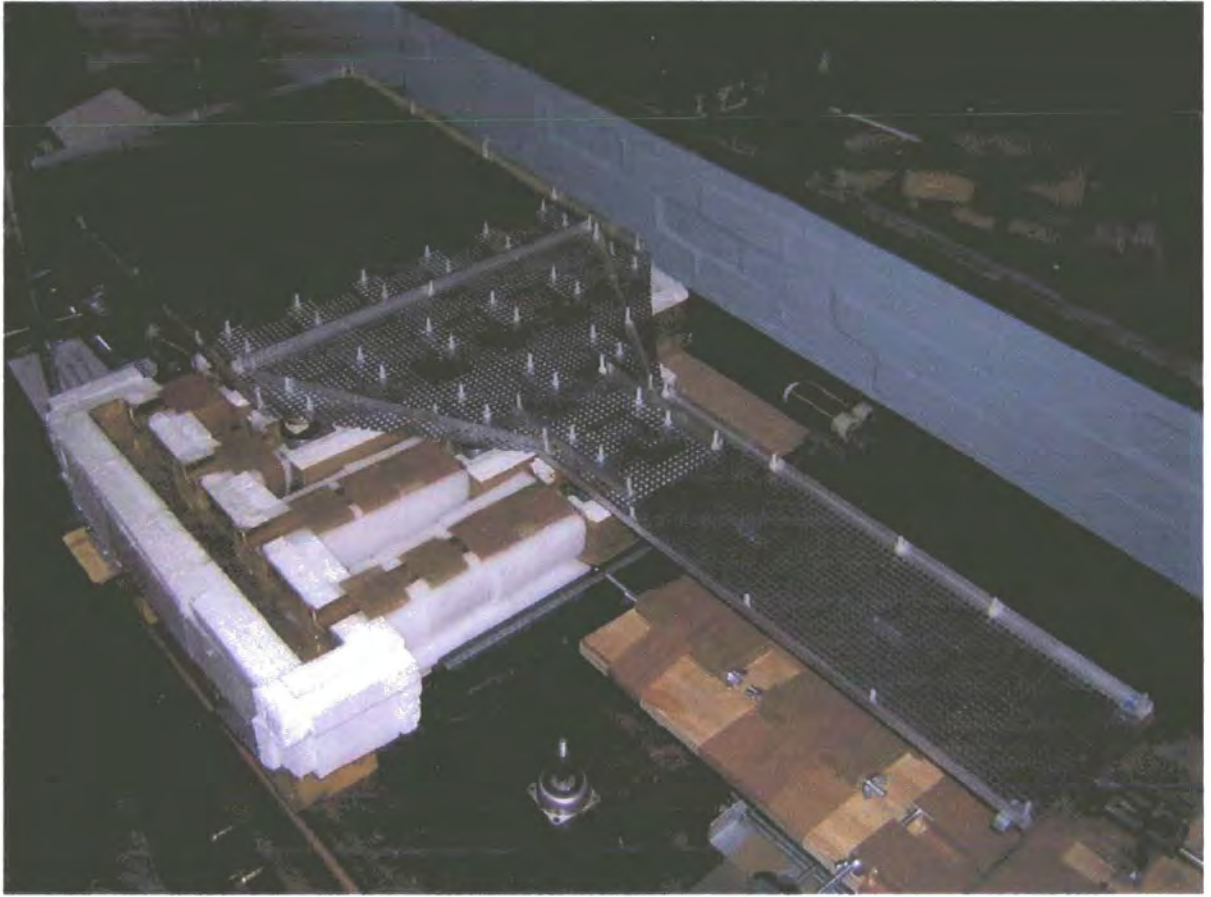
Figure 5.4.8, Prototype final rig with Frame in place.

Figure 5.4.8 shows the frame being held in place by clamps. Non-ferrous spacers were used to set the height of the superconducting levitation before the liquid nitrogen was added to field cool the superconductors. Figure 5.4.6 shows the frame levitating after the addition of liquid nitrogen.
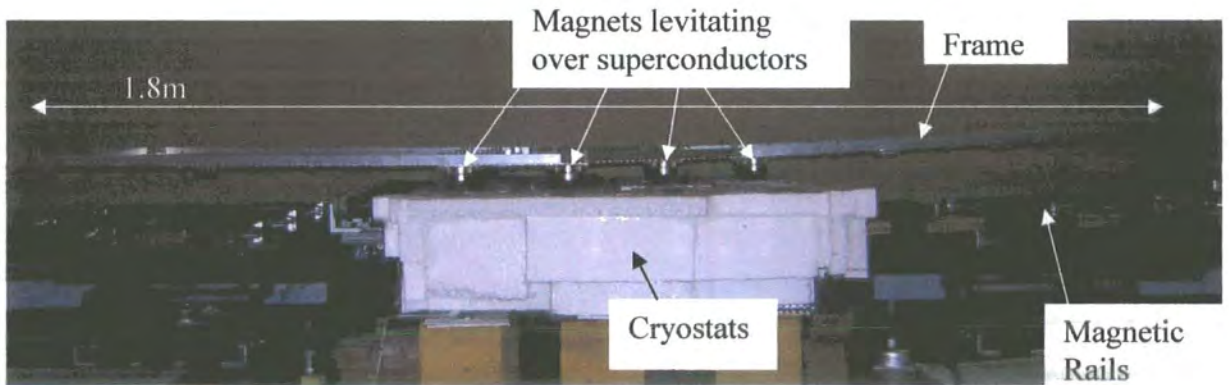


Figure 5.4.6, Large Scale Prototype Rig Levitating.

The levitation height varied from the central superconducting section where the height was 15mm, to the magnet on magnet section where the height was 70mm. The fixed magnets on the base were lower than the superconductors to mimic the increased height change at the front and rear of an F1 car, as it was easier to change the height of the floor than to change the height of the frame. Figure 5.4.6 shows that there was some give in the frame that allowed the front and rear sections to flex upwards as the height of the scissor platforms were increased causing the levitating magnets to move up as well. The model was changed for the later tests in the wind tunnel so that the front and rear sections were raised to represent the outline of an F1 car, and the superconductors and magnets were at the same level under the floor of the wind tunnel.

5.5, Bench testing of the final system.

The system was tested in situ on the bench to ascertain its capabilities. Maximum lift tests and maximum drag tests were performed with various different arrangements of the permanent magnets to provide varying amounts of lift. The first test was run with the magnetic rails with a distance of 25mm between them, and with the superconductors field cooled at a height of 15mm. Calibrated masses were then loaded onto the frame. This configuration gave a maximum levitation force of 200N, mainly supplied by the superconductors, because of the distance between the rails the magnets provided only a small amount of lift as the system had been configured for maximum stability. For the second run the gap between the rails was reduced to 10mm. In this configuration the system was able to support 250N. The system was then tested for drag force. Each of the six electromagnets had 400 turns, and each electromagnet drew 5 Amps. The electromagnets were positioned 50mm behind the superconductors and electromagnets in order to allow space for insulation. The maximum drag force attained was 90N before the levitating frame started to move. As with previous drag force tests it was found that the drag force that could be resisted increased as the current in the electromagnets increased. Through the use of electromagnets with more turns and larger power supplies the maximum drag force that can be resisted will be considerably increased.

5.5.1, Modular Expansion of the Superconducting Magnetic Levitation System.

As mentioned previously, only a fraction of the superconductors that were intended to be used in the original design were used to build the large scale prototype of the Superconducting Magnetic Levitation System. Seventeen Yttrium Barium Copper Oxide superconducting bulks with a diameter of 44mm were used; depending on whether circular or square superconductors were used up to 80 superconductors of similar dimensions would be able to fit into the available space. This would at least quadruple the load carrying capacity of the superconductors. The limiting factor to the amount of levitation force that the magnetic rails can produce is the stability and damping that the superconductors produce, such a large increase in the numbers of superconductors used will greatly increase the stability and damping that the system possesses and will allow much larger loads to be supported by the magnets.

Based on a frontal area of an F1 car of $1.5m^2$, the system operating with the reduced number of superconductors the system would be capable of supporting a lightweight, 10 kg model at 30 $ms^{-1}$ with modest lift and drag coefficients of -1.14 and 0.70 respectively. Increasing the number of superconductors used would make it possible to support vertical forces of 1000 N and horizontal forces of 360 N. These forces would correspond to a 35 kg, 40% Formula 1 car model at 30$ms^{-1}$ with lift and drag coefficients of -4.0 and 2.5 respectively.
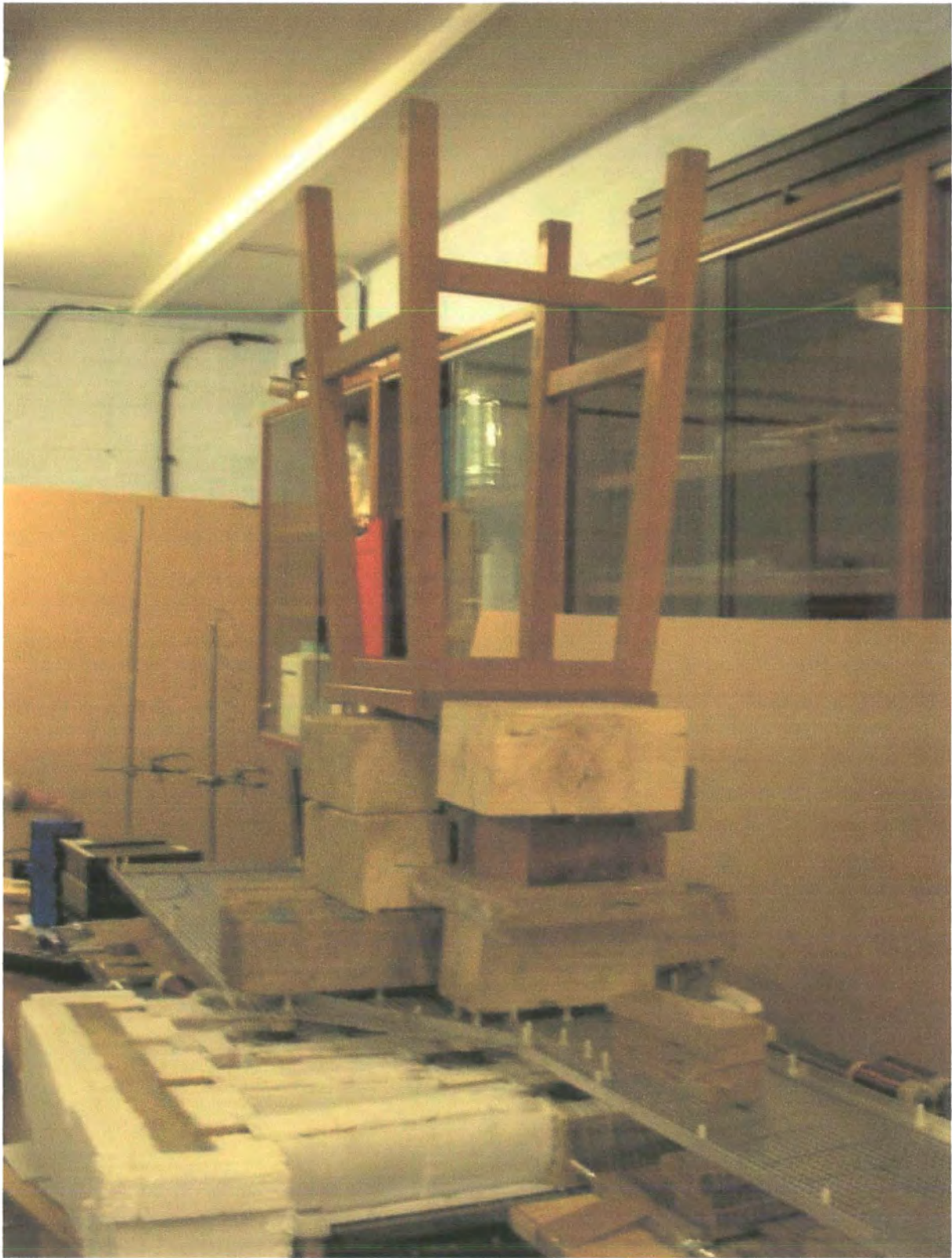
Figure 5.5.1, Demonstration of the Systems Load Carrying Capability.

The system was also run with an aluminium sheet in place over the superconductors to demonstrate that is did not cause any problems for the system. The levitation height of the magnet-magnet levitation at the front and back of the system could be adjusted whilst in operation.



Figure 5.5.2, Superconducting Magnetic Levitation System with Aluminium Floor

5.6, Testing of the Superconducting Magnetic Levitation System in the Durham 2m Wind Tunnel.

The Superconducting Magnetic Levitation System was designed for use in conjunction with a rolling road. A purpose built rolling road had been designed for use with the system inside the Durham 2m wind tunnel. Unlike standard rolling roads which have three rollers the rolling road was designed with four rollers to allow space inside the belt to position a six component force balance with the Superconducting Magnetic Levitation System on top of it. The rolling road was made of 60mm square section steel beams and was designed so that when it was not in use it could be lowered to allow a turn table to be mounted on top of it to run yaw testing. A 3mm thick aluminium platen was used in the rolling road. A diagram of the rolling road is shown in figure 5.6.1.
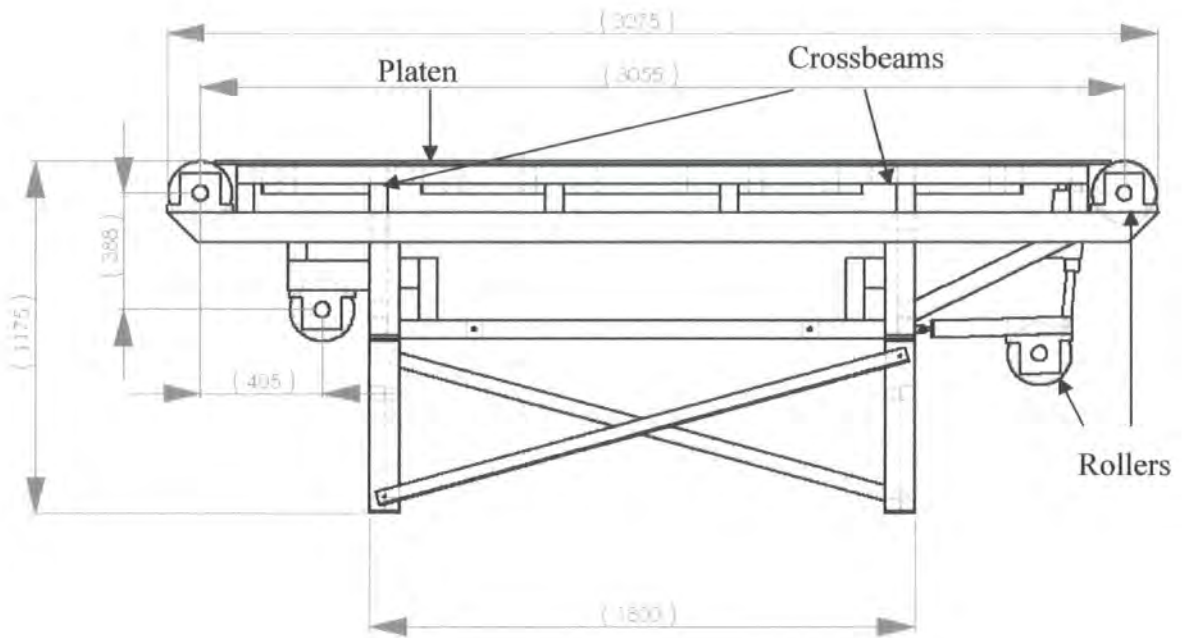
Figure 5.6.1, Rolling road frame (Dimensions in mm)

The aluminium frame for the Superconducting Magnetic Levitation System on which the levitating magnets were mounted was designed to be 40% of the length of a Formula 1 car at 1800mm. The supporting structure of the system was 2000mm long. The rolling road in the Durham 2m Wind Tunnel was designed with two 60mm square section steel supports running across the width of the rolling road as shown in figure 5.6.1. The distance between the beams was 1500mm, 500mm shorter than the overall length of the Superconducting Magnetic Levitation System.

In order to fit the Superconducting Magnetic Levitation System into the available space within the rolling road the supporting system was shortened whilst keeping the length of the levitating frame the same. The layout of the superconductors in the central section was kept the same although the supporting optical benches were moved closer together and the electromagnets were moved closer to the superconductors. The major reduction in length was achieved by removing one of the magnetic rails in the front section of the system that was perpendicular to the direction of the airflow. The layout of the shortened version of the Superconducting Magnetic Levitation System is shown in figure 5.6.2.
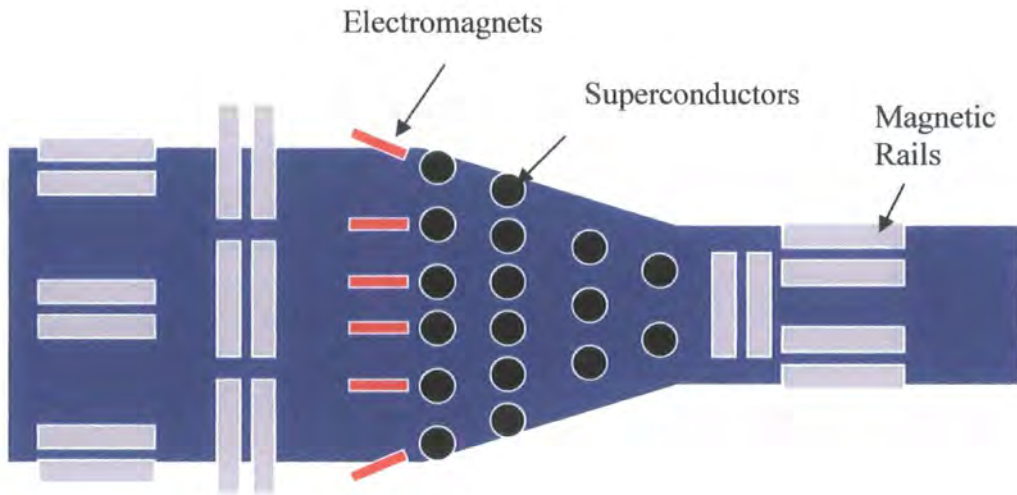
Figure 5.6.2, Cut down version of system.

The Superconducting Magnetic Levitation System was mounted on a steel frame used to represent the dimensions of the force balance normally used for fixed ground testing. Figure 5.6.3 shows how the Superconducting Magnetic Levitation System was integrated into the rolling road.
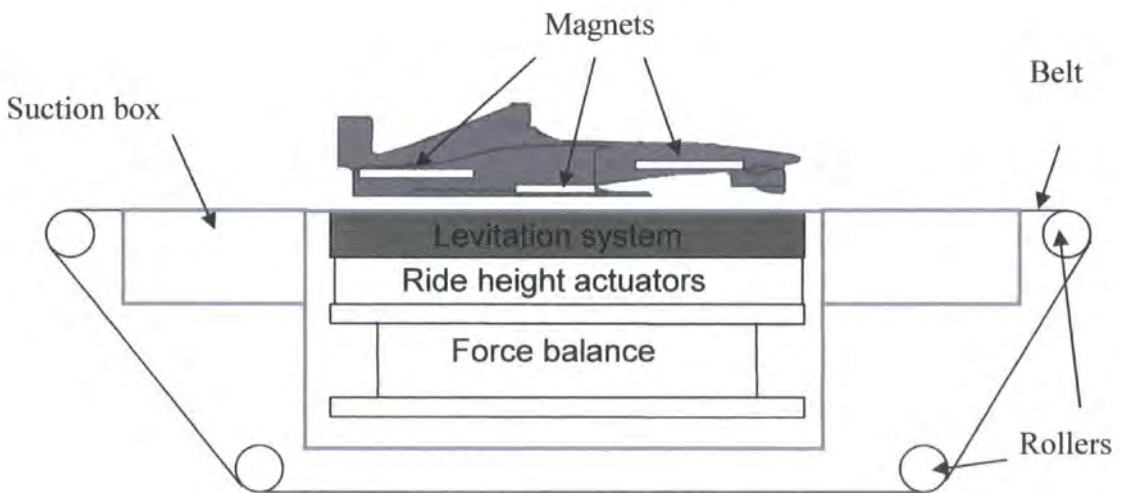


Figure 5.6.3, Schematic of the system integrated into the rolling road

Figures 5.6.4 and 5.6.5 show the system installed in the rolling road within the 2m Durham Wind Tunnel.
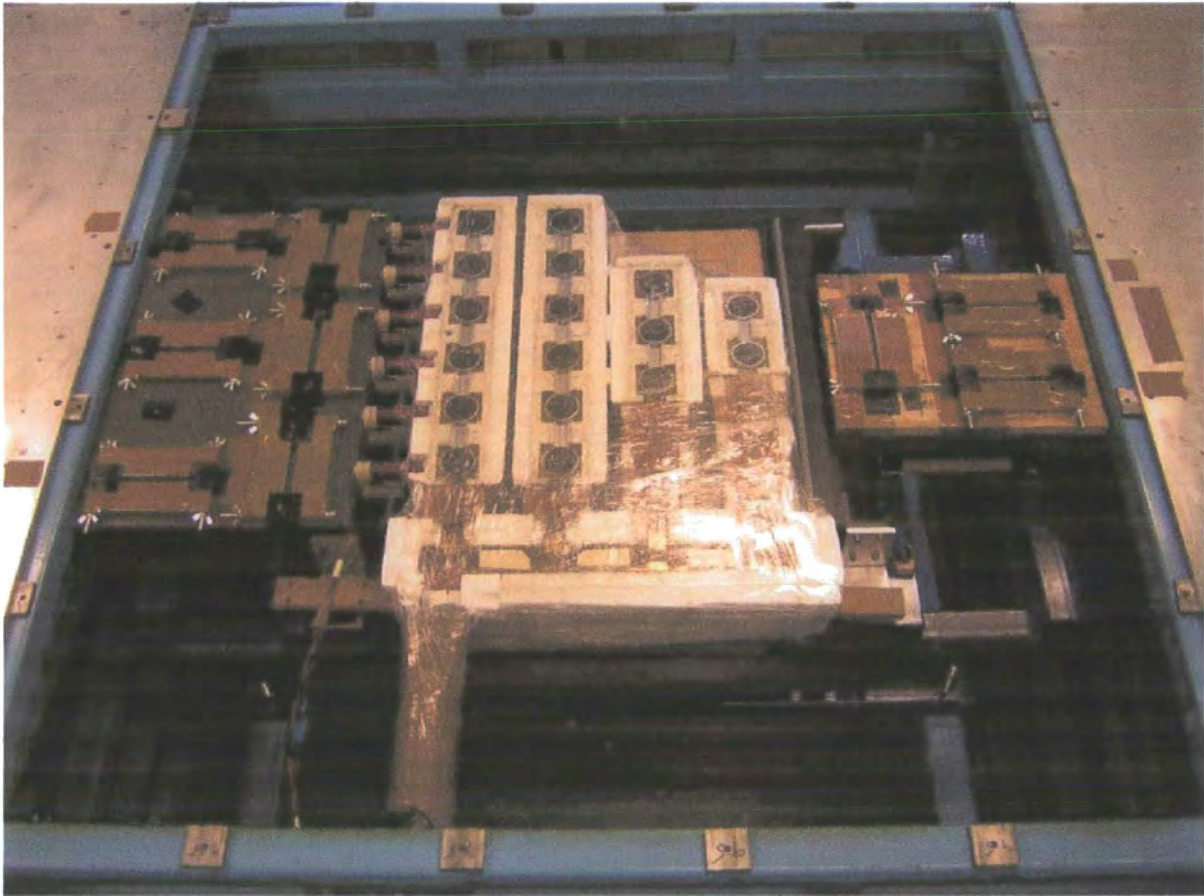
Figure 5.6.4, Superconducting Magnetic Levitation System Installed in the Rolling Road

Figure 5.6.5, Superconducting Magnetic Levitation System in the Durham 2m Tunnel.

In order to prevent convection due to the airflow from causing the liquid nitrogen to boil off at an increased rate the cryostats were covered in clingfilm, whilst ensuring the system was still vented to prevent pressure build up. In order to allow continuous cooling of the superconductors when the aluminium platens were in place, a feeder pipe was connected to an exterior inlet to allow the addition of liquid nitrogen whilst the system was in operation. Figure 5.6.6 shows the Superconducting Magnetic Levitation System installed inside the rolling road in the Durham 2m wind tunnel with the platen in place. No part of the system protruded above the level of the floor, thereby providing no impediments to the normal operation of the rolling road.
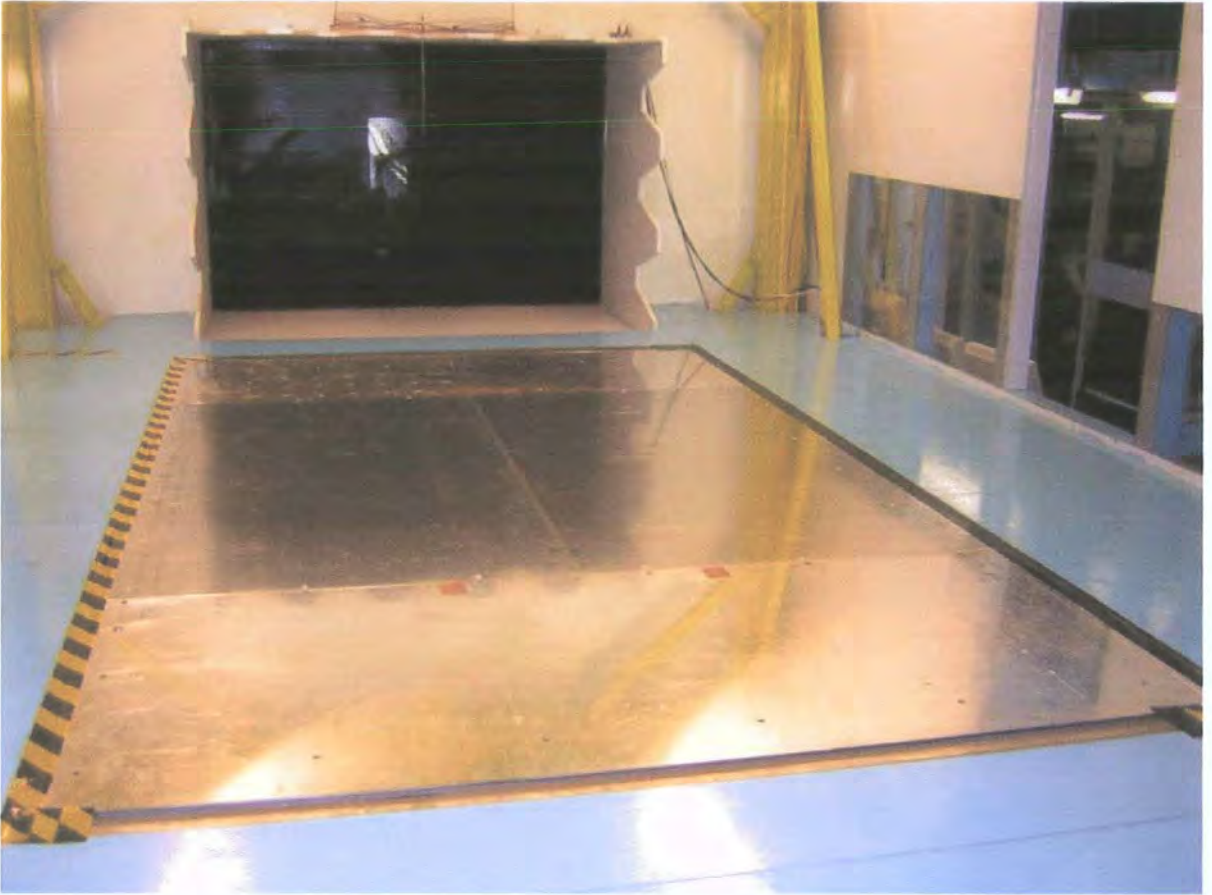
Figure 5.6.6, Superconducting Magnetic Levitation System with Platen in Place.

In order to provide a more realistic set of conditions for the testing of the Superconducting Magnetic Levitation System in the 2m Durham wind tunnel, the frame used to support the levitating magnets was mounted inside a model designed to approximate the body shell of a Formula 1 car. When the system was tested on the bench the frame had all the magnets at the same height and the height differences for the system were introduced by setting the magnetic rails at a lower height than the superconductors. For the tests in the wind tunnel the height changes were incorporated into the model. The magnets in the central section of the model were kept at the same height and the magnets for the front and rear magnet only sections were raised. The underneath of the frame was covered with aluminium sheeting to provide a flat underside for the model. In order to provide drag to act on the system a polystyrene shell was added to the frame to act as a bluff body and induce unsteady oscillations in the system to test the damping capabilities of the Superconducting Magnetic Levitation System. The levitation height of the system was set by field cooling the

superconductors with the model in place using 10mm spacers. The levitation height at the front of the model was 70mm, and the levitation height at the rear of the model was 30mm, although these heights could be adjusted by changing the height of the scissor platforms on which the magnetic rails were mounted. Figures 5.6.7 and 5.6.8 show the Superconducting Magnetic Levitation System in operation. In order to allow the current in the electromagnets to be adjusted during the operation of the system the leads were run to the exterior of the wind tunnel where they were connected to the power supplies. The Superconducting Magnetic Levitation System was demonstrated to be stable at a range of wind speeds up to 20ms$^{-1}$. There was some oscillation of the nose of the model at higher wind speeds due to the flexible nature of the frame intended to allow changes in the ride height to occur without the need to reposition the magnets inside the model. This problem would be solved by making the frame stiffer as demonstrated in the rear section of the model where no oscillation occurred due to the damping from the superconductors and the stiff frame.
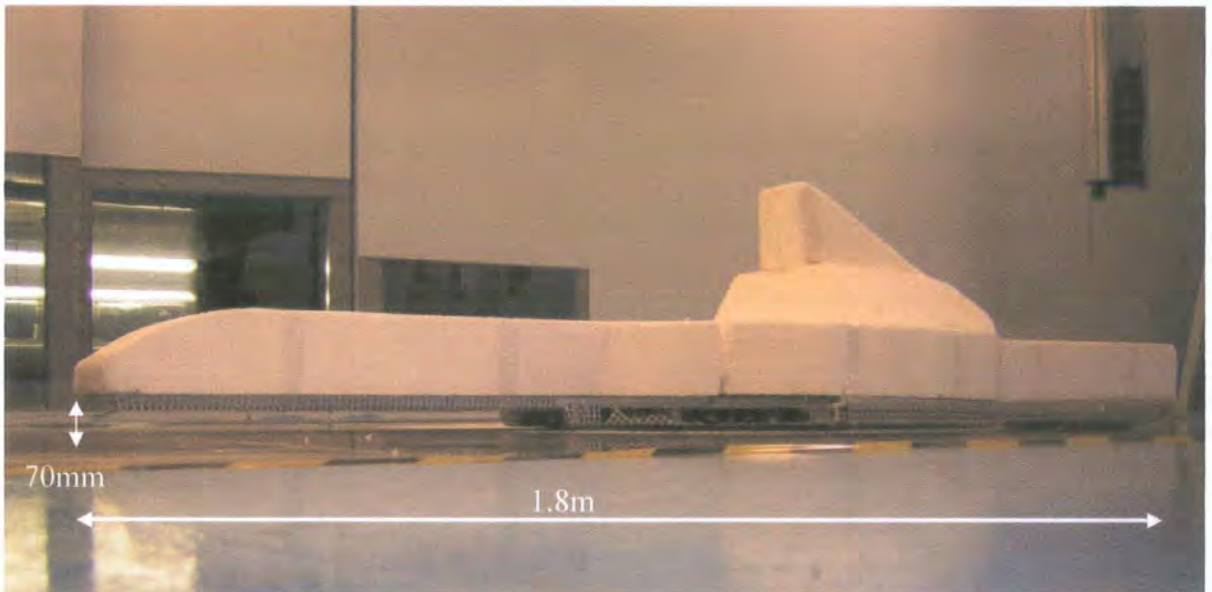


Figure 5.6.7, Superconducting Magnetic Levitation System in Operation.
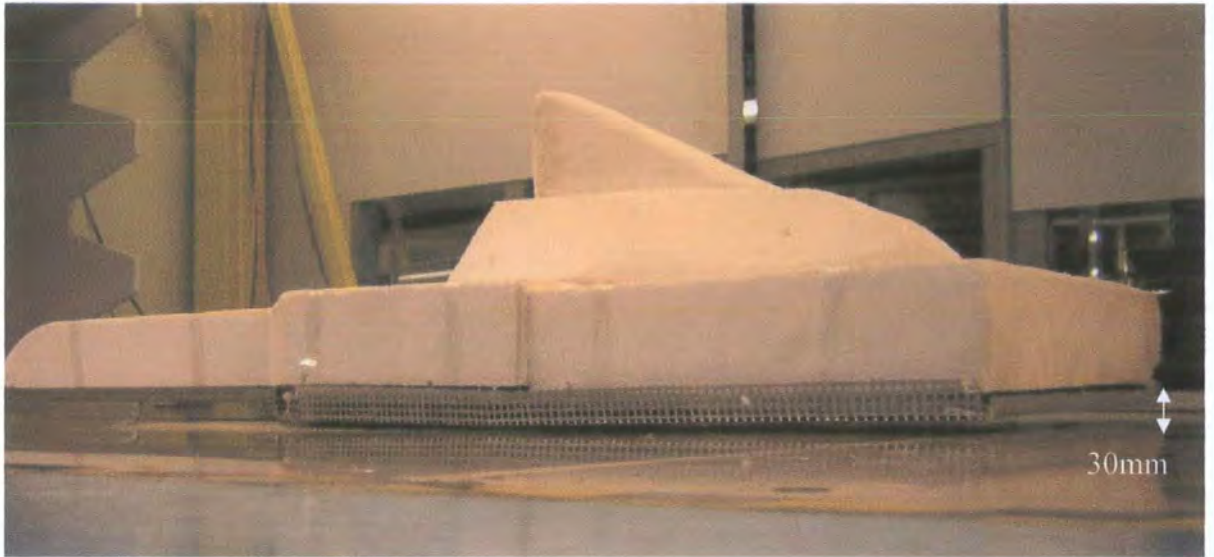
Figure 5.6.8, Superconducting Magnetic Levitation System in Operation.

5.7, Summary of Experimental Results

It has been demonstrated that permanent magnet only levitation can be used to augment superconducting levitation. The magnetic "rail" reduces the instability of magnet only levitation and the orientation of the rails affect the directional stability of the system.

A large scale Hybrid Superconducting Magnetic Levitation System was built to support a 40% scale F1 car. The system has been demonstrated to work both in tests on the bench and in the wind tunnel. The system has been demonstrated to be stable at a speed of $20 \text{ms}^{-1}$. The modular nature of the system allows for straightforward scaling to accommodate changes in vehicle size. These results were published by the author (Muscroft et al 2006).

## 6. Discussion

### 6.1 Introduction

Aerodynamic testing of racings cars with a moving ground plane requires the use of struts and wheel stings to hold the vehicle in position. Hetherington and Sims-Williams (2004 and 2006) showed that these supporting struts and stings significantly disrupt the air flow around the vehicle. The supports can be several orders of magnitude larger than some of the aerodynamic element on the vehicles. In cases where the vehicle's aerodynamics are already highly refined, the effect of subtle shape changes may be considerably smaller than the errors introduced by the supporting struts. The large overhead strut is situated directly in front of the highly loaded rear wing. The supports cause the conditions to deviate from those experienced on track, and the resulting test data is therefore inaccurate. It has been demonstrated that the overhead strut can also affect the airflow underneath the model. The interference effects are model and configuration dependant and are not cumulative, making the use of correction factors unfeasible.

The ideal solution to the problem of support strut interference would be to remove the physical supports and support the vehicle non-intrusively. The Magnetic Suspension and Balance System was developed for aerospace applications; used most notably by NASA (1991) to test the space shuttle. Currently the largest Magnetic Suspension and Balance System in the world operates at the National Aerospace Laboratory of Japan (Sawada 2001). The MSBS operates in a 600mm x 600mm wind tunnel, requires active control and draws 40kW, yet the system can only support light weight models weighing less than 7kg producing less than 16N of drag. Using such a system for ground vehicle application would severely reduce its effectiveness. Scaling the system up to allow the support of a 40% vehicle is problematical as the force acting between two magnetic dipoles decreases with the inverse cube of the distance between them. The power supplies required for a system of sufficient size to support a 40% vehicle and also allow the walls far enough away to provide a low blockage ratio would be prohibitively large.

6.2 Superconductivity

Superconductivity occurs in a material when electrons overcome their repulsion and pair up to form Cooper pairs (Bardeen et al 1957). This happens when the material is cooled below its critical transition temperature. The paired electrons possess equal and opposite values of momentum and spin vectors. When the electrons collide with the lattice structure of the superconductor the Cooper pair is not affected unless the energy generated is sufficient to cross the energy gap, and therefore there is no resistance to flow. The energy gap increases as the temperature of the material is reduced. Type II High Temperature Superconductors (HTS) possess higher critical current densities than the predominantly elemental type I superconductors, and therefore produce greater levitation forces. The Yttrium Barium Copper Oxide superconductor has a critical temperature above the boiling point of liquid nitrogen, unlike previous superconductors which required cooling with expensive liquid helium.

The usefulness of a YBCO superconducting bulk for levitation application depends on the quality of the sample. The levitation force produced by the superconductor depends on the manufacturing process and the resulting structure of the crystal lattice. Superconducting samples that consist of a single domain allow an external magnetic field to induce a supercurrent with a diameter comparable to that of the sample. Yang et al (2002) showed that the relationship between domain size and levitation force is not linear. A sample with a single domain produces significantly greater levitation force than the sum of two samples of half the size. The levitation force that a sample produces is inversely proportional to the length of the domain boundary perimeter. The trapped magnetic flux in a superconducting sample is at a maximum at the centre of the sample and decreases towards the boundary of the sample. A crack in a superconducting sample that splits the crystal lattice acts to increase the boundary length of the sample, and therefore reduces the trapped flux and hence the resulting levitation force, dramatically reducing the usefulness of the sample as demonstrated in section 3.3.2. To maximise the effectiveness of a superconducting levitation system only single domain superconductors should be used.

The Meissner effect (Meissner and Ochsenfeld 1933) is where a superconductor will expel any magnetic field impinging on its volume. A magnet will stably levitate over a superconductor in the Meissner state if the superconductor is several orders of magnitude larger than the magnet. For a magnet to levitate over superconductor of similar dimensions, the superconductor must be in the vortex state. In the vortex state the magnetic flux is trapped in superconducting vortices at imperfections in the crystal lattice of the superconductor. These imperfections are intentionally created in the production process and are microscopic which, unlike the macroscopic imperfections such as cracks, do not affect the flow of current within the superconductor or create multiple domains.

Superconducting levitation in the vortex state is intrinsically damped and the levitating magnet will resist any force that acts on it. This levitation forms the basis for the superconducting pod, as described in section 3.2, that is used in the Superconducting Magnetic Levitation System that has been developed as part of the present work. The air gap at which superconducting levitation can occur is directly proportional to the magnetic field strength of the levitating magnet. Rare-earth permanent magnets possess much higher magnetic fields than standard ferrite magnets. Neodymium-Iron-Boron magnets possess the highest magnetic field of all the permanent magnets and therefore produce the greatest levitation height. Neodymium magnets are essential for levitation applications and were therefore used throughout this project.

6.3 The Superconducting Pod

The Superconducting Pod forms the basis of the Superconducting Magnetic Levitation System. The superconducting pod consisted of a rare-earth magnet levitating over a YBCO superconducting bulk in the vortex state surrounded by electromagnets to counteract the effect of the wind force acting on the levitating magnets. One pod was tested in a wind tunnel and was demonstrated to be stable at $20ms^{-1}$ (Muscroft 2002). The position of the levitating magnets could be controlled by adjusting the current in the electromagnets. The Superconducting pod is passive and as such does not require constant adjustment to remain in a stationary position.

Electromagnetic Finite Element Analysis was carried out on a two dimensional representation of the Superconducting Pod to evaluate the effectiveness of the electromagnets used to resist the force of the wind acting on the levitating magnets. Several different configurations of electromagnets were tested with varying angles of incidence to the horizontal and increasing angles of bend in the electromagnets from $0°$ to $90°$. It was shown that straight horizontal electromagnets produced the greatest horizontal restoring force. The simulations were also tested with the levitating magnets at different air gaps which showed that the restoring force decreased as the air gap increased. This result tallied with the experimental results from the force testing of the superconducting pod on the force balance as described in section 3.6.

A larger system consisting of three Superconducting Pods was then designed and built. The increased aspect ratio of the system removed the problem of the levitating magnets pitching as the current in the electromagnets was adjusted to compensate for the effect of the wind force. The three pod system was shown to be stable and allowed complete horizontal positional control of the system through the adjustment of the current in the electromagnets. The system was also tested with a metallic non-ferrous floor to demonstrate that it does not affect the operation of the system, as shown in section 3.7.

6.4 Magnetic Reinforcement and the magnetic "Rail".

Superconducting levitation is stable and intrinsically damped but, because of the mirror effect, the air gap at which levitation can occur is limited. Magnetic levitation is capable of producing greater forces at larger air gaps. However one permanent magnet levitating over another permanent magnet will always be unstable. The magnetic rail was invented as a means of reducing the instability of magnet only levitation. The magnetic rail consists of one permanent magnet levitating over two permanent magnets with a given separation. The levitating magnet rests in a magnetic "well" created by the magnetic fields of the two base magnets. This results in a configuration that is stable in one horizontal direction and unstable in the perpendicular horizontal direction. Increasing the ratio of the length of the rails to the length of the levitating magnets reduces the instability of the system as shown in section 4.4.

The use of the magnetic rail to reinforce the superconducting levitation allows for more weight to be supported without introducing large amounts of instability into the system. The magnetic rail can be tuned to provide more load bearing capacity or increased stability depending upon the current requirements of the system. For situations such as yaw testing, multiple magnetic rails positioned at right angles to each other can be altered to provide a restoring force in a particular direction when a displacement is applied to the levitating magnets.

## 6.5 The Hybrid Superconducting Magnetic Levitation System

The magnetic rail and the superconducting pod were amalgamated to form a hybrid superconducting magnetic levitation system, combining the stability and damping of the superconducting levitation with the high ground clearance and large load bearing capability of magnetic levitation. Such a system is suited to providing support for racing cars which are comprised of regions of both high and low ground clearance. The superconductors provide levitation for the low ground clearance areas of the vehicles and the magnet only levitation provides support for the high ground clearance areas. The first hybrid system that was built was based on a 20% Le Mans style racing car and used superconducting levitation for the low ground clearance at the front axle of the car and permanent magnet levitation for the high ground clearance at the rear axle.

The number of magnetic rails used and the direction in which they were arranged affected both the stability and restoring force the system produced. Magnetic rails positioned at the rear of the system and aligned to be stable in the direction of the airflow reduced the stability of the system because of the large lever arm over which the destabilising force was able to act. When the magnetic rails are aligned to be stable in the direction perpendicular to the airflow the destabilising force acts uniformly against the superconductors without being amplified by the lever arm of frame and the resulting configuration is more stable. Reducing the lever arm of the frame by increasing the number of superconductors used in the system or shortening the frame would increase the stability. In order to create the most versatile system an equal number of rails perpendicular to each other were used. This arrangement produced an almost neutrally stable system of magnetic levitation which was

then stabilised by the superconducting levitation. Such a configuration can then be tuned to provide extra stability in a desired direction depending upon the requirements put on the system. This system provided positional control through the adjustment of the current in the electromagnets and ride height control through the adjustment of the scissor platforms on which the magnetic rails were mounted as shown in section 5.2. The superconducting levitation allowed for a ground clearance of up to 35mm. The permanent magnet levitation allowed for adjustment of the ground clearance up to 80mm. The system was also tested with an aluminium sheet to represent the platen of the rolling road to demonstrate it did not affect the operation of the system. An important advantage of the hybrid system is that it is passive and requires only low power supplies to operate. The 20% system drew less than 200W.

The hybrid superconducting magnetic levitation system was extended to support a 40% Formula 1 car. Unlike Le Mans style cars, Formula 1 cars have raised nose sections, making the front section unsuitable for support through the use of superconducting levitation. The central section of Formula 1 cars are designed with low ground clearance therefore the superconductors were situated there. The high front and rear sections of the model were supported through the use of magnetic rail configuration. The modular nature of the superconducting magnetic levitation system allowed for easy restructuring to support the larger vehicle of dissimilar design. The larger system used fives times more superconducting material than the 20% Le Mans style configuration. This allowed the superconductors to be positioned to provide an increased lever arm between the superconductors both parallel and perpendicular to the direction of the air flow. Increasing the distance between the superconductors resulted in an increased resistance to rotation of the system. The magnetic rails at the front and rear of the model were mounted on scissor platforms which allowed the ride height of the system to be easily controlled. The superconducting levitation allowed for a ground clearance of up to 35mm. The permanent magnet levitation allowed for adjustment of the ground clearance up to 80mm. Positional control of the levitating frame was achieved through control of the currents in the electromagnets as demonstrated in section 5.5. The 40% system could support 250N of downforce on top of the weight of the frame and magnets and could resist 90N of drag. The modular nature of the system means that at least four times the superconducting material

could be used in the design which would at least quadruple the load bearing capability of the system.

6.6 Wind Tunnel Tests of the Superconducting Magnetic Levitation System

To test the ability of the system to withstand the unsteady oscillations caused by the air flow acting on a vehicle under test in a wind tunnel, the hybrid superconducting magnetic levitation system was installed in the Durham 2m Wind Tunnel. The system was installed inside a custom made rolling road equipped with four rollers to provide space within it to locate the system mounted on a six component force balance. The rolling road was constructed of 60mm square steel beams but, despite strong magnetic fields being used in the system, there were no problems of interference. A 3mm aluminium platen was used on top of the rolling road. A representation of the body shell of a Formula 1 car was mounted on top of the frame connecting the levitating magnets to act as a bluff body to induce drag and cause unsteady flow to test. All of the components of the superconducting magnetic levitation system were situated either underneath the platen of the rolling road or within the levitating frame. No part of the system encroached into the airflow. The system was tested up to a speed of $20\text{ms}^{-1}$ and was demonstrated to be stable in section 5.6. The results of these tests were published by the author (Muscroft et al 2006).

## 7. Conclusions and Recommendations for Future Work

### 7.1 Conclusions

### 7.1.1 Wind Tunnel Testing with a Moving Ground Plane.

Testing of ground vehicle wind tunnel models with a moving ground plane requires the use of struts and wheel stings to hold the model in position. It has been shown that these supports considerably disrupt the air flow over the test vehicle, resulting in flawed test data. The ideal solution to this problem is to support a vehicle under test without using physical supports. Previous methods of non-intrusive support have been limited to aerospace applications. A Magnetic Suspension and Balance System (MSBS) uses very high power electromagnets to support a test vehicle. The largest MSBS is based at the National Aerospace Laboratory of Japan, and it is limited to operation in a test section of dimensions 600mm x 600mm and is only capable of supporting a model weighing 7kg. The power supplies required for a MSBS of sufficient size to support large scale heavy test vehicles are prohibitive.

### 7.1.2 Superconducting Levitation and Crystal Quality

It has been demonstrated that a permanent magnet will stably levitate over a type II superconductor when the superconductor is in the vortex state. The levitation force that a superconductor can produce depends upon its size and quality. For a superconductor to produce the maximum levitation force it must consist of only one domain. The external magnetic field induces a current loop within the crystal lattice of the superconductor; the larger the radius of the current loop, the greater the force produced. Cracks within the superconductor or misalignment of the c-axis between adjacent grains disrupt the flow of current, and if they extend throughout the sample can result in the sample consisting of two or more domains. Superconductors with multiple domains produce considerably less levitation force than single domain superconductors of comparable size, and therefore only single domain superconductors must be used for levitation applications.

## 7.1.3 The Magnetic Rail

One permanent magnet levitating directly over another permanent magnet will always be in a state of unstable equilibrium; any movement of one of the magnets will result in a force acting to further destabilise the magnets. Therefore the addition of this type of levitation to a system will always introduce greater instability. The magnetic rail was invented to reduce the instability of permanent magnet only levitation. Through the creation of a magnetic "well" in which the levitating magnet rests in the dip in field created by two fixed magnets and is then stable in two degrees of freedom. By increasing the length of the fixed magnets compared to the levitating magnet the instability of the system can be further reduced. The magnetic rail thereby allows permanent magnet levitation to augment superconducting levitation without introducing large amounts of instability, increasing the effectiveness of such a levitation system.

## 7.1.4 Electromagnetic Finite Element Analysis

Simulations of a two dimensional representation of the superconducting pod indicated that straight horizontal electromagnets provided the greatest horizontal restoring force to a displacement of the levitating magnets.

## 7.1.5 Development of the Hybrid Levitation System

It has been demonstrated that a levitation system solely utilising superconducting levitation is limited in its effectiveness for the support of a ground vehicle wind tunnel model. Augmentation of superconducting levitation with permanent magnet levitation will introduce instability, however through the use of the magnetic rail configuration the instability is minimised. Superconducting levitation provides damping and support for regions of low ground clearance whilst permanent magnetic levitation provides support for regions of high ground clearance. The magnetic rails can also be tuned to provide a restoring force in a particular direction in response to a displacement.

## 7.1.6 Testing of the Hybrid Levitation System

The hybrid levitation system was scaled up to allow the support of a vehicle with the dimensions of a 40% Formula 1 car. The system is modular allowing for straightforward implementation for differing vehicle design. This system was tested on both the bench and in the wind tunnel to evaluate its effectiveness. The system was found to be able to support 250N of downforce and 90N of drag and was tested at speeds of up to $20ms^{-1}$ in the 2m Durham wind tunnel and was shown to be stable. The prototype system used a quarter of the superconducting material that the design called for, through the use of the system with a full compliment of superconductors it is likely that it will be able to support 1000N of downforce which is comparable with the operating parameters of a Formula 1 car at test scale.

This thesis has demonstrated for the first time that it is feasible to create a passive non-intrusive method of supporting ground vehicle wind tunnel models, capable of operating in large scale wind tunnels and requiring only low power to operate. The superconducting magnetic levitation system requires less than half a kilowatt to run and because the vehicle is solely supported by magnetic fields from below the floor of the wind tunnel, the walls and ceiling of the wind tunnel can be as far away as desired to provide a low blockage ratio. The system is the largest wind tunnel magnetic levitation system in the world.

7.2 Future Work

7.2.1, Tiling of Superconducting Bulks.

To increase the effectiveness of the system more superconducting material could be fitted into the available space beneath the test vehicle. The use of cylindrical superconductors similar to those used to construct the previous systems would result in large quantities of dead space not providing levitation. Superconducting bulks can be machined into either square or hexagonal shapes which could then be tiled to maximise the use of space. Square superconductors are easier to machine but reduce the diameter of the supercurrent that can flow in the sample. Hexagonal superconductors produce a supercurrent path that is closer to the ideal circular path but are more difficult to produce.

Testing of the system with an increased quantity of superconducting material would also show how the extra damping provided would increase both the stability of the model and the ability of the system to hold the model stationary in the airflow.

7.2.2, Testing of the system with a detailed model.

Operation of the system with a detailed model running levels of drag and lift comparable to those produced by a Formula 1 car at test scale would assess the capabilities of the system. The model would not necessarily need to include the aerodynamic elements situated on the chassis of the vehicle, as utilised in Formula 1. Instead larger front and rear wings than those allowed in F1 could be used to compensate for the extra downforce and drag normally produced by the chassis located aerodynamic elements.

7.2.3, Remote Ride Height Control.

The inclusion of remotely adjustable platforms supporting the separate elements of the system would allow ride height changes to be made to the vehicle during testing. Stepper motors would be used to control the height of the platforms; multiple axis platforms would allow independent pitch and roll control.

7.2.4, Yaw Testing.

Mounting the superconducting magnetic levitation system onto a turntable would allow testing of the system at yaw angles. Testing of vehicles at yaw angles would apply differing loads to the system. This would require adjustments to be made to the system to apply restoring forces at an angle to the direction of the airflow. This could be achieved through the use of electromagnets positioned to resist the forces acting on the sides of the system. Tuning of the magnetic rails would also allow a displacement to result in a force acting in a desired direction.

7.2.5, Testing of the System with a Force Balance.

Tests on the system mounted on top of a force balance will show the level of repeatability that the system is capable of producing.

7.2.6, Quantification of Support Strut Interference.

The superconducting magnetic levitation system would be an effective means of quantifying the effects of support strut interference. The non-intrusive method of support would allow the use of a moving ground plane and removable "dummy" struts that would show the effects they have on the airflow and other aerodynamic elements on a test vehicle.

## 8. References

Akehurst, A. (2003). The Development of an Invisible Wind Tunnel Support Sting. M. Eng Dissertation, School Of Engineering, University of Durham

Bardeen, J. Cooper L. N., Schrieffer J. R. (1957). Theory of Superconductivity. Physical Review. Vol. 108. Issue 5. Pages 1175-1204.

Barlow, J. B., Rae, W. H., Pope, A. (1999). Low Speed Wind Tunnel Testing. 3$^{rd}$ Edition. Wiley, New York

Beams, J. W. (1954). Magnetic-Suspension Ultracentrifuge Circuits. Electronics Vol. 27. Issue 3. Pages 152-155.

Bednorz, J. G.; Mueller, K. A. (1986). Possible high Tc superconductivity in the barium-lanthanum-copper-oxygen system. Zeitschrift fuer Physik B: Condensed Matter. Vol. 64. Issue 2. Pages 189-193.

Boyden, R.P.; Britcher, C.P.; Tcheng, P. (1985). Status of Wind Tunnel Magnetic Suspension Research. SAE TP-851898 October 1985.

Britcher, C. (1997) Research Related to Multi Degree of Freedom Magnetic Suspensions. National Aeronautics and Space Administration Langley Research Centre. NASA-CR-205208; NAS 1.26:205208, 19970801; Aug. 1997.

Buzea, C., Robbie, K. (2005). Assembling the puzzle of superconducting elements: a review. Superconductor Science and Technology. Issue 1. Pages R1-R8.

Campbell, A. M.; Cardwell, D. A. (1997). Bulk high temperature superconductors for magnet applications. Cryogenics. Vol. 37. Issue 10. Pages 567-575.

Coey, J. M. D. (1995). Rare-earth magnets. Endeavour Vol. 19, Issue 4. Pages 146-151.

Coey, J. M. D. (2002). Permanent Magnet Applications. Journal of Magnetism and Magnetic Materials. 248, Pages 441-456.

## 8. References

Devenport W. J., Agarwal, N. K., Dewitz, M. B., Simpson, R. L., Poddar, K.(1990). Effects of a fillet on the flow past a wing-body junction. American Institute of Aeronautics and Astronautics. Vol. 28. Issue 12. Pages 2017-2024

Devenport, W. J., Simpson, R. L., Dewitz, Agarwal, N. K. (1992). Effects of a Leading Edge Fillet on the Flow Past an Appendage-Body Junction. American Institute of Aeronautics and Astronautics Journal. Vol. 30. Issue 9. Pages 2177-2183

Diko, P., Zmorayova, K., Babu, N. H., Cardwell, D. A. (2003). Shape change during solidification of bulk, single grain Y-Ba-Cu-O samples fabricated by top seeded melt growth. Physica C: Superconductivity. Vol. 398. Issue 1-2. Pages 1-7.

Docton, MKR (1997) The Simulation of Transient Cross Winds on Passenger Vehicles, PhD Thesis, University of Durham.

Dullin, H. R., Easton, R. W. (1999). Stability of Levitrons. Physica D: Nonlinear Phenomena Vol. 126. Issue 1-2. Pages 1-17.

Earnshaw, W. (1842). On the nature of the molecular forces which regulate the constitution of the luminiferous ether. Transactions of the Cambridge Philosophical Society. Vol. 7. Pages 97-112.

F.I.A., (2004), Formula 1 rules and regulations, http://www.formula1.com/insight/rulesandregs/14/479.html, Date accessed 10/07/2004.

Feng, Y.; Pradhan, A. K.; Zhao, Y.; Wu, Y.; Koshizuka, N.; Zhou, L. (2001). Influence of Ho substitution for Y on flux pinning in melt-processed YBCO superconductors. Physica C: Superconductivity, 357-360, Part 1, Pages 799-802.

Ferrari (2004), F2004 Photo Gallery, http://www.ferrariworld.com/FWorld/fw/index.jsp, Date accessed 01/07/2004

# 8. References

Fleming, J. L., Simpson, R. L., Devenport, W. J. (1991) An Experimental Study of a Turbulent Wing-Body Junction and Wake Flow. VPI&SU Report VPI-AOE-179. Virginia Polytechnic Institute and State University Blacksburg Department of Aerospace and Ocean Engineering.

Gov, S.; Shtrikman, S.; Thomas, H. (1999). On the dynamical stability of the hovering magnetic top. Physica D: Nonlinear Phenomena. Vol. 126. Issue 3-4. Pages 214-224.

Hadfield, D. (1962). Permanent Magnets and Magnetism. Wiley. New York.

Hetherington, B., Sims-Williams D. B. (2004). Wind Tunnel Model Support Strut Interference. SAE 2004 World Congress, Detroit Michigan, March 2004

Hetherington, B., Sims-Williams D. B. (2006). Support Strut Interference Effects on Passenger and Racing Car Wind Tunnel Models. SAE 2006 World Congress, Detroit Michigan, April 2006

Hoerner, S. F. (1965). Fluid-Dynamic Drag. Published by the author

Holmes, F. T. (1937) Axial Magnetic Suspensions. Review of Scientific Instruments Vol. 8. Pages 444-447.

Hor, P. H., Gao, L., Meng, R. L., Huang, Z. J., Wang, Y. Q., Forster, K., Vassilious, J., Chu, C. W., Wu, M. K., Ashburn, J. R., Torng, C. J. (1987). High-Pressure Study of the New Y-Ba-Cu-O Superconducting Compound System. Physical Review Letters. Vol. 58. Issue 9. Pages 911-912.

Hucho, W-F. (1998). Aerodynamics of Road Vehicles. 4th Edition. Society of Automotive Engineers Warrendale, PA

Jones, W. (1980). Earnshaw's theorem and the stability of matter. European Journal of Physics Issue 2. Pages 85-88.

## 8. References

Kamerlingh Onnes, H. (1913). Investigations into the properties of substances at low temperatures, which have led, amongst other things, to the preparation of liquid helium. Nobel lecture. December 1913.

Kedves, F. J.; Meszaros, S.; Vad, K.; Halasz, G.; Keszei, B.; Mihaly, L. (1987). Estimation of maximum electrical resistivity of high Tc superconducting ceramics by the meissner effect. Solid State Communications. Vol. 63. Issue 11. Pages 991-992

Ketterson, J. B., Song, S. N. (1999). Superconductivity. Cambridge University Press.

Kittel, C. (1996) Introduction To Solid State Physics. 7th Edition. Wiley New York.

Knowles, R. D., Saddington, A. J., and Knowles, K., (2002). Simulation and Experiments on an Isolated Road Wheel Rotating in Ground Contact, 4th MIRA International Vehicle Aerodynamics Conference, Warwick, UK, 16-17 October 2002.

Krabbes, G.; Fuchs, G.; Verges, P.; Diko, P.; Stover, G.; Gruss, S. (2002). 16 T trapped fields in modified YBaCuO: materials aspects. Physica C: Superconductivity. Vol. 378-381. Issue 1. Pages 636-640.

LaFleur, R. S., Langston, L. S. (1993). Drag Reduction of a Cylinder/Endwall Junction Using the Iceform Method. Journal of Fluids Engineering. Vol. 115. Pages 26-32

Leblond, C., Monot, I., Bourgault, D., Desgardin, G. (1999). Effect of the oxygenation time and of the sample thickness on the levitation force of top seeding melt-processed YBCO. Superconductor Science and Technology. Vol. 12. Pages 405-410.

Li, M. S. (2003). Paramagnetic Meissner effect and related dynamical phenomena. Physics Reports. Vol. 376. Issue 3. Pages 133-223.

MEGA (2000)Version V6.28 Manual, Applied Electromagnetic Research Centre, University Of Bath.

# 8. References

Meissner, W., Ochsenfeld, R. (1933). A new effect concerning the onset of superconductivity. Die Naturwissenschaften. Vol. 21. Page 787.

Milgrom, M. (1998). Suspension and levitation in nonlinear theories. Physics Letters A Vol. 243. Issue 1-2. Pages 33-37.

Monk, P. (2003). Finite Elements for Maxwell's Equations. Clarendon, Oxford.

Motorsport.com (2003), The Sauber Wind Tunnel
http://www.motorsport.com/photos/select.asp?Y=2003&S=F1&E=Sauber_present_wind_tunn e#, Date Accessed 06/09/2004

Murakami, M. (1992). Processing of bulk YBaCuO. Superconductor Science and Technology Vol. 5. Issue 4. Pages 185-203.

Muscroft, R. J. M. (2002). Superconduting Magnetic Levitation of Wind Tunnel Models. M. Eng Dissertation, School Of Engineering, University of Durham

Muscroft, R. J. M., D. B. Sims-Williams, D. A. Cardwell (2006). The Development of a Passive Magnetic Levitation System for Wind Tunnel Models. SP-1991, SAE 2006 World Congress, Detroit Michigan, April 2006, SAE 2006 Transactions Journal of passenger cars mechanical systems.

NASA (1991), NASA Langley Magnetic Suspension/Balance System
http://grin.hq.nasa.gov/ABSTRACTS/GPN-2000-001920.html, Date accessed 10/9/2004.

Ogawa, N.; Hirabayashi, I.; Tanaka, S. (1991). Preparation of a high-Jc YBCO bulk superconductor by the platinum doped melt growth method. Physica C: Superconductivity Vol. 177. Issue 1-3. Pages 101-105.

Ohm, G. S. (1827), The galvanic circuit investigated mathematically. New York : D. Van Nostrand Co.

# 8. References

ONERA (2005), Testing of the A380, http://www.onera.fr/photos-en/windtunnels/a380.php, Date accessed 18/01/2006.

Page, M., Winkler, J., Roberts, N., Huschilt, T., Smyth, D., Kane, B. (2002). Recent Upgrades to the Swift 8ft x 9ft Rolling Road Wind Tunnel. SAE Paper 02-MSEC-85.

Reddy, E. S., Babu, N. H., Shi, Y., Cardwell, D. A. (2005). Effect of size, morphology and crystallinity of seed crystal on the nucleation and growth of single grain Y-Ba-Cu-O. Journal of the European Ceramic Society. Vol. 25. Issue 12. Pages 2935-2938.

Reissner, M. (1997). Surface versus bulk pinning in a $HgBa_2Ca_2Cu_3O_{8+x}$ ceramics. Physica C: Superconductivity. Vol. 290. Issue 3-4. Pages 173-187.

Rohlf, J. R. (1994). Modern Physics from $\alpha$ to $Z^0$. Wiley, New York.

Sarangi, S., Chockalingam, S. P., Mavinkurve, R. G., and Bhat, S.V. (2005). Experimental Evidence for Zero DC Resistance of Superconductors. Department of Physics, Indian Institute of Science, Bangalore 560012, India. cond-mat/0506426.

Sawada, H., Kunimasu T. (2001). Status of MSBS Study at NAL. 6th International Symposium on Magnetic Suspension Technology. Politechnico di Torino.

Sengupta, S., Corpus, J., Agarwal, M., Gaines Jr, J. R. (1998). Feasibility of manufacturing large domain YBCO Levitators(TM) by using melt processing techniques. Materials Science and Engineering B. Vol. 53. Issue 1-2. Pages 62-65.

Shimura, K., Daitoh, Y., Yano, Y., Terashima, T., Bando, Y., Matsuda, Y., Komiyama, S. (1994). Superconductivity in the surface of $YBa_2Cu_3O_{7-\delta}$ films. Role of the charge reservoir block on the occurence of the superconductivity in one-unit-cell thick $YBa_2Cu_3O_{7-\delta}$. Physica C: Superconductivity. Vol. 228. Issue 1-2. Pages 91-102.

Simpson, Roger L. (2001). Junction Flows. Annual Review of Fluid Mechanics. Vol. 33. Issue 1. Pages 415-443.

# 8. References

Sims-Williams, D. B., Dominy, R. G. (2002). The Design of an Open-Jet Wind Tunnel for Model Testing. SAE Motorsports Engineering Conference, Indianapolis, Indiana, December 2002. 2002-01-3340. P-382.

Sonier, J. E. (2004). Investigations of the core structure of magnetic vortices in type-II superconductors using muon spin rotation. Journal of Physics: Condensed Matter. Vol. 16. Pages 4499-4513.

Stephens, T. (1969). Design, Construction, and Evaluation of a Magnetic Suspension and Balance System for Wind Tunnels. Tech. Rep. February 1966-November 1969. Rep. No. MIT-DSR-75396. MIT-TR-136; NASA CR-66903. Page 187

Taoufik, A.; Senoussi, S.; Tirbiyine, A. (2002). The critical current density and the vortex pinning in high-quality $YBa_2Cu_3O_{7-\delta}$ thin films. Physica B: Condensed Matter. Vol. 321. Issue 1-4. Pages 332-336.

Teshima, H. (1997). Effect of eddy current dampers on the vibrational properties in superconducting levitation using melt-processed YBaCuO bulk superconductors. Physica C: Superconductivity. Vol. 274. Issue 1. Pages 17-23.

Teshima, H.; Sawamura, M.; Morita, M.; Tsuchimoto, M. (1997). Levitation forces of a single-grained Y-Ba-Cu-O bulk superconductor of 48 mm in diameter. Cryogenics. Vol. 37. Issue 9. Pages 505-509.

Testardi, L. R., Meek, R. L., Poate, J. M., Royer, W. A., Storm, A. R., and Wernick, J. H. (1974). Preparation and analysis of superconducting Nb-Ge films. Physical Review B; Condensed Matter. Issue 11. Pages 4304-4317.

THEVA (2004), HTS Bulk Material
http://www.theva.com/index.php?option=com_content&task=view&id=15&Itemid=13, Date Accessed 17/09/2004.

## 8. References

Tournier, M., Laurenceau, P. (1957) Magnetic Suspension of a Model in a Wind Tunnel. La Recherché Aeronautique. Vol. 59. Pages 21-27.

Toyota (2003), TF103 Gallery http://www.toyota-f1.com/public/en/gallery/index.html, Date Accessed 01/07/2004

Tristan Jover, D.; Wijngaarden, R. J.; Schilling, A.; Ott, H. R.; Griessen, R. (1994). Pressure dependence of the superconducting critical temperature Tc of $HgBa_2Ca_2Cu_3O_{8+x}$ up to 26 GPa. Physica C: Superconductivity. Vol. 235-240 Part 2. Pages 893-894.

Tuttle, M. H., Moore, D. L., Kilgore, R. A., (1991). Magnetic Suspension and Balance Systems - a comprehensive annotated bibliography. NASA Center for AeroSpace Information. NASA-TM-4318.

Wu, M. K., Ashburn, J. R., Torng, C. J., Hor, P. H., Meng, R. L., Gao, L., Huang, Z. J., Wang, Y. Q., Chu, C. W. (1987). Superconductivity at 93K in a New Mixed-Phase Y-Ba-Cu-O Compound System at Ambient Pressure. Physical Review Letters. Vol. 58. Issue 9. Pages 908-910.

Yang, W. M.; Zhou, L.; Feng, Y.; Zhang, P. X.; Wu, M. Z.; Zhang, C. P.; Wang, J. R.; Du, Z. H.; Wang, F. Y.; Yu, Z. M. (1998). The effect of excess $Y_2O_3$ addition on the levitation force of melt processed YBCO bulk superconductors. Physica C: Superconductivity. Vol. 305. Issue: 3-4. Pages 269-274.

Yang, W. M.; Zhou, L.; Feng, Y.; Zhang, P. X.; Zhang, C. P.; Yu, Z. M.; Tang, X. D. (2001) Effect of perimeters of induced shielding current loops on levitation force in melt grown single domain $YBa_2Cu_3O_{7-x}$ bulk. Applied Physics Letters. Vol. 79, No. 13. Pages 2043-2045.

Yang, W. M.; Zhou, L.; Feng, Y.; Zhang, P. X.; Zhang, C. P.; Yu, Z. M.; Tang, X. D.; Nicolsky, R.; Andrade, Jr., R. (2002). Identification of the effect of grain size on levitation force of well-textured YBCO bulk superconductors. Cryogenics. Vol. 42. Issue 10. Pages 589-592.

# 8. References

Yang, Y. (1997) Research Related to Multi Degree of Freedom Magnetic Suspensions. NASA Center for AeroSpace Information. NASA-CR-205208.

Yeh, W., Chen, L., Xu, F., Bi, B., and Yang, P. (1987). Persistent current in Ba-Y-Cu-O in liquid nitrogen. Physical Review B; Condensed Matter. Vol. 36. Issue 4. Page 2414.